INFECTION-RESPONSIVE BIOMATERIALS: BACTERIOPHAGE INTEGRATED PROTOTYPE WOUND DRESSINGS FOR A TARGETED THERAPY

JOHN BARKER

A thesis submitted in partial fulfilment for the degree of Doctor of Philosophy

November 2019

The University of Brighton

School of Pharmacy and Biomolecular Sciences

Abstract

While the advent of antibiotics has proved to be one of the most important medical triumphs of the 20th century, antimicrobial resistance is threatening the return of a pre-antibiotic era. Wound pathogens can exhibit antibiotic resistance; significantly increasing patient morbidity and the associated financial costs of treatment and prevention of nosocomial outbreaks. Accordingly, attention is now focused towards alternative approaches to infection control. Bacteriophage therapy, well-established in Eastern Europe and the former Soviet Union (FSU), is increasingly being considered as one option. Lytic bacteriophage are viruses that infect and kill bacteria through cell lysis, releasing virion progeny to continue the bacteriolytic process.

The objective of this study was to produce and characterise virulent bacteriophage-integrated and immobilised wound dressings which demonstrate lytic activity against clinically relevant bacteria *in vitro*. Through judicious material design; the material structure, and bacteriophage stability, infectivity and release characteristics were characterised and modified to achieve enhanced antibacterial efficacy. Bacteriophage distribution, orientation and integrity were determined using a range of direct and indirect, techniques. Finally, the developed bacteriophage-integrated biomaterials were evaluated for cytotoxicity in preliminary studies to determine suitability for the proposed application.

The candidate wound dressing materials developed for bacteriophage integration were built upon the base material, plasticised agarose (PLAg), to which two novel modifications were made dependant on the approach to bacteriophage integration. Surface charge modification of PLAg was achieved by application of a highly charged cationic polymer, poly(vinyl amine) (PVAm), to produce a cationic interface (PVAm-PLAg) for bacteriophage adsorption. Results presented in this thesis reveal the preferential immobilisation and increased infectivity of bacteriophage adsorbed to the surface of PVAm-PLAg films when compared to unmodified PLAg. The modification of surface charge, determined by surface zeta potential measurements and elemental analysis, suggests orientated attachment of the negatively charged bacteriophage capsid to PVAm-PLAg, leaving the infective machinery available to initiate bacterial infection. Synthesis of a composite material, comprised of PVAm modified PLAg and an alginate hydrogel (Alg-PVAm-PLAg), allowed integration of bacteriophage within the porous matrix of the alginate hydrogel, protecting viral particles

from harsh external conditions and demonstrating a further increase in antimicrobial efficacy.

As reports of bacteriophage efficacy in *in vitro* and *in vivo* studies amass, delivery of bacteriophage to the target site will be of utmost importance. This study demonstrates the successful integration of bacteriophage with two novel wound dressing materials; PVAm-PLAg and Alg-PVAm-PLAg. Extensive comparative characterisation of PLAg and PVAm-PLAg films allowed a compilation of physical and chemical profiles of the developed materials, also suggesting no cytotoxic effects of the base material.

Acknowledgements

To my friends and family; you have kept me motivated through the good and the bad and provided me with endless support and encouragement. For that I thank you wholeheartedly.

I would like to express my sincere gratitude to my supervisors, Dr Iain Allan, Dr Cressida Bowyer, Prof. Stephen Denyer, and Dr Irina Savina for your continued support and guidance throughout my PhD. Your scientific knowledge and enthusiasm has allowed me to complete this project to the best of my ability.

I would also like to thank my good friend Ben Burrowes, your introductions to vital members of the bacteriophage community and the generosity you have shown has been incredible. Joe Hawthorne, Bertie Berterelli, and Heather Catty; thank you for providing invaluable technical support in the microbiology laboratory over the years. It has always been a pleasure to work alongside you. Rora Wisby, for volunteering as a laboratory assistant and providing invaluable practical support during an extremely busy period.

Further thanks are extended to Pascale Schellenberger (University of Sussex, UK) and Richard Thorogate (UCL, UK) for your expertise in TEM and AFM, respectively. Lorraine Draper's laboratory at the University College Cork, for the sequencing of my unidentified bacteriophage; your generosity was invaluable to this project and your friendship made my time at conferences even more enjoyable.

Finally, I would also like to acknowledge the generosity of BASF and Malvern Panalytical. BASF kindly provided me with PVAm samples for use throughout this study, while Malvern provided me with training and the loan of surface zeta potential equipment. These proved to be significant factors in the development of this project.

Author’s declaration

I declare that the research contained in this thesis, unless otherwise formally indicated within the text, is the original work of the author. The thesis has not been previously submitted to this or any other university for a degree and does not incorporate any material already submitted for a degree.

Signed

Dated

Contents

ABSTRACT ..... **I**

ACKNOWLEDGEMENTS ..... **III**

CONTENTS ..... **V**

LIST OF FIGURES ..... **XI**

LIST OF TABLES ..... **XVI**

ABBREVIATIONS ..... **XVII**

1 INTRODUCTION **2**

1.1 Wound infections **5**

1.1.1 Skin: a natural defence 5

1.1.2 Acute and chronic wounds 5

1.1.3 Wound infections 6

1.2 *Staphylococcus aureus* **9**

1.2.1 Pathogenesis and virulence factors 9

1.2.1.1 Membrane damaging toxins 10

1.2.1.2 Superantigen TSST-1 10

1.2.1.3 Enzymes 11

1.3 *Escherichia coli* **12**

1.3.1 Pathogenesis and virulence factors 12

1.3.1.1 Outer membrane proteins (ompT) 12

1.3.1.2 Cytotoxic necrotising factor (CNF1) 13

1.3.1.3 Haemolysin A 13

1.4 Antibiotic resistance **14**

1.4.1 Methicillin-resistant *S. aureus* (MRSA) 14

1.4.2 Multi-drug resistant *E. coli* 15

1.4.3 Biofilm formation 16

1.5 Bacteriophage **18**

1.5.1 Discovery 18

1.5.2 Classification and ecology 18

1.5.3 Bacteriophage life cycle 19

1.5.3.1 Lytic life cycle 20
1.5.3.2 Lysogenic life cycle 20
1.5.4 Bacteriophage as a novel antimicrobial 20
1.5.4.1 Advantages and considerations 22
1.5.5 Prospective bacteriophage for this study 25
1.5.5.1 Bacteriophage T4 25
1.5.5.2 Bacteriophage T3 26
1.5.5.3 Bacteriophage K 26
1.5.5.4 Bacteriophage 44AHJD 27

1.6 Polymeric wound dressings 28
1.6.1 Polymers 28
1.6.1.1 Agarose hydrogels and dehydrated films 29
1.6.1.2 Plasticisers 30
1.6.1.3 Alginate hydrogels 30
1.6.1.4 Poly(vinyl amine) 31

1.7 Bacteriophage delivery formulations 35
1.7.1 Surface immobilization 35
1.7.2 Integration within hydrogels 37

1.8 Research aims 40

2 GENERAL MATERIALS AND METHODS 42

2.1 Materials 42
2.1.1 Microorganisms and bacteriophage 42
2.1.2 Chemicals 42

2.2 Methods 44
2.2.1 Microbiological techniques 44
2.2.1.1 Bacterial strains 44
2.2.1.2 Bacterial growth conditions 45
2.2.1.3 Bacterial culture and production of stocks 45
2.2.1.4 Bacterial enumeration 46
2.2.1.5 Bacteriophage purification from crude lysate 46
2.2.1.6 Bacteriophage propagation and purification 47
2.2.1.7 Bacteriophage enumeration by plaque assay 48
2.2.2 Synthesis of PLAg films 49
2.2.2.1 Preparation of choline chloride (ChCl)/urea-based plasticiser 49

2.2.2.2 PLAg film production 49
2.2.3 Synthesis of PVAm-PLAg films 49
2.2.3.1 Purification of PVAm 49
2.2.3.2 Surface coating of PLAg with PVAm to produce PVAm-PLAg 50
2.2.4 Synthesis of Alg-PVAm-PLAg composites 50
2.2.4.1 Alginate cross-linking by the oxidation of Fe(II) 50
2.2.4.2 Alginate cross-linking by the $CaCO_3$ – GDL system 51

3 BACTERIOPHAGE CHARACTERISATION 53

3.1 Background 53

3.2 Methods 55
3.2.1 Bacterial strains 55
3.2.2 Transmission Electron Microscopy 55
3.2.2.1 Principles of TEM 55
3.2.2.2 TEM methodology 55
3.2.3 Bacteriophage host range 56
3.2.4 Bacteriophage infection of planktonic bacterial cultures 56
3.2.5 One-step growth curve of bacteriophage 57
3.2.6 Adsorption kinetics 58
3.2.7 Zeta potential of bacteriophage 58
3.2.8 Statistical analysis 59
3.2.8.1 Student's t-test 59

3.3 Results 60
3.3.1 Plaque morphology 60
3.3.2 Bacteriophage morphology 61
3.3.3 Bacteriophage host range 63
3.3.4 Bacteriophage and host interactions under planktonic growth conditions 66
3.3.5 Bacteriophage growth characteristics 67
3.3.6 Zeta potential of bacteriophage 69

3.4 Discussion 70

4 BIOMATERIAL SYNTHESIS AND CHARACTERISATION 76

4.1 Background 76
4.1.1 Base material - PLAg 76

4.1.2 Surface modification of PLAg 77
4.1.3 Alg-PVAm-PLAg composite material 79

4.2 Methods 81
4.2.1 SEM and EDS analysis 81
4.2.1.2 Principles of EDS 81
4.2.1.3 SEM and EDS methodology 82
4.2.2 MTS cytotoxicity assay of PLAg leachate 82
4.2.3 FTIR spectroscopy 83
4.2.3.1 Principles of FTIR 83
4.2.3.2 FTIR methodology 85
4.2.4 NMR spectroscopy 85
4.2.4.1 Principles of NMR spectroscopy 85
4.2.4.2 ^{1}H-NMR analysis of purified PVAm 86
4.2.5 Contact angle analysis 86
4.2.6 AFM imaging 86
4.2.7 XPS surface analysis 86
4.2.7.1 Principles of XPS 86
4.2.7.2 XPS methodology 87
4.2.8 Moisture vapour permeability rate 87
4.2.9 Swelling ratio 88
4.2.10 Surface zeta potential 89
4.2.10.1 Principles of surface zeta potential 89
4.2.10.2 Surface zeta potential measurements 90
4.2.11 Statistical analysis 90
4.2.11.1 Student's t-test 91
4.2.11.2 One-way ANOVA 91

4.3 Results 92
4.3.1 Synthesis and characterisation of PLAg films 92
4.3.1.1 Synthesis and physical evaluation 92
4.3.1.2 SEM analysis 94
4.3.1.3 FTIR analysis 95
4.3.1.4 Cytotoxicity of PLAg film leachate 98
4.3.2 PVAm purification and characterisation 99
4.3.2.1 FTIR analysis of stock and purified PVAm 99
4.3.2.2 NMR analysis of purified PVAm 101
4.3.2.3 Evidence of PVAm degradation 102
4.3.3 Surface modification and characterisation of PLAg and PVAm-PLAg 104

4.3.3.1 Atomic force microscopy 104
4.3.3.2 FTIR analysis 106
4.3.3.3 Contact angle measurements 107
4.3.3.4 MVPR and swelling studies 108
4.3.3.5 XPS surface analysis 110
4.3.3.6 SEM and EDS analysis 114
4.3.3.7 Surface zeta potential 116
4.3.4 Synthesis of Alg-PVAm-PLAg composite materials 119
4.3.4.1 Alginate gelation by oxidation of Fe(II) 119
4.3.4.2 Alginate gelation by internal liberation of calcium ions 120

4.4 Discussion 123
4.4.1 PLAg film synthesis and characterisation 123
4.4.2 Purification and characterisation of PVAm 126
4.4.3 Characterisation of PVAm-PLAg films 128
4.4.4 Identification and stability of PVAm at the PVAm-PLAg interface 128
4.4.5 General characterisation of PLAg and PVAm-PLAg films 129
4.4.6 Alg-PVAm-PLAg composite synthesis and macroscopic evaluation 132

5 BACTERIOPHAGE-BIOMATERIAL INTEGRATION AND CHARACTERISATION 135

5.1 Background 135
5.1.1 Bacteriophage adsorption and immobilisation 135
5.1.2 Bacteriophage integration within hydrogel matrices 138

5.2 Methods 140
5.2.1 Bacteriophage sensitivity to ionic liquid plasticiser 140
5.2.2 Bacteriophage integration with PLAg 140
5.2.2.1 Bacteriophage integration and release from hydrated PLAg hydrogels 140
5.2.2.2 Bacteriophage infectivity subsequent to adsorption by air drying on the surface of PLAg films 142
5.2.3 Spontaneous charge-based adsorption of bacteriophage to the surface of PLAg and PVAm-PLAg films 142
5.2.4 AFM of bacteriophage adsorbed to the surface of PVAm-PLAg 143
5.2.5 Bacteriophage integration with Alg-PVAm-PLAg 144
5.2.6 Bacteriophage dissociation and enumeration 144
5.2.6.1 Bacteriophage dissociation and release from PLAg and PVAm-PLAg 144
5.2.6.2 Bacteriophage enumeration by direct plating 144

5.2.6.3 Bacteriophage release from Alg-PVAm-PLAg composites 144
5.2.7 Statistical analysis 145
5.2.7.1 Student's t-test 145
5.2.7.2 Two-way ANOVA 145

5.3 Results 146
5.3.1 Bacteriophage sensitivity to ionic liquid plasticiser 146
5.3.2 Bacteriophage integration within hydrated PLAg hydrogels 148
5.3.3 Bacteriophage physisorption by desiccation on the surface of PLAg films 150
5.3.4 Assessment of enumeration methods for spontaneous bacteriophage adsorption 152
5.3.5 Quantification of bacteriophage adsorption to the surface of PLAg and PVAm-PLAg films... 155
5.3.6 Spontaneously immobilised bacteriophage T3 release from PLAg and PVAm-PLAg films159
5.3.7 AFM of *E. coli* infective bacteriophage at the PVAm-PLAg film interface 161
5.3.7.1 Bacteriophage T4 161
5.3.7.2 Bacteriophage T3 164
5.3.8 Bacteriophage release from Alg-PVAm-PLAg composite materials 165

5.4 Discussion 169

6 GENERAL DISCUSSION AND CONCLUSIONS 178

6.1 General discussion 178

6.2 Experimental limitations 180
6.2.1 Microbiological 180
6.2.2 Imaging of bacteriophage at the film interface 181
6.2.3 PLAg cytotoxicity assay 182

6.3 Investigative outcomes, novel contributions and conclusions 183
6.3.1 Investigative outcomes 183
6.3.2 Novel contributions 185
6.3.3 Conclusions 186

6.4 Future work 187

7 REFERENCES 189

8 APPENDICES 214

List of figures

Figure 1.1 - Schematic of acute wound healing and chronic wound attributes. 5
Figure 1.2 - Representation of the wound infection continuum. 7
Figure 1.3 - A representation of virulence factors expressed by *S. aureus*. 10
Figure 1.4 - A representation of the stages of biofilm formation. 17
Figure 1.5 - A representation of the stages of the lytic and lysogenic bacteriophage life cycles. 19
Figure 1.6 - Chemical structure of an agarose subunit. 29
Figure 1.7 - Chemical structures of alginate depicting M-blocks (MMM), G-blocks (GGG), and alternating blocks (MGM). 31
Figure 1.8 - The synthesis of PVAm from the hydrolysis of poly-NVF (left), and the Hofmann rearrangement of poly-acrylamide (right). 32
Figure 1.9 – Schematic of the hydrolysis of NVF to PVAm and the formation of formic acid or formate dependant on acid or base hydrolysis. 33
Figure 2.1 - Representation of the three distinct layers following final centrifugation at 3,000 g for 15 min. Purified phage lysate was extracted ensuring the PEG layer was not disrupted. 48
Figure 3.1 – A graphical representation of the one-step growth curve. The green line represents chloroform treated samples (total bacteriophage) and the blue line represents the number of free viruses. Eclipse period (E), latent period (L) and burst size (B) are denoted by their respective letters on the graph. 57
Figure 3.2 - Images of bacteriophage K, 44AHJD, T4 and T3 plaque morphologies on bacterial lawns (A). T3 plaques were larger with halo zones surrounding the plaques (B). 60
Figure 3.3 - Transmission electron micrograph images of bacteriophages T4 (A), bacteriophage K (B), T3 (C) and 44AHJD (D). Bacteriophage were purified by PEG precipitation prior to analysis. All samples were stained with 1% uranyl acetate. Scale is indicated by the bars. 61
Figure 3.4 - Transmission electron micrograph image of separated bacteriophage K capsid and tail. Scale is indicated by the bar. 62
Figure 3.5 - Transmission electron micrographs of bacteriophage T4. (B) shows a bacteriophage with a contracted tail and deformed capsid. Scale is indicated by the bars. 62
Figure 3.6 - Examples of *E. coli* strain sensitivities to bacteriophage T3 infection. Dark green: S, light green: SI, orange: I, and red: R. 63
Figure 3.7 - OD growth curves for E. coli 8545 (top left), E. coli 11303 (top right), S. aureus 10788 (bottom left), and S. aureus MR027 (bottom right) incubated with bacteriophage T3, T4, 44AHJD and bacteriophage K, respectively (MOIs of 0.1, 1, and 10). Graphs show the mean values of five independent experiments (N-5) ± SD. 66
Figure 3.8 - Free phage concentrations of bacteriophage T3 (top left), T4 (top right), 44AHJD (bottom left) and bacteriophage K (bottom right), normalised to percentage of initial inoculum after exposure to host bacterial cultures at a MOI of 0.01 over a period of 10 min. Data points reflect

mean data of three independent experiments (N=3) ± SD. Non-linear one-phase exponential decay curves were fitted using GraphPad Prism 5 software to obtain adsorption rate constants. 67
Figure 3.9 - One step growth curve data for bacteriophage T3 (top left), T4 (top right), 44AHJD (bottom left) and bacteriophage K (bottom right), at an MOI of 0.001. Chloroform treated samples show the total bacteriophage concentration and untreated samples show free bacteriophage concentrations. Data represents mean values from three independent experiments (N=3) ± SD. Eclipse period, latent period and burst size are denoted on the graphs by E, L, and B, respectively. . 68
Figure 3.10 - Net zeta potential values for bacteriophage T3, T4, 44AHJD, and phage K. Zeta potential values were obtained at 25°C and pH 7 ± 0.2 in deionized water. Mean values from a minimum of five repeats (N=5), each comprising of 10-100 sub-runs. 69
Figure 4.1 - Schematic of the complexation reaction between choline chloride and urea (1:2M ratio). .. 77
Figure 4.2 - Theoretical representation of cationic surface modification with PVAm and orientated attachment of bacteriophage to the film interface. 78
Figure 4.3 – Schematic representing a bacteriophage loaded composite material, where bacteriophage have been entrapped within a protective alginate hydrogel layer. 79
Figure 4.4 - Representation of the vibrational modes of a molecule upon exposure to infrared light. 84
Figure 4.5 - Images of plasticised (50% DES) and non-plasticised agarose films, depicting the differences in physical characteristics. 93
Figure 4.6 - SEM micrographs of PLAg films (50% DES) showing surface topography at 10,000x magnification (A) and 150,000x magnification (B). 94
Figure 4.7 - FTIR spectra obtained from PLAg films containing incremental concentrations of plasticiser; IL0 (red), IL15 (blue), IL30 (green), and IL50 (magenta) DES. 96
Figure 4.8 - FTIR spectra obtained from PLAg films prior to (red), and subsequent to soaking in bacteriophage buffer (blue) for 24h at room temperature and atmospheric pressure. 97
Figure 4.9 - Cell viability of 3T3 fibroblasts after 24h incubation with PLAg film leachate as measured by MTS assay. Cell viability was calculated by relation to the cell control. Mean values were calculated from nine independent experiments (N=9) ± SD. 98
Figure 4.10 - FTIR spectra of commercially available PVAm (blue) and PVAm which had undergone hydrolysis and dialysis (red). 100
Figure 4.11 - NMR spectrum of purified PVAm, outlining the chemical structure of the purified sample. The sample was analysed using 16 run scan analysis at 400 MHz, with D_2O used as solvent. 101
Figure 4.12 - Evidence of PVAm degradation subsequent to 12 months storage (RT and atmospheric pressure) by FTIR analysis. Top spectrum (purple) was obtained from the analysis of newly purified PVAm, while the bottom spectrum (blue) was obtained from PVAm produced 12 months prior and stored under ambient conditions. 102
Figure 4.13 - FTIR spectra of a number of storage conditions subsequent to 12 months storage under each condition (with the exception of newly purified PVAm). From top to bottom; Newly purified

(ORANGE), NITROGEN ROOM TEMPERATURE (GREEN), AIR ROOM TEMPERATURE (MAGENTA), NITROGEN -20°C (BLUE), AND AIR -20°C (BROWN). 103
FIGURE 4.14 - 2D (LEFT) AND 3D (RIGHT) AFM IMAGES OF DEHYDRATED PLAG (A) AND PVAM-PLAG (B) FILMS OBTAINED UNDER AMBIENT CONDITIONS. IMAGES WERE COLLECTED USING TAPPING MODE WITH A SILICON TIP. SCALES ARE INDICATED BY THE BARS. 105
FIGURE 4.15 - FTIR SPECTRA OF PLAG (PURPLE) AND PVAM-PLAG (BLUE) FILMS, ALLOWING IDENTIFICATION OF PVAM BY THE PRESENCE OF FUNCTIONAL GROUPS UNIQUE TO THE POLYMER COATING. 106
FIGURE 4.16 - CONTACT ANGLE (CA) MEASUREMENTS OF PLAG (TOP) AND PVAM-PLAG (BOTTOM) FILMS USING SESSILE DROP TECHNIQUE. MEAN CA MEASUREMENTS WERE CALCULATED FROM SIX INDEPENDENT MEASUREMENTS (N=6). 107
FIGURE 4.17 - MOISTURE VAPOUR PERMEABILITY RATE OF PLAG AND PVAM-PLAG FILMS (50% DES) AT 37°C FOR 24H AT 33.6 RH (A),AND SWELLING MEASUREMENTS OF PLAG AND PVAM-PLAG FILMS IN PBS (MAINTAINED AT 37°C) MONITORED OVER A 40 MINUTE PERIOD (B). ALL VALUES WERE CALCULATED AS THE MEAN OF THREE INDEPENDENT EXPERIMENTS (N=3) ± SD. 109
FIGURE 4.18 - XPS SURVEY SCAN SPECTRA OF UNCOATED PLAG (TOP LEFT), PVAM COATED PLAG (TOP RIGHT), PRE-SOAKED UNCOATED PLAG (BOTTOM LEFT) AND PRE-SOAKED PVAM COATED PLAG (BOTTOM RIGHT). PRE-SOAKING WAS CONDUCTED IN BACTERIOPHAGE BUFFER FOR 24H AT 4°C TO DETERMINE DETACHMENT OF PVAM SURFACE COATINGS FROM THE POLYMER FILM. EACH SPECTRUM REPRESENTS THE MEAN VALUE OF THREE INDEPENDENT MEASUREMENTS. 111
FIGURE 4.19 - HIGH RESOLUTION C1S CORE LEVEL SPECTRA ALLOWING DECONVOLUTION OF C BONDING. UNCOATED PLAG (TOP LEFT), PVAM COATED PLAG (TOP RIGHT), PRE-SOAKED UNCOATED PLAG (BOTTOM LEFT) AND PRE-SOAKED PVAM COATED PLAG (BOTTOM RIGHT). PRE-SOAKING WAS CONDUCTED IN BACTERIOPHAGE BUFFER FOR 24 H AT 4°C TO DETERMINE DETACHMENT OF PVAM SURFACE COATINGS FROM THE POLYMER FILM. EACH SPECTRUM REPRESENTS THE MEAN VALUE OF THREE INDEPENDENT MEASUREMENTS. 113
FIGURE 4.20 - EDS SPECTRA OBTAINED FROM SEM MICROGRAPHS OF PLAG (BLACK) AND PVAM-PLAG (RED) IN THE ABSENCE OF FIXATION AND SPUTTER COATING. IMAGES WERE OBTAINED AT LOW MAGNIFICATION (25K X) TO AVOID SAMPLE DEGRADATION. 114
FIGURE 4.21 - SEM MICROGRAPH OF PVAM-PLAG AT 25K X MAGNIFICATION (TOP) AND EDS SPECTRA OF FOUR POINTS (A TO D – BELOW) ALLOWING ELEMENTAL ANALYSIS AT SPECIFIC POINTS WITHIN THE IMAGE. 115
FIGURE 4.22 - SURFACE ZETA POTENTIAL MEASUREMENTS OF PLAG AND PVAM-PLAG FILMS IN BACTERIOPHAGE BUFFER (PH 7.2, 25°C). PVAM-PLAG FILMS WERE FORMULATED WITH A SURFACE COATING CONCENTRATION OF 0.5 % W/V. UNMODIFIED POLYSTYRENE LATEX TRACER PARTICLES WERE USED FOR PLAG AND NR3+ MODIFIED PARTICLES FOR PVAM-PLAG FILMS. MEAN VALUES WERE OBTAINED FROM THREE INDEPENDENT EXPERIMENTS (N=3) ± SD. 116
FIGURE 4.23 - SURFACE ZETA POTENTIAL MEASUREMENTS OF PVAM-PLAG FILMS IN BACTERIOPHAGE BUFFER (PH 7.2, 25°C). PVAM-PLAG FILMS WERE FORMULATED WITH A SURFACE COATING CONCENTRATION OF 0.06% TO 1% W/V. NR3+ MODIFIED PARTICLES WERE USED FOR PVAM-PLAG FILM MEASUREMENTS. EACH VALUE DEPICTS THE

mean of three independent measurements (N=3) ± SD. Statistical analysis was conducted using one-way ANOVA and analysed using Tukey's multiple comparisons post-hoc test. 117
Figure 4.24 - Images of alginate hydrogels cross-linked by the air oxidation of iron(II) to iron(III). Images show the Alg-PVAm-PLAg composite (top left), alginate hydrogel formed in the bottom of a 25 ml beaker (bottom left), and alginate hydrogels formed within wells of a 12-well plate. 119
Figure 4.25 - Image of an alginate hydrogel, formed within a 15 ml bijoux bottle, cross-linked using the $CaCO_3$-GDL system of internal liberation of Ca^{2+} ions. Final concentrations of the hydrogel formulation were as follows; 1.5 % alginate, 1 % GDL, and 1 % $CaCO_3$. 120
Figure 4.26 - Images of Alg-PLAg film composites synthesised by the addition of alginate-GDL-$CaCO_3$ to the surface of PLAg films and allowed to cross link for 2h under ambient conditions. No affinity was observed between the alginate hydrogel layer and PLAg film base material (N=5). 121
Figure 4.27 - Images of Alg-PVAm-PLAg film composites synthesised by the addition of alginate-GDL-$CaCO_3$ to the surface of PLAg films and allowed to cross link for 2 h under ambient conditions. High affinity was observed between the alginate hydrogel layer and PVAm-PLAg film base material (N=5). 122
Figure 4.28 - Theoretical representations of the consequences of low PVAm concentration (A1), low salt concentration (A2), and no surface coating (A3) on the hydrophilicity of polymer films. A1 represents misalignment of the polymer exposing the hydrophobic alkyl chain, A2 represents flat polymer (orange line) deposition, and A3 represents the leaching of plasticiser from uncoated PLAg (green arrows). Row B represents the theoretical approaches circumvent factors in row A, by increasing PVAm concentration (B1), increasing salt concentration (B2), and application of the surface coating (B3). 131
Figure 5.1 - Representation of uncontrolled adsorption (top) and orientated adsorption (bottom) of bacteriophage to a solid substrate. 136
Figure 5.2 - Images of bacterial filter units utilised for bacteriophage adsorption and dissociation studies. 143
Figure 5.3 - Bacteriophage sensitivity to ionic liquid plasticiser at incremental concentrations (0% to 50% v/v) following 3 h exposure at 30°C. Each value represents the mean of three independent measurements (N=3) ± SD. 147
Figure 5.4 - Incorporation and release of bacteriophage K and T3 from within the PLAg gel matrix. Each value represents the mean of three independent experiments (N=3) ± SD. (A) proportional release in relation to the starting inoculum (%), and (B) qualitative measure of bacteriophage release by direct plating. Statistical significance between bacteriophage release was calculated using student's t-test. * indicates statistical significance (* = P <0.05, ** = P <0.01, *** = P <0.001). .. 149
Figure 5.5 – Bacteriophage K and T3 viability subsequent to air drying at 30°C on the surface of PLAg films for 0 h to 24 h. Bacteriophage viability was quantified by the reconstitution method. Each data point represents the mean values of three independent experiments (N=3) ± SD. 151

FIGURE 5.6 - SPONTANEOUS ADSORPTION METHODOLOGY VALIDATION USING UNCOATED PLAG FILMS AND BACTERIOPHAGE T3 AT 4°C FOR 24 H. **SUPERNATANT**: TOTAL BACTERIOPHAGE SORPTION, **WASHING**: WEAKLY ASSOCIATED BACTERIOPHAGE, **PLATING**: ADSORBED AND INFECTIVE BACTERIOPHAGE. EACH DATA POINT REPRESENTS THE MEAN VALUES OF THREE INDEPENDENT EXPERIMENTS (N=3) ± SD. 153

FIGURE 5.7 – EXAMPLE OF DIRECT PLATING OF PLAG (BOTTOM LEFT) AND PVAM-PLAG (BOTTOM RIGHT), SUBSEQUENT TO BACTERIOPHAGE ADSORPTION AT AN EXPOSURE INOCULUM OF 10^4 PFU/FILM. CONTROL PLATES ARE PLAG (TOP LEFT) AND PVAM-PLAG (TOP RIGHT) WHICH HAD NOT BEEN EXPOSED TO BACTERIOPHAGE. 154

FIGURE 5.8 - SPONTANEOUS ADSORPTION OF BACTERIOPHAGE T3 (TOP LEFT), T4 (TOP RIGHT), 44AHJD (BOTTOM LEFT), AND K (BOTTOM RIGHT), TO PLAG (BLUE) AND PVAM-PLAG (GREEN), AS DETERMINED BY PERCENTAGE REDUCTION FROM THE STARTING SUPERNATANT INOCULUM (10^3 PFU, 10^4 PFU, 10^5 PFU, AND 10^6 PFU). EACH DATA POINT REPRESENTS THE MEAN VALUES OF THREE INDEPENDENT EXPERIMENTS (N=3) ± SD. STATISTICAL ANALYSIS BETWEEN EACH INOCULUM AND FILM VARIANT WAS CONDUCTED USING TWO-WAY ANOVA AND BONFERRONI MULTIPLE COMPARISONS POST-HOC TESTS, FOLLOWING LOG TRANSFORMATION OF RAW DATA. * INDICATES STATISTICAL SIGNIFICANCE (***** = P <0.05, ****** = P <0.01, ******* = P <0.001, ******** = P <0.0001)... 156

FIGURE 5.9 - RELEASE OF BACTERIOPHAGE T3 SPONTANEOUSLY ADSORBED TO THE SURFACE OF PLAG (TOP) AND PVAM-PLAG (BOTTOM) FILMS, OVER A 48 H PERIOD AT 4°C (BLUE LINE) AND 37°C (RED LINE). THE NUMBER OF BACTERIOPHAGE ADSORBED TO THE SURFACE OF EACH FILM VARIANT WAS ESTIMATED BY THE REDUCTION IN SUPERNATANT TITRE FOLLOWING 24 H ADSORPTION AT 4°C. EACH DATA POINT REPRESENTS THE MEAN VALUES OF THREE INDEPENDENT EXPERIMENTS (N=3) ± SD. 160

FIGURE 5.10 - AFM IMAGE OF BACTERIOPHAGE T4 ADSORBED TO THE SURFACE OF PVAM-PLAG FILMS. THE SCALE IS 5 μM^2, AND HEIGHT MEASUREMENT IS INDICATED BY BAR. 161

FIGURE 5.11 - AFM IMAGES OF BACTERIOPHAGE T4 ADSORBED TO THE SURFACE OF A PVAM-PLAG FILM, SHOWING THE CHARACTERISTIC MORPHOLOGY OF *MYOVIRIDAE*. (A) 1.5 μM^2 AFM IMAGE OF FOUR T4 BACTERIOPHAGE, (B) 500 NM^2 AFM IMAGE OF A SINGLE T4 BACTERIOPHAGE CAPTURED FROM (A), AND (C) 500 NM^2 3D PERSPECTIVE VIEW OF A SINGLE T4 BACTERIOPHAGE. THE SCALE OF EACH IMAGE IS INDICATED BY THE BARS. 162

FIGURE 5.12 - EXAMPLE HEIGHT MEASUREMENTS OF BACTERIOPHAGE T4 CAPSID (BLUE LINE) AND TAIL (WHITE LINE) STRUCTURES BY CROSS-SECTION ANALYSIS USING JPK SPM AFM DATA PROCESSING SOFTWARE. EACH GRAPH SHOWS THE MEASURED HEIGHT (NM) OF THE CAPSID (TOP IMAGE) AND TAIL (BOTTOM IMAGE) OVER THE SELECTED SECTION. 163

FIGURE 5.13 - AFM IMAGES OF BACTERIOPHAGE T3 ADSORBED TO THE SURFACE OF PVAM-PLAG. (A) 5 μM^2 AFM IMAGE OF NUMEROUS T3 BACTERIOPHAGE, (B) 1 μM^2 AFM IMAGE OF THREE T3 BACTERIOPHAGE ENLARGED FROM (A – RED BOX), AND (C) 1 μM^2 3D PERSPECTIVE VIEW OF IMAGE (B) SHOWING THE TAIL STRUCTURE OF BACTERIOPHAGE T3 (WHITE CIRCLE). THE SCALE OF EACH IMAGE IS INDICATED BY THE BARS. 164

FIGURE 5.14 - RELEASE KINETICS OF BACTERIOPHAGE T3 (TOP LEFT), T4 (TOP RIGHT), AND BACTERIOPHAGE K (BOTTOM CENTRE) FROM ALG-PVAM-PLAG COMPOSITE MATERIALS AT 4°C (BLUE LINES) AND 37°C (RED LINES). THREE TITRES WERE TESTED FOR EACH BACTERIOPHAGE; 10^5 PFU (CIRCLE), 10^6 PFU (SQUARE), AND 10^7 PFU (TRIANGLE). EACH DATA POINT REPRESENTS THE MEAN VALUES OF THREE INDEPENDENT EXPERIMENTS (N=3) ± SD. 166

List of tables

TABLE 1.1 - SUMMARY OF A NUMBER OF STUDIES OUTLINING THE PREVALENCE OF BACTERIAL SPECIES AND GENUS' ISOLATED FROM BURN WOUNDS, SSIS AND DIABETIC FOOT ULCERS. 8

TABLE 1.2 - PRESENTING THE ADVANTAGES AND CONSIDERATIONS OF BACTERIOPHAGE AS A NOVEL ANTIMICROBIAL IN COMPARISON TO ANTIBIOTICS. 24

TABLE 1.3 - ADVANTAGEOUS PROPERTIES OF PVAM IN COMPARISON TO CHITOSAN AN ALTERNATIVE INTERFACIAL AGENT. 34

TABLE 2.1 - LIST OF *E. COLI* STRAINS AND SOURCES USED IN THIS STUDY. 44

TABLE 2.2 - LIST OF *S. AUREUS* STRAINS AND SOURCES USED IN THIS STUDY. 45

TABLE 3.1 - SENSITIVITY SCREENING OF BACTERIOPHAGE T3 AND T4 AGAINST A PANEL OF 12 *E. COLI* STRAINS, INCLUDING A CLINICAL ISOLATE (E. COLI B3). 64

TABLE 3.2 - SENSITIVITY SCREENING OF BACTERIOPHAGE K AND 44AHJD AGAINST A PANEL OF 17 *S. AUREUS* STRAINS, INCLUDING 9 CLINICAL ISOLATES. 65

TABLE 3.3 - SUMMARY OF BACTERIOPHAGE GROWTH CHARACTERISTIC DATA FROM ADSORPTION, ONE-STEP GROWTH, AND BURST SIZE INVESTIGATIONS. 72

TABLE 4.1 - FTIR WAVENUMBERS (CM-1) OBTAINED FROM PLAG FILM SAMPLES CONTAINING INCREMENTAL CONCENTRATIONS OF PLASTICISER (0 %, 15 %, 30 %, 50 %). 95

TABLE 4.2 - FTIR WAVENUMBERS (CM-1) OBTAINED FROM UNPURIFIED PVAM AND PURIFIED PVAM, WITH PEAK ASSIGNMENT DESCRIPTIONS. 100

TABLE 4.3 - ELEMENTAL SURFACE CONCENTRATIONS FOR UNWASHED AND WASHED (BACTERIOPHAGE BUFFER, 24H) PLAG AND PVAM-PLAG FILMS DERIVED FROM XPS SURVEY SCAN DATA. 110

TABLE 4.4 - RELATIVE ABUNDANCE OF CARBON BONDS FOR UNWASHED AND WASHED (BACTERIOPHAGE BUFFER, 24H) PLAG AND PVAM-PLAG FILMS, DERIVED FROM C1S CORE LEVEL XPS DATA. 112

TABLE 4.5 - SURFACE ZETA POTENTIAL MEASUREMENTS OF PVAM-PLAG FILMS OF INCREMENTAL SURFACE PVAM CONCENTRATION, IN BACTERIOPHAGE BUFFER (PH 7.2, 25°C). 118

TABLE 5.1 - SPONTANEOUS ADSORPTION VALUES OF BACTERIOPHAGE TO PLAG AND PVAM-PLAG FILMS, SHOWING THE INITIAL INOCULUM, THE REDUCTION IN SUPERNATANT TITRE FOLLOWING THE ADSORPTION CONDITIONS (24 H, 4°C, 80 RPM), CALCULATED THEORETICAL ADSORPTION VALUES, AND THE MEAN PLAQUE COUNT OBTAINED FROM DIRECT PLATING OF THE FILMS. 157

TABLE 5.2 - BACTERIOPHAGE K, T3, AND T4 RELEASE FROM ALG-PVAM-PLAG COMPOSITES FROM 1 TO 48 H TIME POINTS, 10^7 PFU INOCULUM, AND RELEASE TEMPERATURES OF 4°C (BLUE) AND 37°C (RED). 167

TABLE 5.3 – BACTERIOPHAGE K, T3, AND T4 RELEASE FROM ALG-PVAM-PLAG COMPOSITES AT THE 48 H TIME POINT (10^5, 10^6, AND 10^7 PFU INOCULUMS) AND RELEASE TEMPERATURES OF 4°C (BLUE) AND 37°C (RED). 168

TABLE 5.4 - SUMMARY OF CHARACTERISTICS WHICH COULD INFLUENCE THE RELEASE OF BACTERIOPHAGE FROM ALG-PVAM-PLAG COMPOSITES. 175

Abbreviations

3D	Three-dimensional
AFM	Atomic force microscopy
Alg-PVAm-PLAg	Alginate-Poly(vinyl amine)-Plasticised agarose composite material
APCs	Antigen presenting cells
ATCC	American type culture collection
ATR	Attenuated total reflectance
CA	Contact angle
ChCl	Choline chloride
CNF-1	Cytotoxic necrotising factor 1
CRE	Carbapenem resistant Enterobacteriaceae
D_2O	Deuterium oxide
DDS	Drug delivery system
DES	Deep eutectic solvent
dH_2O	Deionised water
DMEM	Dulbecco's modified eagle medium
ECM	Extracellular matrix
EDS	Energy dispersive x-ray spectroscopy
EPS	Exopolysaccharide
eV	Electron volt
ExPEC	Extra-intestinal pathogenic *E. coli*
FBS	Foetal bovine serum
Fe	Iron
FEG-SEM	Field emission gun scanning electron microscopy
FnbpA	Fibronectin binding protein A
FSU	Former Soviet Union
FTIR	Fourier transform infrared spectroscopy
GDL	Glucono delta-lactone
HAMA	Hyaluronic acid methacrylate
HGT	Horizontal gene transfer
hlyA	Hemolysin A
ICTV	International committee on taxonomy of viruses
IgG	Immunoglobulin G
IL	Ionic liquid
IR	Infrared

iSCAT	Interferometric scattering microscopy
IUPAC	International union of pure an applied chemistry
LPS	Lipopolysaccharide
M	Molar
MHC	Major histocompatibility complex
MHz	Megahertz
mM	Millimolar
MOI	Multiplicity of infection
MRSA	Methicillin resistant *S. aureus*
MSCRAMMs	Microbial surface components recognising adhesive matrix molecules
mV	Millivolt
MVPR	Moisture vapour permeability rate
MWCO	Molecular weight cut off
NaCl	Sodium chloride
NaOH	Sodium hydroxide
NCTC	National collection of type cultures
NMR	Nuclear magnetic resonance spectroscopy
NNIS	National nosocomial infections surveillance system
NS	Nanosight
NVF	N-vinylformamide
OD	Optical density
ompT	Outer membrane protein T
PALS	Phase analysis light scattering
PBS	Phosphate buffered saline
PBPs	Penicillin binding proteins
PdI	Poly dispersity index
PEG	Polyethylene glycol
PFU	Plaque forming units
PGA	Polyglycolide
PLAg	Plasticised agarose
ppm	Parts per million
PVAm	Poly(vinyl amine)
PVAm-PLAg	Poly(vinyl amine) coated plasticised agarose
PVL	Panton and Valentine leukocidin
RGIMS	Rajiv Gandhi institute of medical sciences

RH	Relative humidity
rpm	Revolutions per minute
RT	Room temperature
SD	Standard deviation
SSC	Staphylococcal cassette chromosome
SSIs	Surgical site infections
TEM	Transmission electron microscopy
TNTC	Too numerous to count
TSA	Tryptone soy agar
TSB	Tryptone soy broth
TSS	Toxic shock syndrome
TSST-1	Toxic shock syndrome toxin 1
UV	Ultraviolet
XPS	X-ray photoelectron spectroscopy

Chapter One: Introduction

1 Introduction

The discovery of antibiotics has been one of the most important medical triumphs of the last century, saving the lives of millions of people and preventing infection following injury, routine surgery, organ transplants and chemotherapy. The introduction of antibiotics has undoubtably revolutionised the world we live in, not only in the treatment and prevention of clinical infections, but also in the agricultural, aquacultural, and veterinary industries. The emergence of bacteria which have evolved resistance mechanisms against these agents is now threatening the return to a pre-antibiotic era, where previously treatable infections are difficult or impossible to treat.

Antibiotic resistance is already causing a significant global threat to the successful treatment of *Clostridium difficile*, Enterobacteriaceae and *Pseudomonas aeruginosa* infections, with a host of other organisms being classed as 'serious' and 'concerning' [1]. These antibiotic-resistant bacteria are now presenting a significant risk to almost all areas of clinical practice that involve the prevention and management of bacterial infection. It has been estimated that some 23,000 deaths occur annually as a direct result of infection by resistant organisms in the USA, and 5,000 deaths in the UK [1]; resistant organisms therefore have significant implications for healthcare expenditure. The estimated financial burden is €1.5 billion per year in the EU [2], and $20 billion per year in the USA [3]. It has recently been estimated that antibiotic resistance will result in 10 million deaths worldwide per year by 2050, potentially making it the world's single biggest killer above cancer, heart disease and stroke [4].

The antibiotic crisis has been attributed almost exclusively to the inappropriate use of these medications, including prescribing for viral infections, extensive and indiscriminate agricultural use, and the ready availability of antibiotics over the counter in many countries. The development of new antibiotics by the pharmaceutical industry has also stalled, due to economic and regulatory obstacles, which has further exacerbated the problem. One area that has particularly suffered has been the management of chronic wounds, resulting in significant burdens to the patient and healthcare system. For example, in the USA, the cost of chronic wounds has been estimated at $6.5 billion per year and the cost of a single diabetic ulcer has been estimated at nearly $50,000 [5].

Awareness of the antibiotic resistance has grown over recent years, with a number of major regional and worldwide initiatives emerging over the past two decades:

- World Health Assembly (WHA) resolutions on antimicrobial resistance (1998) [6]
- World Health Organisation (WHO) global strategy for containment of antimicrobial resistance (2001) [7]
- EU banned the use of antibiotics for animal growth promotion (2003) [8]
- EU strategic action plan against the rising threats from antimicrobial resistance (2011) [9]
- EU council conclusions (2012) [10]
- FDA banned the arbitrary use of antibiotics on animals unless prescribed by a veterinarian (2012) [11]
- UK five year antimicrobial resistance strategy 2013 – 2018, and the recently published 2019 – 2024 strategy [12]

A feature common to most of these strategies is providing funding to explore therapeutic alternatives to traditional antibiotics. In the case of chronic wounds infected by antibiotic resistant bacteria, research is now focused on novel methods of management, including novel vaccination formulations, antibiotic uptake mechanisms, and alternative modalities. The use of vaccines to prevent bacterial infections still offer potential in preventing bacterial infections, by employing innovative vaccine technologies such as reverse vaccinology, novel adjuvants, and advanced polysaccharide conjugation and antigen design [13]. To circumvent inadequate penetration of antibacterial agents, the use of efflux pump inhibitors and active uptake transporters may provide adjuncts to increase the efficacy of traditional antibiotics [14]. Finally, several alternative approaches and modalities are currently under consideration, including the targeting of host factors, reduction of bacterial virulence, and the use of monoclonal antibodies [13], nanomaterials [15, 16] and mollusc mucus [17, 18]. A further alternative approach to bacterial the management of bacterial infections is bacteriophage therapy which involves the use of bacteriolytic viruses; these may offer many advantages when used alone and in combination with traditional antibiotics [19].

Once a new antimicrobial agent is established, it is important to consider its delivery to the target site. Over the years, a vast array of wound dressings have been developed in order to protect the open wound from bacterial colonisation, whilst also promoting the wound healing process. For example, the use of occlusive dressings (air and water tight) supports the inflammatory phase by reducing oxygen tension, while traditional dry gauze dressings limit the amount of wound exudate enabling autolytic debridement [20]. Semipermeable

films and hydrogels, however, are now more commonly used permitting air and water vapour transmission while restricting microbial and liquid penetration.

These biomaterials, along with novel antimicrobial agents, are now of considerable interest in the management of chronic wounds infected by antibiotic resistant bacteria. Accordingly, the investigations presented in this thesis are directed towards furthering our understanding of the integration of bacteriophage with novel polymer films and hydrogels.

1.1 Wound infections

1.1.1 Skin: a natural defence

Our largest organ system, the skin, is composed of three distinct layers: epidermis, dermis and hypodermis. The skin performs functions that include thermoregulation, fluid homeostasis, provision of sensory information, and metabolic and immunological support; while presenting a continuous anatomical barrier from the external environment. Breach of this microbial defence can allow exposure and colonisation of the deeper tissues to endogenous or exogenous bacteria. Proliferation of colonised bacteria can follow, exacerbated by exposure to the moist, warm and nutritive deeper tissues; leading to infection and inflammation of the affected area.

1.1.2 Acute and chronic wounds

Acute wounds follow a normal healing process defined by haemostasis, inflammation, proliferation and growth of new tissue, and tissue maturation. A wound which does not follow these stages in an anticipated time period can be considered chronic, often characterised by a prolonged phase of inflammation [21], imbalance of tissue production and degradation, and increased risk of infection [22] (Figure 1.1). Chronic wounds primarily develop due to predispositions which affect the nervous, circulatory and immune systems.

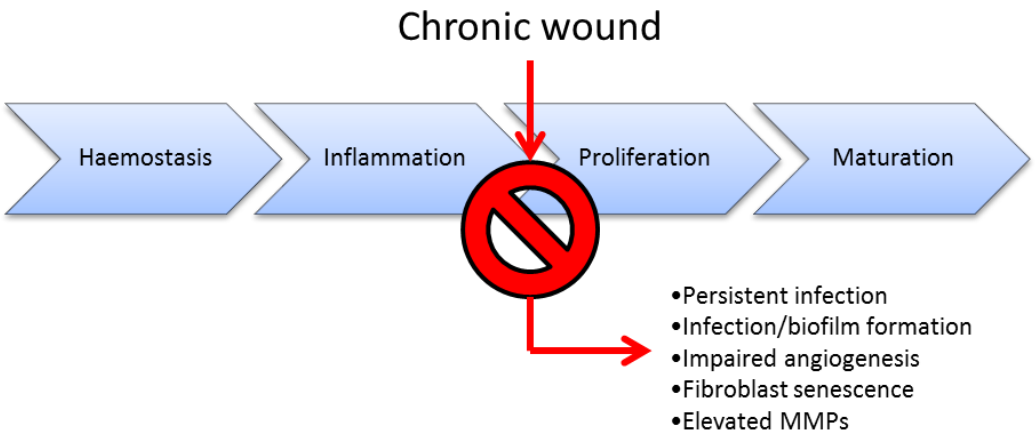

Figure 1.1 - Schematic of acute wound healing and chronic wound attributes.

A high proportion of chronic wounds can be placed into one of four categories: diabetic ulcers, venous ulcers, pressure sores and ischemic ulcers [23]. While the vast majority of superficial wounds follow the normal pathway, the process may fail at numerous stages during the healing process, especially when there is an underlying disease such as diabetes. Age also seems to be an important factor, with the average age of clinical presentation for diabetic ulcers [24], pressure sores [25], and venous ulcers [26] being over 60 years old.

1.1.3 Wound infections

Microbiological exposure and consequent infection most commonly arises from lesions caused by external factors which breach the anatomical defence against endogenous and exogenous contamination, most commonly surgery, trauma and burns. Colonisation of both acute and chronic wounds will delay the healing process, however in chronic wounds this can result in a non-healing, persistent infection and the formation of complex microbial communities (biofilms). These can evade the host immune defence and withstand antibiotic exposure, allowing the wound to persist indefinitely [27].

Subsequent to the inevitable colonisation of wounds by microorganisms, a number of host and bacterial responses will influence the wound bioburden and consequent healing outcome. The route to wound infection is believed to follow a number of stages, often referred to as the infection continuum [28] (Figure 1.2). Early contamination of wounds by microorganisms must result in their prompt adaptation and acclimatisation, as without suitable nutritive and physical conditions, or the ability to evade the host immune response, the contaminants will not multiply or persist. During the colonisation stage, microbial species successfully grow and divide, often due to a compromised local environment, such as the presence of necrotic tissue and foreign bodies, tissue hypoxia, and impaired immune response [29]. At this stage the microorganisms may persist by forming biofilms and expressing virulence factors which could result in interrupted wound healing without inducing apparent clinical signs of infection, a stage referred to as the ‘critical colonisation threshold’ which without identification may lead to the clinical manifestations of infection [29].

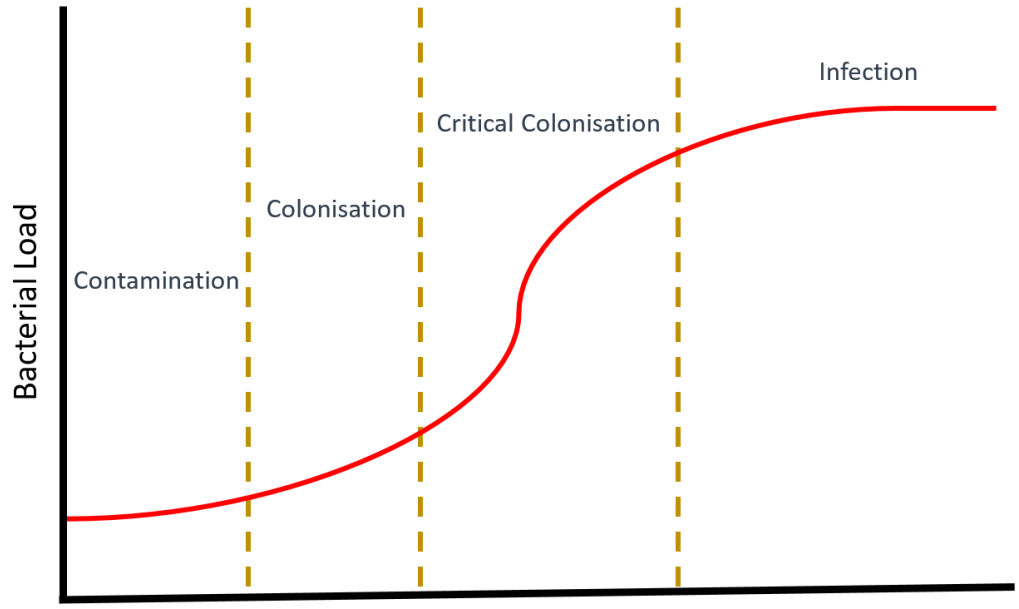

Figure 1.2 - Representation of the wound infection continuum.

General classification for wound infection is 10^4 CFU/gram of tissue in surgical site infections (SSIs), or CFU/cm^2 of wound in burns patients [30, 31]. Wound colonisation is commonly polymicrobial, causing further difficulties in management, a rise in treatment cost and increased trauma to the patient [32]. This is exacerbated by the inability to distinguish between pathogenic and non-pathogenic species in infected wounds, causing difficulties in identifying the etiological agent [33]. This has led to the argument that all species associated with microbial infection should be considered as potentially synergistic, rather than restrict thinking to the traditional view of a single species being causative [34].

There have been many studies identifying the bacterial species prevalent in various categories of acute and chronic wounds (Table 1.1). While etiological pathogens differ based on various factors including wound site, stage and type, it is generally accepted that facultatively anaerobic or aerobic organisms such as *Staphylococcus aureus* and *Escherichia coli* are more often implicated in the delayed healing of both acute and chronic wounds [35]. However, a common oversight in many reports is the inclusion of obligately anaerobic organisms, despite being reported to contribute significantly to bacterial populations [36]. This could be due to a combination of factors, including: anaerobes not generally being considered as detrimental to wound healing, the cost of isolation and culture of anaerobes when compared with aerobic bacteria, and difficulties in specimen collection and transportation [32]. Table 1.1 summarises from a small number of studies, the organisms responsible for colonisation of burns, SSIs, and diabetic foot ulcers.

Table 1.1 - Summary of a number of studies outlining the prevalence of bacterial species and genus' isolated from burn wounds, SSIs and Diabetic foot ulcers.

Study	Geographical Location	Wound Type	Bacterial Species	Prevalence
Agnihotri N *et al.* (2004) [37]	India	Burn	*P. aeruginosa*	59%
			S. aureus	17.9%
			Acinetobacter spp.	7.2%
			Klebsiella spp.	3.9%
			Enterobacter spp.	3.9%
			Proteus spp.	3.3%
Bayram Y *et al*. (2013) [38]	Turkey	Burn	*Acinetobacter baumannii*	23.6%
			Coagulase negative *Staphylococci*	13.6%
			P. aeruginosa	12%
			S. aureus	11.2%
			E. coli	10%
National Nosocomial Infections Surveillance System (NNIS) (1986-1996) [39]	Participating hospitals in the NNIS (USA)	SSI	*S. aureus*	20%
			Coagulase negative *Staphylococci*	14%
			Enterococcus spp.	12%
			E. coli	8%
			P. aeruginosa	8%
			Enterobacter spp.	7%
			K. pneumoniae	3%
			P. mirabilis	3%
			C. albicans	3%
Citron D *et al*. (2007) [40]	USA	Diabetic Foot Ulcer	*S.aureus*	34%
			Streptococcus spp.	15.5%
			Enterococcus spp.	13.5%
			Enterobacteriaceae	12.8%
			P. aeruginosa	3.5%
Benwan K *et al.* (2012) [41]	Kuwait	Diabetic Foot Ulcer	*Enterobacteriaceae*	28.5%
			P. aeruginosa	17.4%
			S. aureus	11.8%
			Methicillin resistant *S. aureus*	7.7%
			Anaerobic gram-negative organisms	10.8%
			Enterococcus spp.	7%

1.2 *Staphylococcus aureus*

Members of the *Staphylococcus* genus (from the Greek: *staphylē*, "grape" and *kókkos*, "granule") are Gram positive, catalase positive, cocci which generally proliferate in clusters due to the division along two axes. *Staphylococci* are typically between 0.5 - 1.5 μm in diameter, non-motile, facultative anaerobes, able to grow in relatively high salt concentrations and within a wide range of temperatures (18 - 40°C). The genus is formed of at least 40 species, a number of which are human pathogens including S*taphylococcus aureus*, *S. capitis*, *S. epidermidis* and *S. haemolyticus*.

S. aureus is a ubiquitous, commensal bacterium of the human microbiota which can often be found in the nostrils, skin, gastrointestinal tract and urinary tract. *S. aureus* is present in approximately 30% of the human population persistently or intermittently [42], without causing any symptoms. However, it is also a known pathogen of a number of diseases, including bacteraemia, pneumonia, meningitis and wound infections. Due to *S. aureus* being a component of the skin microbiota, it is easily spread from person to person via direct contact (skin to skin) or indirect contact (contact with contaminated objects). The latter presents difficulties in controlling spread within the healthcare setting and, as a consequence, *S. aureus* is also frequently responsible for nosocomial outbreaks and medical device-related infections [43].

1.2.1 Pathogenesis and virulence factors

S. aureus can express an array of structural components, toxins and enzymes which aid in the evasion of host defence mechanisms and onset of disease (Figure 1.3). Initial adherence of the pathogen to host tissue is achieved via microbial surface components-recognising adhesive matrix molecules (MSCRAMMs) expressed during exponential growth, including fibronectin-binding protein A (FnbpA). Another MSCRAMM is protein A, which causes binding to the Fc region of immunoglobulin G (IgG) antibodies in an incorrect orientation, with consequent suppression of the humoral immune response and evasion from phagocytosis [44]. The role of protein A in *S. aureus* pathogenesis has been clearly outlined in a number of animal studies, with one reporting that protein A deficient mutants were less virulent than the counterpart [45].

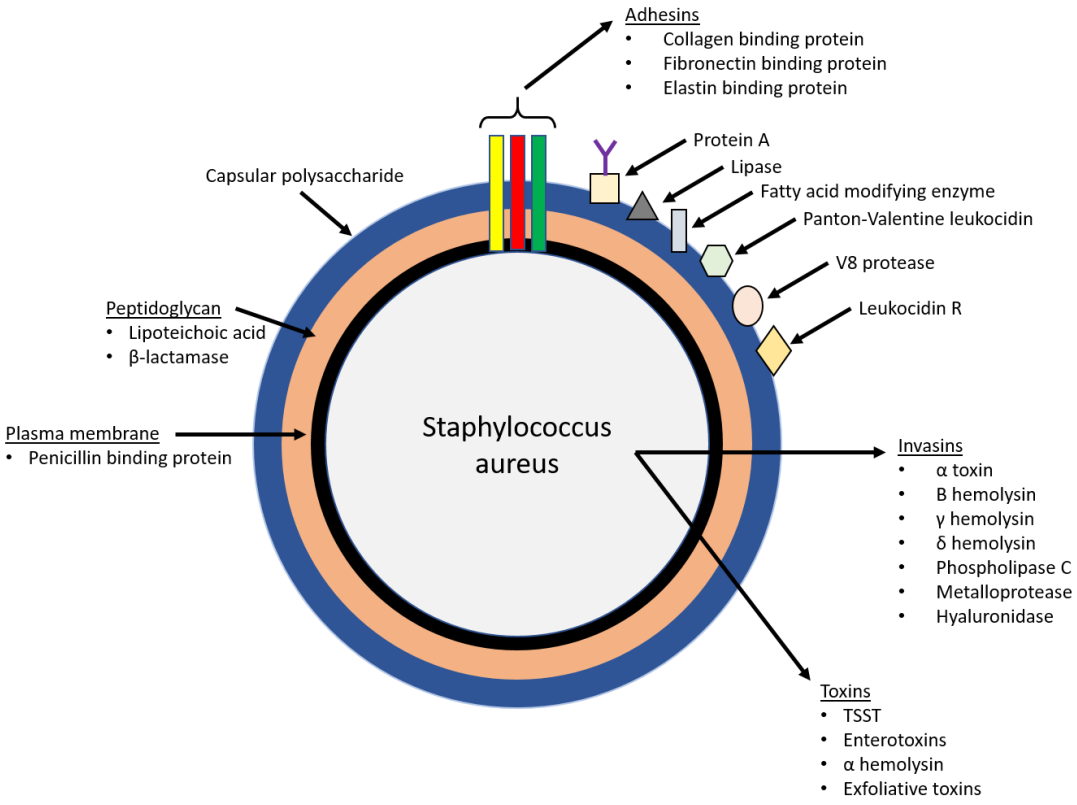

Figure 1.3 - A representation of virulence factors expressed by *S. aureus*.

1.2.1.1 Membrane damaging toxins

S. aureus produces numerous toxins which increase virulence, including cytolytic toxins, enterotoxins, exfoliative toxins and toxic shock syndrome toxin-1 (TSST-1). Cytolytic toxins include α, β, δ, γ toxins and Panton and Valentine leukocidin (PVL), of which α-toxin is the best characterised and most potent [46]. These toxins lyse the cytoplasmic membrane by forming a β-barrel pore across the lipid bi-layer, causing electrolyte imbalance, cell swelling and lysis [47].

1.2.1.2 Superantigen TSST-1

TSST-1 is one of >20 superantigens identified in *S. aureus* isolates, with approximately 60% of all clinical isolates expressing at least one [48]. This group of exotoxins cause non-specific activation of T lymphocytes and antigen presenting cells (APCs) by crosslinking Vβ regions (T-cell) with major histocompatibility complex (MHC) class II molecules (APC) resulting in a significant release of cytokines and chemokines [49]. Up to 30% of T-cells may be activated in this manner, with toxic shock syndrome (TSS) symptoms expressed as fever, rash, hypotension and multi-organ failure. TSST-1 is responsible for 90% of

menstrual TSS cases and approximately 50% of non-menstrual cases, primarily from SSIs and burns [50].

1.2.1.3 Enzymes

S. aureus secretes an array of extracellular enzymes including lipases, nucleases, hyaluronidase, staphylokinase and proteases which can manipulate host defence mechanisms and disrupt host cells [51]. Coagulase is produced by all strains of *S. aureus*, allowing the conversion of fibrinogen to fibrin which can encapsulate the bacterial cell which allows evasion from phagocytosis. Staphylokinase converts plasminogen to plasmin, which degrades fibrin clots allowing the spread of infection and penetration through the skin barrier. While definitely an undesirable factor, conversely staphylokinases have also been reported to reduce skin infection severity by opening abscesses and allowing drainage in an animal model [52].

1.3 *Escherichia coli*

Members of the *Escherichia* genus are Gram negative, facultatively anaerobic bacilli belonging to the family Enterobacteriaceae. *Escherichia spp.* are generally between 1.0 - 1.5 µm in diameter and 2.0 - 6.0 µm in length. Unlike *Staphylococcus spp.* some possess peritrichous flagella to allow motility, with most strains also expressing fimbriae allowing for specific functions (e.g. adhesion). Many *Escherichia spp.* are commensal bacteria of the gut microbiota, but are also acknowledged as being significant human pathogens, most notably *E. coli*.

E. coli is a common inhabitant of the lower intestine and colonisation by non-pathogenic serotypes can benefit the host by producing vitamin K [53] and inhibiting gut colonisation by pathogenic bacteria [54]. While commonly associated with gastroenteritis and urinary tract infections, *E. coli* has also been implicated as a causative agent of wound infections including SSIs [55] and burns [56]. Often studies investigating the prevalence of bacterial species isolated from wounds name *S. aureus* and *P. aeruginosa* as most commonly isolated (Table 1.1). However, *E. coli* is also shown to be an important causative agent of chronic wound infections, with a study spanning 7 years and covering 3 continents, naming *E. coli* as the third most prevalent species, only dominated by *S. aureus* and *P. aeruginosa* [57]. Despite this, *E. coli* strains isolated from wound infections remain largely uncharacterised, with only a small number of studies determining the virulence and antibiotic susceptibility profiles of pathogenic *E. coli* isolates from surgical and traumatic wounds, foot ulcers, and pressure sores [58].

1.3.1 Pathogenesis and virulence factors

While virulence factors relating to extra-intestinal pathogenic *E. coli* (ExPEC) remain largely unknown, a study conducted by Petkovšek *et al.* (2009) [58] defined the virulence profiles of 102 pathogenic *E. coli* isolated from foot ulcers and surgical/traumatic wounds. They found that the most prevalent virulence factor was ompT (80%), followed by CNF1 (32%) and hlyA (30%). It has also been suggested that ExPEC belong to the same serogroups and share similar virulence factors to *E. coli* isolates from urinary tract infections and bacteria, and can exhibit a remarkable and comparable virulence potential [58].

1.3.1.1 Outer membrane proteins (ompT)

Outer membrane protein T (ompT) is a member of the omptin protease family, located on the outer membrane of *E. coli* and some other Gram-negative species. OmpT serves to

degrade foreign peptide material encountered in its surrounding environment. Degradation of cationic antimicrobial peptides secreted during the innate immune response allows colonisation and enhanced risk of infection [59, 60].

1.3.1.2 Cytotoxic necrotising factor (CNF1)

Cytotoxic necrotising factor 1 (CNF1) is commonly expressed in *E. coli* strains causing uropathogenic and neonatal meningitis, and is a protein toxin which acts by interfering with the host cell cytoskeleton organisation, flattening the cell body and causing it to acquire a multinucleated phenotype [61].

1.3.1.3 Haemolysin A

Haemolysins are primarily proteinaceous compounds which lyse red blood cells by disruption of the cell membrane. Haemolysin A (hlyA) is a common exotoxin, facilitating membrane lysis by enzymatic cleavage and formation of transmembrane pores of the phospholipid bilayer [62]. In addition to causing damage to erythrocytes, hlyA has also been demonstrated to be toxic to a wide variety of cells including monocytes [63], granulocytes [64], neutrophils [65] and endothelial cells [66].

Other virulence factors of ExPEC include Dr adhesins, K antigen and fimbriae; these are beyond the scope of this study. Further investigation into wound isolates would be prudent to identify specific virulence mechanisms, considering the high prevalence of *E. coli* in wound infections.

1.4 Antibiotic resistance

Antimicrobial resistance can be defined as the innate or acquired mechanisms that confer decreased or complete lack of susceptibility to antibiotic exposure [67]. The spread of antibiotic resistance has been fuelled by the inappropriate use of antibiotics, lack of patient compliance, and environmental pollution from antibiotic over-use for livestock prophylaxis and as pesticide, a particular consequence has been the presence of sub-inhibitory concentrations which serve to enrich and maintain resistant populations [68]. Organisms can become resistant to multiple antibiotics, possessing and sharing mechanisms which render an array of antimicrobial drugs ineffective. There are numerous mechanisms of antibiotic resistance including: inactivation or modification via drug altering enzymes, alteration of the target site which decreases binding capability, bypass of the targeted metabolic pathway, overproduction of the antimicrobial target, active efflux, and reduced uptake [69]. Antibiotic resistance has been frequently associated with the formation of bacterial biofilms, with documented antibiotic tolerances of up to 1,000 fold higher in biofilm residing bacteria than their planktonic counterpart [70].

1.4.1 Methicillin-resistant *S. aureus* (MRSA)

MRSA is a significant contributor to the elevated morbidity, mortality and healthcare costs associated with antibiotic resistance and is a prevalent pathogenic bacterium of both acute and chronic wounds [71-73]. It has been reported that in 2005 there were approximately 94,000 invasive MRSA infections in the USA, resulting in over 18,000 deaths [74]. MRSA incidence has increased dramatically over the past 10 years and MRSA-skin and soft tissue infection-related discharges tripled from 2004 to 2011 [75]. Commonly associated with the healthcare and community setting, MRSA is presenting a world-wide threat to public health.

Methicillin is a narrow spectrum β-lactam antibiotic of the penicillin class of antibiotics. Less than a year after the discovery of penicillin by Alexander Fleming in 1929 it was recognised that *S. aureus* were able to mutate and become resistant, later becoming resistant to other antibiotics [76]. By the 1950s epidemics of penicillin resistance were being reported and by the 1960s penicillin resistance was considered as pandemic [76]. Methicillin was introduced in 1959 however resistance was reported a year later, spreading worldwide with further reports of MRSA becoming resistant to and array of antibiotics. The acronym MRSA is now used as a blanket term for identifying *S. aureus* strains resistant to β-lactam antibiotics.

β-lactam antibiotics act by competitively inhibiting bacterial cell wall synthesis, entering the periplasmic space through bacterial porins and binding to the transpeptidase enzyme (or penicillin-binding proteins (PBPs)) ordinarily required for the crosslinking of peptidoglycan. Resistance arises due to the production of PBP2a, a modified PBP upregulated by mutations in the regulatory genes that is resistant to the action of methicillin at therapeutic levels. PBP2a is a 76kDa protein encoded by the *mecA* gene, a component of the larger *mec* element or staphylococcal cassette chromosome (SSC) [77]. Upstream of *mecA* are *mecR1*and *mecI*, the regulatory genes of PBP2a, responsible for the methicillin-resistant phenotype and production of PBP2a [78].

1.4.2 Multi-drug resistant *E. coli*

While multi-drug resistant *P. aeruginosa* has arguably been the best known therapeutic challenge amongst Gram-negative bacteria, the focus has now extended to members of the Enterobacteriaceae family, including *Klebsiella*, *E. coli* and *Enterobacter* [79]. The prevalence of multi-drug resistant *E. coli* has increased significantly over recent years and with the lack of newly developed Gram-negative antimicrobial agents these infections are causing an emerging threat to public health.

Carbapenem-resistant *Enterobacteriaceae* (CRE) can be defined as bacteria which show resistance to the carbapenem and extended-spectrum cephalosporin classes of antibiotics. As members of the β-lactam family of antibiotics the mechanism of action of antibacterial activity in *E. coli* is identical to that of MRSA, however the mechanism of bacterial resistance differs somewhat. Several mechanisms exist for resistance in CRE, including active efflux [80], mutation or loss of porins reducing antibiotic intake [81] and secretion of carbapenemases [82].

Carbapenemases belong to a family of β-lactamases capable of hydrolysing penicillins, cephalosporins, monobactams and carbapenems [83]. Class B carbapenemases are metallo-β-lactamases containing zinc at the active site. While this class of enzyme has high prevalence in *P. aeruginosa* isolates, there are increasing reports of expression in the *Enterobacteriaceae* [83-85].

1.4.3 Biofilm formation

Biofilm formation follows three discrete yet complex stages, typically remaining consistent regardless of circumstances, site and organisms present [86]. These stages are as follows: initial attachment of planktonic bacteria to a surface (abiotic or biotic), followed by exopolysaccharide (EPS) production and the formation of microcolonies, and finally maturation and dissemination of microbes from the biofilm (Figure 1.4). Bacterial adhesion in *E. coli* is facilitated by both preformed adhesins such as flagellum and pili, and conditionally synthesised adhesins such as the exopolysaccharide *E. coli* PGA (poly-β-1,6-*N*-acetyl-d-glucosamine) which allows for temporary to permanent attachment transition [87] while *S. aureus* attaches by hydrophobic interactions or MSCRAMMs [88]. Bacteria may attach as a monolayer or multilayer, with the former exclusively adhering to the surface, and the latter adhering to both the surface and neighbouring bacterial cells [89]. Flagella have been reported to promote surface adhesion of motile planktonic bacteria, with flagellar impedance resulting in the absence of both multilayer and monolayer biofilm formation [90]. Pili have also been implicated in Gram-negative bacterial biofilm attachment, with this structural component allowing motility along the surface via attachment and retraction [91]. Following this transient attachment, stable and specific attachment is achieved via proteinaceous appendages which allow for adhesion to other bacterial cells and eukaryotic cells [89]. Bacterial cell-cell adhesion is mediated by appendages such as curli fimbriae and biofilm associated proteins, encoded by *csgBAC* and *Bap* loci, respectively [89, 92] in *E. coli* and MSCRAMMs in *S. aureus* [88].

Once attached, bacterial cells are encapsulated by a highly hydrated (<97 % water) biofilm matrix, composed of polysaccharides, proteins, DNA, lipids, glycolipids, membrane vesicles and ions [89]. The bacterial exopolysaccharide is the predominant component of biofilm matrices, with cellulose, PGA, and colonic acid often implicated in *E. coli* biofilm formation and poly-N-acetylglucosamine (PNAG) in *S. aureus* biofilms [93]. Distinct genetic loci encode for the synthesis of these polysaccharide components, with *bcsABZC-bcsEFG* [94], *pgaABCS* [95], and *wca* [95] implicated in *E. coli* cellulose, PGA and colonic acid synthesis, respectively, while the *ica* locus is implicated in the production of *S. aureus* PNAG exopolysaccharide [96]. Genetic mutants defective in the synthesis of these matrix components were unable to form multilayer biofilms [89].

Gene expression for biofilm formation is moderated via quorum sensing, a chemical mediator and autoinducer-dependant crosstalk mechanism operating between bacterial cells. Once a threshold has been met, the accumulation of secreted chemical mediators in the biofilm matrix results in the activation of quorum sensing which allows co-ordination of gene expression, which in Gram-negative bacteria such as *E. coli* is often facilitated via the

LuxI/LuxR system [97]. In this process, autoinducers are synthesised via LuxI proteins which initiate LuxR, activating and moderating gene expression [89].

It should be noted that biofilm formation is highly dynamic and in the presence of unfavourable environmental conditions adherent bacteria may return to a planktonic state resulting in biofilm dispersal. While this could be seen as a desirable trait, with many avenues of pharmaceutical biofilm reduction targeting matrix disruption in order to trigger biofilm dispersion, secondary infections may result due to the release of bacterial cells and further biofilm establishment in an alternative niche.

Biofilms have been associated with low sensitivity to antibiotics as a result of poor penetration of antibiotics across the exopolysaccharide layer, inhibition via altered pH, altered osmotic environment which decreases bacterial permeability, and a dormant state which can be comparable to bacterial spore formation [98]. Furthermore horizontal gene transfer (HGT) allows for the spread of antibiotic resistance genes under stressed conditions such as exposure to low antibiotic levels, resulting in a biofilm reservoir for transferable antimicrobial resistance [99]. HGT comprises of three mechanisms of resistance transfer: transduction, transformation, and conjugation. In brief, transduction utilises bacteriophage in the transfer of bacterial genes, transformation occurs via the uptake of environmental genomic material, and conjugation via plasmid transfer mediated by bacterial pili. Once acquired, the genes conferring antimicrobial resistance may be integrated into the bacterial chromosome by recombination or transposition, allowing expression of resistant traits.

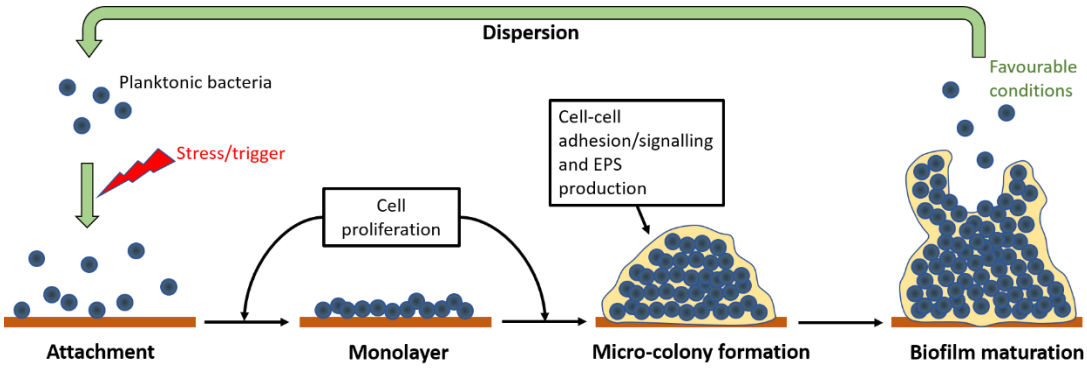

Figure 1.4 - A representation of the stages of biofilm formation.

1.5 Bacteriophage

1.5.1 Discovery

Bacteriophage are obligate intracellular viruses which only infect and replicate within bacteria. With cell lysis occurring due to the release of virion progeny, bacteriophage have been of considerable interest in the search for a novel antimicrobial approach. Recognised as one of most abundant entities on earth [100], bacteriophage research boasts a rich and notable past, perhaps first unfolding in 1896 when Ernest Hankin described a component of river water taken from sources in India which had antibacterial properties against *Vibrio cholerae*, although their actual discovery was made independently by Fredrick Twort in 1915 and Felix d'Herelle in 1917. With the development of conventional antibiotics in the 1940s and unreliable results from early trials, the potential for bacteriophage in the treatment of infection was promptly pushed aside in the West, however research continued in Eastern Europe and the former Soviet Union, initially in part due to the lack of access to antibiotics. The collapse of the Soviet Union in 1989 lead to the unrestrained distribution of much Soviet research, including supporting evidence of bacteriophage therapy, precipitating the interest of western researchers just as the antibiotic resistance crisis was in its infancy.

1.5.2 Classification and ecology

Generally, bacteriophage can be found wherever bacteria are present, in water, soil, human and animal skin, faeces, digestive tract and our food. It has been reported that approximately 10^8 viable phage can be isolated per gram of fresh or processed meat [101], 10^{10} per litre of surface seawater [102] and 10^8 per gram of topsoil [103]. Bacteriophage have been identified as the most abundant and ubiquitous microorganisms on earth, estimated to be in the order of 10^{32} existing in the biosphere [104]. It has also been estimated that around 10^{23} bacteriophage infections of bacteria occur every second [105], destroying half of the world's bacterial population every 48 hours [106].

Bacteriophage are classified according to the International Committee for Taxonomy of Viruses (ICTV) based on a number of characteristics, such as nucleic acid composition and morphology. Their genomes can be ssRNA, ssDNA, dsRNA or dsDNA and exhibit a vast range of shapes, sizes and structures. Under the current bacteriophage classification order, *Caudovirales* are the largest group and are characterised by dsDNA genomes (18 kbp to 500 kbp in length), icosahedral head, and flexible tail [107]. It has been estimated that 96% of the all bacteriophage belong to the *Caudovirales* order which is composed of three families:

Myoviridae (contractile tail), *Podoviridae* (short non-contractile tail), and *Siphoviridae* (long non-contractile tail) [108].

1.5.3 Bacteriophage life cycle

The life cycle of bacteriophage begins with two common stages, adsorption and injection of genetic material; this then culminates in the initiation of either the lytic or lysogenic life cycle (Figure 1.5). Since bacteriophage are non-motile, they rely on random encounters with host bacteria to initiate the first stage of infection. Once an encounter occurs, both lytic and lysogenic bacteriophage adsorb to the bacterial cell by the association of tail fibres (or other equivalent structures in non-tailed bacteriophage) with specific bacterial surface receptors. The bacterial surface receptor sites are diverse and vary by species and strain, causing the high specificity of bacteriophage infection. However, bacterial receptor sites are not specifically designed to enable bacteriophage infection, rather they are essential components of the bacterial membrane such as lipopolysaccharides (LPS), pili and surface proteins. Once bacteriophage absorption has occurred, injection of genomic material into the bacterial cytoplasm follows. In the case of the *Myoviridae*, this occurs by contraction of the tail fibres, drawing the base plate towards the bacterial cell and penetration of a needle-like complex which injects the bacterial genome in a syringe-like motion. At this point, dependant on whether the bacteriophage is lytic or lysogenic (temperate), the bacteriophage life cycle will follow one of two courses.

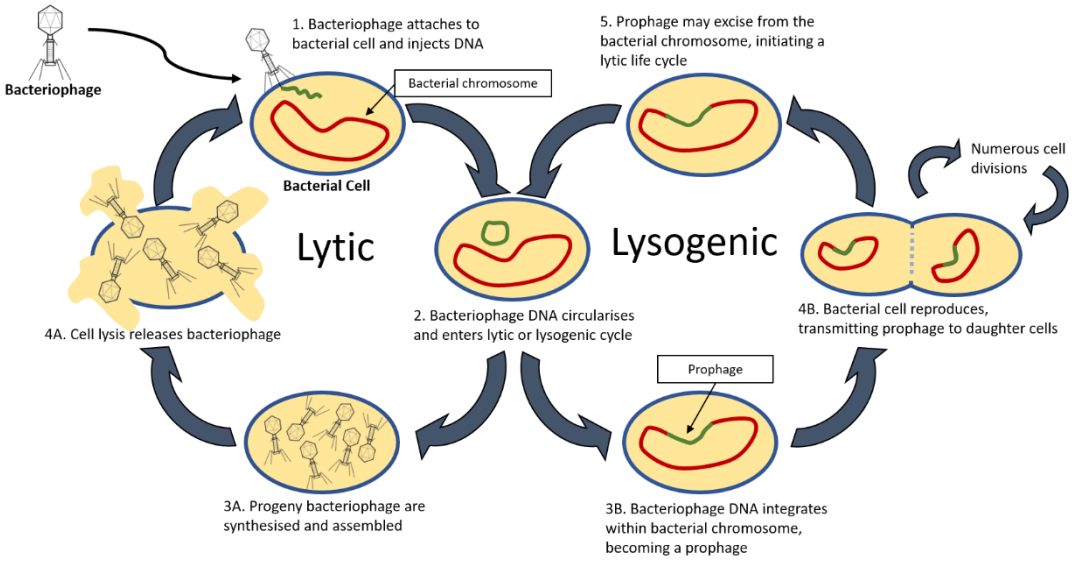

Figure 1.5 - A representation of the stages of the lytic and lysogenic bacteriophage life cycles.

1.5.3.1 Lytic life cycle

If the bacteriophage is lytic, then following absorption and injection the bacteriophage genomic material will hijack the host cell's reproductive machinery to produce virion progeny. In the case of DNA viruses, the nucleic acid is transcribed into mRNA utilising the host RNA polymerases, culminating in preferential production of bacteriophage products. Bacteriophage assembly follows, with head capsids (constructed separately) spontaneously assembling with tail portions. Once virion progeny have assembled, bacteriophage are released from the bacterial cell by membrane lysis. This process is initiated by small bacteriophage produced proteins called holins which form pores in the cell membrane, allowing lytic enzymes (lysins) to degrade bacterial peptidoglycan [109] thereby releasing hundreds of virion progeny to initiate subsequent cycles of bacteriophage infection.

1.5.3.2 Lysogenic life cycle

Lysogenic bacteriophage follow the same aforementioned initial stages, however once the nucleic acid has been deposited within the bacterial cell it integrates within the bacterial genome, resulting in the formation of prophage. Prophage reside in a dormant state in the bacterial cell for an undefined period, being transmitted to each bacterial daughter cell during division, but without initiating bacteriophage replication and bacterial lysis. However, upon induction, caused by events which cause host cell damage, the prophage is excised from the bacterial genome retaining the ability to initiate the lytic life cycle.

1.5.4 Bacteriophage as a novel antimicrobial

As previously mentioned, the potential for bacteriophage to be used as antimicrobial agents is largely associated with the use of lytic bacteriophage, due to the efficient reduction of bacterial cell numbers through cell lysis; ideally this reduction is of such magnitude that it leads to complete eradication or to a level in which the immune system is able to eliminate any remaining pathogens. As research into the use of bacteriophage as an antibacterial agent has developed, a number of prerequisites have been identified as necessary for the production of therapeutic bacteriophage preparations:

- Bacterial eradication or reduction to a level at which the immune system is able to successful eliminate any survivors.
- Compliance with safety requirements: all bacteriophage preparations should be of high purity, free from bacterial components and associated toxins.

- Thorough understanding of bacteriophage specific biology and bacteriophage-host interaction.
- Assessment of storage conditions, ensuring the bacteriophage preparation contains and remains at a known titre for a defined period.
- Knowledge of bacteriophage-host resistance profile.
- Bacteriophage preparations should be tested in animal models to assess bacteriophage efficacy *in vivo*.
- No transduction rates and no genetic evidence of temperate or lysogenic life cycles.
- Biofilm degrading capabilities desirable.

While the above prerequisites may be assessed and met, many regulatory guidelines are yet to be defined causing delays in the efficient and successful progression of bacteriophage therapy research into clinical use. Despite this, there is now an abundance of *in vitro* and *in vivo* (using an array of administration routes) studies demonstrating the efficacy of bacteriophage therapy against a host of clinically relevant bacteria. While comprehensive investigations of topical bacteriophage administration in animal models and human subjects are somewhat lacking, a number of studies have shown promise for this application [110-115]. These studies report efficacy in the treatment of wound infections, intransigent diabetic foot ulcers, endocarditis and chronic otitis. Pulmonary delivery of bacteriophage in animal models and *in vitro* studies has been reported in a number of papers, using various administration methods including nebulisation [116, 117], intraperitoneal injection [118, 119], and intranasal delivery [120-122]. Oral delivery perhaps presents one of the more significant challenges in bacteriophage therapy, due to the extreme conditions to which bacteriophage are exposed in the gastrointestinal tract. A number of studies have utilised bacteriophage encapsulation systems [123-125], and antacids such as calcium carbonate [125-129] to prevent bacteriophage inactivation. With the exception of bacterial infections localised to external extremities, such as chronic wounds, parenteral bacteriophage delivery has proved one of the most popular methods of administration for *in vivo* animal models [122, 130-136]. A considerable advantage of this administration method over oral administration, is the rapid delivery of bacteriophage to the systemic circulation, bypassing deleterious conditions associated with the gastrointestinal tract.

In 2009, Wright *et al* conducted the first regulated, double blind, placebo controlled, randomised phase I/II trial of bacteriophage therapy in the treatment of chronic otitis caused by antibiotic resistant *P. aeruginosa* [114]. 24 participants were selected for this study, all having had chronic otitis for a duration of several years, with an antibiotic resistant strain of *P. aeruginosa* sensitive to a test bacteriophage, Biophage-PA. Upon treatment, it was found

that clinical indicators for the bacteriophage treated group improved relative to the placebo group, with *P. aeruginosa* counts significantly lower, and no adverse events reported. This study provided a solid grounding to the efficacy and safety of bacteriophage use as a novel antimicrobial in human subjects. In addition to bacteriophage preparations entering early stage clinical trials in the West, there are a growing number of commercial bacteriophage companies entering the market, showing a desire for this therapy to be an integral component of modern medicine.

1.5.4.1 Advantages and considerations

Bacteriophage are known to possess many desirable characteristics when compared with traditional antibiotics, the most notable of which have been presented in the table below (Table 1.2). Bacteriophage are highly specific and tend to only recognise and infect a specific strain of bacteria. This could be highly advantageous in reducing damage to the normal microbiota, which can cause dysbiosis when broad-spectrum antibiotics are used. However, this can also be a limiting factor, as unless the specific strain of bacterium is known on an individual case-by-case basis, failure of therapy may occur. This factor has been experimentally overcome by the use of bacteriophage 'cocktails', numerous bacteriophage specific to an array of bacterial species and strains, however this could counteract the potential advantage of reduced damage to the normal microbiota and may need to be adapted on an individual basis. It has also been reported that bacteriophage can elicit a strong antibody response at high concentrations, associated with endotoxin release, and therefore their extended use is ill advised [137]. Bacteriophage replication at the site of bacterial infection is an important advantage, as it could reduce side effects associated with antibiotic use, while biofilm degradation may aid in the eradication of persistent infections, such as chronic *P. aeruginosa* colonisation seen in patients with cystic fibrosis [138]. The main focus of bacteriophage therapy is no longer exclusively on whole virion particles, with many studies now investigating the efficacy of isolated bacteriophage depolymerases and lysins on biofilm permeability and bacterial lysis, respectively [139, 140]. Due to bacteriophage only replicating in the presence of the target bacteria, it could be considered that 'auto-dosing' occurs, with bacteriophage numbers increasing upon administration, then reducing once the infection has subsided. It has also been reported that bacteriophage have a low resistance potential, evolving with the spontaneous and acquired bacterial mutations [141]. While studies have provided evidence of bacterial resistance to bacteriophage infection [142], bacteriophage reportedly maintain the ability to co-evolve with host bacteria. Additionally, with the vast number of bacteriophage active against a specific bacterium this factor may be easily overcome. It has been reported that bacteriophage can

carry and express enzymes [143-145], or activate enzymes within the host genome [146] which degrade the extracellular matrix of biofilms and promote diffusion of the viral particles. Isolation and purification of such enzymes may present further novel therapeutics to combat persistent bacterial infections.

Table 1.2 - Presenting the advantages and considerations of bacteriophage as a novel antimicrobial in comparison to antibiotics.

Characteristic	Bacteriophage	Antibiotics	Comments
Specificity	Strain/Species	Non-specific	Bacteriophage are highly specific which reduces damage to the normal flora. A common side effect of antibiotic use is dysbiosis, caused by the eradication of commensal bacteria.
Replication at infection site/auto-dosing	Replicate at site of infection	Do not concentrate at infection site	Bacteriophage replicate exponentially at the site of infection, reducing the need for frequent administration. Antibiotics are metabolised and eliminated from the body, reducing concentrations at the target site.
Side effects	Limited side effects	Many side effects	Minor side effects of bacteriophage therapeutics due to liberation of bacterial toxins, a phenomenon also observed with antibiotics. Multiple side effects for antibiotic use including digestive disorders, allergies and secondary infections.
Resistance	Possible	Widespread	While bacteriophage resistance is possible, - resistant bacteria remain susceptible to alternative bacteriophage. Antibiotic resistance is commonly seen and not limited to target bacteria.
Discovery	Rapid and cost effective	Time consuming and expensive	Identifying new bacteriophage involves rapid techniques, taking only days or weeks. Antibiotic development can take years and is extremely expensive. It can also be argued that for every antibiotic or bacteriophage resistant bacterium, there are bacteriophage capable of infection.
Development and manufacture	Standardised procedures and regulatory pathways have yet to fully emerge	Established procedures	As more products reach clinical trial and licensing stages the manufacturing and quality assurance processes will become more established

Safety concerns may arise from bacteriophage/bacterium interaction due to liberation of bacterial toxins, causing the potential for harmful side-effects. Bacteriophage have been shown to interact with non-infected tissues, with some being absorbed into the blood via specific epithelial interactions, however it has been reported that these factors do not result in side-effects [147]. Immunological analysis of bacteriophage interactions have provided similar safety characteristics, with one explanation being the high exposure of humans to bacteriophage over the course of evolution [147]. One concern, however, is the ability of some bacteriophage to modify bacteria causing them to express increased virulence through HGT.

This is especially concerning when isolating bacteriophage which may be lysogenic, which do not 'kill' the bacterium, but could convey lysogenic resistance to the infecting bacteriophage, modification of the bacterial phenotype, and even increase resistance via transduction in the absence of bacterial lysis [147]. These bacteriophage should therefore not be considered for use in bacteriophage therapy. Another consideration is the lack of efficacy in bacteriophage treatment of intracellular infections such as that seen in *Chlamydia trachomatis* and some uropathogenic *E. coli* infections, due to the inability of bacteriophage to recognise and infect the bacterium within the human cell. Finally, the release of bacterial toxins from lysed cells, such as Gram-negative outer membrane proteins and LPS, should be considered to avoid secondary illness.

1.5.5 Prospective bacteriophage for this study

1.5.5.1 Bacteriophage T4

Bacteriophage T4 is a complex lytic virus, belonging to the *Myoviridae* family, comprising of over 40 proteins and consisting of a protein shell, 172 kbp dsDNA genome, contractile tail and tail fibres [148]. *E. coli* serves as the permissible host. The tail fibres allow for host cell recognition and are implicated in the high strain specificity associated with bacteriophage infection [149]. The tail allows for DNA delivery into the bacterial cell, packaged via the dodecameric portal protein within the portal vertex of the bacteriophage head [149]. Bacteriophage T4 is an obligate lytic bacteriophage, with initial adsorption occurring via OmpC and R-type LPS interactions with T4 long tail fibres, triggering permanent attachment via six short tail fibres with a heptose moiety within the LPS [150]. The bacteriophage tail then penetrates the bacterial outer membrane due to baseplate conformational change, followed by lysozyme mediated degradation of the peptidoglycan

layer and transfer of genetic material into the bacterial cytoplasm [151]. Lysozyme is a component of the base plate protein gp5, located at the penetrating end of the bacteriophage tail [150]. DNA replication, translation and assembly of virion progeny follows, resulting in bacterial cell lysis and release of virion progeny into the external environment.

Bacteriophage T4 has been documented to possess desirable characteristics in the treatment of *E. coli* infections, such as the penetration of biofilm matrices. Doolittle *et al*. (1995) reported that *E. coli* biofilm extracellular matrix was not a sufficient barrier to bacteriophage T4 infection and that the infected cells were present within the biofilm formed on the surface of polyvinylchloride [152]. This early observation was reportedly the first of its kind, with previous studies suggesting that bacteriophage could not infect and multiply within cells growing as a biofilm. Further research within this field has now discovered that bacteriophage can possess polysaccharide degrading enzymes which serve to break down the exopolymeric matrix allowing diffusion into the biofilm [145, 153, 154].

1.5.5.2 Bacteriophage T3

Bacteriophage T3 is a member of the *Podoviridae* family of *Caudovirales* and is closely related to bacteriophage T7 in structure [155]. *E. coli* serves as the permissible host, however it has been reported that the host range includes certain strains of *Shigella sonnei* [156], *Klebsiella pneumoniae* [157], and *Salmonella typhimurium* [158]. The virion structure consists of an icosahedral head of approximately 50 nm diameter, attached to a non-contractile tail of 20 nm length. Bacteriophage T3 has a dsDNA genome of approximately 40 kbp [159]. As research into the use of bacteriophage as a novel antimicrobial has progressed, recent reports have used bacteriophage T3 in nanoencapsulation systems [160], as antibiofilm agents [161], and novel drug delivery vehicles [162].

1.5.5.3 Bacteriophage K

Bacteriophage K is a member of the *Myoviridae* family and possesses the ability to infect both coagulase-positive and coagulase-negative staphylococci [163]. Early genome sequencing has revealed a linear DNA genome of 127-kbp, encoding modules for lysins, structural components, DNA replication and transcription [164]. However, a recent study conducted by Gill *et al* (2014) presented a revised sequence including 12-kbp of additional sequence omitted from the genome described previously [165]. It has been documented that this bacteriophage utilises *N*-acetylglucosamine in teichoic acid of the bacterial cell wall to facilitate adsorption [166]. Interestingly, genome analysis has also revealed that

bacteriophage K is morphologically identical to bacteriophage Au2 [167] and indistinguishable from the polyvalent bacteriophage phi 812 [168]. The morphology of bacteriophage K has been determined by transmission electron microscopy and reported to comprise an icosahedral head of approximately 70 nm diameter, attached to a long, thin (210 nm x 15 nm) contractile tail, terminating in a complex basal appendage [169].

As with phage T4, staphylococcal bacteriophage K has been extensively investigated for use in human therapy [170-173]; with studies suggesting lytic ability against clinically isolated MRSA, vancomycin-resistant *S. aureus* (VRSA) and teicoplanin-resistant strains [170].

1.5.5.4 Bacteriophage 44AHJD

S. aureus bacteriophage, 44AHJD, is a member of the *Podoviridae* family and is composed of an icosahedral head of 75 nm, with a short non-flexible and non-contractile tail of approximately 27 nm in length, and has a genome length of 16,784 bp [174]. While literature describing the potential use of bacteriophage 44AHJD in the therapeutic treatment of bacterial infections in lacking, this species has been reported to be particularly virulent in nature and may therefore be a suitable candidate for bacteriophage therapy [175].

1.6 Polymeric wound dressings

Prior to the 19th century wound management and dressing products were surrounded by myth and superstition, with materials ranging from cobwebs to animal fat in use [176]. However, towards the end of the 19th century Sir Joseph Lister, the British pioneer of antiseptic surgery, demonstrated the role of aseptic practice and good quality wound dressings in the prevention of sepsis [176]. From this point, until the 1960s, the prerequisites for wound dressings were to provide a clean, dry environment for wound healing by fulfilling the following criteria [177]:

- High moisture vapour and oxygen permeability
- Absorbent
- Act as a barrier to bacteria and external contaminants
- Flexible and strong
- Biocompatible
- Sterile
- Low cost

While the concept of 'dry wound healing' has largely remained unaltered and is still in practice today, modern wound care has shifted towards wound dressings which provide a balanced moisture environment while performing specific functions based on the type of injury, presence of infection, and other parameters which define a specific type of wound [178]. While occlusive dressings such as films, foams and hydrocolloids have been reported to favour bacterial proliferation in the wound bed [179], this proliferation is reported as lower than that of traditional dry dressings [180]. In providing predefined moisture vapour transmission rates, advanced wound dressings manage wound exudates, preventing tissue maceration and irritation by gaseous exchange while remaining an effective barrier to bacterial contamination.

1.6.1 Polymers

Wound dressings comprise of a group of materials including films, foams, gels, composites and sprays. Many emerging dressings are based on natural or synthetic polymers, used independently or in composite with other materials. Polymers can be defined as multiple assemblies of simple structural units which are able to form 3-dimensional constructs [181]. There are a vast array of available polymers, holding the ability for tuneable physical, chemical and biological properties thus allowing formulations to be optimised for very

specific applications [181]. This current research study focuses on the use of the natural polymers, agarose and alginate, and the synthetic polymer poly(vinyl amine).

1.6.1.1 Agarose hydrogels and dehydrated films

With intrinsic biocompatibility, biodegradability and remarkable similarity to the extracellular matrix (ECM), natural polymers are widely used in the management of wound infections. Natural base materials include polysaccharides, heteroglycans, proteins and peptides.

Of the polysaccharide natural polymers, agarose has shown promise in wound dressing applications although this polymer has yet to be used in the clinical setting as a lone matrix [182]. Agarose is a linear polymer comprising repeating units of a D-galactose and 3,6-anydro-L-galactopyranose disaccharide linked by α-(1→3) and β-(1→4) glycosidic bonds (Figure 1.6). Agarose is a natural polymer derived from marine algae and is abundantly available. It has also been reported that agarose is highly biocompatible (not harmful or toxic to living tissue) [183-186], increasing its desirability as a wound dressing base material.

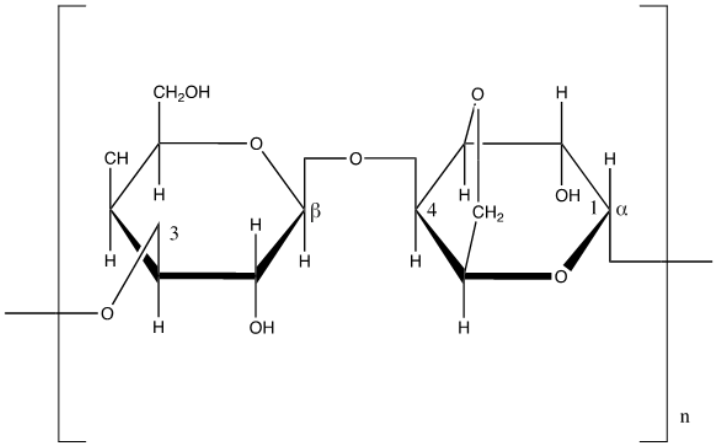

Figure 1.6 - Chemical structure of an agarose subunit.

Individual agarose chains form helical fibres containing in the region of 800 galactose molecules. Upon exposure to solvent, these fibres aggregate to form supercoiled structures with a radius of 20-30nm [187]. Agarose, available commercially in powder form, dissolves in boiling water and forms a gel when cooled. This gel is formed by the helical fibres forming a 3-dimensional matrix supported by hydrogen bonding with pore size a function of

agarose concentration. Upon dehydration of agarose gels, the agarose network contracts forming a strong but brittle film.

While agarose hydrogels provide potential as wound dressing materials due to their porous structure and potential to release compounds into the external environment, in this form the gel strength is not sufficient for the application. In contrast, dehydrated agarose films are strong but lose flexibility due to the contraction of the agarose network. With strength and flexibility are important factors in the development of novel wound dressings, neither agarose gels nor agarose films alone would suffice for this application. These properties can, however, be achieved with the addition of certain plasticising additives which increase free volume between polymer units.

1.6.1.2 Plasticisers

The International Union of Pure and Applied Chemistry (IUPAC) provide a definition of plasticers as "a substance or material incorporated into a material to increase flexibility, workability and distensibility". Plasticisers often exhibit their effect by increasing free volume between polymer units [188] and comprise an array of low molecular weight, non-volatile compounds used extensively in polymer industries [189]. At present, the worldwide production of plasticisers is approximately 5 million tons per year, being applied to around 60 polymers and over 30 groups of products [190]. Over recent years there has been safety concerns commonly relating to the migration of phthalate and synthetic plasticisers leading to an increasing interest in low toxicity, often naturally-based alternatives. Selection of plasticisers for specific applications is generally determined not only by toxicity, but also plasticiser-polymer compatibility, desired properties of the end product (thermal, electrical and mechanical), permanence and cost[189].

1.6.1.3 Alginate hydrogels

Alginic acid is another naturally occurring polysaccharide which is isolated from brown algae. Structurally, it is a linear copolymer with homopolymeric units of (1,4)-linked β-D-mannuronate (M) and α-L-guluronate (G) residues which covalently link in different sequences (i.e. MMMM, GGGG, and GMGM). As with agarose, alginate can form hydrogels by various cross-linking methods, producing materials which are similar in structure to the ECM and provide many of the same advantageous characteristics for use as wound dressing materials.

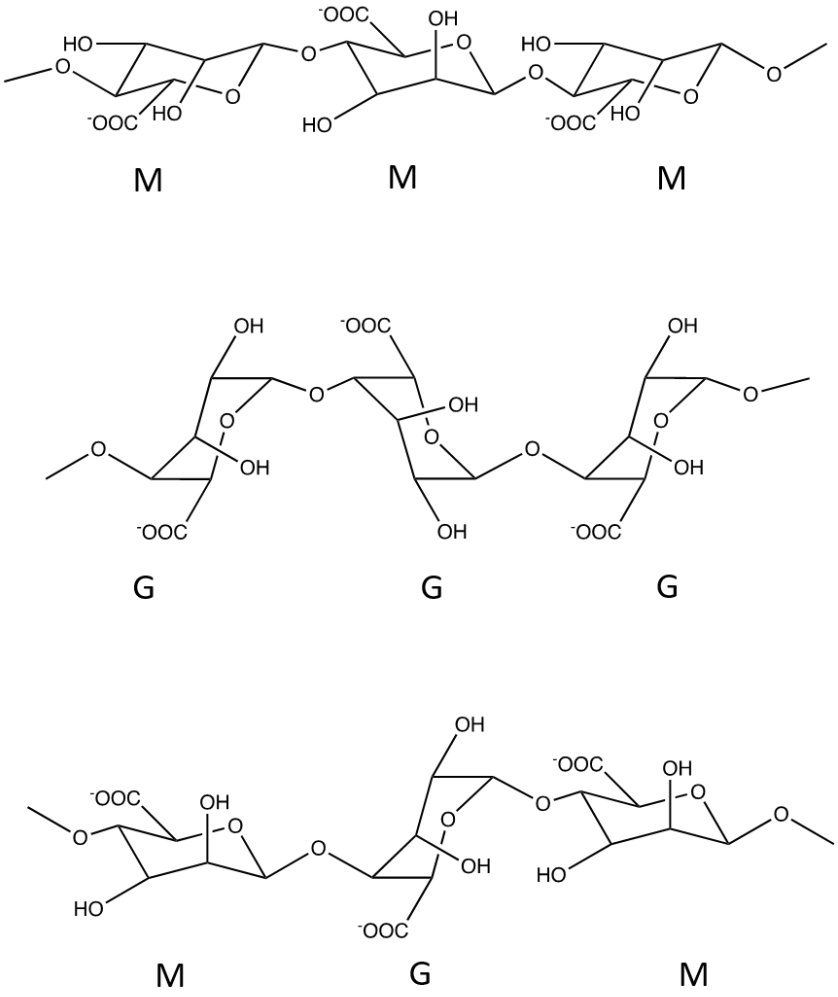

Figure 1.7 - Chemical structures of alginate depicting M-blocks (MMM), G-blocks (GGG), and alternating blocks (MGM).

Cross-linking of alginate to form hydrogels is most commonly achieved by the addition of divalent cations (e.g. Ca^{2+}) which form ionic bonds between polymer chains. It is believed that only the G-blocks are involved in intermolecular cross-linking, making the M and G ratio, sequence, G-block length and molecular weight important factors which determine the physical properties of the hydrogels [191].

1.6.1.4 Poly(vinyl amine)

The range of available synthetic polymers has grown extensively in recent years, with common polymers used in biomedicine including: polyolefins, poly(tetrafluoroethylene), poly(vinyl chloride), silicones, polyacrylates, polyesters, polyethers, polyamides and

polyurethanes. This list grows exponentially when synthesis is modified to produce varied chain lengths, crystallinity, side groups and co-polymers [181]. While synthetic polymers are generally beyond the scope of this study there is one polymer of interest, poly(vinyl amine) (PVAm).

PVAm is a linear homopolymer most commonly based on the free radical polymerisation and subsequent hydrolysis of N-vinylformamide (NVF), a water-soluble isomer of acrylamide (Figure 1.8). Alternative routes to PVAm synthesis include Hofmann rearrangement of polyacrylamide, which was once considered preferable due to the low cost of precursors. However, the Hofmann reaction requires treatment at high pH, conditions that can lead to side reactions and chain scission.

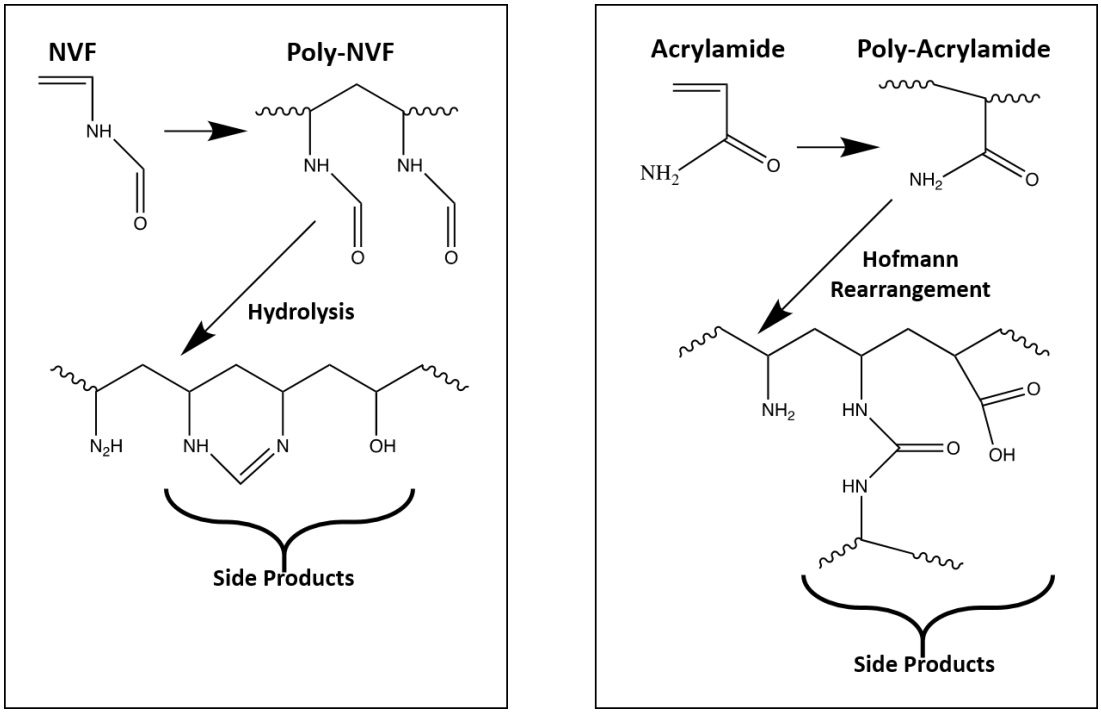

Figure 1.8 - The synthesis of PVAm from the hydrolysis of poly-NVF (left), and the Hofmann rearrangement of poly-acrylamide (right).

Polymerisation of NVF to poly-NVF produces high MW (0.8 kDa to >1 MDa) [192] water soluble polymers which upon partial hydrolysis form PVAm-*co*-NVF copolymer, and on complete hydrolysis produces pure PVAm polymer. Major side products of poly-NVF hydrolysis include sodium formate (alkaline hydrolysis) and formic acid (acidic hydrolysis) which may be removed by exhaustive dialysis with suitable molecular weight cut off (MWCO) followed by lyophilisation (Figure 1.9).

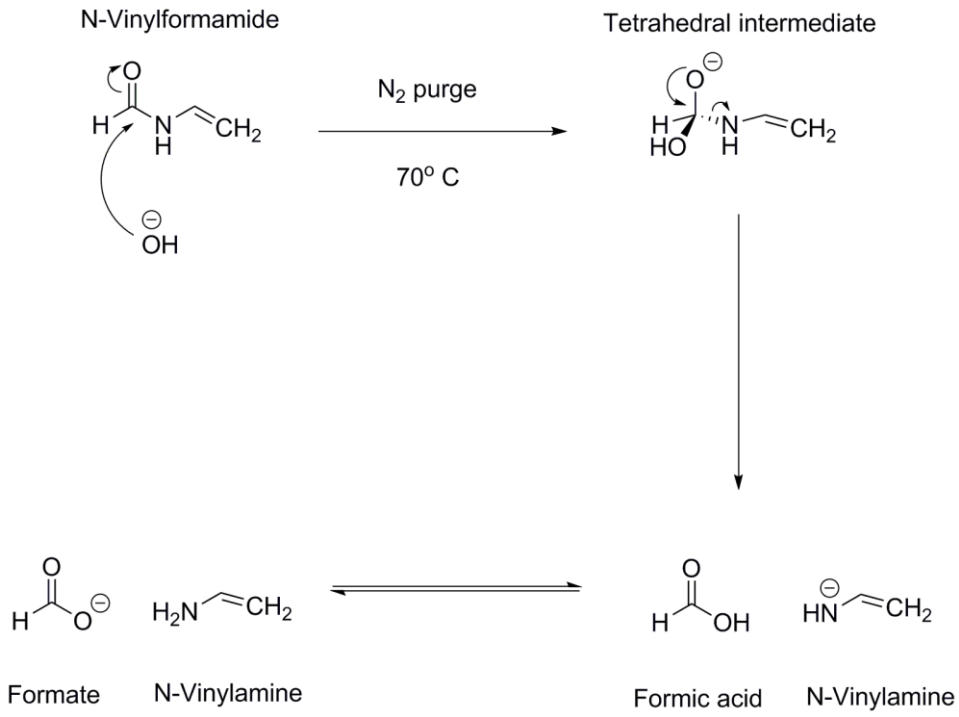

Figure 1.9 – Schematic of the hydrolysis of NVF to PVAm and the formation of formic acid or formate dependant on acid or base hydrolysis.

With the highest content of primary amine groups of any synthesised polymer and advances in commercial synthesis [193], PVAm is coming to the forefront of material surface modification and functionalisation research. When dispersed in water, PVAm irreversibly and spontaneously adsorbs to most surfaces, creating a cationic interface capable of charge-based adsorption/repulsion and further functionalisation such as co-polymer synthesis. Unlike lower Mw analogues, such as ethylamine, PVAm remains partially ionised below pH 10 due to interactions between neighbouring amine groups. Much of the literature around this polymer relate to PVAm synthesis and the interaction of PVAm with cellulose, due to its commercial application as a paper making additive. However an emerging body of literature is now showing novel applications ranging from oil recovery to gene delivery [193]. The beneficial characteristics of PVAm as an interfacial agent can be compared to that of commonly used alternative interfacial agents such as chitosan (Table 1.3).

Table 1.3 - Advantageous properties of PVAm in comparison to chitosan an alternative interfacial agent.

Property	**Chitosan**	**PVAm**
Primary amine content	Low content	Highest density of any polymer
Flexibility of synthesis	Low synthetic flexibility	*N*-vinylformamide hydrolysis allows flexibility in Mw and synthesis of micro/macrogels and copolymers
Reactivity	Low nitrogen content and low reactivity	Amenable to conjugation of molecules and oligomers
Solution properties	Not water soluble	Water soluble and positive charge at pH 2-11

1.7 Bacteriophage delivery formulations

With high porosity polymeric wound dressings already being exploited as drug delivery carriers of traditional antibiotics [194] and the clear potential for bacteriophage in the management of bacterial infection, the immobilisation of bacteriophage within wound dressings could provide a novel solution to the treatment of chronic antibiotic resistant wound infections. Bacteriophage are fundamentally different to all other therapeutic classes due to their large size and ability to propagate within targeted bacteria. Delivery of bacteriophage to the target site has therefore become an integral component of bacteriophage therapy research. To facilitate bacteriophage delivery, various formulations and administration methods have been developed including aqueous formulations, impregnated hydrogels, encapsulation technologies, and surface immobilisation.

When envisaging drug delivery systems (DDS) in the context of bacteriophage therapy, it is important to consider the infectivity of bacteriophage as the 'therapeutic substance'. Bacteriophage stability can be disrupted by an array of external physical and chemical factors, including temperature, pH, UV exposure, salinity and ion exposure [195, 196]. Therefore, a suitable DDS would be protective against external factors which jeopardise bacteriophage viability. Over the years, reports of efficacy have grown in the literature spanning a range of DDS techniques for the therapeutic delivery of bacteriophage. These techniques can generally be partitioned into one of five categories: aqueous formulations, hydrogels, surface immobilisation, encapsulation, and nebulisation. For the purpose of this thesis, the surface immobilisation of bacteriophage and their integration within hydrogels as a device for wound treatment will be discussed: the other methods lie outside the scope of this study.

1.7.1 Surface immobilization

Surface immobilisation of bacteriophage offers the potential to produce bioactive surfaces. Substrates have been functionalised with specific recognition elements for use as bacterial detection biosensors or as antimicrobial surfaces for medical applications and food preservation [197].

Immobilisation of bacteriophage on the surface of solid substrates is an area of emerging interest, with literature describing potential use in a variety of applications from bacterial sensing platforms to industrial chemistry [198]. Microbial colonisation on the surface of medical devices is a significant healthcare concern, accounting for the majority of medical device associated infections [199]. Immobilisation of bacteriophage on the surface of

medical devices provides a novel method of bacterial control and anti-biofilm properties when *in situ*.

A number of studies have exploited the intrinsic charge difference between the bacteriophage capsid and tail fibres to orientate bacteriophage on various substrates [200-203], allowing immobilisation of the negatively charged bacteriophage capsid to the surface of the material, leaving the infective machinery (tail fibres) available to initiate bacterial infection. The use of polyelectrolytes to immobilise viral particles on various substrates using layer by layer assembly has been explored by a number of researchers [203-208]. For example, a study published in 2006 reported assembly of filamentous bacteriophage driven by competitive electrostatic binding, leading to spontaneous inter-diffusion and production of a dense bacteriophage monolayer [207]. It was later reported, by the same group of researchers, that spontaneous assembly of bacteriophage in this manner was highly dependent on the use of high molecular mobility polymers, facilitating lateral movement of the assembling bacteriophage monolayer [208].

An alternative method of bacteriophage immobilisation is covalent attachment, typically taking advantage of amino acid residues present on the viral capsid. The amino acids lysine, glutamic acid, aspartic acid, cysteine and tyrosine allow for common protein conjugation techniques to immobilise the phage capsid to an array of substrates [199]. A recent study conducted by Pearson *et al* reported successful covalent immobilisation of bacteriophage to plasma-treated polymer substrates via primary amine groups located on the phage capsid effectively lysing bacteria and eliminating biofilm formation [209]. While it has been reported that covalent immobilisation of bacteriophage can result in significantly higher phage surface densities (up to 37-fold) when compared to physisorption [210], it has also been suggested that high surface densities are restricted by strong covalent bonding inhibiting lateral mobility of the viral layer [211]. Furthermore, reaction conditions generally required for covalent attachment can often be detrimental to bacteriophage viability, with extremes in pH, chemicals and temperature all jeopardising viral integrity. Cost is also an important consideration, with the tendency for covalent attachment being more labour intensive and costly than other methods.

Genetic modification of the bacteriophage capsid and bacteriophage display technology involves the insertion of DNA fragments encoding specific proteins into bacteriophage coat protein genes. Exploitation of the expression of the proteins encoded by the inserted gene allows for bacteriophage immobilisation on substrates coated with ligands specific to the newly expressed peptide. This method of immobilisation allows for highly specific and tailorable associations between displayed phage capsid proteins and the ligand present on the

substrate interface. However, it must be considered that any genetic modification of bacteriophage may alter the infective behaviour of the modified virus [212]. Furthermore, genetic modification requires genomic information and molecular techniques that may be time and cost inhibitory to using phage cocktails or where bacteriophage need to be regularly updated to avoid bacterial resistance; it may also add to the regulatory burden during product licensing.

With various methods of bacteriophage immobilisation outlined, it is important to consider the correlation between bacterial infection efficacy and bacteriophage surface density. In a paper by Naidoo *et al*, it was reported that bacterial capture efficiency increased with bacteriophage surface density until a threshold was met [213]. Exceeding this equilibrium point resulted in a significant decrease in bacterial capture efficiency, hypothesised as due to one of or a combination of three factors. Firstly, it could be considered that above optimal bacteriophage surface density the tail fibres become entangled, resulting in inhibited bacterial recognition and adsorption. Secondly that electrostatic repulsion between bacteriophage capsids when in closer proximity could result in reduced bacteriophage surface density. Finally, depositing bacteriophage on the surface of a substrate may change the intrinsic associations of that material with bacteria [214].

1.7.2 Integration within hydrogels

Bacteriophage entrapment within microporous matrices provides distinct advantages over methods of delivery which leave viral particles exposed to the external conditions, which may threaten bacteriophage viability. This structural and functional stabilisation of viral particles may be achieved by entrapment within the porous matrix of hydrogels.

Hydrogels are a group of three-dimensional (3D) water-engorged materials derived from polymeric cross-linking and represent the first group of biomaterials designed for use within the human body [215]. The biophysical properties of these hydrogels has been widely exploited in the field of biomaterials due to their remarkable similarity to soft biological tissues [216]. Many advantageous characteristics have been identified, namely: high biocompatibility, low interfacial tension, physical similarities to soft tissue, high permeability, and the innate ability to allow for controlled release of entrapped or encapsulated molecules [217]. Further advantages include, low protein absorption and cell adhesion, low friction reducing consequent irritation, surface and internal modification, and the ability to inject as a solution and initiate cross-linking at body temperature [217]. When considering hydrogels as bacteriophage delivery systems it is also important to value the high water content of hydrogels, thus providing a high humidity environment which is

crucial to bacteriophage viability and a useful tool when using lyophilised bacteriophage preparations [218].

Hydrogels are formed by either physical or chemical cross-linking. The latter typically occurs due to covalent bonding of linear polymer chains in the presence of a chemical initiator. The use of chemical cross-linking for biomaterial applications is limited primarily due to the toxicity of cross-linking agents [217, 219], with removal (leaching) of the cross-linking agent from the hydrogel leading to loss of integrity and significant safety concerns. Physical cross-linking occurs via chain entanglement, hydrophobic interaction, hydrogen bonding or the formation of ionic complexes [220]. Unlike chemical cross-linking, these cross-linking points are generally reversible and the resulting structures tend to be mechanically weaker in the swollen state [217].

One potential concern when considering hydrogels as a bacteriophage delivery system is the entrapment matrix could act as a barrier between the bacteriophage and target bacterium, inhibiting initiation of the bacteriophage infection process and decreasing antimicrobial efficacy. One way of counteracting this concern is the use of controlled release technologies to disperse the bacteriophage into the surrounding environment under certain conditions, or by a predetermined 'trigger'. This technology would allow for a highly adaptable bacteriophage DDS unique to the application, whether it be a wound dressing material, antimicrobial coating on the surface of medical devices, or antimicrobial food packaging. Release of the bacteriophage from the hydrogel matrix is dependent on degradation of the polymer network, and therefore the material composition may be highly dependent on intended external conditions. For example, Bean *et al* developed a hydrogel composite bilayer composed of an agarose base layer containing bacteriophage K, and a cross-linked hyaluronic acid (HAMA) superficial layer [221]. The common inhabitant of chronic wound infections, *Staphylococcus aureus*, secretes hyaluronidase, an enzyme which degrades the superficial HAMA and acts as the bacteriophage release 'trigger'. In such a way, exposure of the material composite to a wound infection colonised by *S. aureus* would result in the release of a therapeutic dose of bacteriophage into the external environment.

PhagoBioDerm® is a commercial product developed in Georgia, which has proved successful in the treatment of various types of superficial wounds [222]. The product is a thin biocomposite film based on a poly(ester amide) matrix, containing a bacteriophage cocktail lytic against five prominent wound bacteria (*Pseudomonas aeruginosa*, *Escherichia coli*, Staphylococci, Streptococci and *Proteus*), together with the antibiotic ciprofloxacin, benzocaine (painkiller) and proteolytic enzymes. While the polymer film acts as a vehicle for therapeutic delivery of bacteriophage and drugs to promote wound healing,

PhagoBioDerm® has also been designed to control moisture transmission and accelerate macrophage activity by controlled degradation of the polymer film. In a study conducted from 1999-2000 in Tbilisi, Georgia, 107 patients with ulcers which did not respond to conventional treatment interventions were treated with PhagoBioDerm; 70% were reported to have healed completely, demonstrating potential in the management of refractory wounds [223].

The use of hydrogels for drug delivery has been an area of growing interest in recent years [216, 224-227]. Incorporation of bacteriophage within the hydrated matrix of these materials has the potential of providing stabilised and triggered delivery to the infection site [221, 228-230]. While care must be taken in the selection of compatible polymers and cross-linking initiators to prevent viral deactivation and toxicity, the potential of this delivery system spans many areas of infection control. The addition of polymer stabilisers to aqueous formulations, and the stabilisation within hydrogels may also provide solutions for long term bacteriophage storage. This factor will become all the more important if bacteriophage are to become commonplace in clinical practice.

1.8 Research aims

While there is an abundance of studies demonstrating the efficacy of planktonic bacteriophage reducing or eliminating bacterial colonisation from *in vitro* and animal studies and a few clinical trials, there have been few studies of bacteriophage efficacy when immobilised and combined with various biomaterials targeted at wound infection. In addition to this, there are limited studies which characterise bacteriophage-material combinations enabling further understanding of release mechanisms for optimisation of infective capacity.

The applications for such biomaterial-bacteriophage developments could range from immobilisation within medical implants to incorporation with hospital hygiene products, providing an antibacterial effect upon contact with the target bacterium even before the clinical signs of infection are evident. Clear industrial and biotechnological applications also exist for immobilised bacteriophage incorporated materials, such as rapid water decontamination following a contamination event and control of biofouling on the surface of engineering structures.

The objective of this research study, therefore, is to prepare and characterise virulent bacteriophage-integrated prototype wound dressing materials which demonstrate lytic activity against clinically relevant bacteria *in vitro.* It is also intended that a technology platform for further development will be established by the end of the project. Through judicious compositional design, the release characteristics of bacteriophage from the material will be established and modified to achieve enhanced bacterial control. Material structure and bacteriophage distribution and integrity will be examined using image analysis and other analytical techniques to help engineer these novel materials towards clinical application, and the bacteriophage-immobilised biomaterials will be evaluated for cytotoxicity against a fibroblast cell line.

The work presented in this thesis will be divided into three sections:

I. Selection and characterisation of virulent bacteriophage (and suitable bacterial hosts) for antimicrobial wound dressing development.
II. Development and characterisation of novel polymer films, hydrogels, and composite materials as candidate wound dressing materials.
III. Integration of bacteriophage selected in section I with materials developed in section II. Bacteriophage integrated candidate wound dressings will then be characterised and optimised accordingly.

Chapter Two: General Materials and Methods

2 General Materials and Methods

2.1 Materials

2.1.1 Microorganisms and bacteriophage

Culture collections have been used as the primary source for bacteria and bacteriophage unless otherwise stated.

Escherichia coli (Table 2.1)

Staphylococcus aureus (Table 2.2)

Bacteriophage K (ATCC 19685-B1)

Bacteriophage 44AHJD (Felix d'Herelle Reference Center for Bacterial Viruses, Quebec, Canada)

Bacteriophage T4 (ATCC 11303-B4)

Bacteriophage T3 (ATCC 11303-B3)

2.1.2 Chemicals

All chemicals are of general laboratory grade unless indicated otherwise.

Agarose (Sigma-Aldrich)

Chloroform (Fisher Scientific)

Choline chloride (Fisher Scientific)

Deuterium oxide (D_2O) (Sigma-Aldrich)

Ethanol (Fisher Scientific)

Gelatin (Sigma-Aldrich)

Glutaraldehyde (Sigma-Aldrich)

Magnesium sulphate heptahydrate ($MgSO_4$ $7H_2O$) (Fisher Scientific)

Phosphate buffered saline (Sigma-Aldrich)

Poly(vinyl amine) (BASF)

Polyethylene glycol (PEG) 8000 (Fisher Scientific)

Sodium cacodylate buffer (Sigma-Aldrich)

Sodium chloride (NaCl) (Fisher Scientific)

Sodium hydroxide (NaOH) (Fisher Scientific)

Technical agar (Fisher Scientific)

Tris(hydroxymethyl)aminomethane (Fisher Scientific)

Tryptone soya agar (Fisher Scientific)

Tryptone soya broth (Fisher Scientific)

Urea (Sigma-Aldrich)

2.2 Methods

2.2.1 Microbiological techniques

2.2.1.1 Bacterial strains

A number of strains of *E. coli* and *S. aureus* were utilised for the characterisation of bacteriophage and the identification of a suitable host bacterium for use in further studies. The strains of *E. coli* and *S. aureus* are listed in Table 2.1 and Table 2.2, respectively. Each bacterial strain was sub-cultured a minimum of three times prior to any investigation.

Table 2.1 - List of *E. coli* strains and sources used in this study.

***E. coli* strain**	**Type**
EPI-300	Molecular strain (TransforMax)
8196	NCTC
10418	NCTC
10240	NCTC
10385	NCTC
8545	NCIMB
5933	NCTC
9270	NCTC
8739	ATCC
12900	NCTC
11303	ATCC
B3	Clinical isolate

Table 2.2 - List of *S. aureus* strains and sources used in this study.

***S. aureus* strain**	**Type**
10788	NCTC
12702	NCIMB
13143 (EMRSA-16)	NCTC
8511	NCTC
6538	ATCC
6571	NCTC
12493	NCTC
9518	NCTC
010	Clinical isolate
06310	Clinical isolate
06311	Clinical isolate
06312	Clinical isolate
06313	Clinical isolate
06314	Clinical isolate
06315	Clinical isolate
MR027	Clinical isolate
MRSA16	Clinical isolate

2.2.1.2 Bacterial growth conditions

Unless stated otherwise, *S. aureus* and *E. coli* were both cultured by inoculation of tryptone soya broth (TSB) or tryptone soya agar (TSA). In the case of planktonic culture, TSB was inoculated from a single isolated colony and incubated with constant shaking (120 rpm) for 24 h at 37°C. All inoculated agar plates were incubated inverted for 24 h at 37°C.

2.2.1.3 Bacterial culture and production of stocks

S. aureus and *E. coli* were obtained from the University of Brighton bacterial culture collection. Each strain was sub-cultured three times from a single isolated colony to ensure monoclonal bacterial populations and resume typical life cycles.

API tests (BioMérieux, UK) were performed prior to preparation of bacterial stocks to ensure the correct organisms were under investigation. Briefly, single isolated colonies were inoculated into 5 ml sterile phosphate buffered saline (PBS) and vortexed to ensure homogeneity. The API test was then conducted as per manufacturer instructions. After

confirmation of the bacterial species identities, stocks were produced for use throughout the research period by transferring single isolated colonies to cryovials with 1.5 ml TSB containing 15 % v/v glycerol and storing at -80°C.

2.2.1.4 Bacterial enumeration

The enumeration of bacterial cells in planktonic culture can be estimated by numerous methods, the most commonly used of which is the standard colony count. Using this method, ten-fold serial dilutions in PBS of the original culture were spread in 100 µl volumes onto the surface of TSA plates and incubated inverted for 24 h at 37°C. After incubation, individual colonies were identified and enumerated, allowing an estimation of the number of bacterial colony forming units per millilitre of the original culture (Equation 2.1).

Equation 2.1 - Enumeration of bacterial cell numbers in planktonic culture from standard colony counts.

$$cfu\ ml^{-1} = \frac{Average\ colony\ count}{d\ x\ V}$$

Where *d* stands for dilution factor of the original culture and *V* for the volume of the relevant dilution.

2.2.1.5 Bacteriophage purification from crude lysate

Isolation of a single viral plaques obtained from a preliminary plaque assay (section 2.2.1.7) was conducted to ensure the propagation of a monoclonal bacteriophage population. The wide end of a sterile Pasteur pipette was used to pick a viral plaque, which was then re-suspended within a sterile Eppendorf tube containing 1 ml of sterile lambda buffer (also referred to as bacteriophage buffer) (see Appendix I for composition). The Eppendorf tubes were then wrapped in tin foil to avoid exposure to UV light and placed in a refrigerator at 4°C for 24 h to allow for bacteriophage release. Further plaque assays were conducted using the supernatant from each plaque, and this purification process repeated a minimum of three times in total. Monoclonal bacteriophage populations were confirmed visually by assessing plates for uniform plaque morphology.

2.2.1.6 Bacteriophage propagation and purification

Propagation and purification of the crude phage stock was conducted based on a polyethylene glycol (PEG) precipitation protocol described by Yamamoto *et al* (1970) [231]. 1 ml of an overnight host bacterial culture was inoculated into 100 ml of TSB in a 250 ml sterile conical flask and incubated at 37°C for approximately 4 hr with shaking (120 rpm). The optical density (OD) was measured at hourly intervals (calibrated with sterile TSB) until an OD_{600nm} of 0.5 was reached. 1 ml of isolated phage suspension was then added to the culture, gently mixed and incubated at 37°C for 15 min under static conditions to allow the phage particles to adsorb to the host bacterial cells. The culture was then incubated for 24 hr at 37°C on a rotary shaker (120 rpm). Bacterial lysis was indicated by macroscopic observation of the presence of cellular debris after this incubation step. 10 ml (10% v/v final concentration) chloroform was added and incubated at 37°C for 15 min on a rotary shaker (150 rpm). 5.84 g of NaCl (1M) was then dissolved within the culture while being held on ice, with gentle mixing every 10 min. The suspension was then transferred to a sterile centrifuge tube and spun at 11,000 g for 10 min at 4°C, and the supernatant transferred to a sterile 250 ml conical flask. 10 g (10% v/v) PEG 8000 was dissolved within the supernatant at room temperature using a magnetic stirrer. The flask was then placed in a polystyrene box containing ice ensuring full coverage around the suspension and left at 2°C for 24 hr. After transferring to a sterile centrifuge tube, centrifugation proceeded as before (11,000 g, 10 min, 4°C). The supernatant was then discarded, and the pellet re-suspended in 2 ml lambda buffer, vortexed, and transferred to a 50 ml Iwaki (chloroform resistant) centrifuge tube. 2 ml of chloroform was added and the tube vortexed for 30 s before centrifugation at 3,000 g for 15 min at 4°C. This resulted in the formation of three distinct layers, with the bacteriophage within lambda buffer residing in the uppermost layer (Figure 2.1). This layer was transferred to a sterile bijou bottle using a Gilson pipette, wrapped in tin foil to protect from UV light and stored at 4°C until required.

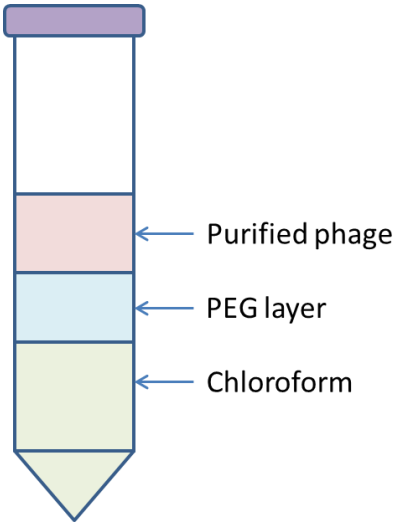

Figure 2.1 - Representation of the three distinct layers following final centrifugation at 3,000 g for 15 min. Purified phage lysate was extracted ensuring the PEG layer was not disrupted.

2.2.1.7 Bacteriophage enumeration by plaque assay

A viral plaque assay was performed in order to calculate the titre of the purified bacteriophage stock (expressed as PFU/ml). Individual 5ml bottles of overlay agar (see Appendix II for composition) were placed in a water bath at 100°C, and once molten placed in a water bath at 45°C to prevent the agar from setting. Serial dilutions (1:10) of the phage suspension were performed in sterile Eppendorf tubes using sterile lambda buffer as a diluent. 100 µl of an overnight bacterial culture was added followed by 100 µl of the appropriate bacteriophage dilution, the contents mixed and poured onto a TSA plate ensuring complete coverage. The plates were allowed to set before incubating inverted at 37°C for 24 hr. All dilutions were plated in triplicate and plates with 30-300 plaques selected for enumeration. The mean plaque count was used to calculate the PFU/ml using Equation 2.2. Control plates included bacterial host alone within overlay agar, and sterile lambda buffer within overlay agar, in order to test for viability of the host organism and sterility of lambda buffer, respectively.

Equation 2.2 - Enumeration of bacteriophage numbers by plaque assay.

$$pfu\ ml^{-1} = \frac{Average\ plaque\ count}{d\ x\ V}$$

Where *d* is the relevant dilution factor and *V* is the volume of phage inoculum.

2.2.2 Synthesis of PLAg films

2.2.2.1 Preparation of choline chloride (ChCl)/urea-based plasticiser

ChCl/urea-based ionic liquid plasticiser was prepared by a complexation reaction previously described by Abbott *et al.* (2003) [232]. Choline chloride and urea were mixed at a 1:2 molar ratio in a Duran bottle and heated to 100°C until a homogenous solution was formed. Ionic liquid was stored in a 60°C oven in the presence of silica desiccant until required.

2.2.2.2 PLAg film production

ChCl/urea ionic liquid (at varying concentrations) was mixed with an appropriate volume of distilled water (dH_2O), which was dependent on the selected cast size, and maintained under continuous stirring until the plasticiser had dispersed. The appropriate quantity of agarose was then added, and the mixture placed in a water bath at 100°C until the agarose had completely dissolved (forming a transparent solution). The PLAg solution was then poured into an appropriately sized (size dependant on water volume, just sufficient to cover) Teflon coated baking tray and allowed to gel at room temperature. Once a solid gel had formed, PLAg disks were excised using a circular plastic cutting tool and excess peripheral material removed. PLAg disks were then rigorously dried at 60°C for 24 h to form a dried film. An example formulation for a 25 cm (L) x 17 cm (W) x 2.5 cm (D) Teflon coated tray was as follows; 2.86 ml ionic liquid, 2.86 g agarose, 140 ml dH_2O, resulting in a 1:1 ratio (50 %) of plasticiser to agarose.

2.2.3 Synthesis of PVAm-PLAg films

2.2.3.1 Purification of PVAm

PVAm was used to modify the surface charge of PLAg films. PVAm samples of varying molecular weight and charge density were kindly provided by BASF (UK). To ensure complete hydrolysis of parental poly-NVF and residual formic acid impurities (see Section 1.6.1.4), samples were reacted with 5 % NaOH at 70°C for 48 h under nitrogen purge, transferred to dialysis tubing cellulose membranes (MWCO 14 kDa) (Sigma-Aldrich, UK), dialysed against dH_2O for 10 days, and lyophilised in a Christ Alpha 2-4 LDC-1M freeze drying cabinet (Martin Christ, Germany) prior to use. Purified PVAm samples were stored in Duran bottles sealed with parafilm tape (unless otherwise stated) to avoid absorption of atmospheric moisture.

2.2.3.2 Surface coating of PLAg with PVAm to produce PVAm-PLAg

PLAg films were modified by the addition of positively charged PVAm to the film surface. Three film coating methods were evaluated. All methods initially utilised 0.5 % PVAm dissolved in 0.005 M NaCl solution adjusted to pH 10 with 1 M NaOH (unless otherwise stated).

Drying method: 500 µl of 0.5 % PVAm dispersed in 0.005 M NaCl adjusted to pH 10 was spread on the surface of plasticised agarose films and the surface coating dehydrated at 60°C for 24 h.

Adsorption method: 500 µl of 0.5 % PVAm dispersed in 0.005 M NaCl adjusted to pH 10 was spread onto the surface of plasticised agarose films and left to spontaneously adsorb for 15 min at 25°C. The modified surface was then washed 5x with dH_2O to remove unbound PVAm and dehydrated at 60°C for 24 h.

Gel dehydration method: 500 µl of 0.5 % PVAm dispersed in 0.005 M NaCl adjusted to pH 10 was spread on the surface of plasticised agarose in gel form (prior to dehydration). Plasticised agarose gels were then dehydrated at 60°C for 24 h to form a film.

2.2.4 Synthesis of Alg-PVAm-PLAg composites

Alg-PVAm-PLAg composite materials were synthesised by the addition of an alginate hydrogel layer to PVAm-PLAg films. The cross-linking of alginate was achieved by two methods; oxidation of Fe(II) to Fe(III), and internal liberation of calcium ions using the $CaCO_3$ – GDL system. Both methods utilised PVAm-PLAg films produced as described previously (Section 2.2.3)

2.2.4.1 Alginate cross-linking by the oxidation of Fe(II)

The method of alginate gelation by air oxidation of Fe(II) was based on work conducted by Narayanan *et al* (2012) [233]. A solution of 2 % w/v alginate solution was prepared by adding 2 g of sodium alginate powder to 1 L of dH_2O and stirred for 24 h until a homogenous solution was formed. To 9.5 ml of sodium alginate solution, 300 µl of Fe(II) chloride (500 mM to 1 M) was added dropwise over a 30 minute period under vigorous stirring. Care was taken to add the Fe(II) solution extremely slowly so as to avoid clumping,

and to achieve a homogenous solution. Once a homogenous alginate-Fe(II) solution was achieved, 5 ml of the solution was transferred to the surface of a PVAm-PLAg film, contained within a filtration unit (as described in Section 5.2.6) and allowed to crosslink at room temperature and atmospheric pressure. Fe(II) concentrations of 500 mM to 1 M solidified within 48 h to 2 h, respectively.

2.2.4.2 Alginate cross-linking by the $CaCO_3$ – GDL system

In situ liberation of calcium ions was achieved by the addition of the hydrolysing proton donor D-glucono-δ-lactone (GDL) to alginate containing dispersed $CaCO_3$. To produce 10ml of pre-gel solution, 0.1g of $CaCO_3$ (100 mM) was thoroughly dispersed in 7.5 ml of 2% alginate and then 2.5 ml of 4 % GDL (225 mM) added to initiate cross-linking and mixed thoroughly. Final concentrations were as follows; 1.5 % w/v alginate, 1 % w/v $CaCO_3$, and 1% w/v GDL. Immediately after the addition of GDL, 5 ml of solution was transferred to the surface of PVAm-PLAg films, contained within filter units (as described in Section 5.2.6), and allowed to cross-link for 1 hr (sol-gel transition occurs at approximately 30 min at room temperature and atmospheric pressure). Once gelled, PVAm-PLAg-Alg composites were removed from the filter units for further study.

Chapter Three: Bacteriophage Characterisation

3 Bacteriophage characterisation

The focus of this chapter is the selection and characterisation of bacteriophage which infect common wound pathogens, *E. coli* and *S. aureus*. Initial selection was based on the preference for obtaining morphologically distinct bacteriophage from both the *Myoviridae* and *Podoviridae* families, allowing comparison of symmetric and asymmetric bacteriophage immobilisation in future work. Previously characterised bacteriophage K and 44AHJD were selected for use against *S. aureus* strains, while bacteriophage T4 and T3 were selected for use against *E. coli*. Each bacteriophage was then assigned a host bacterial strain based on the efficacy of plating, and characterised by assessment of its morphology, host range, viral-bacterium interactions, growth parameters and electro-kinetic potential. Characterisation using these parameters was done to provide reference information which would prove necessary for subsequent investigations in this project.

3.1 Background

The first two stages of developing novel bacteriophage formulations are isolation and characterisation of the candidate bacteriophage. These initial steps are essential to produce a final formulation of the required efficacy; inappropriate selection and instability has resulted in a number of early failures of commercially available bacteriophage products. These considerations were promptly addressed in a guide for the preparation of therapeutic bacteriophages, authored by Felix d'Hérelle in 1938 [234].

In order to obtain suitable samples from which to isolate bacteriophage, one must consider the source and ecology of the bacterial strains to be targeted. In the case of gastrointestinal pathogens such as *E. coli*, it may be considered that if the target bacterium is present on the patient and in the surrounding environment, it is also likely to be found plentifully in the wastewater systems. As bacteriophage require a bacterial host to replicate, it would be expected that environments rich in bacteria would also contain an abundance of bacteriophage specific to the bacteria of interest. These environments, therefore, provide opportunities for isolation of bacteriophage highly specific to the bacterium of interest. For example, a recent study reported the isolation of bacteriophage infective of multi-drug resistant bacteria (*P. aeruginosa, S. aureus, K. pneumoniae* and *E. coli*) collected from patients with septic wounds at the Rajiv Gandhi Institute of Medical Science (RGIMS), Kadapa [235]. In this study, to increase the likelihood of obtaining bacteriophage infective

of the collected pathogenic bacteria, bacteriophage were isolated and propagated from raw sewage at the RIMS municipal sewage plant. The authors reported isolation of bacteriophage active against all the aforementioned bacteria.

Once isolated, it is essential to characterise a bacteriophage to determine its suitability as a therapeutic agent. Morphological assessment by transmission electron microscopy (TEM) is considered a standard characterisation step for all isolated bacteriophage [236]. Whilst allowing taxonomic classification of the viral particles into families, TEM may also allow for the identification of novel bacteriophage and estimation of DNA size from the capsid diameters [108]. As many of the standard isolation methods require the addition of chloroform to lyse bacterial cells, it should be recognised that the majority of bacteriophage assessed at this stage will be members of the lipid-free, linear dsDNA genome, *Caudovirales* order.

Once morphological evaluation has been conducted by direct imaging, the host range of the bacteriophage against both culture collection deposited, and clinical bacterial isolates should be investigated. Ideally the host range should be clinically reflective of the prevalent pathogens of the intended target bacteria. Host range is often determined by the spot test method, whereby a small volume of bacteriophage is applied to a continuous inoculum of bacteria and observed for bacterial lysis. At this stage it is common to assess the efficacy of bacteriophage cocktails (formulations containing multiple bacteriophage), potentially increasing the therapeutic range and decreasing the effect of bacterial resistance.

Another crucial step in the characterisation of bacteriophage is the characterisation of the of viral life cycle, such as adsorption rate, latency period, and burst size. For the purpose of bacteriophage therapy, it may be considered that bacteriophage with a relatively high adsorption rate, short latent period, and large burst size will be most desirable. These characteristics, however, are seldom found together. In addition to this, the method employed for bacteriophage isolation will often bias towards the selection of viruses with short latency periods, potentially resulting in the loss of bacteriophage with longer latency period but a burst size which is significantly greater [237].

Once morphological identification and bacteriophage-host characterisation has been conducted, further characterisation of bacteriophage is primarily focused on the intended application and often dictated by the technical possibilities of the laboratory. Often these will include the stability of bacteriophage and their resilience against external conditions.

3.2 Methods

3.2.1 Bacterial strains

In this chapter, a number of bacterial strains were utilised for the characterisation of bacteriophage and the identification of a suitable host bacterium for use in further studies. The strains of *E. coli* and *S. aureus* are listed in Table 2.1 and Table 2.2, respectively. Each bacterial strain was sub-cultured a minimum of three times prior to any investigation.

3.2.2 Transmission Electron Microscopy

3.2.2.1 Principles of TEM

Transmission electron microscopy (TEM) is a significant analytical imaging method used in the physical, chemical and biological sciences; finding applications in cancer research, nanotechnology and virology. TEM has long been used for observation of bacteriophage and still remains the gold standard for the identification and classification of bacteriophage particles [238]. The TEM operates by accelerating electrons through an electromagnetic lens to produce a condensed high-energy beam that is transmitted through a specimen. Interactions of the electrons with the specimen allows generation of magnified two-dimensional micrographs; these interactions are categorised as either transmitted (un-scattered) or diffracted (scattered). Specimens with low atomic number generally have low electron interactions and are therefore negatively stained with heavy metal salts such as uranyl acetate or phosphotungstic acid to enhance the contrast between the material and background [239].

3.2.2.2 TEM methodology

The bacteriophage were purified by polyethylene glycol (PEG) precipitation prior to TEM analysis. Prior to sample deposition, 300 mesh carbon-coated copper grids (Agar Scientific, UK) were ionised under UV for 30 minutes to increase bacteriophage adherence. 5 µL of bacteriophage lysate (10^9 PFU/mL) was then deposited on the surface, allowed to adsorb for 1 minute and then negatively stained with 1% (w/v) uranyl acetate (pH 4) for 30 seconds. All samples were allowed to air dry prior to visualisation using a JEOL JEM-1400Plus transmission electron microscope, operated at 120 KV (pixel = 0.1nm) and equipped with a

Gatan OneView 4K CMOS digital camera. Bacteriophage size estimations were based on a minimum of five single bacteriophage images from different areas of the TEM grid.

3.2.3 Bacteriophage host range

Bacteriophage sensitivities against the aforementioned bacterial isolates (Table 2.1 and Table 2.2) were established using the spot test method. 100 µl of overnight bacterial host culture was spread onto TSA plates and allowed to dry at 37°C for 20 min. 10 µl of purified bacteriophage lysate (approx. $1x10^9$ PFU/ml) was dropped onto the agar surface and allowed to air dry before incubating inverted at 37°C for 24 h. This method was conducted for all available strains of *S. aureus* (13 strains) and *E. coli* (11 strains) contained in the University of Brighton bacterial culture collection. The plates were then examined, and each bacterial strain recorded as sensitive, intermediate or resistant to phage infection (Figure 3.6). These sensitivity profiles were based on: clear zones of lysis (sensitive), evidence of bacterial regrowth (intermediate), or no evidence of lysis (resistant). An additional category of SI (sensitive/intermediate) was used due to the spectrum of susceptibility in intermediate strains. Two bacterial strains for each bacterial species were then chosen for further study based on these parameters and the desirable characteristics relevant to the study (e.g. antibiotic resistance, clinical isolate, extent of published characterisation).

3.2.4 Bacteriophage infection of planktonic bacterial cultures

Planktonic growth of untreated and bacteriophage treated bacterial cultures was compared by monitoring optical density over time using an iEMS Reader MF (Thermo Labsystems, UK) incubated plate reader, allowing examination of the bacteriophage-host interactions and detection of emerging bacteriophage-resistant bacteria. Overnight bacterial cultures were diluted 1:1000 in TSB (OD_{620} 0.1) and 100 µl added to each well of a 96-well plate. Plates were incubated at 37°C for 2 h prior to the addition of bacteriophage at MOIs of 0.1, 1, and 10. Plates were then incubated for a further 20 h under the same conditions, with OD_{620} readings taken every 15 minutes with orbital shaking for 5 seconds immediately prior to each measurement. Reagent background measurements and positive controls comprised of wells constituting medium alone and bacteria grown in the absence of bacteriophage, respectively. Data was analysed using Excel (Microsoft, USA) and GraphPad Prism 5 (GraphPad Software Inc., USA).

3.2.5 One-step growth curve of bacteriophage

Bacteriophage growth parameters (latent period, eclipse period and burst size) were determined using the one-step growth method. This method is based on the periodical evaluation of free and total phage numbers over a specified time period. An overnight bacterial culture was diluted 1:1000 in TSB and incubated at 37°C until mid-exponential phase. The bacteria were then harvested by centrifugation (7,000 g, 10 min, 4°C) and resuspended in TSB to an OD_{600} of 1. Bacteriophage was then added to obtain a MOI of 0.001 and allowed to adsorb for 5 min at room temperature. The unadsorbed bacteriophage were then removed by centrifugation as above, and the pellet resuspended in 10 ml TSB and incubated under constant shaking at 37°C for 1 h. Two samples were taken every 5 minutes; the first samples being plated by plaque assay immediately, and the second set of samples plated after treatment with 1 % (v/v) chloroform for 30 min to release intracellular virions. Each series time-point was then serially diluted, titrated by triplicate overlay plaque assay and bacteriophage concentrations enumerated after 24 h incubation at 37°C.

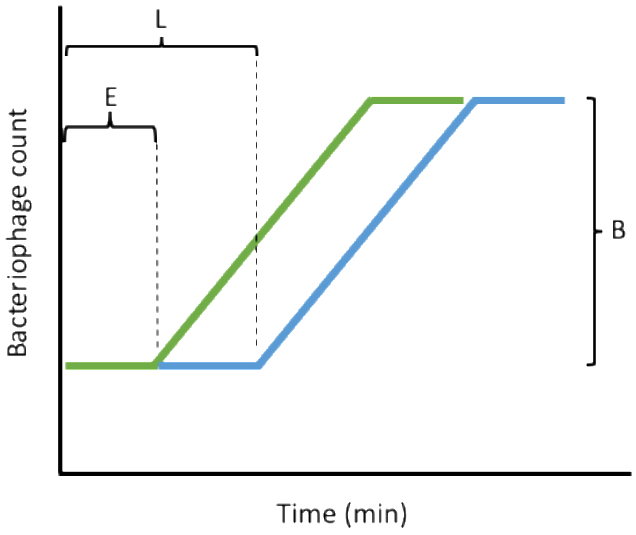

Figure 3.1 – A graphical representation of the one-step growth curve. The green line represents chloroform treated samples (total bacteriophage) and the blue line represents the number of free viruses. Eclipse period (E), latent period (L) and burst size (B) are denoted by their respective letters on the graph.

Bacteriophage latent period, the duration over which virions attach to susceptible bacteria and subsequently terminate cell lysis, was described as the time period of the initial plateau of free bacteriophage (Figure 3.1 – B). The eclipse period, from virion adsorption ending in the maturation of the first bacteriophage particles, was described as the time period of the

initial plateau of total bacteriophage (Figure 3.1 – E). The bacteriophage burst size was calculated using the following equation:

Equation 3.1 - Burst size of bacteriophage

$$Burst\ size = \frac{(P_1 - P_0)}{P_1}$$

Where P_0 is phage titre at plateau prior to rise and P_1 is phage titre at plateau post-rise.

3.2.6 Adsorption kinetics

All media was pre-warmed to 37°C prior to preparation of bacterial and bacteriophage solutions. Bacteriophage solutions were prepared by diluting 100 µl of bacteriophage in 10 ml pre-warmed TSB to obtain a titre of 10^6 PFU/ml. Bacterial cultures were prepared by centrifuging a 10ml overnight culture (7,000 g, 10 min, 4°C) and resuspending in 10 ml pre-warmed TSB. Bacterial cultures were diluted to a concentration of 10^8 CFU/ml. Bacteriophage and host solutions were then mixed (MOI 0.01) and incubated at 37°C in a water bath with gentle agitation (60 rpm). Aliquots were taken at predetermined time points over 10 minutes incubation and filtered through a 0.45 µm syringe filter to determine free phage concentration. Free phage concentration was normalised by converting to percentage of initial inoculum. Non-linear one-phase exponential decay curves were fitted using GraphPad Prism 5 software (GraphPad Software Inc., USA) to obtain adsorption rate constants.

3.2.7 Zeta potential of bacteriophage

Zeta potential can be described as the difference in electrostatic potential between a conducting medium and the ionic stationary layer surrounding suspended particles. This information can provide insight into the magnitude of surface charge displayed by the suspended particles. In this case, bacteriophage are considered as suspended particles. Under application of an external electric field, particles will migrate towards the oppositely charged electrode at a certain velocity. This phenomenon, termed particle electrophoretic motility, allows for calculation of the particle zeta potential by applying Henry's equation:

Equation 3.2 - Zeta potential of bacteriophage

$$\upsilon_E = \frac{2\,\varepsilon\,Z\,f(ka)}{3\,\pi}$$

Where υ_E is the electrophoretic motility (μm cm $V^{-1}s^{-1}$), ε is the dielectric constant, Z is the zeta potential (mV), *f(ka)* is the Henry's function and η is the medium viscosity (cP).

Bacteriophage zeta potential values were obtained using a Malvern Zetasizer nano ZS90 (Malvern Instruments Ltd., UK) operating in zeta potential mode at 25°C. A zeta potential transfer standard reference (-42 mV) was used to validate instrument calibration prior to analysis (see Appendix III). Bacteriophage lysate solutions were diluted in filtered (0.2 μM pore size) deionised water to obtain a final concentration of 10^8 PFU/ml. Bacteriophage samples were then injected into DTS1070 folded zeta capillary cells for analysis. Mean data was obtained from a minimum of 5 replicates, each replicate being comprised of 10-100 runs, automatically determined by the software when stable readings were achieved. The pH of samples was 7.0 ± 0.2 in all cases.

3.2.8 Statistical analysis

The sizes of population data sets are expressed as (N) throughout this thesis, with values being reported as the mean averages ± standard deviation (SD), unless otherwise stated. All statistical analysis was conducted using GraphPad Prism version 8 (GraphPad Software, USA).

3.2.8.1 Student's t-test

Student's t-tests were used to compare mean zeta potential values for bacteriophage K, 44AHJD, T3 and T4. P values of < 0.05 indicate statistical significance.

3.3 Results

3.3.1 Plaque morphology

Bacteriophage were serially diluted and plated by plaque assay to assess plaque morphology. Plaques produced by all bacteriophage were circular of varying size (Figure 3.2a). Bacteriophage K plaques were between 1.5 mm and 2.0 mm in diameter, 44AHJD plaques were between 1.6 mm and 2.2 mm in diameter, T4 plaques were between 1.4 mm and 1.8 mm in diameter, and T3 plaques were between 5.5 mm and 7.2 mm in diameter. Large, 2 mm to 2.5 mm halo zones were observed around T3 plaques (Figure 3.2b), possibly indicating the diffusion of enzymatic molecules expressed by the bacteriophage. This characteristic was unique to the T3 bacteriophage.

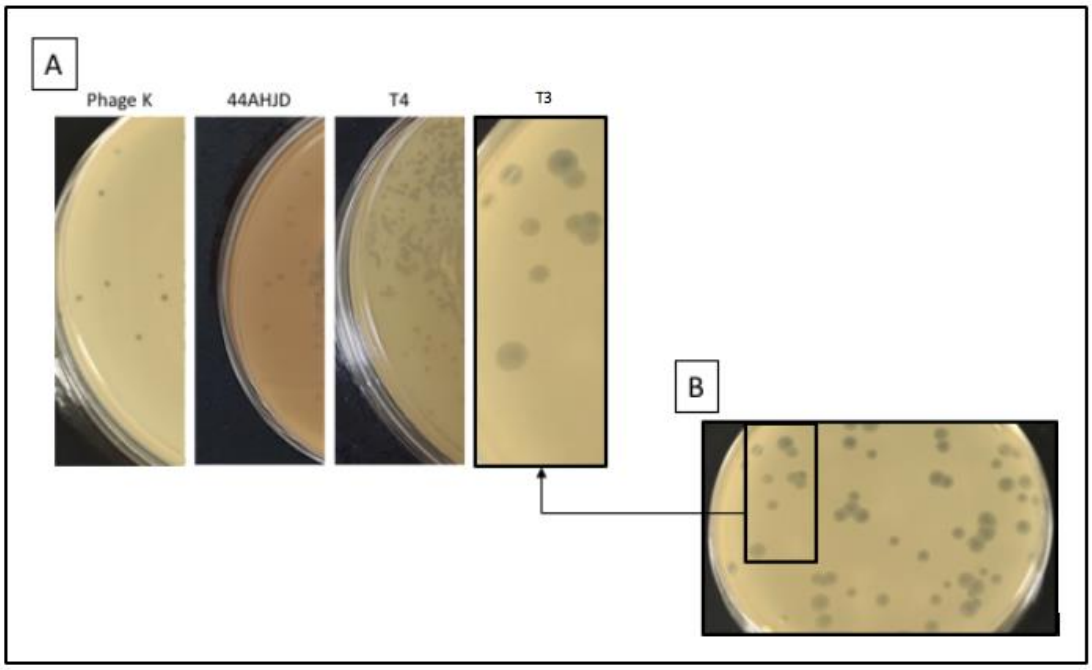

Figure 3.2 - Images of bacteriophage K, 44AHJD, T4 and T3 plaque morphologies on bacterial lawns (A). T3 plaques were larger with halo zones surrounding the plaques (b).

3.3.2 Bacteriophage morphology

The morphology of bacteriophage selected for use in this study was observed by TEM (Figure 3.3). Previously characterised bacteriophage K [164] and T4 [240] were confirmed as members of the *Myoviridae* family, while bacteriophages 44AHJD [174] and T3 [241] were confirmed as members of the *Podoviridae* family; based on morphological evaluation consistent with Ackermann classification [108]. All bacteriophage were of the order of *Caudovirales*. Bacteriophage T4, K, T3 and 44AHJD all had icosahedral heads approximately 86.7 nm, 96 nm, 60 nm, and 45.7 nm in diameter, respectively. T4 and bacteriophage K show long contractile tails of 120 x 19 nm, and 232 x 24 nm, respectively. No tail fibres were visible, however both T4 and bacteriophage K have clear baseplate structures at the terminal end of the tail. T3 and 44AHJD have short tails of approximately 10 x 7.5 nm and 17.4 x 6.5 nm, respectively. Baseplate structures were observed for 44AHJD; however, no such structures were observed for T3.

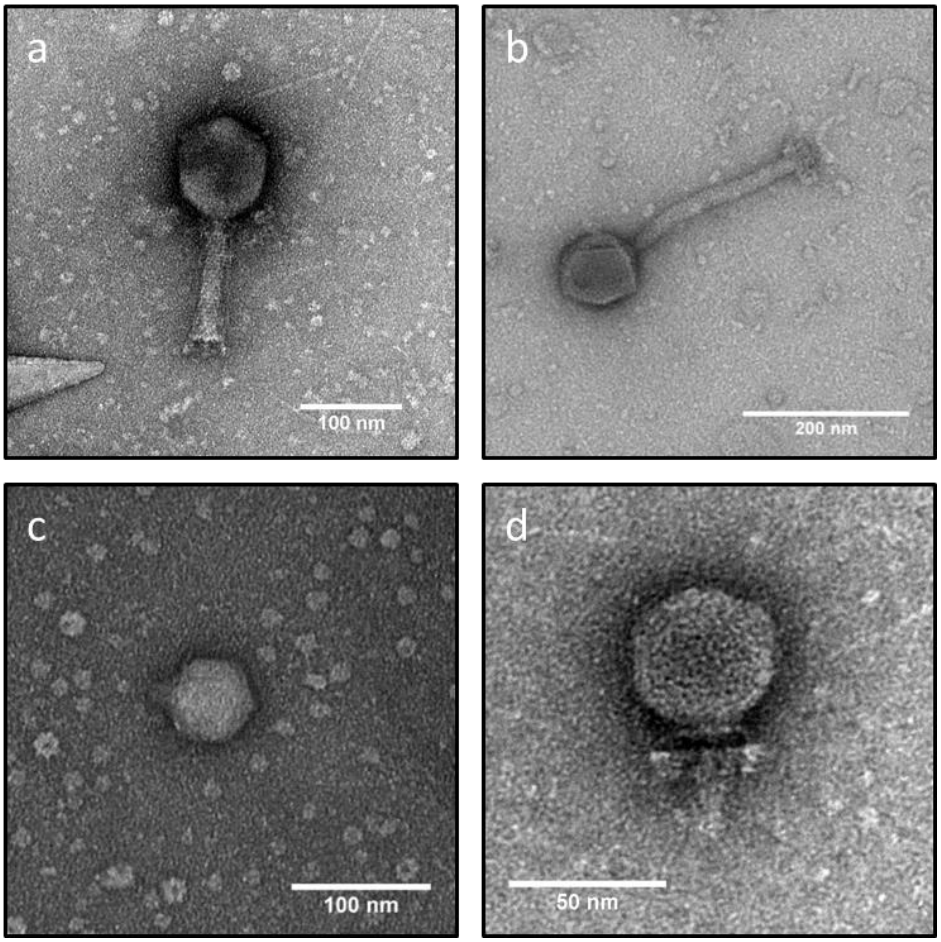

Figure 3.3 - Transmission electron micrograph images of bacteriophages T4 (A), bacteriophage K (B), T3 (C) and 44AHJD (D). Bacteriophage were purified by PEG precipitation prior to analysis. All samples were stained with 1% uranyl acetate. Scale is indicated by the bars.

Bacteriophage preparations from both *Myoviridae* bacteriophage showed the presence of separated capsids and tails on the TEM grid (Figure 3.4). This observation is typical of chloroform treated *Myoviridae* preparations due to release of viral components from lysed bacteria, prior to their complete assembly.

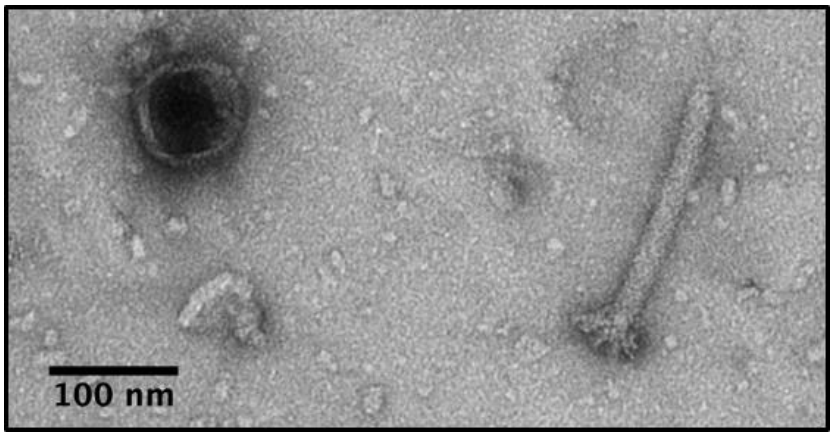

Figure 3.4 - Transmission electron micrograph image of separated bacteriophage K capsid and tail. Scale is indicated by the bar.

A small number of bacteriophage T4 were visualised with contracted tails and deformed capsids indicating release of genetic material triggered by an unknown stimulus (Figure 3.5).

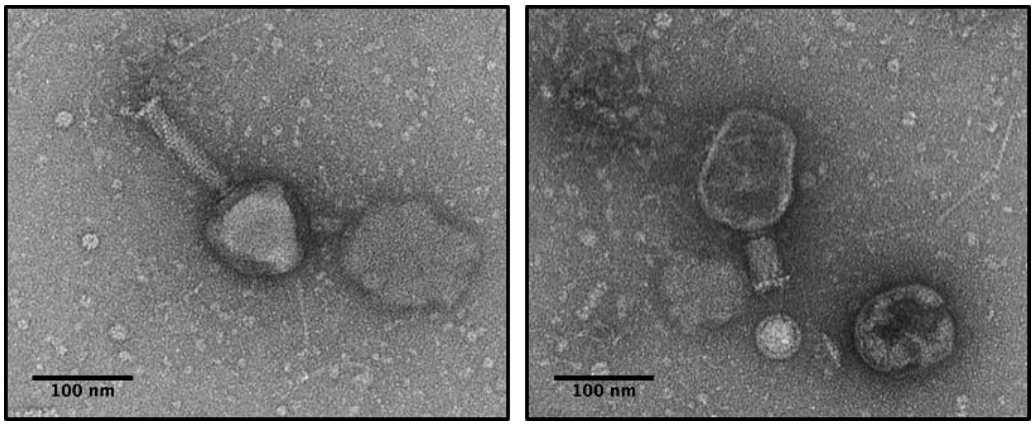

Figure 3.5 - Transmission electron micrographs of bacteriophage T4. (B) shows a bacteriophage with a contracted tail and deformed capsid. Scale is indicated by the bars.

3.3.3 Bacteriophage host range

The bacteriophage selected for use in this study were evaluated for their lytic activity against a small range of host strains. T3 and T4 were assessed against a total of twelve *E. coli* strains, while 44AHJD and bacteriophage K were assessed against a total of seventeen *S. aureus* strains, both comprising a mixture of reference culture collection strains and clinical isolates. Host range for all bacteriophage was determined by spot test method. Sensitivity was based on clear plaques (sensitive), evidence of regrowth (intermediate) or no evidence of bacterial lysis (resistant). An additional category of SI (sensitive/intermediate) was used due to the spectrum of susceptibility in intermediate strains. Representative plaques for each category (*E.*coli/T3) are shown in Figure 3.6.

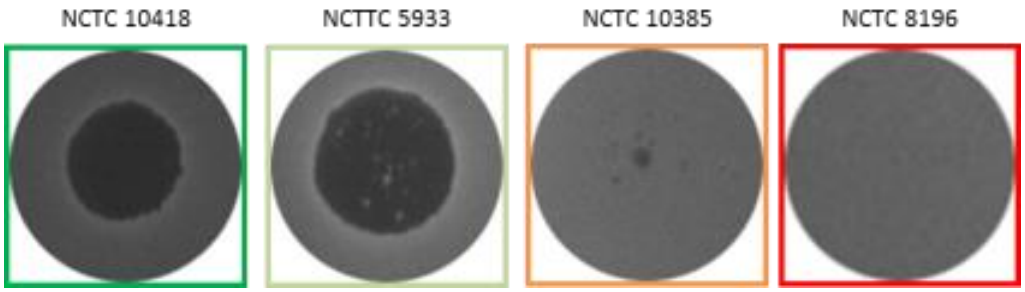

Figure 3.6 - Examples of *E. coli* strain sensitivities to bacteriophage T3 infection. Dark green: S, light green: SI, orange: I, and red: R.

Plaque morphology analysis during bacteriophage spot test sensitivity assays demonstrated the highly specific nature of phage activity. **R** bacterial strains demonstrated complete absence of bacterial lysis, **I** strains showed very limited areas of lysis, **SI** showed comparatively clear zones but with evidence of bacterial regrowth or resistant colonies, and **S** strains demonstrated clear zones with no evidence of bacterial regrowth or resistance. Table 3.1 and Table 3.2 show the sensitivity profiles of the four bacteriophage. Lytic activity was determined by the presence of plaques, this included bacterial strains in the **S**, **SI** and **I** categories. T3 showed the highest level of lytic activity against the strains tested, with 83.3% coverage. Both 44AHJD and phage K demonstrated 70.6% coverage and T4 as 50% coverage.

Table 3.1 - Sensitivity screening of bacteriophage T3 and T4 against a panel of 12 *E. coli* strains, including a clinical isolate (E. coli B3).

***E. coli* strain**	**T3**	**T4**
EPI-300	S	S
8196	R	R
10418	S	R
10240	SI	S
10385	SI	S
8545	S[Ł]	I
5933	SI	R
9270	I	R
8739	SI	I
12900	S	R
11303	S	S[Ł]
B3	R	R
% Resistant	16.7%	50%
% S/SI/I	83.3%	50%

* Dark green: Sensitive, light green: Sensitive/Intermediate, orange: Intermediate, and red: Resistant.

Ł Bacterial strains selected as bacteriophage hosts for future studies. Selection was based on the outcome of spot testing and plaque analysis.

Table 3.2 - Sensitivity screening of bacteriophage K and 44AHJD against a panel of 17 *S. aureus* strains, including 9 clinical isolates.

***S. aureus* strain**	**44AHJD**	**Phage K**
10788	S[I]	S
12702	R	S
13143 (EMRSA-16)	S	S
8511	I	SI
6538	S	SI
6571	I	S
12493	R	R
9518	S	SI
010	R	SI
06310	S	R
06311	S	R
06312	S	R
06313	R	S
06314	R	R
06315	S	S
MR027	SI	S[I]
MRSA16	SI	SI
% Resistant	29.4%	29.4%
% S/SI/I	70.6%	70.6%

* Dark green: Sensitive, light green: Sensitive/Intermediate, orange: Intermediate, and red: Resistant.

Ɨ Bacterial strains selected as bacteriophage hosts for future studies. Selection was based on the outcome of spot testing and plaque analysis.

3.3.4 Bacteriophage and host interactions under planktonic growth conditions

The infection of relevant bacterial broth cultures with bacteriophage K, 44AHJD, T4, and T3 was assessed by monitoring OD_{620} readings under planktonic growth conditions (Figure 3.7). Bacteriophage at MOIs of 0.1, 1, and 10 were introduced to bacterial cultures and incubated for 20 hours. Complete lysis of host bacteria at 20h was only observed for bacteriophage K/*S. aureus* MR027 cultures (MOI 0.1, 1 and 10); with some inhibition of bacterial growth evident after approximately 5 h (MOI 0.1 and 1), and complete inhibition of bacterial growth with MOIs of 10. T3, T4 and 44AHJD (incubated with their respective bacterial hosts) all showed near complete inhibition of bacterial hosts initially, followed by emergence of bacteriophage resistant mutants from approximately 10h, 14h and 14h, respectively. All MOIs of T3 and 44AHJD resulted in the emergence of bacteriophage resistant mutants, while only the lower MOI of 0.1 resulted in the same outcome for T4 infected cultures.

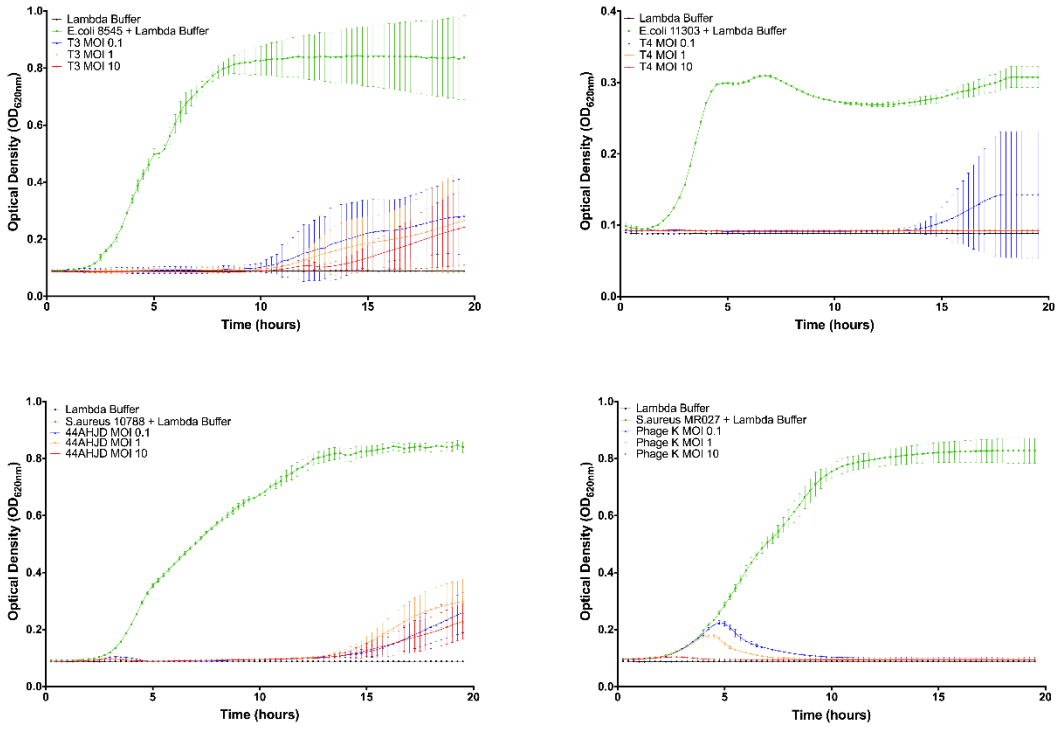

Figure 3.7 - OD growth curves for E. coli 8545 (top left), E. coli 11303 (top right), S. aureus 10788 (bottom left), and S. aureus MR027 (bottom right) incubated with bacteriophage T3, T4, 44AHJD and bacteriophage K, respectively (MOIs of 0.1, 1, and 10). Graphs show the mean values of five independent experiments (N-5) ± SD.

3.3.5 Bacteriophage growth characteristics

Adsorption efficacy of bacteriophage to their respective hosts was estimated by monitoring free bacteriophage reductions over a period of 10 min in early logarithmic bacterial cultures (Figure 3.8). Rate constants for loss of free phage were determined by fitting exponential decay curves; k' = 0.312 min^{-1} (phage K), k' = 0.336 min^{-1} (44AHJD), k' = 0.554 min^{-1} (T4), and k' = 1.106 min^{-1} (T3). After 5 min incubation 75% of phage K, 68% of T4, 78% of 44AHJD, and 93% of T3 were adsorbed to their host bacterium. Additionally, approximately 80% of T3 were adsorbed to the host strain within 2 min incubation.

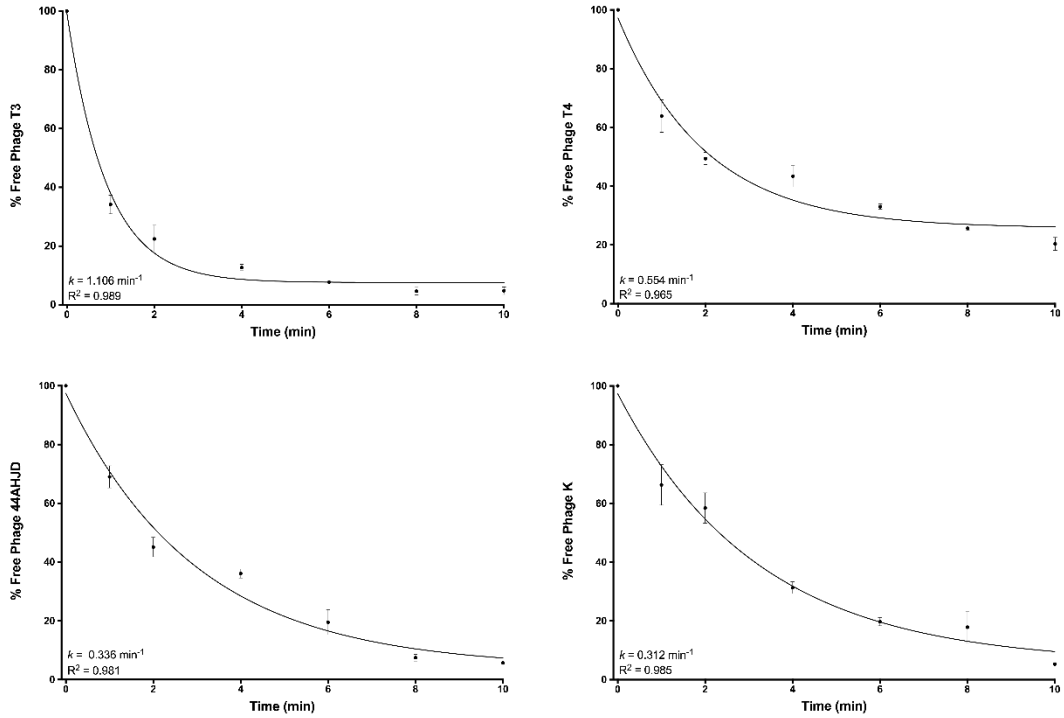

Figure 3.8 - Free phage concentrations of bacteriophage T3 (top left), T4 (top right), 44AHJD (bottom left) and bacteriophage K (bottom right), normalised to percentage of initial inoculum after exposure to host bacterial cultures at a MOI of 0.01 over a period of 10 min. Data points reflect mean data of three independent experiments (N=3) ± SD. Non-linear one-phase exponential decay curves were fitted using GraphPad Prism 5 software to obtain adsorption rate constants.

The growth parameters of T3, T4, 44AHJD and bacteriophage K were identified when grown with their respective host bacteria at 37°C using the one-step growth method (Figure 3.9). The eclipse period (E), latent period (L) and burst size (B) were determined by monitoring the number of free phage and total phage over a time period of 60 min. The latent and eclipse (L/E min) periods were 20/15, 25/15, 15/10 and 20/15 for T3, T4, 44AHJD and bacteriophage K, respectively. Burst sizes per infected cell were estimated at 438 PFU (T3), 181 PFU (T4), 121 (phage K) and 61 PFU (44AHJD).

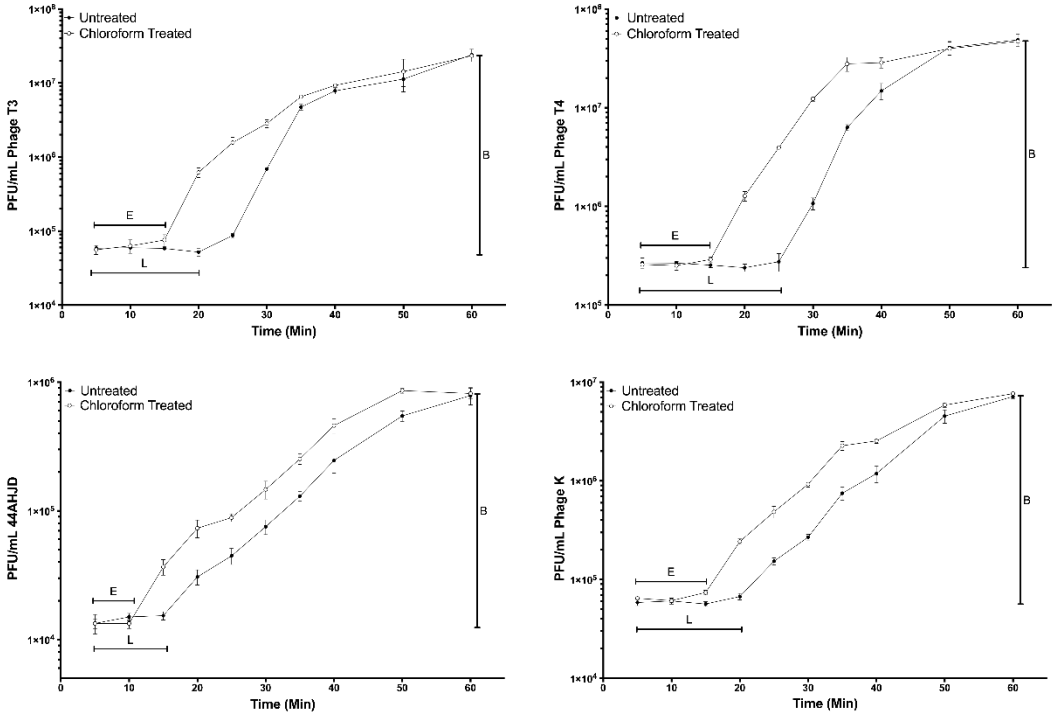

Figure 3.9 - One step growth curve data for bacteriophage T3 (top left), T4 (top right), 44AHJD (bottom left) and bacteriophage K (bottom right), at an MOI of 0.001. Chloroform treated samples show the total bacteriophage concentration and untreated samples show free bacteriophage concentrations. Data represents mean values from three independent experiments (N=3) ± SD. Eclipse period, latent period and burst size are denoted on the graphs by E, L, and B, respectively.

3.3.6 Zeta potential of bacteriophage

Net bacteriophage zeta potential values were determined by dynamic light scattering and electrophoretic mobility of viral particles at pH 7 (Figure 3.10). Zeta potential values (±SD) were -13.12 ± 1.71, -17.66 ± 1.01, -24.01 ± 2.84, and -16.65 ± 2.43 for bacteriophages T3, T4, 44AHJD, and bacteriophage K, respectively. All bacteriophage had negative zeta potential values, and with the exception of T4 vs. bacteriophage K, all differences were statistically significant ($P < 0.05$). Bacteriophage 44AHJD showed a significantly lower negative charge than the other bacteriophage tested ($P < 0.0001$).

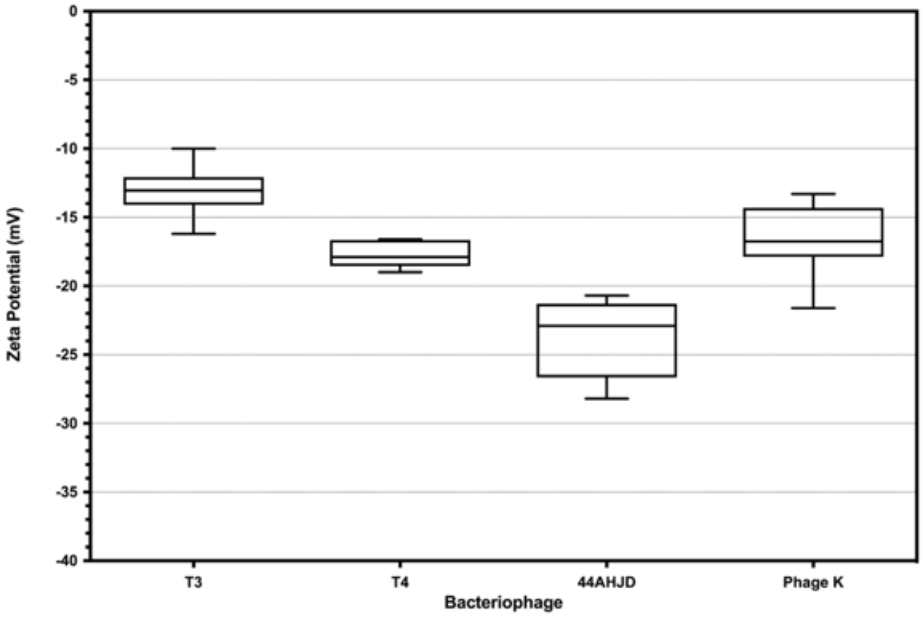

	T3	T4	44AHJD	Phage K
Average (mV)	- 13.12	- 17.66	- 24.01	- 16.65
SD	1.71	1.01	2.84	2.43

Figure 3.10 - Net zeta potential values for bacteriophage T3, T4, 44AHJD, and phage K. Zeta potential values were obtained at 25°C and pH 7 ± 0.2 in deionized water. Mean values from a minimum of five repeats (N=5), each comprising of 10-100 sub-runs.

3.4 Discussion

The work conducted in this chapter has resulted in the characterisation of four bacteriophages which demonstrated lytic activity against the common wound pathogens, *E. coli* and *S. aureus*. Lytic bacteriophage from both the *Myoviridae* and *Podoviridae* families were selected for each bacterial species; allowing comparison between morphologically distinct bacteriophage in further studies, which will focus on bacteriophage compatibility with wound dressing polymeric systems. Based on TEM analysis, bacteriophage K and T4 were confirmed as members of the tailed *Myoviridae* family. Bacteriophage 44AHJD and T3 were confirmed as members of the *Podoviridae* family, identified by the presence of short, non-contractile tails. TEM analysis of each bacteriophage selected showed homogenous morphologies, indicating purity of the bacteriophage preparations.

The plaques produced by both *S. aureus* bacteriophage (phage K and 44AHJD) were small and no visible halo zones were visible. The plaque morphology of bacteriophage T4 was similar, with similar size and no halo zones visible. Plaques produced by bacteriophage T3, however, were significantly different in their morphology. This bacteriophage produced larger plaques, and wide halo zones were visible. Halo zones have been documented as the hallmark feature of bacteriophage-encoded bacterial polysaccharide depolymerases [242]. These enzymes, responsible for the degradation of EPS, CPS or O-polysaccharide, freely diffuse through the soft agar at a higher rate than bacteriophage and can be an integral component of virion particles, or released during bacterial lysis [154]. Enzymatic degradation results in the turbid halo zones as bacteriophage are not actively propagating, therefore producing regions atypical of a plaque produced by bacterial lysis. The presence of halo zones may be advantageous in the selection of bacteriophage for therapeutic applications, due to the intrinsic ability of these bacteriophage to disperse bacterial biofilms and so have the potential to be used as a treatment for chronic bacterial infection where biofilms may be a pathological feature [243].

Plaque size is often considered to be directly proportional to the virion diffusivity in the soft agar, adsorption rate, latent period, burst size, and host density [244]. Higher diffusivity within the cross-linked agar matrix would result in bacteriophage moving further outward during propagation. The contribution of adsorption rate is, however, more complex. The general consensus is that there is an optimal adsorption rate which results in larger bacteriophage plaques [245]. The influence of bacteriophage latent periods seems to be negatively correlated with plaque size, due to the longer period of time in which the bacteriophage is interacting with the bacterial host prior to lysis. A high burst size produced

by a bacteriophage can produce larger plaque sizes, however it has been shown that the impact of burst size diminishes at high bacteriophage levels [246].

Perhaps one of the most important characterisation stages of a bacteriophage is determining the host range; the spectrum of bacteria which the bacteriophage can productively infect. While there are numerous potential methods including plaque and broth-based assay, this parameter is commonly deduced by the simple and rapid spot test assay, where a small volume of concentrated bacteriophage is placed on a lawn of bacteria. The results, however, can often be misleading and potentially result in either an over-or under-estimate of the true spectrum of the bacteriophage lytic range, depending on the methodology used. For example, the spot test assay may provide false positives due to the exposure of high titre bacteriophage preparations inducing lysis from without, a phenomenon where infection of a single bacterium by multiple bacteriophage, or exposure to residual endolysins in the bacteriophage stock, causes bacterial lysis without bacteriophage propagation [247]. Prior to host range determination, it is crucial to conduct a minimum of three rounds of bacteriophage plaque purification to reduce the probability of a heterogenous bacteriophage population producing a broader host range [248]. To-date there is no generally accepted standard procedure for determining bacteriophage host range other than to explicitly state the method of determination and acknowledge the limitations of that technique [248]. With this in mind, data from this study suggests bacteriophage K, 44AHJD, and T3 have broad host ranges of 70.6%, 70.6%, and 83.3% of the potential hosts tested, respectively. Bacteriophage T4 was shown to have a more limited host range at 50%. It should be noted, however, that these values were based on small bacterial sample sizes (12 *E. coli* isolates and 17 *S. aureus* isolates), largely restricted by the available bacterial culture collection. Further studies using a large collection of clinical bacterial isolates would provide more robust data on the host range of the bacteriophage.

Table 3.3 shows the growth characteristics of all four bacteriophage, obtained from various studies. Due to bacteriophage K, 44AHJD and T4 producing plaques of similar size and morphology, one should look at other differences between these bacteriophage and bacteriophage T3 to determine the source of the significant difference in plaque morphology produced by this bacteriophage. From Table 3.3 it is evident that the eclipse and latent periods of T3 are similar to that of the other bacteriophage under investigation. The burst size and adsorption rate constant of bacteriophage T3, however, are notably higher at 438 PFU/infected cell and 1.106 min^{-1}, respectively. This suggests that the individual characteristics, or combined effect, of high burst size and efficient adsorption may be responsible for the large plaque size produced by T3. This combination may be of high interest in the use of bacteriophage as a therapeutic agent, as both characteristics may

increase the probability and speed at which the bacteriophage and their progeny reach the target bacteria, reducing and hence optimising lysis time [249]. In addition to this, if the bacteriophage is able to lyse bacteria faster than they can replicate, a high burst size may reduce the emergence of bacteriophage-resistant bacteria [248]. However, while these traits may prove desirable in static double-agar and planktonic assays, it has been shown that high adsorption rates can be detrimental to bacteriophage fitness in biofilm environments due to the lack of adaptation potential [250].

While this is the first study which outlines adsorption and growth data for bacteriophage 44AHJD, comparisons can be drawn between values obtained for bacteriophage K, T3 and T4, with that of published literature. Bacteriophage T4 is one of the most extensively studied bacteriophage [251] and therefore data relating to its growth characteristics are readily available. Published data for T-even bacteriophage suggest latent periods (L) of 25 – 30 minutes and eclipse periods (E) of approximately 10 minutes [252], while burst size (BS) experiments suggest values in the region of 130 PFU/infected cell [253]. These values align with those reported in this study for bacteriophage T4; L: 25 minutes, E: 15 minutes, and BS: 181 PFU/infected cell. Bacteriophage T3, however, demonstrated a shorter latent period and significantly higher burst size than bacteriophage T4. These findings align with reported values in the literature [254]. Deviations from these values can be explained by the use of supplemented media [255], host cell density [252], and host growth rate [256]. A recent study conducted by Alves *et al* (2014) described the growth characteristics of bacteriophage K, reporting values of; L: 20 minutes, E: 15 minutes, and BS: 125 PFU/infected cell [171]. These data are in conformity with the values obtained in this study for bacteriophage K; L: 20 minutes, E: 15 minutes, and BS: 121 PFU/infected cell. The aforementioned study also reported the adsorption rate constant (*k'*) of bacteriophage K as 0.352 min^{-1} [171], which conforms with the data presented in this study (*k'* = 0.312 min^{-1}).

Table 3.3 - Summary of bacteriophage growth characteristic data from adsorption, one-step growth, and burst size investigations.

Bacteriophage	Eclipse Period (min)	Latent Period (min)	Burst Size (PFU/infected cell)	Adsorption Constant (min^{-1})
T3	15	20	438	1.106
T4	15	25	181	0.554
44AHJD	10	15	61	0.336
Phage K	15	20	121	0.312

The planktonic growth of bacterial hosts in the presence of bacteriophage was monitored by observing bacterial growth (optical density) over a 20h period. While agar plate-based assays provide insight into bacteriophage infectivity in static conditions, planktonic growth experiments were conducted to determine the efficacy of bacteriophage administration in a dynamic environment. Under dynamic conditions, bacteriophage adsorption is lessened due to the bacteriophage only initiating infection upon random encounters with host bacteria. Investigating bacteriophage infectivity in these conditions also allows for the identification of mutation events in both bacteria and bacteriophage over time, thus allowing selection of bacteriophage which are able to overcome the emergence of bacteriophage-resistant bacterial mutants. Planktonic growth data for bacteriophage *E. coli* podovirus, T3, demonstrated the emergence of bacteriophage resistant bacterial mutants, in a concentration dependent manner, after approximately 10 hours incubation (MOIs of 0.1, 1 and 10). From 0 hours to 10 hours incubation, T3 was shown to inhibit all bacterial growth and re-growth of bacterial mutants resistant to T3 infection was lower than that of the untreated bacterial culture. The other *E. coli* specific bacteriophage, T4, was shown to completely inhibit bacterial growth over a 24h period at MOIs of 1 and 10, with bacteriophage resistant mutants only identified after approximately 14 hours incubation at a MOI of 0.1, which plateaued rapidly at approximately 17 hours incubation. Of the *S. aureus* bacteriophage, bacteriophage K demonstrated highly desirable characteristics under planktonic conditions. All MOIs (0.1, 1, and 10) resulted in the complete absence of bacterial growth at 20 hours incubation. While an MOIs of 0.1 and 1 allowed a low level of growth at approximately 3-4 hours incubation, inhibition was noted at approximately 5 hours incubation and no bacterial regrowth was evident subsequently. The phenomenon of bacterial regrowth in this case is unlikely to be due to the emergence of bacteriophage resistant bacterial mutants, but rather the requirement for the propagation of bacteriophage at lower doses to achieve the concentration required for bacterial clearance and inhibition. Conversely, *S. aureus* podovirus 44AHJD demonstrated complete bacterial inhibition from 0-14 hours incubation, with the emergence of bacteriophage-resistant mutants evident at 14-20 hours incubation. Data from these investigations demonstrate the importance of selecting bacteriophage able to adapt to the highly dynamic nature of bacterial mutation, the administered concentration of bacteriophage, and the development of bacteriophage cocktails. This study showed differences in efficacy between two bacteriophage lytic against the same bacterial species, and that the level of bacterial regrowth can be influenced by the factor of bacteriophage MOI. Bacteriophage cocktails, formulations containing a number of bacteriophage specific to the host species, have not only been shown to broaden the host range, but also prevent and delay bacterial mutations which confer resistance to the bacteriophage [257]. Unfortunately, preliminary investigations into the development of bacteriophage cocktails

utilising the bacteriophage used in this study were unable to prevent the emergence of bacterial mutants. The development of bacteriophage libraries containing an array of bacteriophage and their respective data will be of high importance in the future development of effective bacteriophage cocktails for therapeutic applications.

Perhaps a lesser studied characteristic of bacteriophage is the surface charge, or zeta potential. This characteristic becomes of importance when studying the adsorption of bacteriophage to bacteria [258, 259] and the development of bacteriophage-mediated antimicrobial materials [200]. In this study the latter will be explored, and therefore the zeta potential of bacteriophage is an essential characterisation step for future studies focused on electrostatic interactions between the bacteriophage and wound dressing materials. Both bacteria [260] and bacteriophage [200] have been reported to carry a net negative surface charge. However, the individual surface charge of bacteriophage capsids and tail fibres have been reported as negative and positive, respectively [200], allowing for bacteriophage attachment to bacterial cells. This study has investigated the net charge of the four bacteriophage, with net negative surface charges ranging from -24.01 to -13.12. These values could be of high importance when investigating charge-based adsorption of bacteriophage to candidate wound dressing materials.

To date, considerations of bacteriophage characteristics seldom relate to the complexity of the *in vivo* treatment of bacterial infections. While researchers can isolate bacteriophage which are lytic against a given clinical pathogen, assess the host range, develop bacteriophage cocktails to reduce the incidence of bacteriophage resistance and consider practicalities such as bacteriophage stability; it is unclear to what extent growth parameters are compatible with therapeutic success [261]. Bacteriophage therapy is now developing in a methodical, controlled manner, a stark contrast to the pre-antibiotic era where misleading information during bacteriophage characterisation lead to many unsuccessful clinical trials. With a better understanding of bacteriophage-host interactions, and developments in technical approaches to bacteriophage characterisation, bacteriophage therapy may advance further towards regulatory approval.

Chapter Four: Biomaterial synthesis and characterisation

4 Biomaterial synthesis and characterisation

As bacteriophage therapy research progresses, it has become increasingly important to consider delivery of bacteriophage to the target site; an area of research which has to-date received limited attention. This chapter outlines attempts to synthesise and characterise candidate materials suitable for wound dressing applications, with the potential for incorporating or immobilising the bacteriophage identified in Chapter 3; to produce antimicrobial biomaterials targeted against common wound pathogens.

4.1 Background

4.1.1 Base material - PLAg

Plasticised agarose films (PLAg) were identified as a candidate material, prepared with a method previously described by Shamsuri *et al* (2012) [262]. Agarose hydrogels form strong yet brittle films upon dehydration, while hydrated agarose gels are too fragile for use as a wound dressing material. To address these issues plasticisers were utilised to produce highly flexible and strong agarose films following dehydration of the gel. The base polymer, agarose, is a commonly used laboratory material in molecular biology for gel electrophoresis and protein purification. With intrinsic biocompatibility, natural abundance, biodegradability and non-toxicity it seemed prudent to identify a plasticiser with similar desirable characteristics.

As concerns relating to conventional plasticiser safety and toxicity have arisen, research has focused on alternative plasticisers and ionic liquids derived from natural sources. Ionic liquids are a mixture of cations and anions which possess a number of unusual and desirable characteristics [262]:

- Environmentally/chemically inert
- Non-volatile
- Low melting point (<100°C)
- Highly polar
- Non-flammable
- Miscible with water
- Modifiable
- Disrupt bacterial biofilms [263]

Common ionic liquid plasticisers include imidazolium, pyridinium and phosphonium based plasticisers, which are expensive due to the high cost of precursors and difficult to produce [264]. An alternative is the use of eutectic ionic liquids (or deep eutectic solvent (DES)); defined as a mixture of substances in fixed proportions with a lower melting point than either of the individual components [262]. Eutectic solvents are produced by a complexation reaction between quaternary ammonium salts and a complexing agent such as metal chlorides or a hydrogen bond donor.

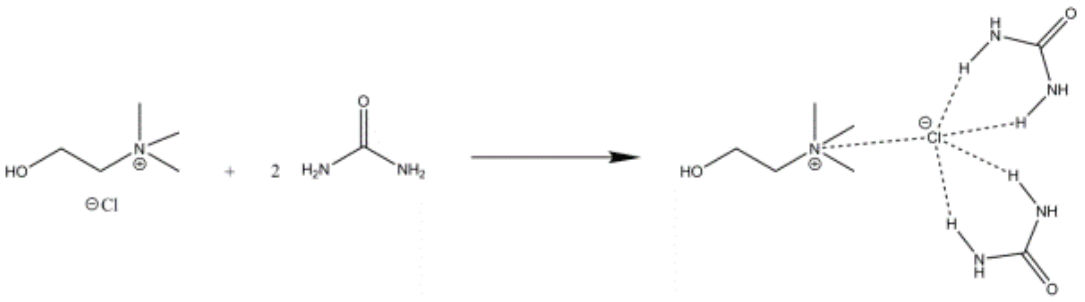

Figure 4.1 - Schematic of the complexation reaction between choline chloride and urea (1:2M ratio).

In this study a choline chloride/urea based eutectic solvent was identified as a suitable plasticiser candidate due to its ease of preparation, cheap production cost, biodegradability and biocompatibility [265]. Choline chloride is a widely used additive in the agricultural industry, whilst urea is a common additive in dermatological products to promote rehydration [266]. The complexation reaction to produce this eutectic solvent is outlined in Figure 4.1. Addition of a choline chloride/urea based eutectic solvent with agarose has been reported to produce flexible and transparent films upon dehydration [262]; utilising the films for the application as a wound dressing, however, requires further characterisation and optimisation. This chapter therefore aims to investigate specific parameters unique to the novel application, building on the initial research conducted by Shamsuri *et al* (2012) [262].

4.1.2 Surface modification of PLAg

It has been reported in the literature that bacteriophage T4 and T7 capsids acquire a negative charge above pH 4, with the tail fibres presenting a positive charge [200]. In a separate study conducted by Esteban *et al* (2016) [259] it was reported that phage K possessed an overall net negative charge, however no investigation was made into the charge difference between the capsid and tail fibres. Agarose carries a net negative charge, primarily due to

the charged sulphate and pyruvate residues on the polysaccharide. With this in mind, spontaneous adsorption of bacteriophage to the film interface would theoretically be via ionic attraction of positively charged tail fibres with agarose, restricting access of these infective components to bacterial receptors and thus reducing the potential infectivity of the film. To counteract this problem, a cationic polymer was identified to produce a positively charged interface for selective bacteriophage capsid adsorption (Figure 4.2). Poly(vinyl amine) (PVAm) is a highly charged cationic polymer with the highest amine content of any polymer [193]. Only recently commercially available and primarily used in the agricultural and paper making industries, this polymer is becoming of considerable interest for many other applications.

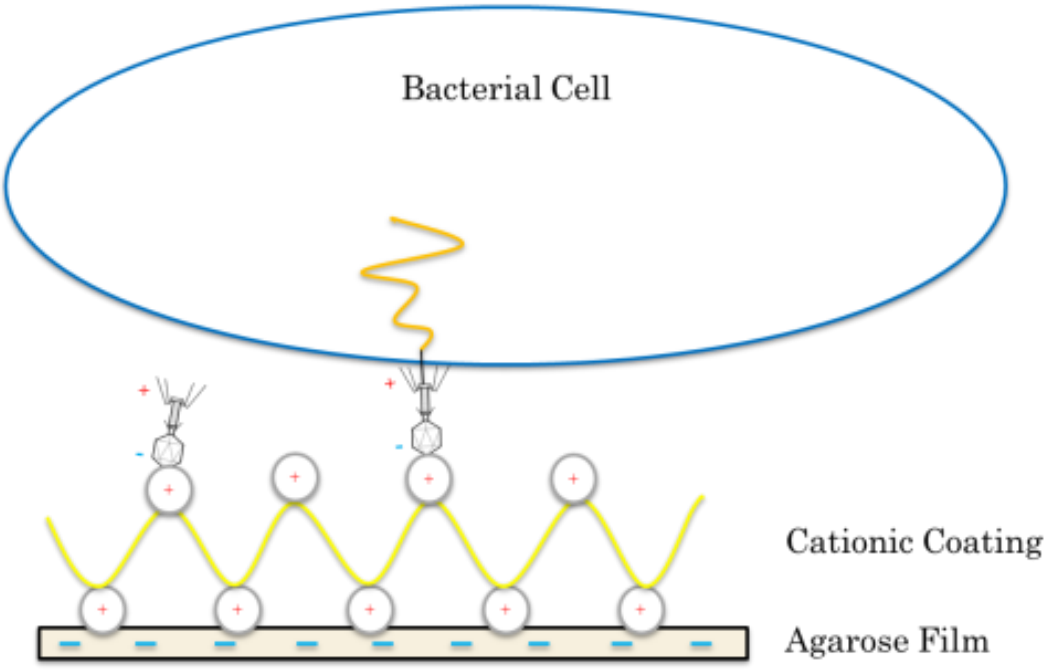

Figure 4.2 - Theoretical representation of cationic surface modification with PVAm and orientated attachment of bacteriophage to the film interface.

Owing to the lack of commercially available laboratory grade PVAm, purification of the industrial grade product was necessary. Impurities generally consisted of N-vinylformamide precursor and the formic acid side product of hydrolysis. A combined hydrolysis and dialysis purification procedure was employed to ensure sufficient purity for the proposed application. Hydrolysis would ensure complete conversion of N-vinylformamide precursor to N-vinylamine, while exhaustive dialysis removed impurities produced by hydrolysis.

Subsequently, the purified end product was chemically characterised to provide evidence of efficacy relating to the purification method. Once verified, numerous methods of PLAg film coating were evaluated, primarily based on preliminary bacteriophage adsorption assays. The selected coating method was then carried forward for further characterisation and assessed for suitability for bacteriophage adsorption studies.

4.1.3 Alg-PVAm-PLAg composite material

While orientated immobilisation of bacteriophage at the surface of substrates provides distinct advantages in the preparation of antimicrobial biomaterials, these viral particles can consequently be left exposed to the external environment, risking their inactivation prior to clinical application. For this reason, composite materials were developed utilising the base material and surface modification platform described previously. An alginate hydrogel layer was attached to the surface of modified PLAg (PVAm-PLAg) films, providing a hydrated matrix encapsulating viral particles, which would subsequently be released upon application of the composite material to the wound site (Figure 4.3).

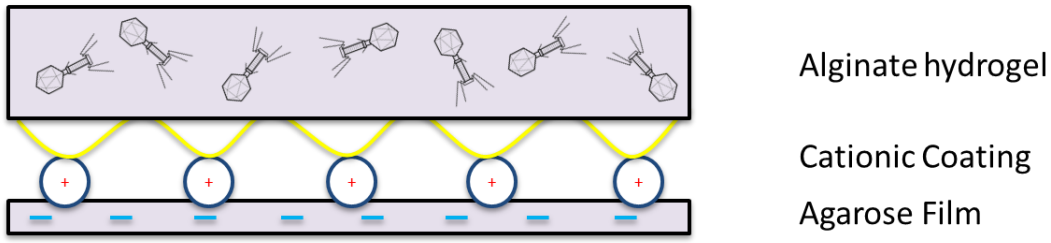

Figure 4.3 – Schematic representing a bacteriophage loaded composite material, where bacteriophage have been entrapped within a protective alginate hydrogel layer.

While synthesis of alginate gel beads using $CaCl_2$ is widely used and has been employed for the formation of encapsulated bacteriophage alginate beads [267-270], this method relies on the ability of $CaCl_2$ to cross-link the alginate polymer instantaneously upon exposure to the polyvalent cation. This method results in the formation of highly heterogenous hydrogels with structural characteristics which are hard to control (i.e. cross-linking density and a polymer concentration gradient) [271]. For the development of the composite material, a more controlled approach was necessary for the entrapment of bacteriophage and adherence of the alginate layer to the modified base material. Therefore, two alternative methods of alginate cross-linking were assessed: oxidation of Fe(II), and a $CaCO_3$/GDL system.

The controlled formation of alginate hydrogels can be achieved by manipulating the oxidation state of iron cations dispersed in alginate. Chemical or electrochemical oxidation of Fe(II) cations to Fe(III) in the presence of sodium alginate has been shown to result in the controlled formation of alginate hydrogels [233, 271]. Due to the decreased ability of Fe(II) to form cross-links with sodium alginate, dissolution of iron cross-linked hydrogels can be induced by oxidative decarboxylation of Fe(III) complexes with carboxylic acids using long wave UV or visible light [233], allowing the potential triggered release of compounds contained within the hydrogel. Furthermore, Fe(II) cross-linked alginate hydrogels have been shown to promote cell proliferation of human dermal fibroblasts [272].

Alginate hydrogels may also be cross-linked by the *in situ* release of Ca^{2+} cations from $CaCO_3$, induced by the hydrolysis of D-glucono-δ-lactone (GDL) to gluconic acid. In aqueous solution with alginate and a calcium salt, the slow hydrolysis of the proton donor, GDL, results in the release of Ca^{2+} by protonation of $CaCO_3$. This method of controlled alginate cross-linking is achieved due to the low solubility of $CaCO_3$ allowing uniform distribution within the alginate solution followed by slow gelation. The gelation of alginate using the $CaCO_3$-GDL system has been used to produce structurally uniform hydrogels for tissue engineering applications [273].

Once both alginate hydrogel cross-linking systems were assessed and optimised, composite materials were produced by attachment of alginate hydrogels to PVAm modified PLAg to produce mechanically robust materials with the potential to contain bacteriophage within the hydrated alginate matrix.

4.2 Methods

The synthesis of PLAg, PVAm-PLAg and Alg-PVAm-PLAg is described in Section 2.2.2, Section 2.2.3, and Section 2.2.4, respectively.

4.2.1 SEM and EDS analysis

4.2.1.1 Principles of SEM

Scanning electron microscopy (SEM) is a routinely used technique with the ability to provide valuable information about a specimen's surface topography by providing pseudo three-dimensional micrographs. Images of specimens are produced by interactions of a highly focused beam of electrons with the conductive surface atoms of the specimen. An electron beam is emitted from the electron gun which passes through condenser lenses (typically one or two), which then focus the beam (0.5nm – 5nm) on the specimen surface. Scanning coils or deflector plates in the electron column deflect the electron beam on the *x* and *y* axes, allowing scanning of the specimen in a raster fashion. Upon interaction of the electron beam with the sample surface the electrons lose energy by back scattering and absorption. This energy exchange results in elastic scattering (direct reflection of electrons with no change in energy state), inelastic scattering (low energy electron absorption and reemission) and emission of electromagnetic radiation typically in the form of X-rays – detected using specific detectors within the SEM instrument. In order for the above principles to work in practice, samples must be conductive to allow interactions of the electron beam with the specimen and to prevent the accumulation of electrostatic surface charge and subsequent thermally induced damage. Samples which do not display these properties can be coated with a thin layer of conductive material, such as platinum, prior to analysis [274].

4.2.1.2 Principles of EDS

Energy dispersive X-ray spectroscopy (EDS) is a supplementary analytical technique to SEM that allows elemental analysis and chemical characterisation of the specimen surface. This technique relies on the principle that under an electron beam, each element will emit a unique and characteristics spectrum of X-rays. The excitation of electrons in a low-energy atomic orbital when exposed to an incident electron beam may cause ejection from the atom and form an 'electron hole' which is simultaneously filled by an electron from an outer high-energy orbital. The excess energy is emitted as characteristic X-rays which is then

recorded as energy (eV) versus intensity (counts per second), allowing the elemental composition of the specimen to be characterised [275].

4.2.1.3 SEM and EDS methodology

SEM and EDS were used to visualise the surface morphology and elemental surface composition of PLAg and PVAm-PLAg films. Film segments were fixed using 2.5 % glutaraldehyde in sodium cacodylate buffer (pH 7.4) for 1 h. Segments were then rinsed three times in sodium cacodylate buffer and dehydrated in increasing concentrations of ethanol (25 %, 50 %, 75 % and two washes in 100 %) for 15 min per wash at room temperature and atmospheric pressure. Fixed, dehydrated segments were then sputter coated with 4nm platinum (Quorum Q150T ES Turbo Pumped Coater Device) and mounted with Leit-C carbon mounts. Film surface topographies were observed at 10,000x to 150,000x magnification and 5kV accelerating voltage on a Zeiss-Sigma-300 field emission gun scanning electron microscope (FEG-STEM) operating in SEM mode using secondary electron detection.

Elemental analysis of uncoated and PVAm modified PLAg films was conducted alongside SEM imaging using a Zeiss Sigma FEG-SEM scanning electron microscope equipped with an 80 mm^2 X-Max energy dispersive X-ray analysis system (Oxford Instruments, UK).

4.2.2 MTS cytotoxicity assay of PLAg leachate

MTS assays were used to determine the cytotoxicity of plasticiser leachate from PLAg films. Prior to conducting the MTS (3-(4,5-dimethylthiazol-2-yl)-2,5-diphenyltetrazolium bromide) assay, 3T3 fibroblast cells (ATCC CRL-1658) were cultured in Dulbecco's Modified Eagle Medium (DMEM; ThermoFisher, UK) supplemented with 10 % Fetal Bovine Serum (FBS; ThermoFisher, UK) at 37°C and 5 % CO_2. PLAg leachate test solutions were prepared by placing pre-prepared and sterilised (UV for 15 min each side) PLAg films into individual wells of a 6-well plate containing 2 ml of DMEM/FBS medium. The 6-well plate was then incubated at 37°C for 24 h to allow plasticiser to leach from the film into the cell culture medium. Tin maleate leachate was collected in the same manner and used as a positive control due to its known cytotoxic properties. After incubation, the leachate was removed from each well and filtered (0.2 μm pore size) to ensure sterility. Fibroblast cell suspensions were then seeded in 96-well plates at a density of 5 x 10^3 cells per well in 100 μl DMEM + FBS and incubated at 37°C and 5 % CO_2 for 24 h. The culture medium was then replaced with 100 μl of the pre-prepared and pre-warmed (37°C) medium

containing plasticiser leachate and incubated for 24 h at 37°C and 5 % CO_2. 8 wells were used for each leachate extract and wells without leachate served as the cell control. A total of 32 wells were used for each treatment group (PLAg and tin maleate leachate), comprised of 8 wells for each 4 samples. After 24 h incubation of cells with PLAg leachate, 20 µl of CellTiter 96 AQueous One Solution reagent (Promega, UK) was pipetted into each well of the 96-well plate and incubated for 4 h at 37°C in 5 % CO_2. The absorbance of each well was then recorded at 490 nm and cell viability calculated using the following equation:

Equation 4.1 - Cell viability by MTS assay

$$Cell\ viability\ (\%) = \frac{absorbance\ of\ sample}{absorbance\ of\ control} \times 100$$

4.2.3 FTIR spectroscopy

4.2.3.1 Principles of FTIR

Infrared (IR) spectroscopy allows for the identification and study of chemicals present in a solid, liquid or gas sample, by interaction with infrared light. The wavelength of the infrared portion of the electromagnetic spectrum is approximately 10 cm^{-1} (adjacent to the microwave region) to 4000 cm^{-1} (approaching the visible light region). Irradiation of IR light through a sample results in vibration of bonds and functional groups, allowing determination and evaluation of chemical composition. A narrow spectrum can be produced using a monochromator, however Fourier transform (FTIR) instruments are more commonly used to investigate IR absorbance across the entire IR spectrum. FTIR instruments direct IR light through an interferometer, a moving mirror inside the instrumentation then alters the distribution of IR light through the sample. Raw data is then converted from light output signal to wavelength (or wavenumber) by Fourier transform, a data processing technique.

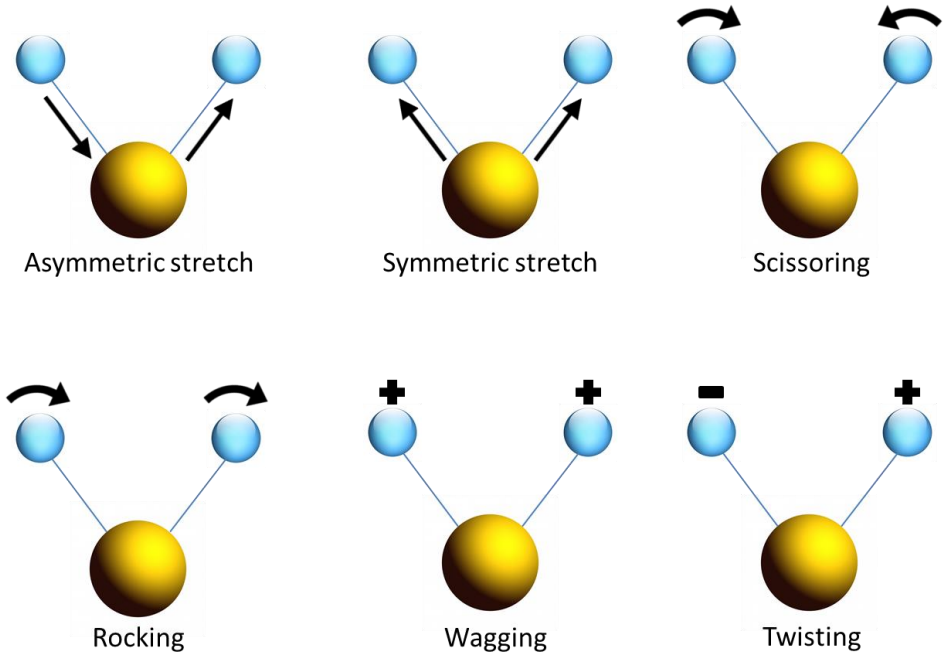

Figure 4.4 - Representation of the vibrational modes of a molecule upon exposure to infrared light.

The energy of molecular vibration only allows a molecule to vibrate at certain frequencies, resulting in a number of vibrational modes illustrated above (Figure 4.4). When exposed to IR radiation, if the frequency matches one of the sample vibrational modes it will absorb energy and the vibrational energy state will increase. These molecules are considered to be IR active, however it is important to note that some vibrations are IR inactive such as stretching of symmetrical double and triple bonds. This is due to the lack of change in dipole moment, a prerequisite for absorption of IR light.

The output spectrum of FTIR delivers data as transmittance % (vertical axis) against wavenumber cm^{-1} (horizontal axis). Peaks can then be assigned to the presence of functional groups with characteristic vibrational modes at specific frequencies. Towards the lower end of the spectrum (500 to 1500 cm^{-1}) is the fingerprint region; an often-complicated series of absorptions used to identify patterns characteristic of complex compounds [276].

FTIR was used throughout this study to determine the composition of solid and liquid samples. The presence and absence of functional groups was important in the characterisation of purified polymers and candidate materials.

4.2.3.2 FTIR methodology

Dependant on sample formulation, preparation for FTIR followed one of two routes. Aqueous samples were concentrated using a rotary evaporator, while solid samples were dried rigorously (60°C atmospheric pressure) prior to analysis. The FTIR spectrometer was then blanked with solvent (aqueous sample) or air (solid sample) to correct for background absorption. Measurements were then taken using a PerkinElmer 65 FTIR spectrometer equipped with a universal attenuated total reflectance (ATR) sampling accessory, linked to the PerkinElmer Spectrum ES software analysing from 650 – 4000 wavenumbers (cm^{-1}). The produced spectrum was based on vibrational frequencies of bonds when exposed to infrared light allowing determination of functional groups.

4.2.4 NMR spectroscopy

4.2.4.1 Principles of NMR spectroscopy

Nuclear magnetic resonance (NMR) spectroscopy is a technique which can be used for determination of molecules within a substance; specifically used for the analysis of molecular structure. NMR exploits the intrinsic quantum spin states of protons and utilises an applied magnetic field to determine the amount of energy required to bring them into the resonant state.

Both protons and electrons have one of two quantum spin states, here designated as $+\frac{1}{2}$ and $-\frac{1}{2}$; having equal energy in the absence of an applied magnetic field. When a magnetic field is applied, a proton's magnetic moment either aligns parallel or antiparallel to the magnetic field; entering a low-energy (ground) or high-energy (excited) state, respectively. The difference between both states increases with application of a stronger magnetic field and protons in the ground state can then be excited by irradiation by radio frequencies. Once in the excited state the magnetic field is removed and molecular nuclei return (relax) to the ground state, emitting a photon which is detected by the NMR and produces spectral lines. Electron shielding reduces the effect of the magnetic field on proton spin, consequently reducing the difference between the ground and excited state. This causes a shift (in ppm) of the NMR frequency, allowing the determination of chemical structure using NMR based on the electron density distribution in the molecular orbitals [277].

NMR spectroscopy was used to validate purification processes utilised in this study and to determine the molecular composition of samples subsequent to chemical alteration. This technique was used in conjunction with FTIR to provide more detailed analysis of PVAm.

4.2.4.2 ^{1}H-NMR analysis of purified PVAm

5-10 mg of purified freeze-dried PVAm was dissolved into 1 mL of deuterated solvent (D_2O) and left to disperse completely for 24 h. The sample solution was then transferred to a 7", 400 MHz NMR tube (Wilmad-Labglass, USA) and capped with a PTFE lid. The tube was then placed in a spinner turbine ensuring the sample solution was positioned across all inner coils of the spectrometer. The Topspin© software was set at 16 run scan analysis at 400 MHz. Proton environments indicated by chemical shift in ppm, outlined by the output spectra, were then evaluated; allowing structural interpretation and purity evaluation.

4.2.5 Contact angle analysis

Contact angle measurements were determined using the DataPhysics OCA15 Contact Angle Analyser and SCA20 software (DataPhysics Instruments GmbH, Germany). PLAg films were produced as described previously and placed on the stage of the contact angle goniometer and 20 µl of ultra-pure water then dispensed from a Hamilton syringe using the standard sessile drop technique. Measurements were made using the SCA20 software with automatic baseline detection and profile extraction.

4.2.6 AFM imaging

The surface topography of PLAg and PVAm-PLAg analysed using a NanoWizard 4 AFM (JPK BioAFM, Bruker, UK) operating in QI mode. Prior to analysis, samples were air dried at 60°C for 24 h with no further preparation. . Samples were processed using intermittent tapping mode, in air, with an AC40 silicon tip on a nitride cantilever (Bruker, UK). Data processing and image analysis was conducted using JPK SPM software (JPK BioAFM, Bruker, UK).

4.2.7 XPS surface analysis

4.2.7.1 Principles of XPS

X-ray photoelectron spectroscopy (XPS) is a quantitative spectroscopic surface analysis technique which enables characterisation to a depth of < 10 nm. XPS complements other elemental analysis techniques by providing information on the chemical state of the atoms present (i.e. the elements to which they are bonded to) [278]. X-ray irradiation of a sample is conducted under ultrahigh vacuum (to prevent sample degradation) which results in excitation of electrons of the superficial layer allowing the photoelectron to break away

from the element. The photo-ejected electrons are then collected by an electron analyser and produces a spectral output of energy (the number of electrons over time) versus binding energy (electron energy prior to leaving the atom). The prominent energy peaks of the spectra correspond to specific elements; and quantification of the elemental composition can be determined by calculation of the respective peak area contributions.

4.2.7.2 XPS methodology

XPS was used to determine the elemental surface composition of PLAg and PVAm-PLAg films. XPS spectra were acquired using an Axis-Ultra DLD XPS instrument (Kratos Analytical, UK) using selected area analysis mode of 900 μm and monochromated Al Kα X-rays producing photons of 1486 eV energy. Due to the charge of PVAm-PLAg films and the use of a monochromated X-ray source, a charge neutraliser was used to prevent charge accumulation at the material interface and resulting distortion of recorded binding energies. Wide survey scans were acquired with a step size of 1 eV, pass energy of 150 eV and range of -10 eV to 1350 eV. Narrow high-resolution core-level C1S scans were acquired with a step size of 0.1 eV, pass energy of 20 eV, binding energy of approximately 285 eV and range of 280 eV to 300 eV. Three areas were analysed for each sample and 5 and 10 scans were obtained per area for wide scans and narrow scans, respectively. The electron emission angle was 0° to the surface and source-to-analyser angle was 60°. Narrow core-level spectra were analysed with CasaXPS (Casa Software) for curve fitting with a Gaussian/Lorentzian product function peak shape model (G/L = 30).

4.2.8 Moisture vapour permeability rate

To quantify the moisture vapour permeability rate (MVPR) of PLAg, PVAm-PLAg and Alg-PVAm-PLAg, methodology based on the international standard of water vapour transmission ASTM E96/E96M-16 was used. 80 ml of dH_2O was dispensed into 2” depth and 2.5” open diameter vapometers and plasticised agarose films (N=3) secured in place between two rubber O-rings. The vapometers were then incubated at 37°C for 24 h (33.6 % Relative Humidity) and vapour transmission quantified by subtraction (weight) from starting weight of dH_2O using the following equation:

Equation 4.2 - Moisture vapour permeability rate of agarose films

$$MVPR = \frac{G}{t\,A}$$

Where *G* is the weight loss of water in grams, *t* is the time in which *G* occurred in hours, and *A* is the sample test area in cm^2.

4.2.9 Swelling ratio

To determine the swelling capacity of PLAg and PVAm-PLAg films, segments were placed in buffer and the change in weight determined as a percentage at regular time points. PLAg and PVAm-PLAg films were produced as previously described (Sections 2.2.2 and 2.2.3, respectively). Subsequent to dehydration at 60°C for 24 h, films were removed from the cast and weighed individually. Films were then placed in individual beakers containing 100 ml PBS (previously equilibrated to 37°C). The beakers were immediately placed in an incubator at 37°C. At predefined time points (0 min – 90 min), films were removed from the beaker, blotted with filter paper to remove residual water and weighed (± 0.001 g). All time point measurements were conducted in triplicate (N=3), with swelling ratio (%) calculated using the equation below.

Equation 4.3 - Swelling ratio of agarose films

$$Swelling\ ratio\ (\%) = \frac{W_s - W_d}{W_d}\ x\ 100$$

Where W_s is swollen weight and W_d is dry weight in grams.

4.2.10 Surface zeta potential

4.2.10.1 Principles of surface zeta potential

Zeta potential measurements are often used to characterise the surface charge of particles in suspension. However, it is also possible to determine the zeta potential of non-suspended material using similar theories. Due to the inability of solid surfaces to undergo electrophoresis (a characteristic exploited in the determination of zeta potential measurements of suspended particles), the technique must be modified. Surface zeta potential can be determined by an alternative technique which measures the electrophoretic mobility of tracer particles at varying distances from a planar surface. The magnitude of electrophoresis and electro-osmosis can then be used to calculate the zeta potential at the sample interface.

Similar to measuring the zeta potential of suspended particles, surface zeta potential measurements can also be determined using the well-established M3-phase analysis light scattering (M3-PALS) technique in a Zetasizer Nano instrument (Malvern, UK). Surface zeta potential measurements can be determined using a specialised dip cell (Malvern ZEN1020) to which the sample is attached and submerged in a medium of interest containing tracer particles. When an electric field is applied via two electrodes either side of the sample the tracer particles will undergo electrophoresis, and electro-osmosis will be established close to the material interface. The sample stage is then moved incrementally by a rotating top cap on the cell, allowing adjustment of the sample displacement. While the tracer particles are in closer proximity to the sample interface electro-osmosis is the dominating force, however as the particle distance from the interface increases this dominance will be reduced to a point where particle mobility is entirely based on electrophoresis. The particles electrophoretic mobility is then measured by phase analysis light scattering (PALS) and plotted as a function of displacement from the surface. Extrapolation of this relationship at the intercept (zero displacement) can then be determined to calculate the surface zeta potential with the following equation:

Equation 4.4 - Surface zeta potential (ζ) of agarose films

$$\zeta\ interface = -intercept + \zeta\ particle$$

4.2.10.2 Surface zeta potential measurements

To determine the surface charge of PLAg and PVAm-PLAg, surface zeta potential measurements were determined by laser Doppler electrophoresis measurements using a Malvern surface zeta potential ZEN1020 dip cell (Malvern, UK). Unmodified PLAg and PVAm-PLAg films were cut into rectangular pieces of 6 mm x 4 mm (L x W) and attached to a sample holder using ethyl cyanoacrylate adhesive (Gorilla Glue, Europe). This adhesive was selected due to the fast curing time and insolubility in the dispersant. Once the adhesive had cured (1-2 h) samples were loaded into the surface zeta potential cell and secured by a tightening screw. Course alignment of the sample stage was then conducted using the height alignment tool included in the ZEN1020 kit. The surface zeta potential cell was then placed into a 10 mm square disposable cuvette containing the dispersant of interest and selected tracer particles (5 µL in 1.2 ml of dispersant to give an optimal derived count rate of approximately 500 kcps). An optimal count rate for surface zeta potential measurements of 250-500 kcps has been reported in the literature [279]. Care was taken to avoid introduction of air bubbles by inserting the cell at an angle of 45°. The ZetaSizer Nano ZS90 (Malvern, UK) was then set to detect forward scattered light at 13° with the attenuator set to eleven (100% transmittance), and voltage as automatic (typically 10 V). Fine alignment of the zero position was then conducted using the count rate meter in the zeta sizer software by rotating the cap clockwise until the count rate fell to zero. Five slow-field reversal measurements were then made at 125 µm, 250 µm, 375 µm and 500 µm from the sample surface, with each measurement comprising of fifteen sub-runs and 1 min between measurements. Finally, three fast-field reversal measurements were performed at a distance of 1000 µm from the sample surface to calculate the electrophoretic mobility of the tracer particles, each measurement comprised of 100 sub-runs with 20s between each measurement. Surface zeta potential measurements were then calculated from Equation 4.4. Each sample was analysed 3 times and a surface zeta potential value expressed as the mean ± SD.

4.2.11 Statistical analysis

The sizes of a population data set are expressed as (N) throughout this thesis, with values being reported as the mean averages ± standard deviation (SD), unless otherwise stated. All statistical analyses were conducted using GraphPad Prism version 8 (GraphPad Software, USA).

4.2.11.1 Student's t-test

Student's t-tests were used to analyse data obtained from MTS cytotoxicity studies and MVPR data. Statistical significance was determined between treatment groups and the cell control (MTS assay), and between PLAg and PVAm PLAg films (MVPR), using a student's t-test at a 95% confidence interval. P values of < 0.05 indicate statistical significance, with the degree of significance indicated on the figures where appropriate.

4.2.11.2 One-way ANOVA

One-way ANOVA with Tukey's multiple comparison post-hoc test was used to determine significance between surface zeta potential values obtained for incremental PVAm concentrations. P values of < 0.05 indicate statistical significance, with the degree of significance indicated on the figures where appropriate.

4.3 Results

4.3.1 Synthesis and characterisation of PLAg films

This section describes the synthesis and characterisation of a PLAg film base material developed as a candidate wound dressing. Optimisation of the plasticiser concentration was conducted based on macroscopic evaluation of the material properties. Once the optimal concentration was identified, the surface topography was assessed by SEM and chemical composition of the films determined by FTIR spectroscopy. As leaching of the plasticiser upon dehydration was of concern, pre-soaked PLAg films were also assessed by FTIR to identify any loss or change in chemical composition. The leachate of PLAg films was then assessed for cytotoxicity in 3T3 fibroblasts.

4.3.1.1 Synthesis and physical evaluation

PLAg films were synthesised by a simple method of dissolving agarose and plasticiser in water, placing the mixture in a boiling water bath until a clear solution was obtained, allowing gelation to occur by cooling in an appropriate cast, then dehydrating for 24 h at 60°C. PLAg films were initially produced with varying plasticiser concentrations of 0 % w/v (IL0) to 50 % w/v (IL50) (Figure 4.5). PLAg films were assessed for flexibility, strength and signs of syneresis by qualitative observations and manual manipulation. Increased flexibility was observed with increasing plasticiser concentration (IL0 to IL50). No signs of syneresis were observed over the range of plasticiser concentrations for up to 4 weeks under ambient conditions. PLAg films were reproducibly produced with a thickness of 0.12 to 0.14 mm (n=10). Batch to batch consistency was also evaluated, with no further variation in thickness or macroscopic qualities observed. PLAg films containing 50 % plasticiser were carried forward for further studies due to the high flexibility and transparency of the material with no signs of plasticiser syneresis under ambient conditions.

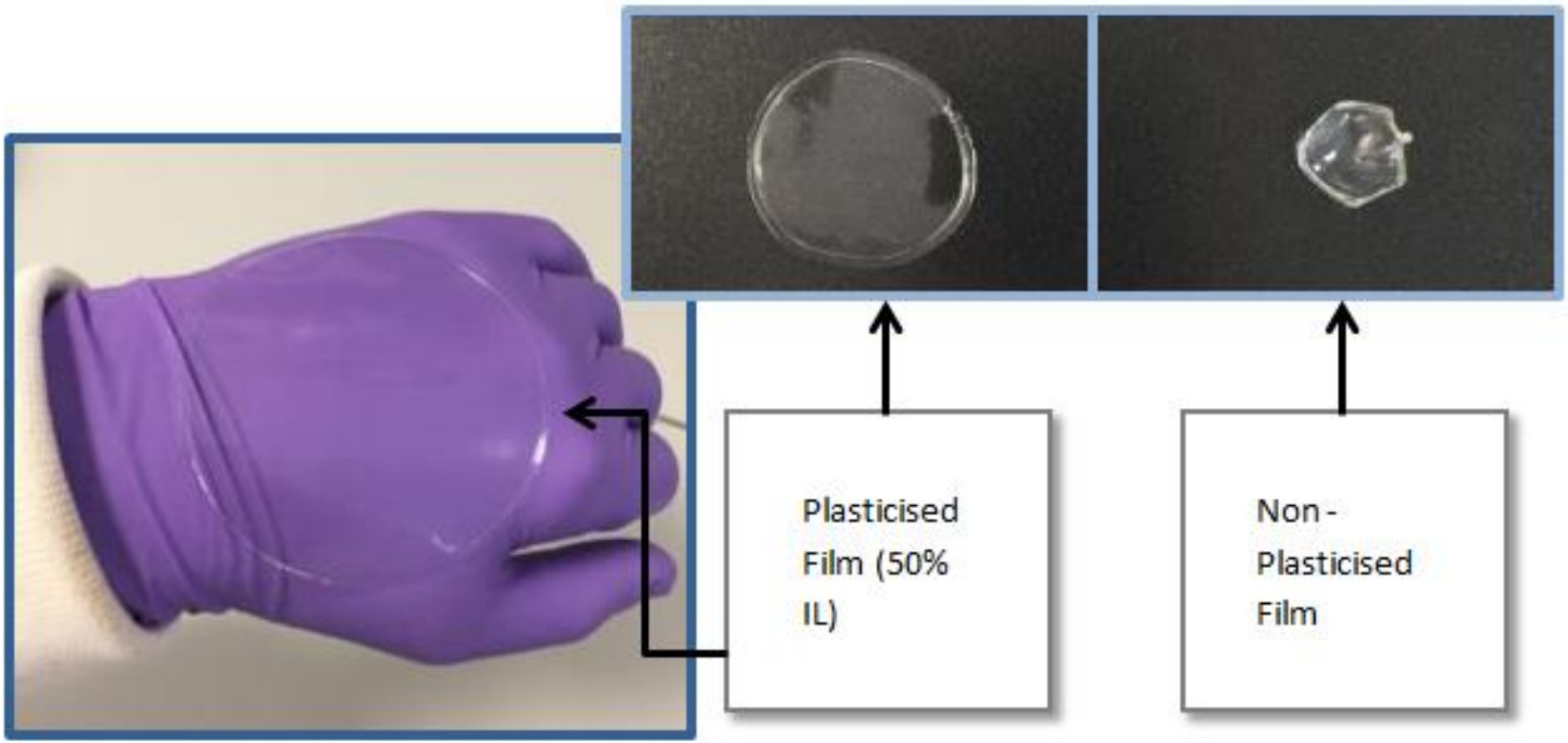

Figure 4.5 - Images of plasticised (50% DES) and non-plasticised agarose films, depicting the differences in physical characteristics.

4.3.1.2 SEM analysis

The surface topography of PLAg films (IL50) was assessed using a Zeiss-Sigma-300 FEG-STEM operating in SEM mode. Sample preparation was conducted using glutaraldehyde in sodium cacodylate buffer as fixative, followed by dehydration in increasing ethanol concentrations and sputter coated in 4nm platinum. At low magnification (Figure 4.6a) the film surface appeared to have a slightly rippled morphology. At high magnification (Figure 4.6b), spherical pores were observed within the peaks and troughs of the sample interface (Figure 4.6b - black arrows). The pore sizes were determined using ImageJ software, allowing simultaneous measurements of all porous structures on a selected image. The average pore size was 14.00 nm ± 5.32 SD (n=513), indicating that PLAg films have a nano-porous structure when in the dehydrated state.

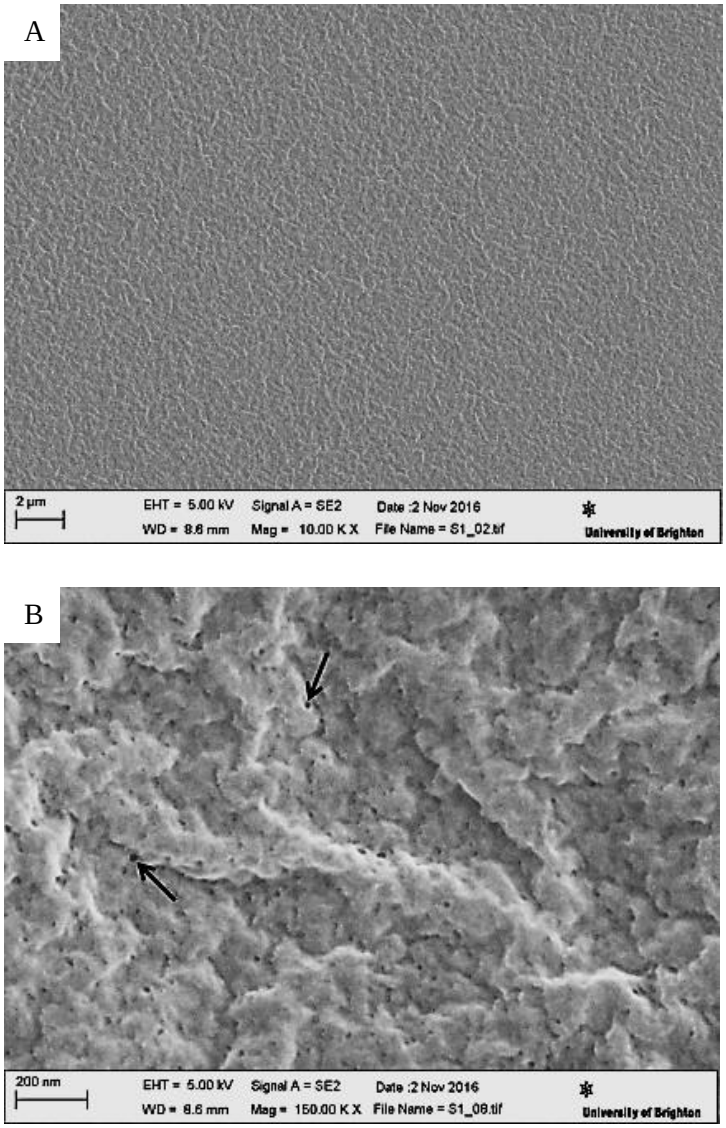

Figure 4.6 - SEM micrographs of PLAg films (50% DES) showing surface topography at 10,000x magnification (A) and 150,000x magnification (B).

4.3.1.3 FTIR analysis

FTIR was conducted on dehydrated PLAg films of incremental DES concentration (IL0 – IL50) to determine the presence of functional groups and intermolecular interactions between agarose and the DES plasticiser. The FTIR spectra of agarose films exhibited strong, broad peaks at approximately 3350 cm^{-1} consistent with -OH bond stretching of alcohol groups present in agarose. Smaller peaks with lesser intensity at approximately 3200 cm^{-1} are consistent with -NH stretching vibrations and are only present in samples containing DES plasticiser. Peaks at approximately 2960 cm^{-1} can be assigned to -CH bonding of agarose and are present in all film samples. Bands with strong intensity were observed at approximately 1600 – 1700 cm^{-1} and can be assigned to -NH bending of urea, only present in films containing plasticiser. There is, however, a peak with low intensity in this region for the sample containing no plasticiser. This could be present due to a weak -CH bend vibration of agarose or an artefact of residual water present in the agarose film. At approximately 1450 – 1500 cm^{-1} peaks were observed in samples containing DES plasticiser due to $-CH_3$ bending of choline chloride. Peaks were present at 1400 cm^{-1}, present for all samples and consistent with C-C bending of agarose. Table 4.1 shows the wavenumbers (cm^{-1}) and functional group designations of PLAg films composed of incremental DES plasticiser concentrations, with the full spectra shown in Figure 4.7.

Table 4.1 - FTIR wavenumbers (cm-1) obtained from PLAg film samples containing incremental concentrations of plasticiser (0 %, 15 %, 30 %, 50 %).

	Wavenumber (cm^{-1})					
DES Concentration	**-OH Stretch**	**-NH Stretch**	**-CH Stretch**	**-NH Bend**	**$-CH_3$ Bend**	**C-C Bend**
50 %	3349	3225	2969	1664	1474	1377
30 %	3347	3238	2978	1667	1477	1386
15 %	3366	3244	2967	1668	1478	1378
0 %	3379	-	2949/1662	-	-	1383

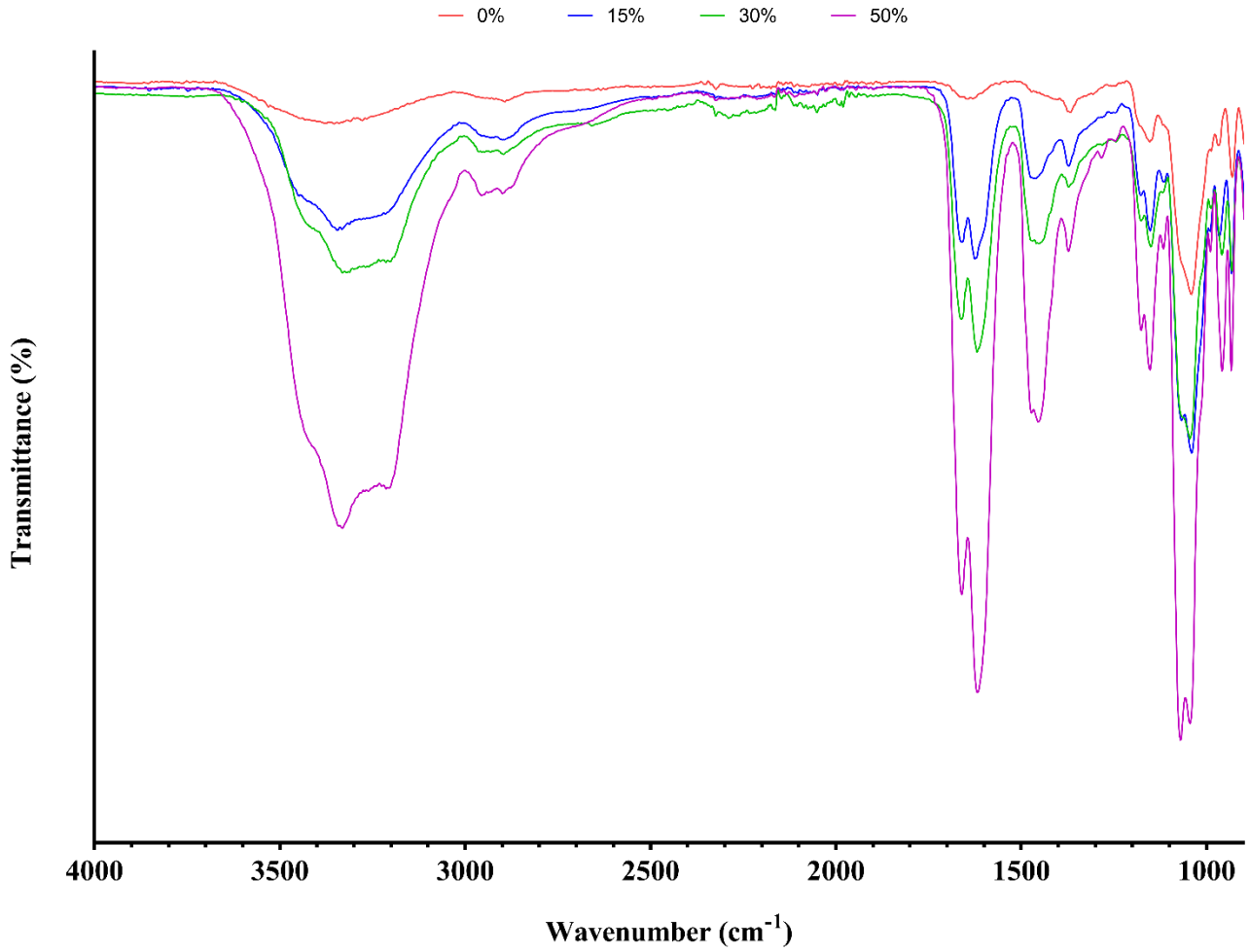

Figure 4.7 - FTIR spectra obtained from PLAg films containing incremental concentrations of plasticiser; IL0 (red), IL15 (blue), IL30 (green), and IL50 (magenta) DES.

The effect of soaking on IL50 PLAg film plasticiser content was then assessed by FTIR analysis prior to, and subsequent to, soaking in bacteriophage buffer for 24 h at room temperature and atmospheric pressure (Figure 4.8). The -NH bend peak associated with the presence of urea (approx. 1650 cm^{-1}) and the $-CH_3$ bending peak associated with the presence of choline chloride (approx. 1450 cm^{-1}) are reduced in soaked samples indicating the release of plasticiser upon rehydration of the PLAg film. Subsequent to soaking in bacteriophage buffer, manual manipulation of PLAg films also suggested loss of plasticiser due to the brittleness of the material.

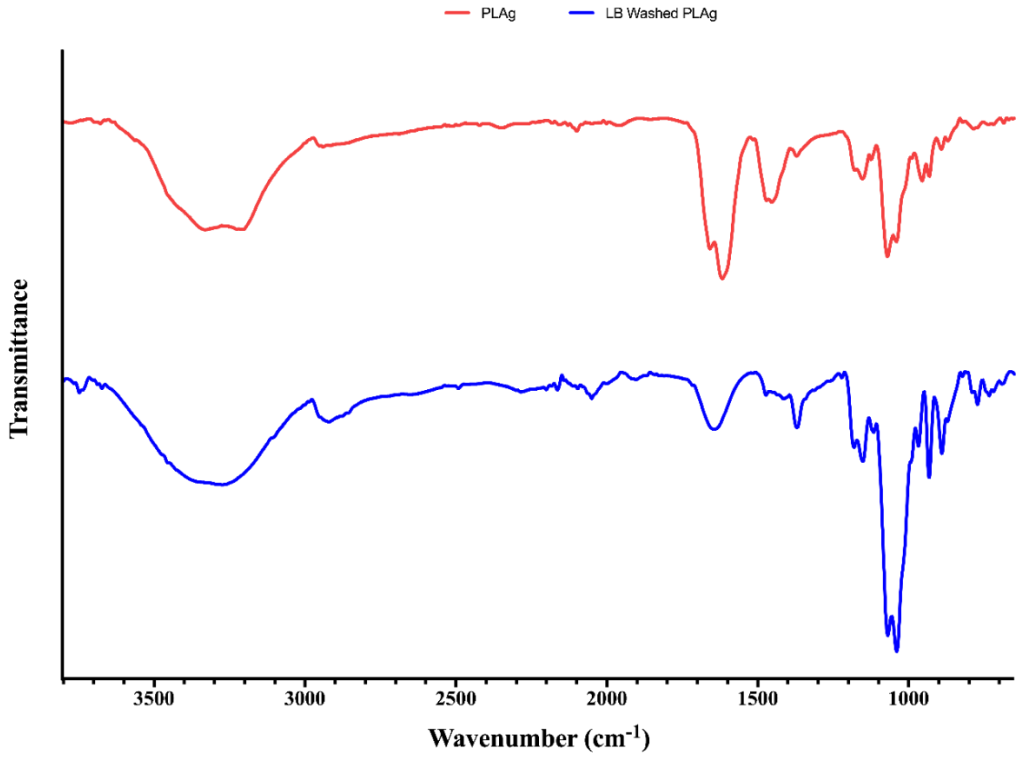

Figure 4.8 - FTIR spectra obtained from PLAg films prior to (red), and subsequent to soaking in bacteriophage buffer (blue) for 24h at room temperature and atmospheric pressure.

4.3.1.4 Cytotoxicity of PLAg film leachate

To determine the clinical implications of plasticiser leaching when applied as a wound dressing, the cytotoxicity of PLAg film leachate was determined by MTS assay (Figure 4.9). MTS is a tetrazolium salt colourimetric assay that detects mitochondrial activity by reduction of MTS to formazan, giving a purple colour, the intensity of which can be quantified at 490 nm. The viability of 3T3 fibroblast cells was assessed after 24 h exposure to PLAg film leachate, with tin maleate leachate used as a positive control due to its known cytotoxic properties. Cell viability was then calculated as a percentage in relation to the cell (negative) control. Exposure of tin maleate leachate to 3T3 cells resulted in residual cell viability of 1.8 % ± 1.4 % after 24 h exposure to the extract. PLAg film leachate was shown to marginally promote cell growth when cultured with 3T3 fibroblasts, with cell viability of 105.5 % ± 2.7 % after 24h exposure. This was not considered statistically significant (P = 0.071) and the variability likely due to minor disparities in cell inoculum numbers in each test well and unlikely to be caused by the plasticiser itself.

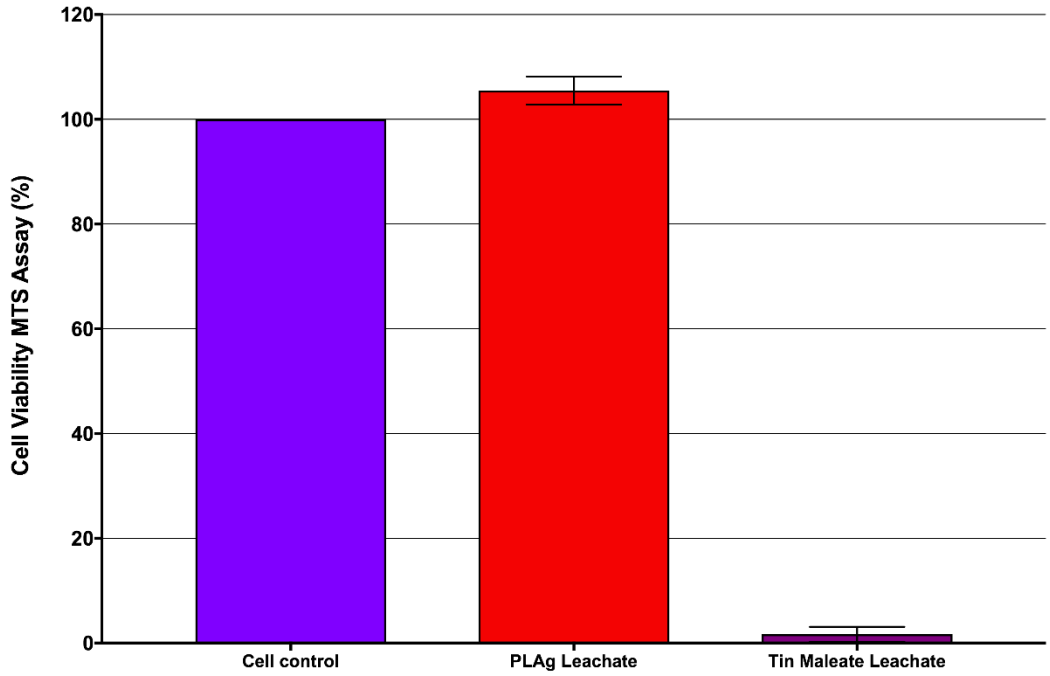

Figure 4.9 - Cell viability of 3T3 fibroblasts after 24h incubation with PLAg film leachate as measured by MTS assay. Cell viability was calculated by relation to the cell control. Mean values were calculated from nine independent experiments (N=9) ± SD.

4.3.2 PVAm purification and characterisation

In this section, PLAg film surfaces were modified with PVAm to obtain a cationic interface for further study. Prior to surface coating, commercially available PVAm was further purified by hydrolysis of the polymer precursor (N-vinylformamide), and the removal of side-product impurities. Once purification had been conducted, FTIR, NMR and DSC analysis were used to determine the composition of purified PVAm and to determine the optimal storage conditions of the lyophilised product.

4.3.2.1 FTIR analysis of stock and purified PVAm

FTIR was conducted on non-purified (as provided) and purified (further hydrolysis/dialysis) PVAm samples to determine the purity and composition of each sample. The FTIR spectra and table containing wavenumbers and peak designations can be found in Figure 4.10 and Table 4.2, respectively. The FTIR spectra of non-purified PVAm showed a broad peak at approximately 3350 cm^{-1} assigned to -OH stretching of carboxylic acid, most likely the formic acid impurity of PVAm synthesis. This broad peak was not observed in the purified sample, indicating the removal of carboxylic acid impurity. In its place were peaks at 3320 cm^{-1} and 3250 cm^{-1} which are typical of primary amines, and 3155 cm^{-1} which is an overtone arising from N-H bending band. In the purified PVAm sample at 1580 cm^{-1} are peaks assigned to NH bending of primary amines. The spectrum obtained therefore indicates the successful hydrolysis of the N-vinylformamide precursor and removal of the side products and impurities. Functional groups indicated from the FTIR spectrum also correlate with the presence of primary amine groups in both samples.

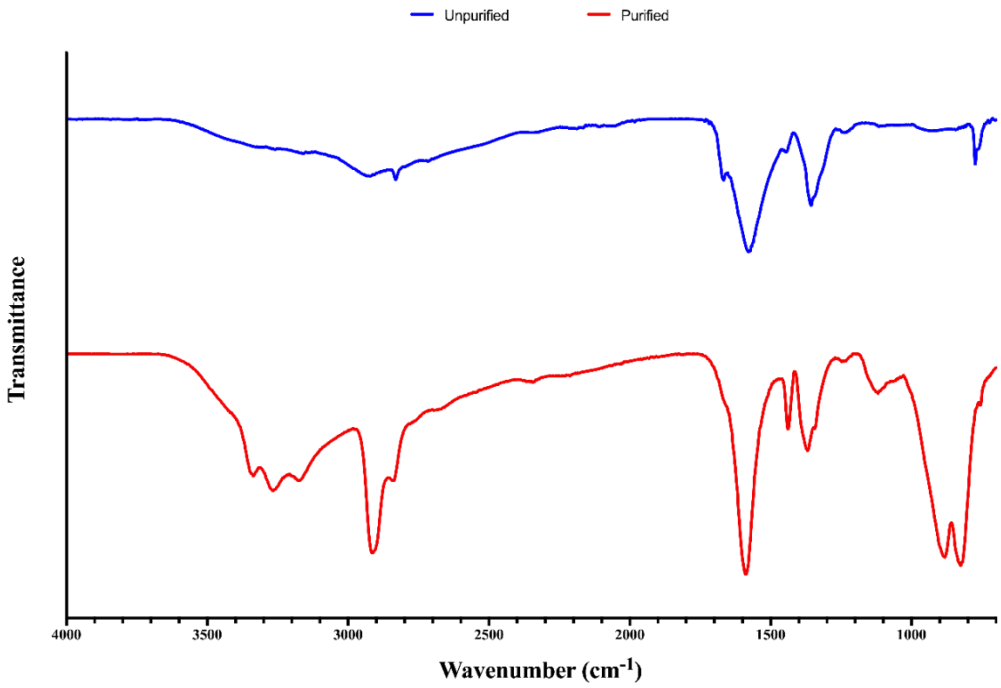

Figure 4.10 - FTIR spectra of commercially available PVAm (blue) and PVAm which had undergone hydrolysis and dialysis (red).

Table 4.2 - FTIR wavenumbers (cm-1) obtained from unpurified PVAm and purified PVAm, with peak assignment descriptions.

Unpurified PVAm				**Purified PVAm**		
Wavenumber (cm^{-1})	**Bond designation**	**Description**		**Wavenumber (cm^{-1})**	**Bond designation**	**Description**
2910	N-H (stretch)	Amine salt		3320	N-H (stretch)	Aliphatic primary amine
2830	N-H (stretch)	Amine salt		3250	N-H (stretch)	Aliphatic primary amine
1664	C=O	Formamide		3155	N-H (bending)	Overtone
1572	N-H (Bending)	Amine		2900	C-H (stretch)	Alkane chain
1355	O-H (Bending)	Formic acid		1580	N-H (Bending)	Primary amine
775	C-H (Bending)	Alkene (Vinyl)		1434	C-H (bend)	Alkane methyl group

4.3.2.2 NMR analysis of purified PVAm

^{1}H-NMR (400MHz, D_2O) analysis of purified PVAm dispersed in D_2O was conducted to determine the molecular structure subsequent to polymer purification. The spectrum shown in Figure 4.11 was produced using Topspin© software set at 16 run scan analysis at 400 MHz. Peak assignments are as follows; 4.75 ppm = D_2O (solvent peak), 1.4 ppm (a) and 3.0 ppm (b) = aliphatic alkyl chain at two separate proton environments. As D_2O was used as the solvent, amine regions were not observed on the NMR spectrum due to the exchange of NH protons with deuterium. However, this data substantiates FTIR spectra (Figure 4.10) and further suggests removal of impurities and hydrolysis of N-vinylformamide to PVAm and provides evidence of the chemical structure of the tested sample.

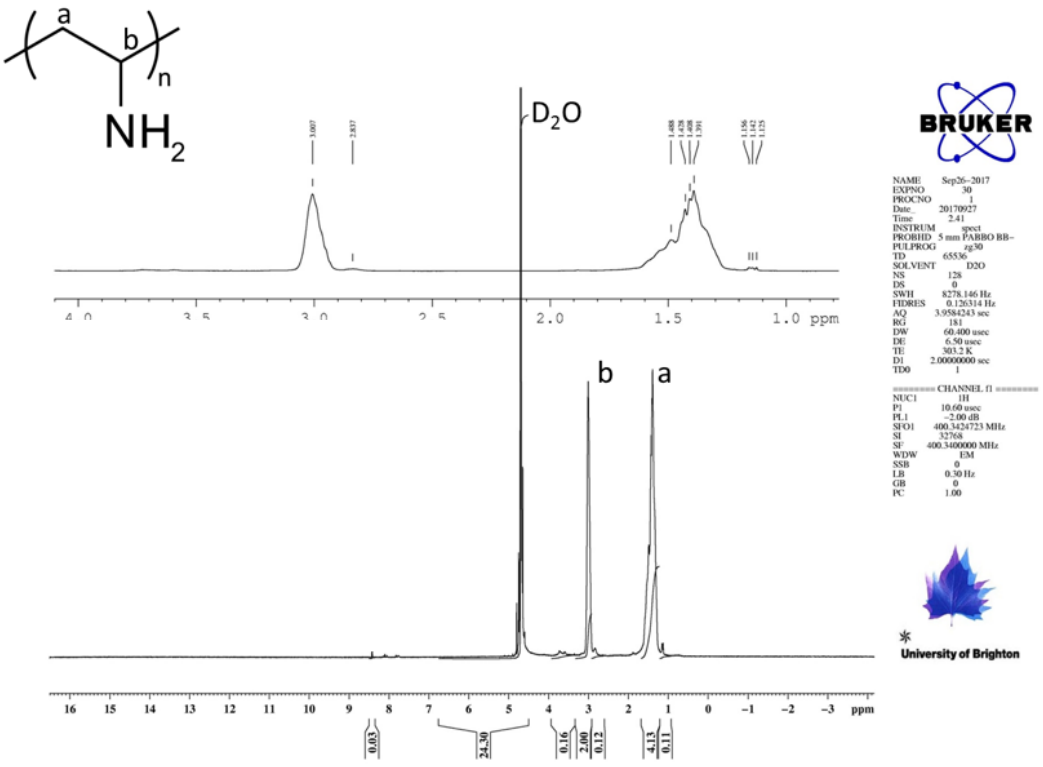

Figure 4.11 - NMR spectrum of purified PVAm, outlining the chemical structure of the purified sample. The sample was analysed using 16 run scan analysis at 400 MHz, with D_2O used as solvent.

4.3.2.3 Evidence of PVAm degradation

The stability of purified PVAm samples was monitored over a 12 month period under various storage conditions: under nitrogen at -20°C and at room temperature (RT), and under atmospheric conditions at -20°C and at RT. Figure 4.12 shows the FTIR spectra of newly purified PVAm, and PVAm produced 12 months prior to analysis, stored under ambient conditions. These results show the introduction of -OH groups after 12 months storage under atmospheric conditions. Figure 4.13 shows FTIR spectra of PVAm stored under the various temperatures and gaseous environments for 12 months. The presence of -OH functional groups are consistent with published literature, which suggests that basic hydrolysis of poly-NVF results in amidine formation, which can decompose leaving an alcohol in place of the amine [280]. Figure 4.13 shows that, if stored under nitrogen at -20°C, purified PVAm degradation is minimised due to the lack of -OH bonding observed on the FTIR spectra. Figure 4.13 also indicates less prominent amine peaks between 3400 cm^{-1} and 3200 cm^{-1} in all samples other than newly produced PVAm and samples stored under nitrogen at -20°C. This further suggests the reduced degradation rate when stored under the aforementioned conditions.

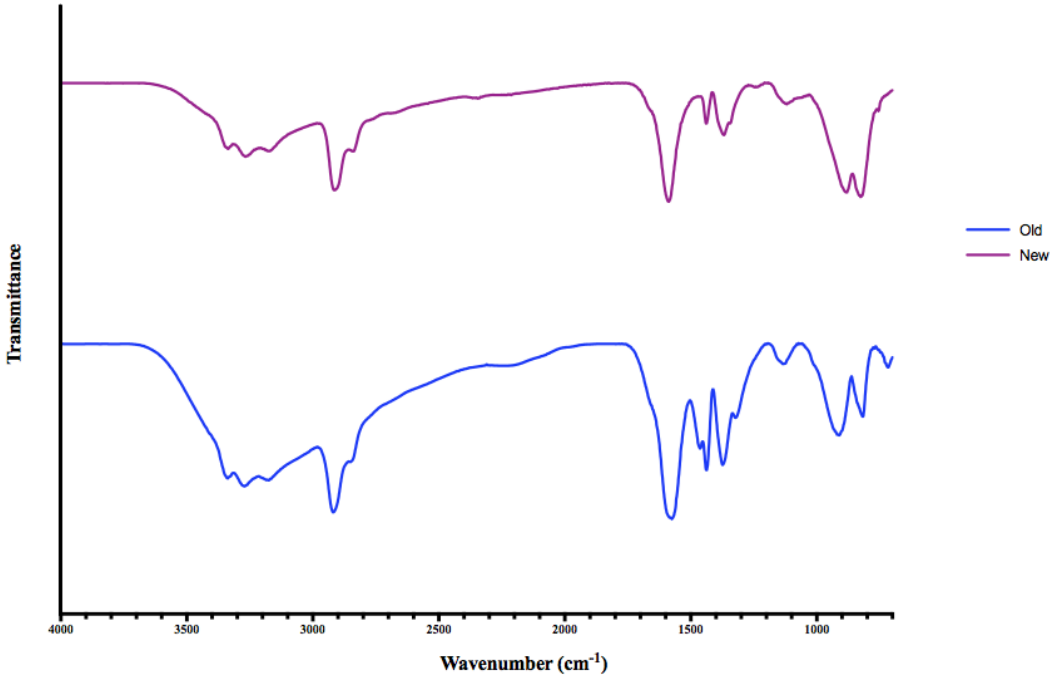

Figure 4.12 - Evidence of PVAm degradation subsequent to 12 months storage (RT and atmospheric pressure) by FTIR analysis. Top spectrum (purple) was obtained from the analysis of newly purified PVAm, while the bottom spectrum (blue) was obtained from PVAm produced 12 months prior and stored under ambient conditions.

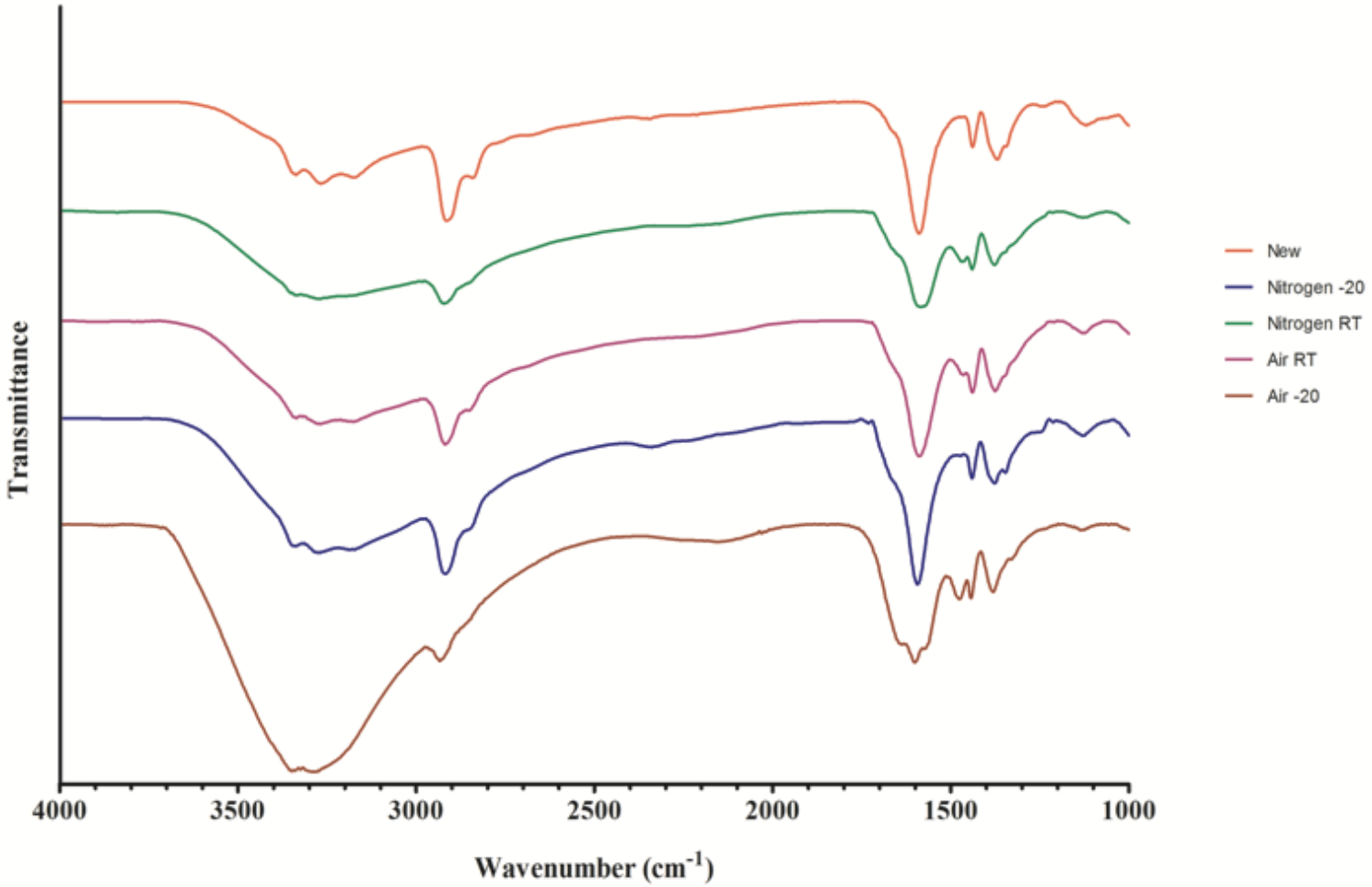

Figure 4.13 - FTIR spectra of a number of storage conditions subsequent to 12 months storage under each condition (with the exception of newly purified PVAm). From top to bottom; Newly purified (orange), Nitrogen room temperature (green), Air room temperature (magenta), Nitrogen -20°C (blue), and Air -20°C (brown).

4.3.3 Surface modification and characterisation of PLAg and PVAm-PLAg

This section outlines the surface modification of PLAg films with PVAm to obtain a cationic interface for bacteriophage attachment in further studies. PVAm was applied to the surface of PLAg films by dehydration on the film interface. Once applied, the surface of PVAm modified PLAg films was characterised by direct imaging and analysis of chemical composition. The stability of the surface coating was also assessed to determine the level of permanence when exposed to aqueous environments. Finally, the surface zeta potential of PLAg and PVAm-PLAg films was determined to distinguish the charge difference after application of the cationic PVAm surface coating.

4.3.3.1 Atomic force microscopy

The surface topography of uncoated PLAg and PVAm coated PLAg (PVAm-PLAg) films was measured by atomic force microscopy (AFM) (Figure 4.14). All samples were observed in ambient conditions without fixation, in tapping mode using a silicon cantilever tip. Unmodified PLAg film topography was shown to be consistent with findings from SEM analysis, with a rippled surface and the presence of pores (Figure 4.14a). These pores, however, appear to have a greater diameter when observed by AFM. The smaller pore size observed in SEM samples may be an artefact of sample fixation, with AFM producing images more reflective of the film topography in ambient conditions. PVAm-PLAg films were shown to have a significantly smoother surface with a lack of pores (Figure 4.14b). This could be explained by the additional polymer layer which fills or masks the pores and troughs of the rippled surface. This hypothesis is further evidenced by the decreased height measured in PVAm-PLAg films.

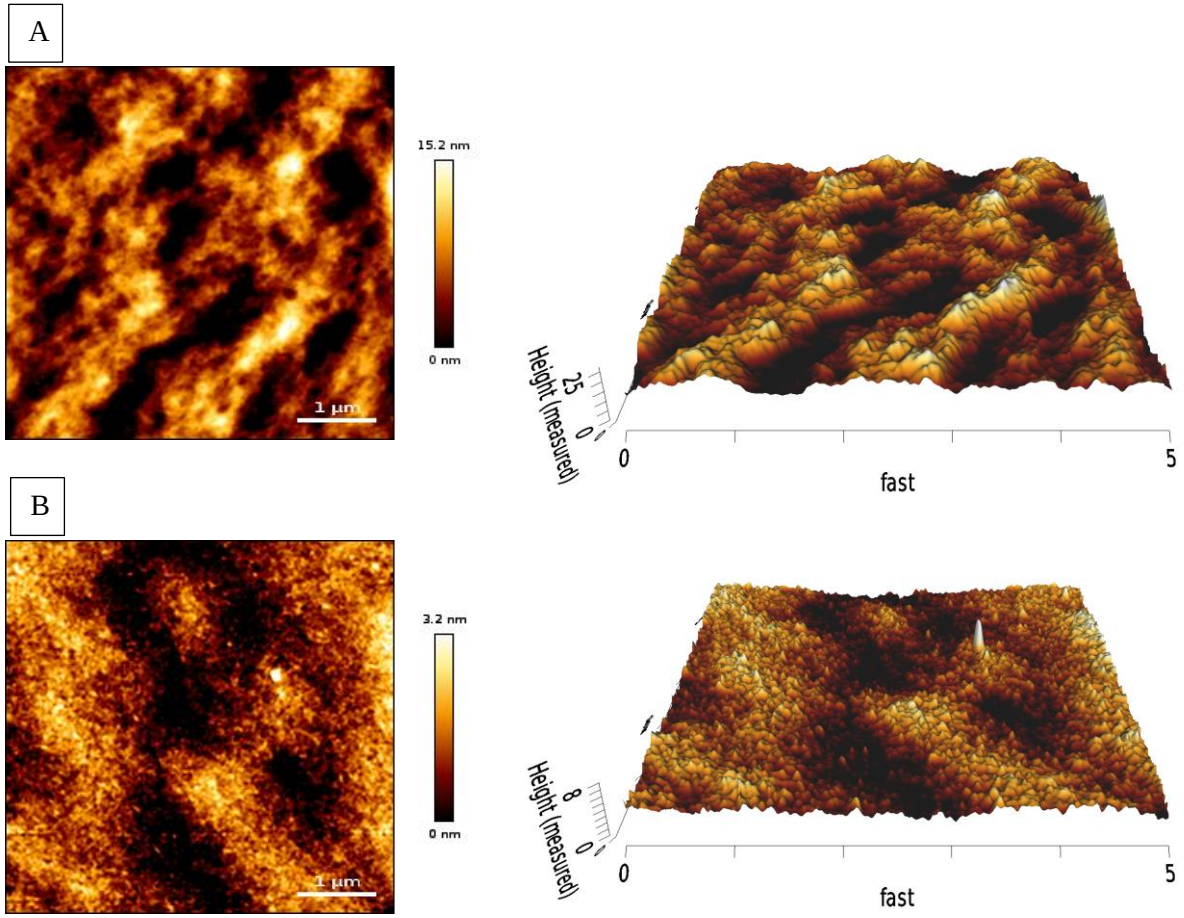

Figure 4.14 - 2D (left) and 3D (right) AFM images of dehydrated PLAg (A) and PVAm-PLAg (B) films obtained under ambient conditions. Images were collected using tapping mode with a silicon tip. Scales are indicated by the bars.

4.3.3.2 FTIR analysis

PLAg and PVAm-PLAg films were analysed by FTIR to identify functional groups attributed to the presence of PVAm surface coating. Figure 4.15 shows the FTIR spectra obtained for both film variants, focused on the fingerprint region at < 2000 cm^{-1}. A band was observed at approximately 1300 cm^{-1} in PVAm-PLAg films, which aligns with the presence of C-N amine regions of PVAm. Higher peak intensity at 1050 to 1085 cm^{-1} observed in PLAg films indicates the presence of primary alcohols, and secondary alcohols at approximately 1125 cm^{-1}. This finding is due to each agarose unit containing four alcoholic functions, three of which being secondary and one being primary. The reduction of peak intensity in PVAm-PLAg films at these wavenumbers may be due to masking of -OH groups by the additional polymer layer, suggesting successful application of PVAm to the surface of PLAg films.

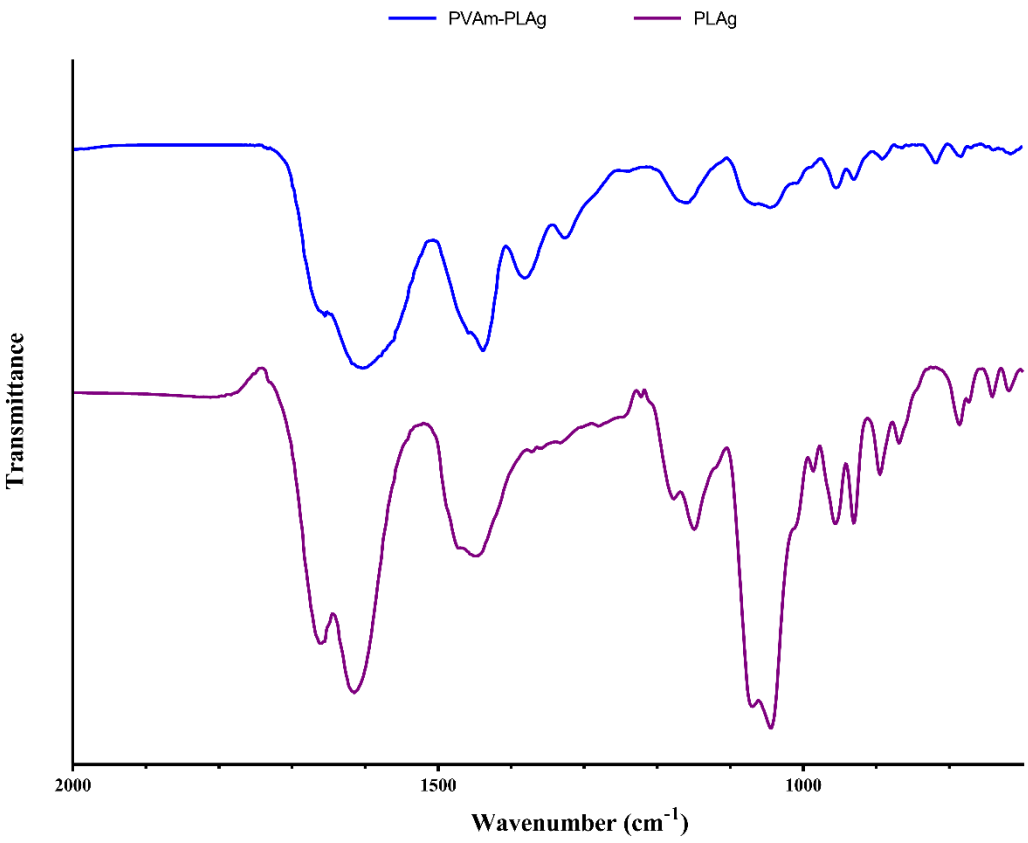

Figure 4.15 - FTIR spectra of PLAg (purple) and PVAm-PLAg (blue) films, allowing identification of PVAm by the presence of functional groups unique to the polymer coating.

4.3.3.3 Contact angle measurements

Contact angle measurements were collected using a DataPhysics OCA15 contact analyser with SCA20 software using the sessile drop technique (20 µl ultra-pure water) (Figure 4.16). Measurements were determined using automatic baseline detection (when possible) and profile extraction. While both PLAg and PVAm-PLAg films were classified as hydrophilic (< 90°), PVAm-PLAg films were found to be significantly 'more hydrophobic' ($P < 0.0001$) with a contact angle of 43.3° ± 2.45°. Due to the polarity of amine regions present on the surface of PVAm-PLAg films, one might expect that these samples would be more hydrophilic than unmodified PLAg films. However, the increased hydrophobicity of PVAm-PLAg films could be explained by a number of factors which are discussed later in this chapter.

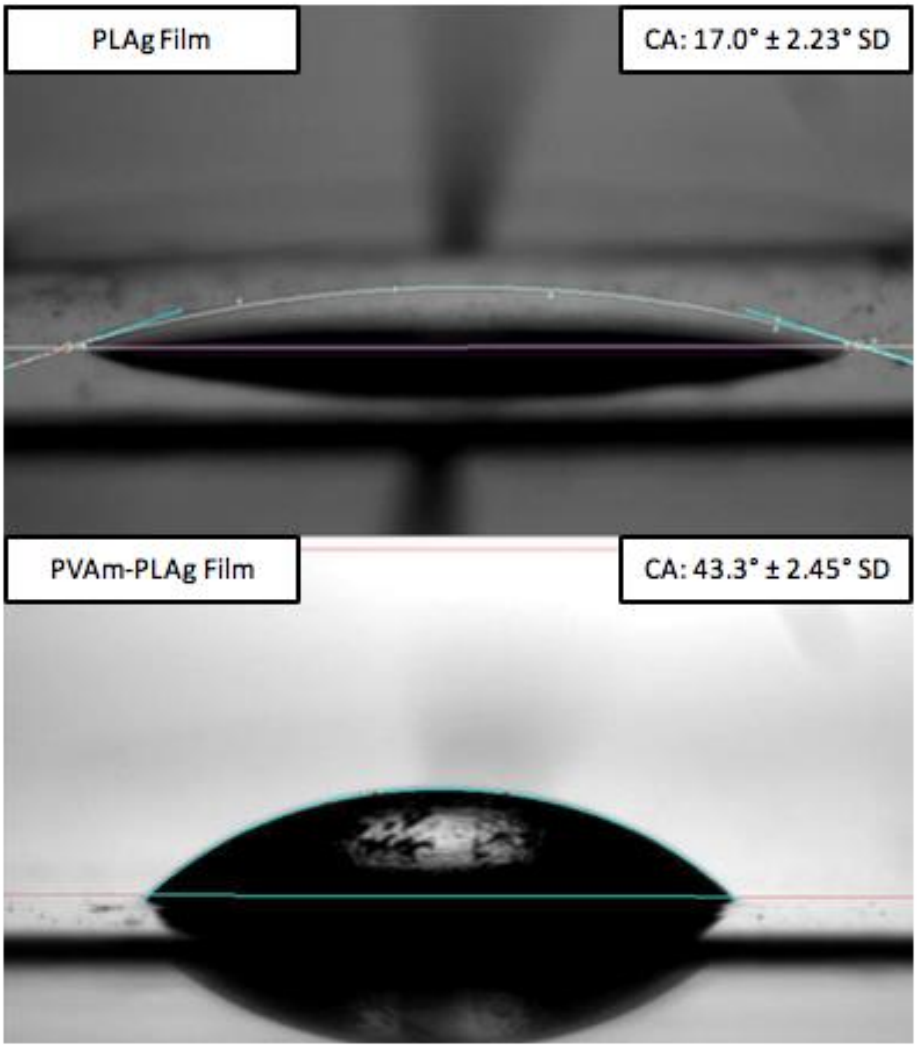

Figure 4.16 - Contact angle (CA) measurements of PLAg (top) and PVAm-PLAg (bottom) films using sessile drop technique. Mean CA measurements were calculated from six independent measurements (N=6).

4.3.3.4 MVPR and swelling studies

The MVPR of PLAg and PVAm-PLAg films was determined by quantifying water vapour movement across the material at 37°C and 33.6 % RH (Figure 4.17a). Control values indicate water loss in the absence of a film barrier. A small difference in MVPR was observed between PLAg and PVAm-PLAg films over a 24 h period (0.1 g/10 cm^2/24 h); this difference was not considered statistically significant (P = 0.055).

Swelling measurements of PLAg and PVAm-PLAg films in PBS (maintained at 37°C) were made over a 30 min period. Subsequent to the removal of residual water, films were weighed and swelling expressed as a percentage of the original weight (Figure 4.17b). PVAm-PLAg films were shown to swell more than PLAg films. The increase in swelling and slight decrease in MVPR observed in PVAm-PLAg films can be explained by the absorption of water by the PVAm polymer layer.

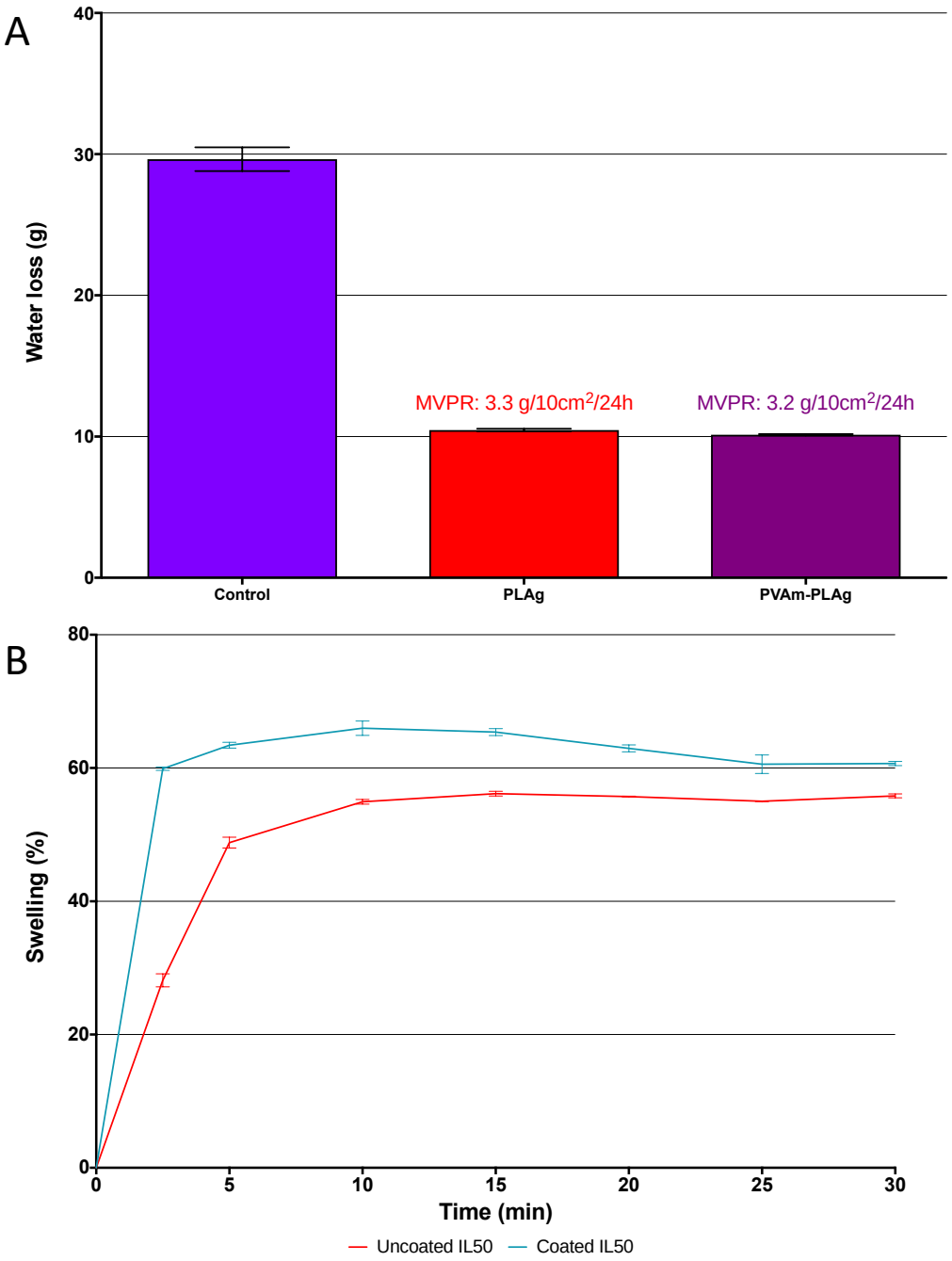

Figure 4.17 - Moisture vapour permeability rate of PLAg and PVAm-PLAg films (50% DES) at 37°C for 24h at 33.6 RH (A),and swelling measurements of PLAg and PVAm-PLAg films in PBS (maintained at 37°C) monitored over a 40 minute period (B). All values were calculated as the mean of three independent experiments (N=3) ± SD.

4.3.3.5 XPS surface analysis

The surface composition of PLAg and PVAm-PLAg films was analysed by x-ray photoelectron microscopy (XPS). Samples were also soaked in bacteriophage buffer to determine the level of PVAm detachment over 24 h at 4°C. Survey scan spectra are presented in Figure 4.18, while mean atomic percentage figures can be found in Table 4.3. For all samples, the dominant peaks present during low resolution survey scans were at approximately 285 eV, 398 eV, and 530 eV, attributed to the presence of C, N, and O, respectively. The presence of these elements is consistent with the base material composition of agarose and plasticiser. As PVAm is exclusively comprised of an alkyl chain with an abundance of amine functional groups, the O peak may be used as a reference point to demonstrate the significant increase in C and N associated with the presence of PVAm. The slight reduction in O demonstrated in PVAm-PLAg films can be attributed to the masking of agarose by PVAm. Cl_2 ions (197 eV) indicate the presence of plasticiser at the material interface.

Samples were then analysed subsequent to 24 h soaking in bacteriophage buffer at 4°C, reflective of the anticipated bacteriophage adsorption conditions in future experiments. Pre-soaked uncoated PLAg films showed a reduced N peak and the complete removal of Cl_2. This indicates leaching of plasticiser during soaking. The presence of Mg (1303 eV) can be attributed to slight adsorption of the cationic component of lambda buffer. Pre-soaked PVAm-PLAg demonstrated a reduction of C in reference to the O peak but negligible reduction in N, indicating loss of plasticiser but retention of the PVAm surface coating.

Table 4.3 - Elemental surface concentrations for unwashed and washed (bacteriophage buffer, 24h) PLAg and PVAm-PLAg films derived from XPS survey scan data.

	Mean atomic %			
Element	**PLAg**	**PVAm-PLAg**	**PLAg (Washed)**	**PVAm-PLAg (Washed)**
N1s	5.61	17.47	1.56	18.66
O1s	29.50	17.24	35.43	21.34
C1s	62.01	63.31	62.80	57.36
S2p	-	-	-	1.88
Cl2p	2.87	1.46	-	0.50
Mg1s	-	-	0.20	0.26

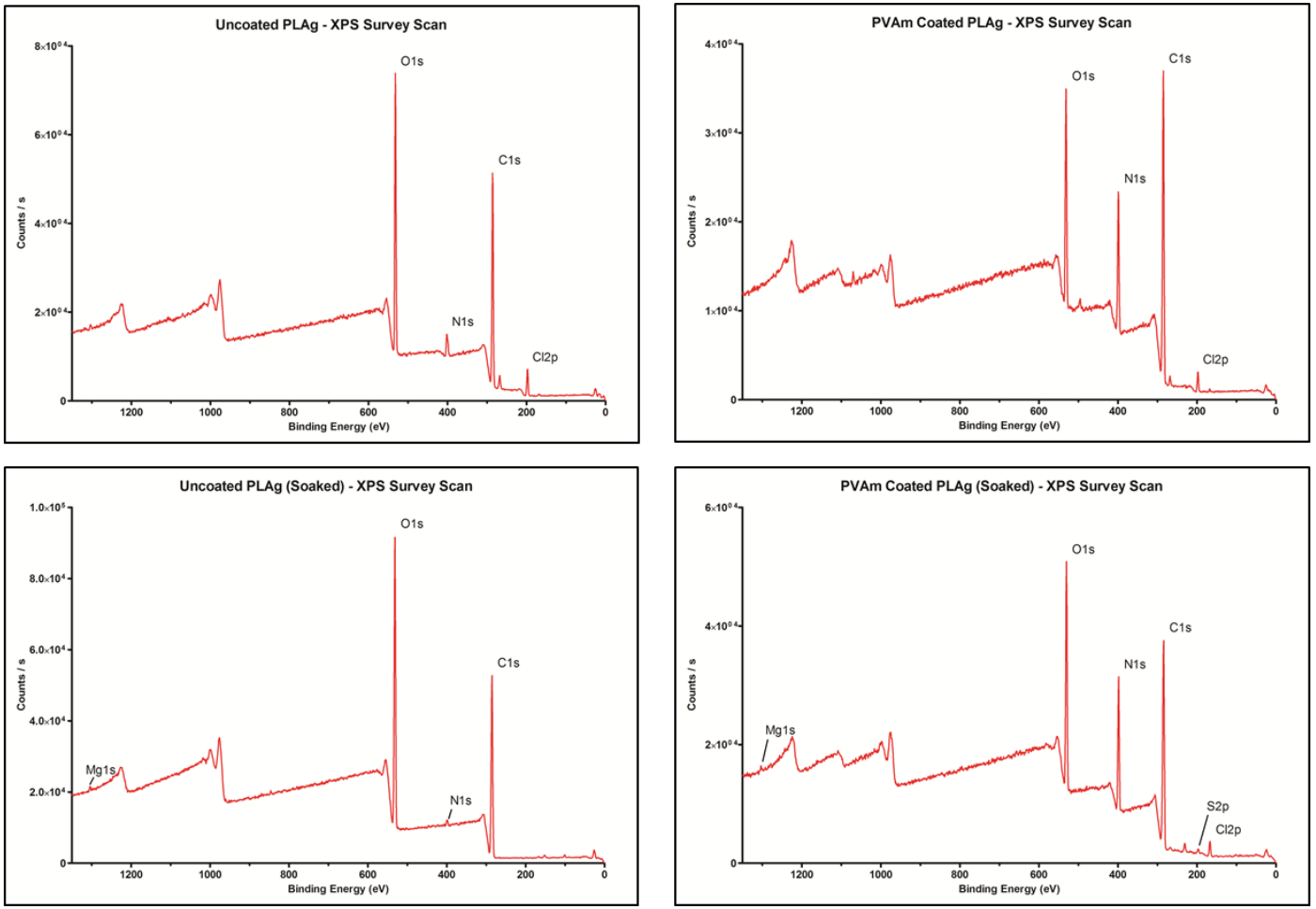

Figure 4.18 - XPS survey scan spectra of uncoated PLAg (top left), PVAm coated PLAg (top right), pre-soaked uncoated PLAg (bottom left) and pre-soaked PVAm coated PLAg (bottom right). Pre-soaking was conducted in bacteriophage buffer for 24h at 4°C to determine detachment of PVAm surface coatings from the polymer film. Each spectrum represents the mean value of three independent measurements.

High resolution spectra of C1s core levels for uncoated and PVAm-PLAg films, prior and subsequent to soaking are presented in Table 4.4 and Figure 4.19. The C peak for uncoated PLAg films was deconvoluted into four major peaks at 285.04 eV, 285.84 eV, 286.74 eV, and 288.11 eV, which were assigned to the presence of C–C, C–N, C–O–C/C–O–H, and N–C=O bonding, respectively. PVAm-PLAg films showed similar elemental base composition, with the addition of –COOH bonding at 288.96 eV. However, consistent with evidence from XPS survey scan data, C–N and C–C bonding is significantly increased in PVAm-PLAg (in reference to alcohol/ester bonding of agarose). PVAm-PLAg samples also showed decreased alcohol/ester and amide bonding, indicating masking of agarose and plasticiser at the interfacial layer.

Pre-soaked, uncoated PLAg showed complete removal of amine bonding, indicating the removal of the urea component of the plasticiser. This finding suggests the deep eutectic solvent is liable to decomposition in aqueous conditions with urea more prone to leaching than ChCl from the interfacial layer. Levels of C-C and C-N bonding in pre-soaked PVAm-PLAg samples were reduced by negligible amounts, providing further evidence of surface coating stability in the pre-soaking conditions tested.

Table 4.4 - Relative abundance of carbon bonds for unwashed and washed (bacteriophage buffer, 24h) PLAg and PVAm-PLAg films, derived from C1s core level XPS data.

	Mean atomic %			
Element	**PLAg**	**PVAm-PLAg**	**PLAg (Washed)**	**PVAm-PLAg (Washed)**
C-C	9.01	33.57	11.43	31.93
C-N	4.91	17.93	-	16.71
C-O-C, C-O-H	71.86	36.58	62.09	33.88
N-C=O	14.23	4.19	17.78	7.23
-COOH	-	7.73	8.69	10.25

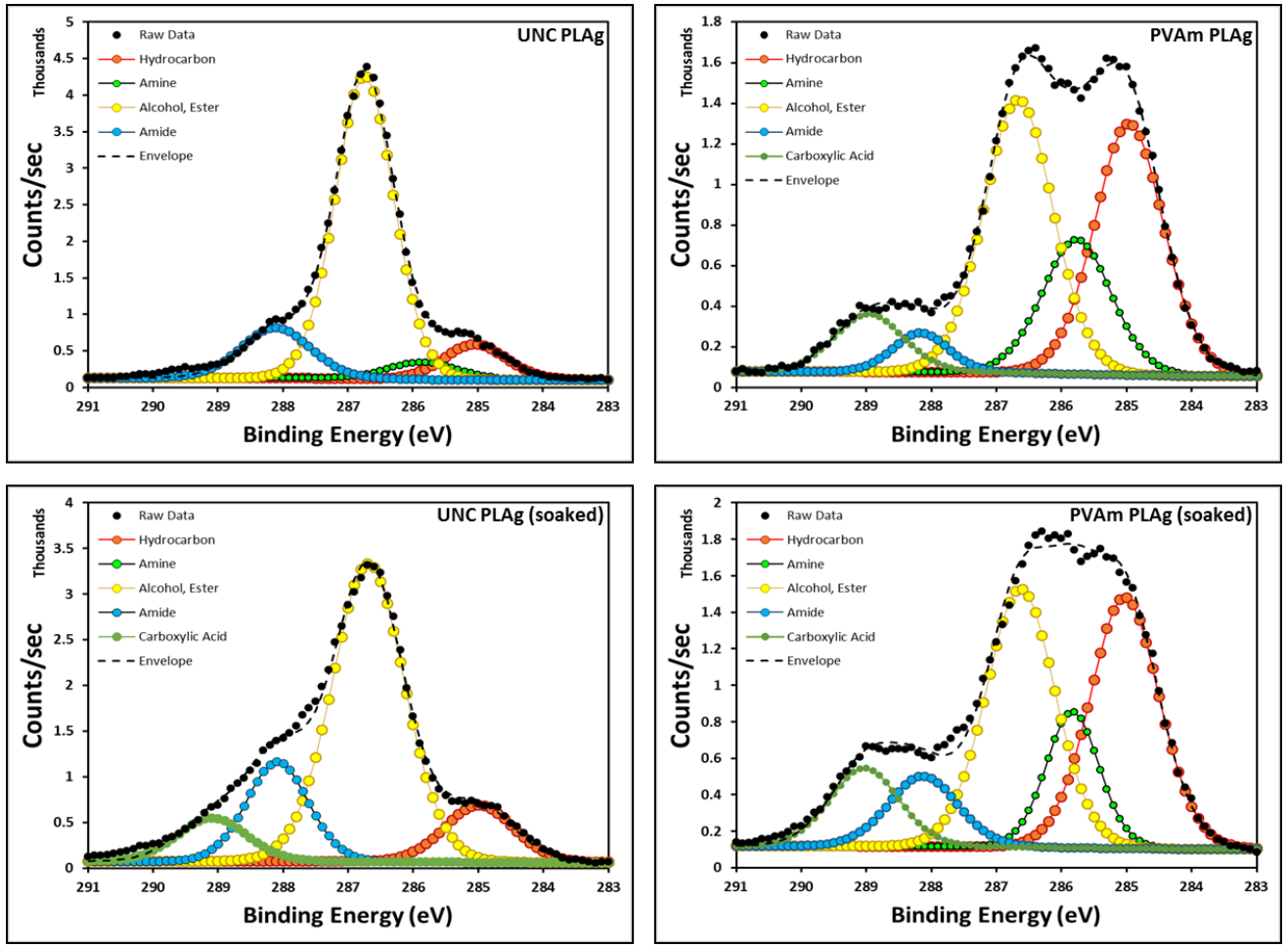

Figure 4.19 - High resolution C1s core level spectra allowing deconvolution of C bonding. Uncoated PLAg (top left), PVAm coated PLAg (top right), pre-soaked uncoated PLAg (bottom left) and pre-soaked PVAm coated PLAg (bottom right). Pre-soaking was conducted in bacteriophage buffer for 24 h at 4°C to determine detachment of PVAm surface coatings from the polymer film. Each spectrum represents the mean value of three independent measurements.

4.3.3.6 SEM and EDS analysis

SEM and EDS analysis were conducted on PLAg and PVAm-PLAg films to determine elemental surface composition. Due to the use of non-fixed samples, only low magnification (25K x) images were obtained. This was as a consequence of sample decomposition at high magnification which impeded identification of surface structures. While no differences in topography were noted at low magnification for the film variants, EDS of PVAm-PLAg films demonstrated an increase in N, decrease in O, and marginal decrease in C, in relation to PLAg films (Figure 4.20). EDS spectra obtained at four points within an PVAm-PLAg image (obtained at 25K x magnification) showed uniformity of the PVAm surface coating with equal levels of C, N, and O at each measurement point (Figure 4.21).

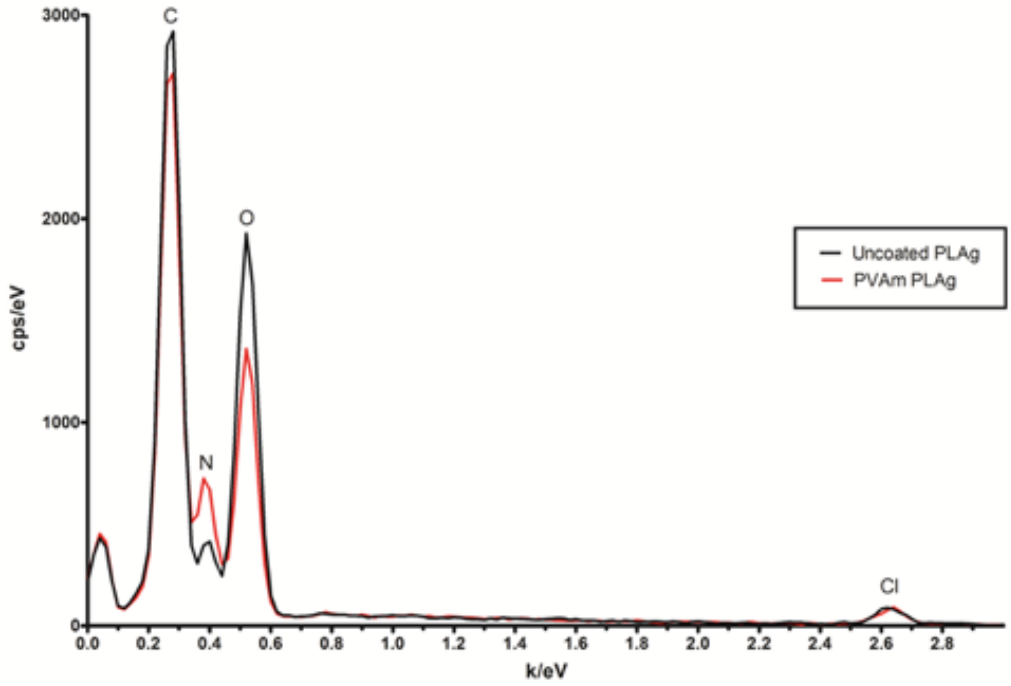

Figure 4.20 - EDS spectra obtained from SEM micrographs of PLAg (black) and PVAm-PLAg (red) in the absence of fixation and sputter coating. Images were obtained at low magnification (25k x) to avoid sample degradation.

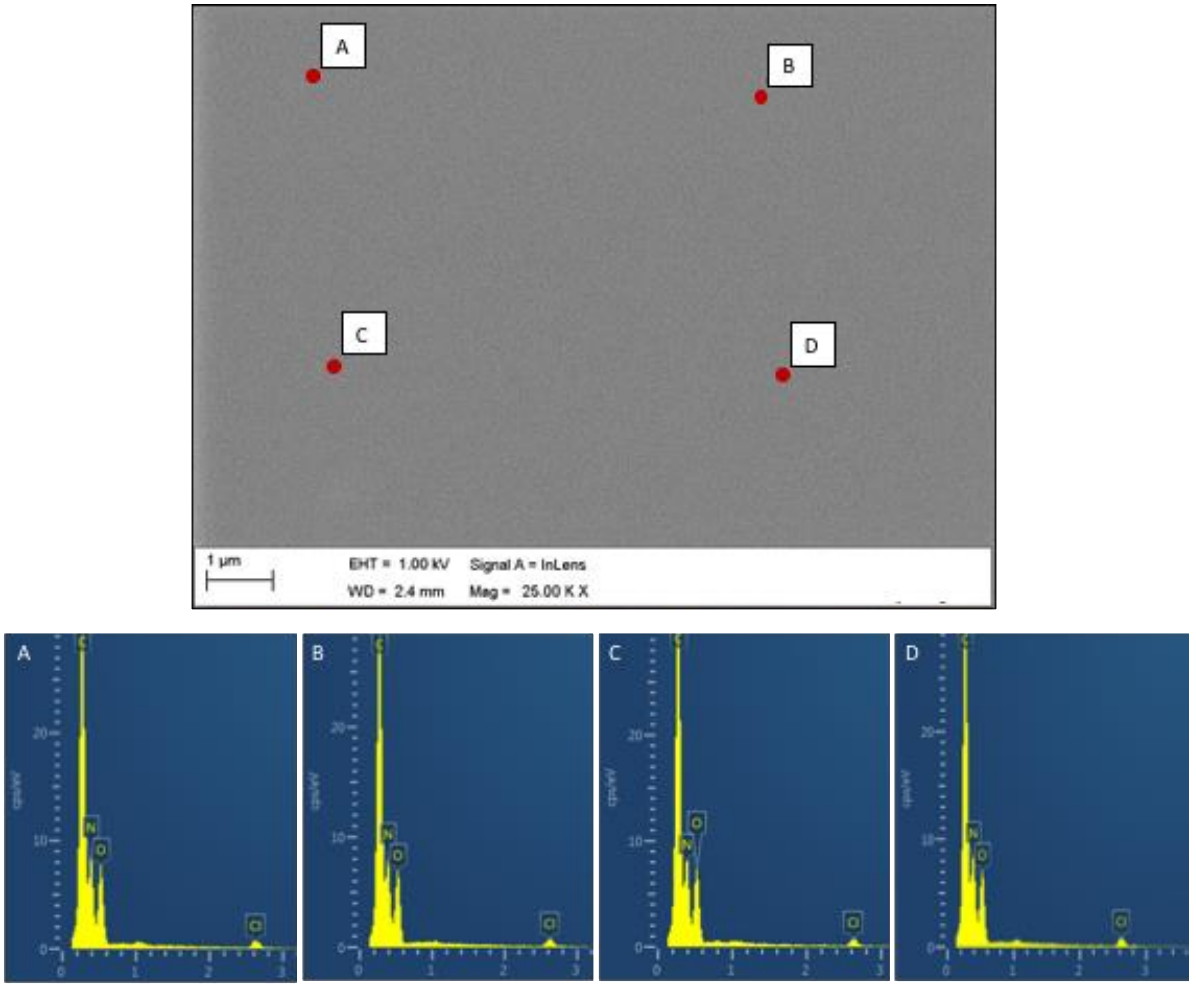

Figure 4.21 - SEM micrograph of PVAm-PLAg at 25k x magnification (top) and EDS spectra of four points (A to D – below) allowing elemental analysis at specific points within the image.

4.3.3.7 Surface zeta potential

Interfacial zeta potential measurements were made using a specialised surface zeta potential cell (ZEN1020) designed for use with the ZetaSizer Nano ZS90. Prior to obtaining measurements for the samples of interest, standards were used to validate the equipment and preliminary studies were conducted to determine methodological approaches, such as tracer particle suitability (see Appendix III). All measurements were made in bacteriophage buffer, at pH 7.2 and 25°C. Once the methodology was established and validated, the surface zeta potential of PLAg and PVAm-PLAg films (0.5 % w/v PVAm) were determined, with uncoated PLAg giving a surface zeta potential value of negative (-)24.1 ± 0.76 mV and PVAm-PLAg of positive (+)22.5 ± 1.62 mV (Figure 4.22). This data demonstrates the successful modification of surface charge from that of anionic to cationic by deposition of PVAm on the surface of PLAg films.

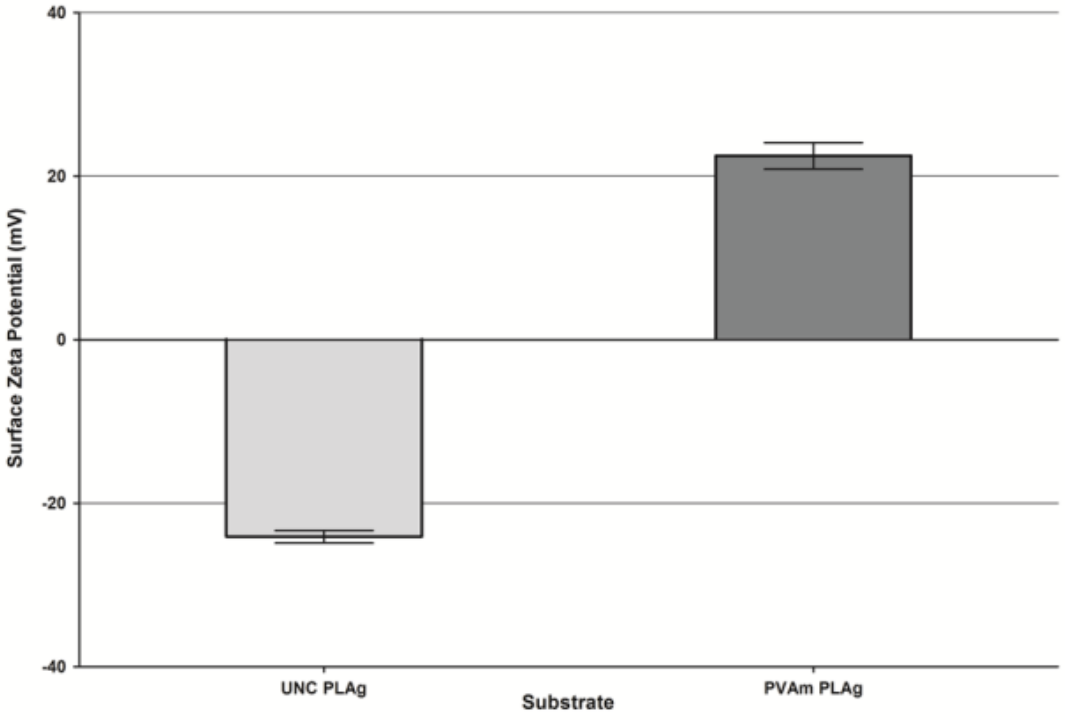

Figure 4.22 - Surface zeta potential measurements of PLAg and PVAm-PLAg films in bacteriophage buffer (pH 7.2, 25°C). PVAm-PLAg films were formulated with a surface coating concentration of 0.5 % w/v. Unmodified polystyrene latex tracer particles were used for PLAg and NR3+ modified particles for PVAm-PLAg films. Mean values were obtained from three independent experiments (N=3) ± SD.

Once the surface charge of PVAm-PLAg films was established, incremental PVAm surface coating concentrations were assessed to determine the optimal PVAm concentration for coating (Figure 4.23 and Table 4.5). The point at which a plateau in surface zeta potential was reached was considered the point at which the entire surface of the unmodified PLAg film was covered with PVAm. A significant difference was observed between PVAm concentrations of 0.06 % and 0.125 % (P = 0.0028), and between 0.125 % and 1 % (P = 0.0394). The plateau, therefore, was considered to have begun at a PVAm concentration of 0.25 % as no significant differences between PVAm was found between this measurement up to 1 % PVAm concentration.

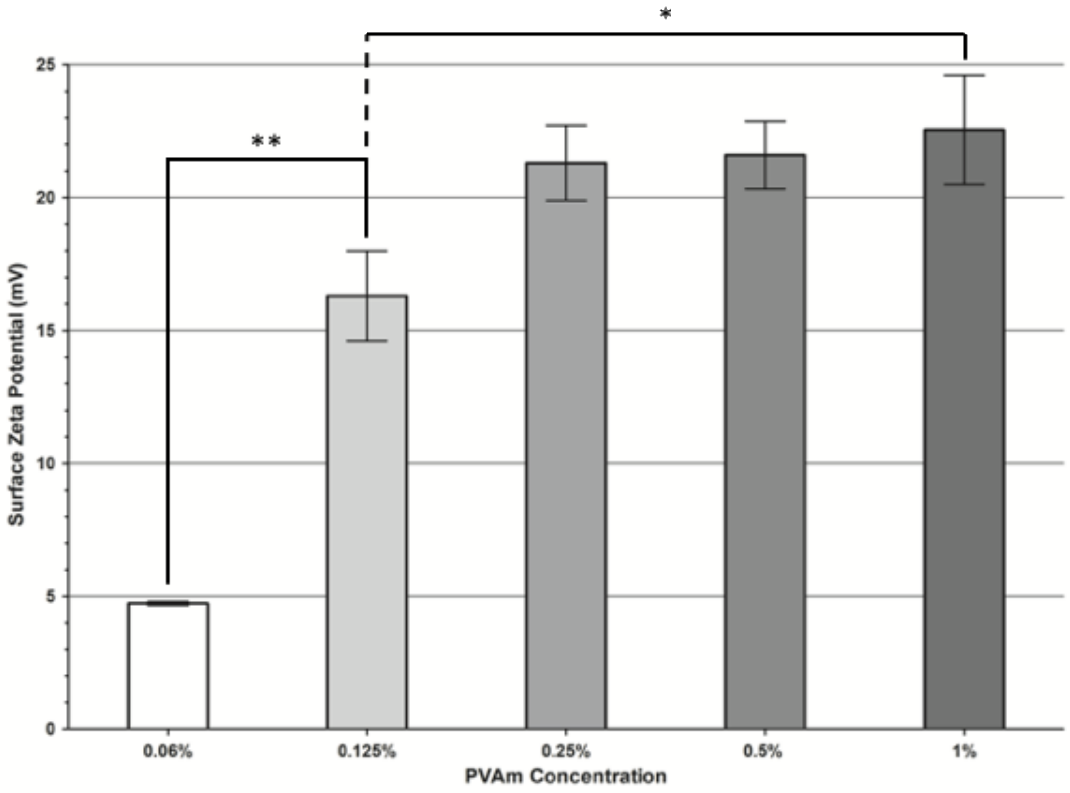

Figure 4.23 - Surface zeta potential measurements of PVAm-PLAg films in bacteriophage buffer (pH 7.2, 25°C). PVAm-PLAg films were formulated with a surface coating concentration of 0.06% to 1% w/v. NR3+ modified particles were used for PVAm-PLAg film measurements. Each value depicts the mean of three independent measurements (N=3) ± SD. Statistical analysis was conducted using one-way ANOVA and analysed using Tukey's multiple comparisons post-hoc test.

Table 4.5 - Surface zeta potential measurements of PVAm-PLAg films of incremental surface PVAm concentration, in bacteriophage buffer (pH 7.2, 25°C).

PVAm concentration (%/film)	Surface zeta potential (mV)	±SD
0.06	4.73	0.057
0.125	16.3	1.697
0.25	21.3	1.414
0.5	21.6	1.273
1.0	22.6	2.051

4.3.4 Synthesis of Alg-PVAm-PLAg composite materials

This section outlines the synthesis of Alg-PVAm-PLAg composite materials, using two methods of alginate hydrogel cross-linking: oxidation of Fe(II), and the $CaCO_3$-GDL system. The base material, PLAg, was used as a structural support for alginate hydrogels, in the presence and absence of PVAm surface coating. The mechanical stability of alginate hydrogels and adsorption to PLAg and PVAm-PLAg films was assessed by manual manipulation of the material.

4.3.4.1 Alginate gelation by oxidation of Fe(II)

Successful gelation of alginate by air oxidation of Fe(II) to Fe(III) was achieved at iron concentrations ranging from 500 mM to 1 M, resulting in a reduction of gelation time from 48 h to 2 h, respectively. Figure 4.24 shows iron cross linked alginate hydrogels at 750 mM concentrations: attached to the surface of a PVAm-PLAg film (top left), formed in the bottom of a 25 ml beaker (bottom left), and formed in a 12 well plate (right). Mechanical strength was manually assessed (by hand) by bending of the composite film shown in Figure 4.24a. Bending of the composite material resulted in splitting of the hydrogel layer at all tested iron concentrations (500 mM to 1 M) and the formulation was therefore omitted from further study due to the inadequate mechanical characteristics. It was discovered, however, that the iron cross linked hydrogel adhered to the surface of PVAm-PLAg films, and not unmodified PLAg films, suggesting an interaction between the alginate hydrogel and the PVAm surface coating.

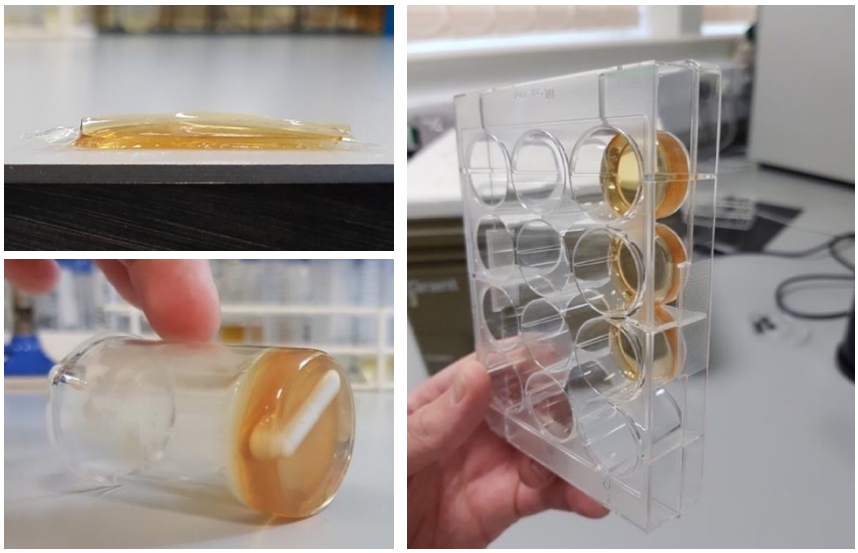

Figure 4.24 - Images of alginate hydrogels cross-linked by the air oxidation of iron(II) to iron(III). Images show the Alg-PVAm-PLAg composite (top left), alginate hydrogel formed in the bottom of a 25 ml beaker (bottom left), and alginate hydrogels formed within wells of a 12-well plate.

4.3.4.2 Alginate gelation by internal liberation of calcium ions

Successful gelation by internal liberation of calcium ions using the $CaCO_3$-GDL system was achieved using final concentrations of 1.5 % w/v alginate, 1 % w/v GDL, and 1 % w/v $CaCO_3$, which resulted in a sol-gel transition at approximately 30 minutes. The aforementioned concentrations were based on a previous study conducted by Draget *et al* (1990), who reported optimal gel strength when using equal concentrations of Ca^{2+} and GDL [281]. Figure 4.25 shows the alginate hydrogel formed in the bottom of a 15ml bijoux bottle (after the sol-gel transition had taken place), 30 minutes after the addition of GDL.

Figure 4.25 - Image of an alginate hydrogel, formed within a 15 ml bijoux bottle, cross-linked using the $CaCO_3$-GDL system of internal liberation of Ca^{2+} ions. Final concentrations of the hydrogel formulation were as follows; 1.5 % alginate, 1 % GDL, and 1 % $CaCO_3$.

Alginate composites were then synthesised by addition of alginate-GDL-$CaCO_3$ in the sol state to the surface of PLAg films, with and without the PVAm surface coating. Hydrogels were then allowed to cross-link at room temperature and atmospheric pressure for 2 h prior to observation. Figure 4.26 shows the composite material composed of the PLAg base material and alginate hydrogel (Alg-PLAg), in the absence of surface modification with PVAm. No affinity was observed between the hydrogel layer and base material for Alg-PLAg materials, with the alginate layer easily coming away from the PLAg.

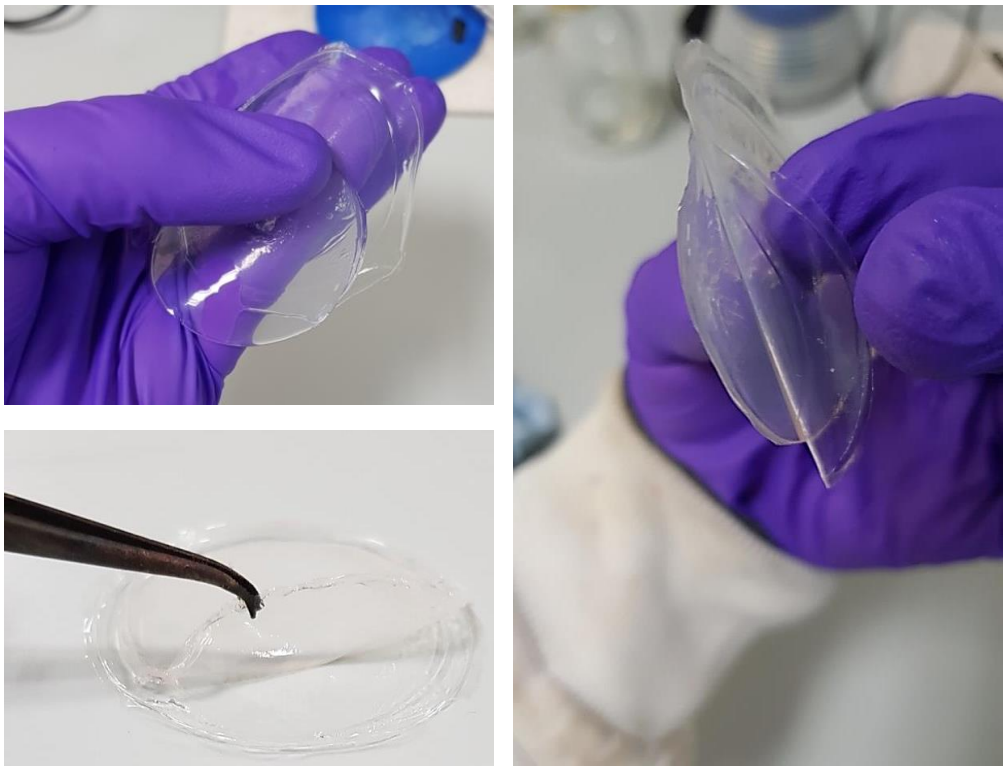

Figure 4.26 - Images of Alg-PLAg film composites synthesised by the addition of alginate-GDL-$CaCO_3$ to the surface of PLAg films and allowed to cross link for 2h under ambient conditions. No affinity was observed between the alginate hydrogel layer and PLAg film base material (N=5).

Composite materials were then synthesised with PVAm-PLAg films as the base material, by addition of alginate-GDL-$CaCO_3$ to the surface of PVAm-PLAg films in the sol state (Alg-PVAm-PLAg). After 2 h cross-linking under ambient conditions, the alginate hydrogel layer demonstrated significant affinity to the PVAm-PLAg film (Figure 4.27). The alginate hydrogel layer remained static on the surface of the PVAm-PLAg film and no areas of weakness were observed when Alg-PVAm-PLAg composites were cut in half and manipulated by hand. The mechanical stability of alginate in the composite form also showed increased mechanical strength and less susceptibility to splitting than when in the composite form (investigated by manual manipulation).

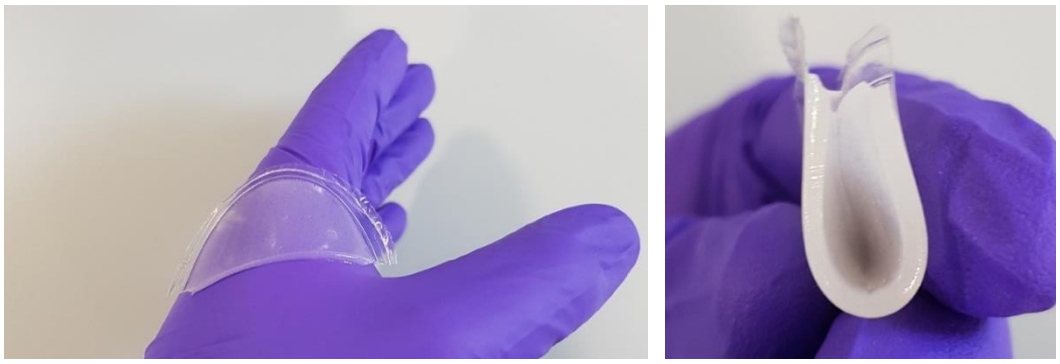

Figure 4.27 - Images of Alg-PVAm-PLAg film composites synthesised by the addition of alginate-GDL-$CaCO_3$ to the surface of PLAg films and allowed to cross link for 2 h under ambient conditions. High affinity was observed between the alginate hydrogel layer and PVAm-PLAg film base material (N=5).

4.4 Discussion

The work conducted in this chapter has led to the synthesis and characterisation of three material variants intended for wound dressing applications: PLAg, PVAm-PLAg, and Alg-PVAm-PLAg. Each material was a progression of the base material, PLAg, which was synthesised based on methods outlined by Shamsuri *et al* (2012) [262]. While a number of characterisation steps were utilised in the referenced study, leaching of plasticiser upon rehydration of the film was an area left unmentioned. Due to the intended application of this material as a wound dressing, the initial phase of the present study investigated the composition of PLAg films with incremental plasticiser concentrations and the loss of plasticiser subsequent to washing steps, by FTIR spectroscopy. The cytotoxicity of PLAg leachate against the 3T3 fibroblast cell line was then determined by MTS assay. The development of PVAm-PLAg resulted in the successful modification of the interfacial layer, to produce a cationic surface for the attachment of bacteriophage in further studies. The development of PVAm-PLAg began with the purification of commercially available PVAm to ensure complete conversion of the polymer precursor and remove impurities produced as a side product of polymer synthesis. Once purified and characterised by molecular methods, PVAm was applied to PLAg films by dehydration on the film surface. The presence and level of permanence of PVAm at the material interface was determined by FTIR, EDS and XPS, while changes in surface topography and physical characteristics were visualised by contact angle analysis and AFM. Finally, a composite material (Alg-PVAm-PLAg) was developed by addition of a hydrogel layer to the surface of PVAm-PLAg films.

4.4.1 PLAg film synthesis and characterisation

Qualitative and macroscopic evaluation of PLAg films indicated an increase in flexibility and transparency with increasing concentrations of plasticiser, with the most notable increase in favourable characteristics observed between 0 % and 30 % w/v plasticiser. No signs of syneresis were observed over long periods of time at room temperature and atmospheric pressure (days to months), suggesting the compatibility of agarose-plasticiser and a level of permanence. Synthesis of PLAg films proved simple and cost effective, with the vast majority of expense associated with the agarose polymer. Subsequent to dehydration, a reduction in film size was noted (approximately 1-2 mm diameter), most likely due to the agarose matrix contracting during removal of the solvent [282]. Film thickness varied with cast size due to agarose concentration/cm^2, therefore the film thickness was optimised for the Teflon casts and remained constant where possible. Based on macroscopic evaluation and manual manipulation, PLAg films containing 50 % w/v

plasticiser (also referred to as IL50) were carried forward for further investigation, unless otherwise stated.

PLAg films containing 50 % plasticiser were analysed by SEM, initially focusing on surface topography. At lower magnification (10,000 x) a rippled surface was observed and higher magnification (150,000 x) revealed the presence of pores within the film surface. Pore size was determined using ImageJ software, allowing simultaneous measurements of all porous structures on a selected image. Average pore size indicated was 14.00 nm ± 5.32 SD (N=513). Pernodet *et al* (1997) [283] measured the pore size of hydrated agarose gels using atomic force microscopy (AFM) under aqueous conditions; recording sizes of approximately 200 nm – 400 nm for a gel of 3 % agarose w/v. An average pore size of 14 nm therefore indicates a significant contraction of the agarose matrix during dehydration, consistent with the reduction of film size; while retaining a nano-porous structure. It should be noted, however, that samples that underwent SEM analysis were fixed in glutaraldehyde prior to ethanol dehydration which could further interfere with pore size measurements. Further problems arose at high magnification, with ionisation of the polymer film and degradation of the material due to the electron induced break down of chemical bonds. To circumvent the limitations of SEM analysis of polymer films, PLAg film samples were analysed by AFM under ambient conditions with no prior sample preparation. The topography of PLAg films determined by AFM was shown to be consistent with findings from SEM analysis, with a rippled surface and the presence of pores. These pores, however, were larger in diameter when observed by AFM. This highlights the importance of using equipment and sample preparation suitable for the sample of interest, to avoid the introduction of artefacts. In the case of polymer films which are easily manipulated and damaged, it may be preferable to utilise techniques which require minimal sample preparation and do not alter structural characteristics during imaging, such as non-contact AFM.

FTIR was conducted on dehydrated PLAg films of incremental plasticiser concentrations (0 % - 50 %) to determine the presence of functional groups and intermolecular interactions of agarose and the plasticiser. The FTIR spectra of agarose films exhibited strong, broad peaks at approximately 3350 cm^{-1} consistent with OH bond stretching of alcohol groups present in agarose. Smaller peaks with lesser intensity at approximately 3200 cm^{-1} are consistent with NH stretching vibrations and are only present in samples containing plasticiser. Peaks at approximately 2960 cm^{-1} can be assigned to CH bending of agarose and is present in all film samples. Bands with strong intensity were observed at approximately 1600 – 1700 cm^{-1} and can be assigned to NH bending of urea, only present in films containing plasticiser. There was, however, a peak with low intensity in this region for the sample containing no

plasticiser. This could be due to a weak CH bend vibration of agarose or an artefact of residual water present in the agarose film. At approximately 1450 – 1500 cm^{-1} peaks were observed in samples containing plasticiser due to CH_3 bending of choline chloride. Peaks at 1400 cm^{-1} were present for all samples, consistent with C-C bending of agarose.

Surface analysis of PLAg films was conducted by XPS and EDS analysis, providing insight into the elemental composition at the material interface. Low resolution XPS survey scans revealed C, N, and O at the material interface, consistent with the presence of agarose and plasticiser. Analysis of core level C1s spectra allowed deconvolution of the C peak to determine the elemental bonding at the interface. High levels of C-O-C and C-O-H bonding arose from the presence of repeating units of D-galactose and 3,6-anhydro-L-galactopyranose found in the agarose polymer. Lower levels of C-C, C-N, and N-C=O bonding are consistent with the presence of choline chloride and urea components of the plasticiser. These findings were in line with EDS analysis, which also revealed the presence of C, N, O, and Cl at the material interface.

The FTIR spectra obtained from incremental concentrations of plasticiser resulted in a change in peak intensity and wavenumber; allowing analysis of the intermolecular interactions between the two components. Notable shifts in wavenumber occur with OH stretching and NH stretching shifting to lower wavenumber as the plasticiser concentration increased. This phenomenon was also evident in NH and OH bending groups. This has been documented previously and can be explained by an increase in hydrogen bonding between hydroxyl groups of agarose and amide groups of ChCl/Urea plasticiser [262]. These data show that there is an interaction between agarose and the plasticiser at a molecular level and may explain the absence of syneresis under ambient conditions. FTIR analysis of pre-soaked PLAg films, however, revealed a reduction in NH (approx. 1650 cm^{-1}) and CH_3 (approx. 1450 cm^{-1}) functional groups, associated with the loss of urea and choline chloride, respectively. Surface analysis of PLAg by XPS, subsequent to soaking in bacteriophage buffer for 24 h at 4°C, indicated a reduction in N and complete removal of Cl_2 from the surface of PLAg. High resolution C1s core level analysis allowed deconvolution of C bonding and showed complete removal of C-N bonding and marginal reduction of C-O-H bonding from the interfacial layer. The findings outlined by FTIR and XPS analysis suggest that the plasticiser is solubilised upon rehydration of PLAg, releasing ChCl and urea into the solvent, with urea more prone to removal at the material interface. These findings are in line with a recent study conducted by Tenhunen *et al* (2017) [284], in which the authors investigated the interactions of cellulose with the same deep eutectic solvent used as plasticiser in this thesis. It was reported that the N of ChCl bound strongly to cellulose and could not be removed with an ethanol washing procedure. Furthermore, in the present study,

macroscopic evaluation of pre-soaked, dehydrated PLAg revealed a reduction in flexibility when compared with non-soaked PLAg, indicating leaching of plasticiser during rehydration.

To investigate any potential cytotoxicity from the PLAg leachate, preliminary MTS assays were conducted using a murine fibroblast cell line (3T3). The percentage cell viability, related to the untreated cell control, was determined subsequent to 24 h exposure of 3T3 cells to PLAg film leachate in standard cell culture media. Results obtained in this study demonstrated no cytotoxic effects of PLAg leachate under the tested conditions. However, it must be noted that the concentration of plasticiser leachate was unknown and may be cytotoxic in higher proportions. Interestingly, some deep eutectic solvents (including ChCl/urea) have been shown to promote cell viability in human keratinocyte cell lines and are becoming of high interest in the pharmaceutical industry [285]. Further work should therefore investigate the cytotoxic effect of PLAg leachate at incremental concentrations in an artificial wound exudate medium.

4.4.2 Purification and characterisation of PVAm

In order to modify the surface charge of PLAg films, a highly charged polymer (PVAm) was applied to the surface of PLAg to obtain a cationic interfacial charge. PVAm was identified as a suitable tool for modifying the surface charge of PLAg due to it containing the highest content of primary amine functional groups of any polymer [193]. Only becoming commercially available over the past decade due to manufacturing challenges, PVAm can now be obtained in the form of copolymers with precursor vinyl monomers, the most common of which being N-vinylformamide (NVF). To synthesise PVAm from NVF, free radical polymerisation with subsequent hydrolysis is employed to obtain high molecular weight, linear, water soluble PVAm-co-NVF. It is generally necessary to purify commercial PVAm products, due to incomplete hydrolysis and the presence of side products such as formic acid [286]. For small-scale laboratory purposes, hydrolysis followed by dialysis and lyophilisation will usually suffice [193]. In this study, Xelorex RS1300 was obtained from BASF (UK) and purified by further hydrolysis, dialysis and lyophilisation. The chemical structure, purity and stability of the purified polymer was then determined using FTIR and NMR spectroscopy.

FTIR analysis was conducted on freeze dried polymers to eliminate the strong broad peaks between 3700 to 3100 cm^{-1} present in aqueous samples, which would mask significant peaks associated with the presence of amine functional groups. FTIR analysis of non-purified PVAm showed a strong broad peak at approximately 3350 cm^{-1} assigned to OH stretching

of carboxylic acid, likely the formic acid impurity of PVAm synthesis. This peak was not observed with the purified sample indicating the removal of a carboxylic acid impurity. Between 1650 cm^{-1} and 1580 cm^{-1} are peaks assigned to NH bending of primary amines, with both samples presenting peaks in this region. Further primary amine regions were observed at 3320 cm^{-1} and 3250 cm^{-1} in purified PVAm samples. The spectra obtained therefore indicates the successful removal of impurities present in the commercial sample. While FTIR analysis allowed determination of functional groups present in non-purified and purified samples, NMR spectroscopy was used to further characterise the molecular composition of purified PVAm. NMR spectroscopy of purified PVAm showed two peaks at 1.4 ppm and 3.0 ppm, which correspond to two separate proton environments of the PVAm aliphatic alkyl chain (Figure 4.11), giving a structural resolution to the polymer. Amine regions were not observed due to exchange of NH protons with deuterium, however alongside data obtained by FTIR these findings suggest the successful hydrolysis of residual precursor (poly-NVF) to PVAm and removal of the associated major side products, such as formic acid.

The synthesis of PVAm by hydrolysis of NVF precursor has been reported to result in reversible amidine formation, which can decompose leaving an alcohol in place of the amine [280]. In order to obtain a cationic interface when applied to the surface of PLAg films, maintaining and monitoring the stability of the purified PVAm for a practical amount of time was of utmost importance. While reports of PVAm decomposition have been made [280], no studies have yet investigated the optimal storage conditions for the polymer. Decomposition of PVAm would result in batch-to-batch inconsistency when applied to PLAg films as a surface coating, and reduced efficacy of the final application. Therefore, the optimal storage conditions of lyophilised purified PVAm were determined over a 12 month period.

FTIR analysis of PVAm stored under ambient conditions for 12 months shows an additional band at approximately 1480 cm^{-1} which can be assigned to -OH bending of alcohol functional groups, suggesting degradation of the polymer over time. To evaluate the stability of PVAm over time, a number of storage conditions were used over a 12 month period followed by further evaluation by FTIR spectroscopy. It was determined that storage of PVAm under nitrogen at -20°C resulted in no discernible presence of -OH functional groups over a 12 month period, with all other storage conditions resulting in the presence of -OH as determined by FTIR analysis. These findings present the first investigations in to the stability of commercially sourced, purified PVAm under various storage conditions.

4.4.3 Characterisation of PVAm-PLAg films

Three methods of surface coating were assessed during the development of PVAm-PLAg films: drying, adsorption and gel dehydration. Air drying of PVAm polymer to the surface of pre-formed PLAg films resulted in an unevenly distributed coating, indicated by an opaque ring of polymer running around the outside edge of the film, and was deemed inappropriate for further investigation. Spontaneous adsorption of PVAm to the surface of pre-formed PLAg films also yielded unacceptable results due to rehydration and subsequent dehydration of the film during the coating procedure, causing film deformation due to loss of plasticiser. Application of PVAm to the surface of PLAg gels prior to dehydration prevented film deformation and produced films macroscopically identical to standard PLAg films, with no opaque regions. This method, termed 'gel dehydration', was therefore identified as the most suitable method of PVAm surface coating and carried forward for further investigation.

Analysis of the surface topography of PVAm-PLAg films, conducted using AFM, revealed a smooth, non-porous surface with a maximum protruding height of 3.2 nm from the lowest measured point. In contrast, analysis of PLAg films by AFM aligned with findings from SEM analysis, showing a porous, rippled surface with a maximum protruding height of 15.2 nm from the lowest measured point. Images obtained from AFM, therefore, indicate a maximum surface coating thickness of approximately 12 nm and alteration of the surface topography when PVAm is applied to the surface of PLAg films.

4.4.4 Identification and stability of PVAm at the PVAm-PLAg interface

Modification of PLAg films, by the gel dehydration method, resulted in the identification of amine functional groups by FTIR spectroscopy. A reduction in transmittance of OH functional groups, when compared to PLAg films, also suggests masking of alcohol functional groups by the additional polymer layer. Once the presence of PVAm was established by FTIR, surface analysis was conducted by XPS and EDS, allowing determination of elemental composition and PVAm stability at the material interface. Low resolution survey scan XPS analysis revealed higher proportions of N at the material interface, when compared to PLAg, which aligns with the high amine content of PVAm. A reduction in O was also observed, which is in agreement with the transmittance reduction in OH functional group regions in FTIR analysis, indicating the masking of agarose by the PVAm layer. High resolution C1s core level spectra indicated a significant increase of C-C and C-N bonding in PVAm-PLAg films, associated with the alkyl chain and amine regions of PVAm, respectively. As with FTIR analysis and survey scan XPS spectra, masking of

agarose in PVAm-PLAg films was evident with reductions of C-O-C, C-O-H, and N-C=O bonding. PVAm stability at the material interface was also determined by XPS, through analysing PVAm-PLAg subsequent to 24 h soaking in bacteriophage buffer; conditions reflective of bacteriophage immobilisation in further studies. Survey scan data indicated a negligible reduction in N, while C1s core level spectra indicated a negligible reduction in C-N and C-C bonding, both indicating retention of the surface coating during immersion in bacteriophage buffer for 24 h.

The mean atomic % data obtained from XPS analysis was the mean of 3 independent measurement areas on the same sample (outer, inner, and middle). All standard deviations were within an acceptable range of <1 %, suggesting continuity of the surface coating across the entire film. Further surface analysis of PVAm-PLAg was conducted by EDS, indicating an increase in N and decrease in O and C in relation to PLAg films and aligning with findings observed during FTIR and XPS analysis. The elemental composition of PVAm-PLAg at 4 points on a 12 μm x 6 μm image was then determined, with all points showing almost identical levels of C, N, and O; further suggesting continuity of the surface coating.

4.4.5 General characterisation of PLAg and PVAm-PLAg films

The concept of moist wound healing was devised by George Winter in 1962 [287]. This theory was based on observation of one of the most significant factors impeding successful healing in burns; wound surface dehydration [288]. Further studies, however, have suggested that excessive fluid retention can result in maceration of the surrounding tissue and poor wound healing [289]. It has more recently been determined that an appropriate balance of moisture loss and retention is required for optimal wound healing [290]. The balance of moisture levels at the wound bed can be achieved by applying wound dressings with the appropriate swelling properties and moisture permeability (MVPR), with both characteristics tuneable by modifying the porosity and hydrophilicity of the material.

Swelling analysis of PLAg and PVAm-PLAg films was conducted in PBS to determine water uptake upon rehydration of the dehydrated material. It was observed that within 10 minutes of rehydration PLAg films reached equilibrium, absorbing 50 % of its dry weight in water. Between 10 minutes and 90 minutes no appreciable increase or decrease in water uptake was observed. The swelling profile of this material may be in part due its nano-porosity. However, it was also observed that upon subsequent dehydration of the material it became slightly less flexible with similar qualities to those of films plasticised to a lesser degree. This could be explained due to the effect of water entering the material, solubilising the plasticiser and replacing the hydrogen bonding, allowing leaching of the plasticiser into

solution; a hypothesis backed up by FTIR analysis. PVAm-PLAg films reached equilibrium after 25 minutes incubation. The swelling % of PVAm-PLAg films was observed as consistently above that of PLAg films, likely due to the additional hydrophilic dehydrated polymer component, absorbing additional water upon rehydration.

While the optimal MVPR of wound dressings is unclear, the rate of water transmission is an important parameter in wound dressing development by allowing determination and regulation of moisture permeability. The MVPR was determined for PLAg and PVAm-PLAg films, with values of 3.3 g/10 cm^2/24 h, and 3.2 g/10 cm^2/24 h, respectively. These findings correlate with the observation of porous structures during SEM and AFM analysis. Interestingly, negligible difference (0.1 g/10 cm^2/24 h) was observed between the MVPR of PLAg and PVAm-PLAg films (P = 0.055). This finding may suggest that upon rehydration of PVAm-PLAg by water vapour, the porosity of the film reverts to similar levels as PLAg films, allowing almost identical water vapour transmission rates across the membrane. These MVPR values correlate with novel chitosan [291] and polyurethane [292] wound dressing materials.

Contact angle (CA) measurements of PLAg films demonstrated highly hydrophilic surface compositions, with an average internal CA of 17°. This hydrophilicity can be explained by agarose comprising of polysaccharides with hydroxyl groups located on planar sugar rings, limiting the ability of molecular rearrangement at the film interface [293]. The addition of the ChCl/Urea plasticiser may also have implications for the hydrophilicity of the PLAg film due to further polar hydroxyl groups, with a study conducted by Abbott *et al* (2006) [294] reporting increased hydrophilicity when coating the surface of cellulose fibres with a choline chloride/urea based ionic liquid. The addition of further exposed hydrophilic amine groups on the surface of PVAm-PLAg films was expected to result in a similar hydrophilicity. However, the average CA of PVAm-PLAg films was 43.3° ± 2.45° SD.

The reduced hydrophilicity observed in PVAm-PLAg films could be a caused by a number of factors outlined in Figure 4.28. Low PVAm coating concentration (Figure 4.28 A1) could result in misalignment of PVAm on the PLAg film interface and exposure of the hydrophobic alkyl chain. This could in turn reduce the number of available bacteriophage binding sites by excessive association of amine regions with the PLAg film interface. However, this theory could be tested by increasing the PVAm coating concentration which would lead to an increase in amine binding sites (Figure 4.28 B1). Another intervention may be increasing the salt concentration of the polymer dispersant. Both conformation in solution and deposition of polyelectrolytes such as PVAm are dramatically influenced by the salt concentration of the polymer dispersant [295]. The absence of additional electrolytes

results in a highly extended polymer conformation due to repulsion of the polyelectrolyte charged groups. The deposition is consequently of a flat nature as depicted in Figure 4.28 A2. Conversely, high concentrations of salt (1-2 M) may result in 'screening' of the repulsive charges and leads to a denser polymer deposition (Figure 4.28 B2). Investigations to date have been conducted using PVAm dispersed in 0.005 M NaCl adjusted to pH 10, therefore an increase in salt concentration of the polymer dispersant could prevent over-association of amine regions to the PLAg film interface at lower PVAm concentrations. Finally, increased hydrophobicity of PVAm coated PLAg films could have been due to the surface coating blocking leaching of hydrophilic plasticiser, creating a 'more hydrophobic' (but still overall hydrophilic) interface than non-modified PLAg (Figure 4.28 A3 and B3).

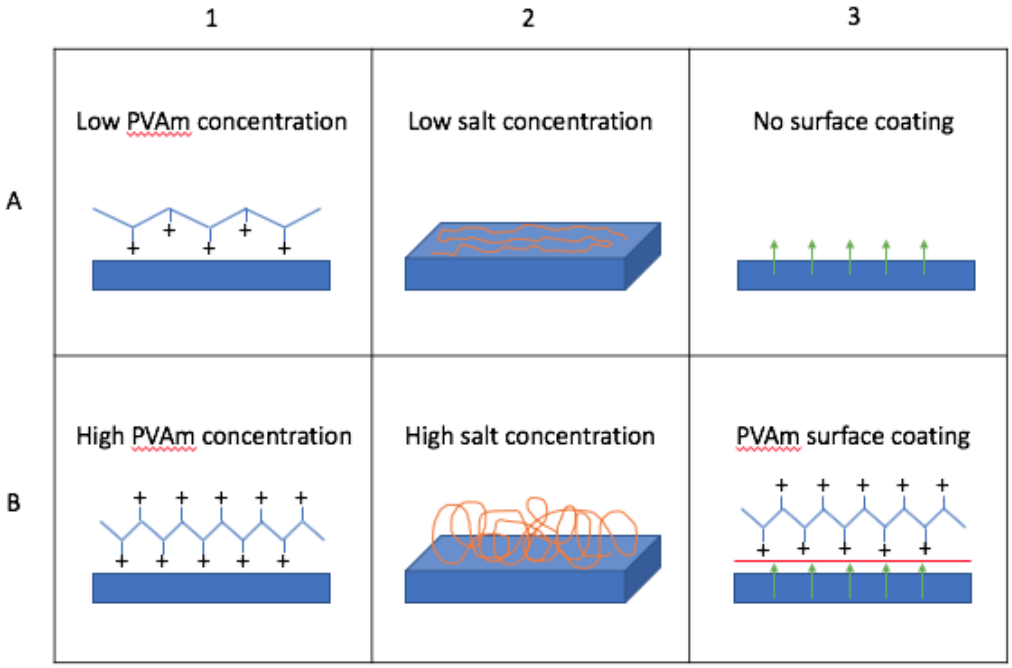

Figure 4.28 - Theoretical representations of the consequences of low PVAm concentration (A1), low salt concentration (A2), and no surface coating (A3) on the hydrophilicity of polymer films. A1 represents misalignment of the polymer exposing the hydrophobic alkyl chain, A2 represents flat polymer (orange line) deposition, and A3 represents the leaching of plasticiser from uncoated PLAg (green arrows). Row B represents the theoretical approaches circumvent factors in row A, by increasing PVAm concentration (B1), increasing salt concentration (B2), and application of the surface coating (B3).

The modification of PLAg films by the application of PVAm was conducted to obtain a cationic interface for bacteriophage adsorption in further studies. It was therefore critical to determine the surface charge of PLAg and PVAm-PLAg films in the relevant adsorption medium (bacteriophage buffer). Surface charge analysis was conducted using a specialised surface zeta potential cell, designed for use with the ZetaSizer Nano series. The surface zeta potential of PLAg and PVAm-PLAg films was determined as negative (-)24.1 ± 0.76 mV

and positive (+)22.5 ± 1.62 mV, respectively. Application of PVAm to the surface of PLAg therefore altered the surface charge from negative to positive. Further surface zeta potential analysis was conducted on PVAm-PLAg films with incremental PVAm concentrations at the material interface (0.06 % w/v to 1 % w/v). Statistically significant increases in surface zeta potentials were observed between 0.06 % and 0.125 % with a plateau occurring between 0.25 % and 1 %. This plateau was considered the point of saturation of PVAm at the material interface. The concentration of 0.5 % w/v PVAm was used in all previous characterisation procedures and was carried forward for bacteriophage adsorption studies due to the theories outlined in Figure 4.28A1/B1. PVAm concentrations of 1 % w/v were omitted due to the labour-intensive nature of PVAm purification for relatively low return in terms of surface zeta potential.

The results presented in this subsection revealed the successful purification of commercially sourced PVAm by further hydrolysis, followed by dialysis and lyophilisation to produce a product free from impurities. Molecular analysis at the material interface demonstrated that the coating method employed was effective and stable, and that the surface properties were modified when PVAm was applied to the PLAg interface. Surface zeta potential measurements further demonstrated a change in surface properties, giving the desired outcome of altering the surface charge of PLAg from anionic to cationic.

4.4.6 Alg-PVAm-PLAg composite synthesis and macroscopic evaluation

While orientated adsorption of bacteriophage to PVAm-PLAg films provides significant theoretical advantages in the preparation of bacteriophage integrated biomaterials, viral particles may be exposed to harsh external conditions which could reduce the antimicrobial potential of the material prior to application. Alg-PVAm-PLAg composite materials were therefore developed, with the rationale for integrating bacteriophage within the hydrated, protective matrix of alginate hydrogels. Alginate hydrogels were selected as suitable vehicles for bacteriophage delivery to the wound site based on numerous favourable characteristics, including high biocompatibility, non-toxicity, flexibility and the capability of absorbing excess wound fluid [296]. One factor of significant interest for the incorporation of bacteriophage is the intrinsic property of alginate hydrogel to degrade in contact with wound fluid, due to the exchange of sodium ions in wound exudate with calcium ions in the hydrogel [297] thus allowing release of bacteriophage upon application to an infected wound. Despite these advantageous characteristics however, alginate hydrogels tend to have poor mechanical stability in the swollen state and can dehydrate easily. To overcome these shortcomings, this section aimed to incorporate an alginate layer

on the surface of PLAg, both increasing mechanical stability and reducing the likelihood of dehydration by addition of a strong polymer film with characterised MVPR and swelling ratio.

Producing alginate hydrogels with homogenous matrices was of considerable importance for the integration of bacteriophage in further study. For this reason, alternative methods of cross-linking were explored to circumvent problems associated with the use of conventional $CaCl_2$ cross-linking. One method of exploration was the controlled formation of alginate hydrogels by air oxidation of Fe(II) to Fe(III). Successful gelation of alginate was achieved at iron concentrations ranging between 500 mM to 1 M, resulting in gelation times of between 48 h to 2 h, respectively. Manual manipulation of iron cross-linked alginate hydrogels resulted in splitting of the hydrogel at all tested concentrations and was therefore omitted from further study. An important finding, however, was that when applied to the surface of PVAm-PLAg films in the sol state and allowed to undergo the sol-gel transition in contact with the film, the alginate hydrogel showed exceptionally high adherence affinity to PVAm-PLAg. This finding was not evident when applied to unmodified PLAg, suggesting an interaction between alginate and PVAm-PLAg at the molecular level.

The second method of alginate cross-linking explored in this study was the internal liberation of calcium ions using the $CaCO_3$-GDL system. This method relies on the hydrolysis of GDL to gluconic acid, resulting in the release of Ca^{2+} by the protonation of $CaCO_3$. Optimisation of this system resulted in a sol-gel transition of approximately 30 minutes, using final concentrations of 1.5 % w/v alginate, 1 % w/v GDL, and 1 % w/v $CaCO_3$. Manual manipulation of alginate hydrogels cross-linked using this method showed significantly higher mechanical strength and less susceptibility to splitting than Fe(II) cross-linked hydrogels. Furthermore, when applied to PVAm-PLAg in the sol state and allowed to undergo the sol-gel transition in contact with the film, high adherence affinity was observed between the hydrogel and PVAm-PLAg. Manual manipulation of Alg-PVAm-PLAg revealed increased mechanical strength when compared to free-standing alginate hydrogels. Due to these factors, and the superiority when compared to Fe(II) cross-linked hydrogels, the $CaCO_3$-GDL system was selected for bacteriophage integration in further study.

Chapter Five: Bacteriophage-biomaterial integration and characterisation

5 Bacteriophage-biomaterial integration and characterisation

Bacteriophage research has provided extensive evidence of antimicrobial action in *in vitro* and *in vivo* studies, which has led to recent reports of efficacy and safety in appropriately controlled clinical trials [114, 298]. Focus can now extend to the integration of bacteriophage with biomaterials for localised delivery. This area of research has received limited attention until now, however there is evidence to suggest these biologically active materials could provide a means to successfully deliver infective bacteriophage to appropriate tissues or surface to control a target bacterium [222, 299-301]. This chapter describes the integration of bacteriophage with two novel wound dressing materials; PVAm-PLAg and Alg-PVAm-PLAg. Bacteriophage distribution, orientation, dissociation and release were investigated using a range of direct and indirect techniques.

5.1 Background

A drug delivery system (DDS) can be defined as an engineered technology (formulation or device) that allows targeted delivery and/or controlled release of therapeutic substances in the body. Often a DDS will facilitate or enhance the therapeutic effect of the pharmacological substance and control the release rate, time and location within the body [302]. With polymeric wound dressings already being exploited as drug delivery carriers of conventional antibiotics [194], and the compelling potential of bacteriophage in the management of bacterial infection, the immobilisation and integration of bacteriophage within this category of wound dressings could provide a novel solution for the treatment of chronic antibiotic resistant wound infections. The clinical success of bacteriophage therapy has been shown to be highly dependent on administration of an appropriate dose of viable bacteriophage to the target site [119-121, 303], which has led to a newly established area of bacteriophage research focusing on formulations and delivery vehicles.

5.1.1 Bacteriophage adsorption and immobilisation

The immobilisation of bacteriophage on the surface of solid substrates is an area of emerging interest, with literature describing the potential of these for use in a variety of applications from bacterial sensing platforms [198] to the development of antimicrobial surfaces for the food [200] and biomedical [301] industries. Success in developing immobilised bacteriophage delivery systems is highly dependent on three factors. First and foremost, and a factor shared with all bacteriophage DDSs, is the retention of bacteriophage

viability post-immobilisation. Second is achieving high viral surface capture density. Lastly, and of high importance due to approximately 95% of isolated phage being asymmetric *Myoviridae* [106], is placement of bacteriophage in an orientation allowing exposure of the tail fibres to the external environment, so that bacteriophage retain their infective capability.

Bacteriophage may attach to inanimate materials by physical adsorption or by chemical interactions. Attachment to surfaces by passive adsorption or physical adsorption is often inefficient due to random orientation of bacteriophage on the substrate which then inhibits bacterial recognition by phage tail fibres (Figure 5.1). This factor is especially important when considering the use of asymmetric bilateral bacteriophages such as *Myoviridae*. The importance of considering the location of bacteriophage binding sites is demonstrated in a study conducted by Hosseinidoust *et al* (2011), reporting decreased bacterial recognition efficacy of tailed bacteriophage compared with symmetric bacteriophage such as *Podoviridae* when covalently immobilised on a substrate [304]. Other disadvantages of physisorption include the ease of viral detachment from the substrate due to changes in temperature, pH, ionic strength or physical shearing.

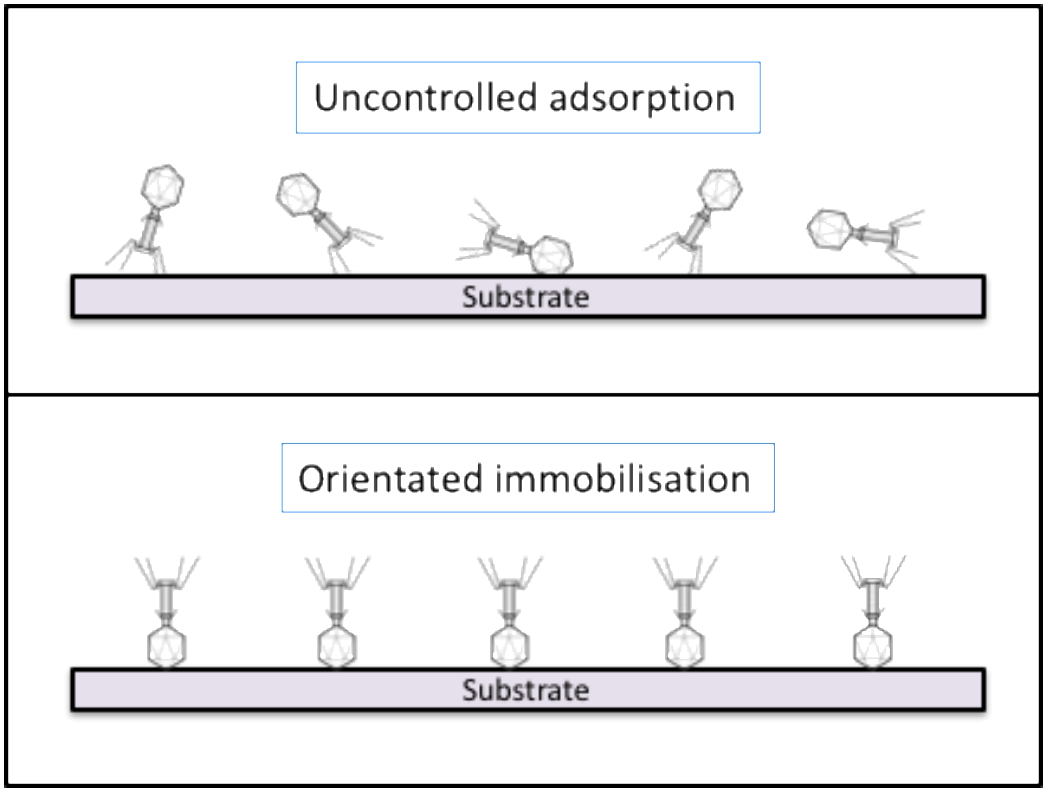

Figure 5.1 - Representation of uncontrolled adsorption (top) and orientated adsorption (bottom) of bacteriophage to a solid substrate.

A number of studies have exploited the intrinsic charge difference between the bacteriophage capsid and tail fibres to orientate bacteriophage on various substrates. While most virions possess a net negative charge at pH 7 [200], it has been suggested there is an inherent charge difference between the viral capsid (negative charge) and tail fibres (positive charge) [200, 305]. A study conducted by Anany *et al* (2011) reported significantly increased bacteriophage capture on the surface of cationic modified cellulose membranes, allowing the control of *Listeria monocytogenes* and *E. coli* growth on meat stored at different temperatures and packaging conditions [200]. This study utilised a highly charged cationic polymer to modify the surface charge of cellulose membranes, acting as an interaction site to allow negatively charged phage capsids to associate with the material interface (Figure 5.1).

While bacteriophage adsorption by electrostatic interactions may be deemed weaker than those of chemical bioconjugation, physico-chemically induced 'shedding' of bacteriophage from the substrate may be preferential when considering the materials' use as a wound dressing. These methods of orientated bacteriophage immobilisation are also likely to be more modest in terms of time and cost, when compared to covalent immobilisation, factors which are of particular importance when considering the highly specific nature of the bacteriophage infection process and the need for rapid manufacture for patients. While bacteriophage therapy is advantageous in reducing potential side effects from dysbiosis, bacterial isolates may need to be cultured prior to treatment, to screen for susceptibility to candidate bacteriophage. Once the bacterial strain and lytic bacteriophage are established, the speed at which the bacteriophage can be integrated with the wound dressing may be critical in successfully resolving the infection.

Preliminary work presented in this chapter describes the sensitivity profiles of the four bacteriophage described in Chapter 3 upon exposure to the ionic liquid plasticiser described in Chapter 4, and integration of the bacteriophage within hydrated PLAg hydrogels and dehydrated PLAg films. Tethering of viral particles to the surface of PLAg, prior, and subsequent, to surface modification with PVAm, was then investigated. Adsorption and dissociation of bacteriophage to PLAg and PVAm-PLAg was quantified using microbiological techniques, while atomic force microscopy (AFM) was employed to visualise bacteriophage at the material interface.

5.1.2 Bacteriophage integration within hydrogel matrices

When envisaging DDSs in the context of bacteriophage therapy, it is important to consider the viability of bacteriophage as the 'therapeutic substance'. Bacteriophage are protein structures and their stability, therefore, can be disrupted by an array of external physical and chemical factors, including temperature, pH, UV exposure, salinity and ion exposure [195, 196]. A suitable DDS would, therefore, need to be protective against external factors which jeopardise viral infectivity. This feature would make bacteriophage delivery systems more comparable to those of biologics, medical products derived from natural sources (human, animal or microorganisms) such as vaccines or cell transplants, than drugs formulated from synthetic chemicals. Bacteriophage entrapment within microporous matrices provides distinct advantages over methods of delivery which leave viral particles exposed to the external conditions, which may threaten bacteriophage infectivity. This structural and functional stabilisation of viral particles may be achieved by entrapment within the porous matrix of hydrogels.

The use of hydrogels for drug delivery has become an area of growing interest in recent years [194, 216, 219, 224-230, 233, 273]. Incorporation of bacteriophage within the hydrated matrix of these materials has the potential to provide stabilisation and triggered delivery to the infection site [221]. While care must be taken in the selection of compatible polymers and cross-linking initiators to prevent viral deactivation and toxicity, the potential of this delivery system spans many areas of infection control. The addition of polymer stabilisers to aqueous formulations, and the stabilisation within hydrogels, may also provide solutions for long term bacteriophage storage. This factor will become all the more important if bacteriophage therapy is to become commonplace in clinical practice. When considering hydrogels as phage delivery systems it is also important to consider the high water content of hydrogels, providing a high humidity environment which is crucial to bacteriophage infectivity, and a useful tool when delivering lyophilised bacteriophage preparations [218].

A number of studies have investigated the antimicrobial efficacy of bacteriophage encapsulated within alginate beads [125, 306, 307]. However, few publications have described the incorporation of bacteriophage within the matrix of macroscopic alginate hydrogel 'slabs'. Other than the factors dictated by the intended application (i.e. encapsulation required for oral administration), the avoidance of large alginate hydrogels could be due to the less desirable mechanical characteristics, which is especially important for wound dressing materials. Chapter 4 described the synthesis of Alg-PVAm-PLAg, a composite material composed of PLAg (base material) with an interfacial alginate hydrogel layer, where the layers are attached to one another by PVAm-mediated cationic surface

modification of PLAg. Addition of the $CaCO_3$-GDL cross-linked alginate hydrogel to PVAm-PLAg to produce the composite material appeared to confer increased mechanical strength to the former, providing a potential carrier for bacteriophage.

This chapter describes the integration of bacteriophage within the alginate hydrogel layer of Alg-PVAm-PLAg composite materials and quantifies their release under storage (4°C) and application conditions (37°C).

5.2 Methods

5.2.1 Bacteriophage sensitivity to ionic liquid plasticiser

Bacteriophage K, 44AHJD, T3 and T4 were screened for their sensitivity to ionic liquid plasticiser by quantifying the loss of infectivity after exposure to incremental concentrations of plasticiser over a 3 h period at 30°C. These conditions were selected based on those used for physical bacteriophage adsorption by desiccation described later in this chapter (section 5.2.2.2). Incremental final concentrations (0 % - 50 % v/v) of plasticiser were prepared with bacteriophage buffer as diluent, and 900 µl aliquots transferred into 1.5 ml Eppendorf tubes. Concentrations of over 50% could not be used due to the high viscosity of the plasticiser solution. 100 µl of bacteriophage (approximately 1 x 10^8 PFU/ml) was then added to each plasticiser concentration, to give a final bacteriophage titre of approximately 1 x 10^7 PFU/ml. After incubation at 30°C for 3 h, plaque assays were performed to determine PFU/ml and quantify loss of bacteriophage infectivity.

5.2.2 Bacteriophage integration with PLAg

5.2.2.1 Bacteriophage integration and release from hydrated PLAg hydrogels

Bacteriophage K and T3 integrated PLAg hydrogels were formulated as follows. PLAg hydrogels were produced by dispersing 410 µl of ionic liquid and 0.41 g of agarose (1:1 ratio) in 20 ml dH_2O and boiling at 100°C until a transparent solution was obtained. Molten plasticised agarose solution was then equilibrated in a 45°C water bath. Once at 45°C, 500 µl of bacteriophage at a known titre (see below) was added, mixed thoroughly, and the molten agarose mixture poured into a plastic petri dish. Hydrogels were allowed to cross-link for 30 min at room temperature prior to being punctured with a sterile boiling tube cap (2.7 cm diameter).

Due to difficulties in quantifying the number of bacteriophage per disk, the PFU/disk was approximated by surface area and PFU per cast (Equation 5.1).

Equation 5.1 - Estimation of bacteriophage numbers within PLAg hydrogels.

$$Estimated\ PFU\ per\ hydrogel\ disk = \frac{Ic}{\left({}^{Sc}/_{Sd}\right)}$$

Where *Ic* is the total applied bacteriophage inoculum per cast, *Sc* is the surface area of the cast in cm^2, and *Sd* is the surface area of each excised hydrogel disk in cm^2.

For example, in the case of T3 preparations:

- 1.83×10^8 PFU per cast
- Surface area of cast = 56.75 cm^2
- Surface area of excised disk = 5.73 cm^2
- Therefore approximately 10 disks per cast
- $1.83 \times 10^8 / 10$ = approximately 1.83×10^7 PFU/DISK
- Note: gel depth was constant at 0.4 cm

Bacteriophage K preparations:

- 4.25×10^8 PFU per cast
- Surface area of cast = 56.75 cm^2
- Surface area of excised disk = 5.73 cm^2
- Therefore approximately 10 disks per cast
- $4.25 \times 10^8 / 10$ = approximately 4.25×10^7 PFU/DISK
- Note: gel depth was constant at 0.4 cm

The release of bacteriophage from PLAg hydrogel disks was then quantified by placing each disk into individual 50 ml glass beakers containing 10 ml of bacteriophage buffer. After 24 h incubation at 4° C with gentle agitation (80 rpm), 1 ml aliquots were removed, and plaque assays performed to quantify bacteriophage released.

5.2.2.2 Bacteriophage infectivity subsequent to adsorption by air drying on the surface of PLAg films

Bacteriophage suspensions of known titre (T4: 3 x 10^6 PFU, Bacteriophage K: 1 x 10^7 PFU) were air dried on the surface of PLAg films by distributing 500 µl of bacteriophage lysate (6.8 cm diameter film) using a sterile plastic spreader and incubating at 30°C and 33.6 % RH for 0 h to 24 h. Air drying on the surface of glass slides was used as a control to account for PLAg film mediated bacteriophage inactivation. The viability of bacteriophage subsequent to air drying on the surface of glass slides and PLAg films for up to 24 h (0 h, 1 h, 3 h, 6 h, and 24 h) was quantified by placing each sample in 10 ml bacteriophage buffer at the relevant time point, incubating at 4°C (80 rpm) for 24 h, then 1 ml aliquots removed for plaque assay.

5.2.3 Spontaneous charge-based adsorption of bacteriophage to the surface of PLAg and PVAm-PLAg films

Analytical bacterial filter units were identified as a suitable vessel for investigating bacteriophage adsorption and release from PLAg film variants, providing a seal to ensure bacteriophage adsorption on a single side and a suitable support to prevent film deformation during rehydration (Figure 5.2). Prior to use, the filter units were disassembled, the supplied filter paper removed, and 1 mm thick silicone rubber cut to replace the supplied cellulosic support pad (creating a seal when reassembled). The units were then re-sterilised under UV for 1 h. The filter unit provided a 47 mm diameter opening for exposure of the films to bacteriophage.

Subsequent to dehydration, PLAg and PVAm-PLAg films were removed from the Teflon cast (Section 2.2.2 and 2.2.3) and placed on the silicone support. The units were then reassembled ensuring a tight seal between the film and the upper chamber. Known titres of bacteriophage (10^3 PFU to 10^6 PFU) suspension were then added to each unit, diluted in 10 ml lambda buffer (pH 7.2) and incubated for 24 h at 4°C under gentle agitation (80 rpm). Prior to enumeration, each film was washed in 10 ml lambda buffer for 10 min at 4°C with gentle agitation (80 rpm) to remove non-associated bacteriophage. The proportion of non-associated bacteriophage was enumerated by quantification of PFU within the supernatant, and the number of associated bacteriophage determined by direct plating of the washed film.

Figure 5.2 - Images of bacterial filter units utilised for bacteriophage adsorption and dissociation studies.

5.2.4 AFM of bacteriophage adsorbed to the surface of PVAm-PLAg

Bacteriophage particles adsorbed to the surface of PVAm-PLAg were visualised using a NanoWizard 4 AFM (JPK BioAFM, Bruker, UK) operating in QI mode. All samples were fixed using 2.5 % glutaraldehyde in sodium cacodylate buffer (pH 7.4) for 1 h. Segments were then rinsed three times in sodium cacodylate buffer and dehydrated in increasing concentrations of ethanol (25 %, 50 %, 75 % and two washes in 100 %) for 15 min per wash, at room temperature and atmospheric pressure. Samples were processed using intermittent tapping mode, in air, with an AC40 silicon tip on a nitride cantilever (Bruker, UK). Data processing and image analysis was conducted using JPK SPM software (JPK BioAFM, Bruker, UK).

5.2.5 Bacteriophage integration with Alg-PVAm-PLAg

Alg-PVAm-PLAg composite materials were prepared using the $CaCO_3$/GDL system as previously described (Section 2.2.4.2). Prior to the addition of GDL, 100 µl of bacteriophage suspended in bacteriophage buffer was added to the alginate (2 % w/v) and $CaCO_3$ mixture to give the desired viral concentration, and mixed gently for 1 min. GDL was then added and mixed for 30 sec, and 5 ml of the mixture transferred to the surface of PVAm-PLAg and allowed to gel at room temperature and atmospheric pressure for 2 h.

5.2.6 Bacteriophage dissociation and enumeration

5.2.6.1 Bacteriophage dissociation and release from PLAg and PVAm-PLAg

Quantification of bacteriophage dissociation from plasticised agarose films was conducted by enumerating viral release in bacteriophage buffer (pH 7.2). Bacteriophage-loaded samples were placed in filtration units (as previously described – Section 5.2.3). 10 ml of fresh bacteriophage buffer was then added before incubating at 4°C for 24 h under gentle agitation (80 rpm). 1 ml aliquots were removed at predetermined time points and plaque assays performed to determine PFU/ml. Total PFU counts were then calculated by multiplication of PFU/ml by the volume of reconstitution buffer.

5.2.6.2 Bacteriophage enumeration by direct plating

Quantification of bacteriophage viability at the film interface was conducted by direct plating. Bacteriophage-loaded films were placed carefully on TSA plates to avoid trapping air bubbles underneath the film, with the "non-infectious surface" in contact with the agar plate. 10 ml of molten bacterial host-inoculated overlay agar (200 µl overnight culture, approx. 10^9 CFU/ml) held at 40°C was then carefully poured over the infective surface of the film and allowed to gel at room temperature for 15 min prior to incubating inverted at 37°C for 24 h. The overlay agar was poured at the periphery of the film to avoid disrupting the bacteriophage adsorbed at the material interface. The total PFU per film was then calculated by enumerating plaque numbers after incubation. If the number of plaques was too high to be accurately quantified, it was considered "too numerous to count" (TNTC).

5.2.6.3 Bacteriophage release from Alg-PVAm-PLAg composites

Bacteriophage release from composite PLAg/Alginate materials was quantified at 4°C and 37°C under constant agitation (120rpm). Composite materials containing bacteriophage of

known titre were placed in filtration units (as previously described – Section 5.2.3) and 10 ml lambda buffer (pH 7.2) dispensed into to the upper chamber above the film. Liberation of bacteriophage from the material was quantified at pre-determined time points over a 48 h period at 4°C (80 rpm) by removing 1 ml aliquots for plaque assay. Total PFU counts were estimated by multiplying PFU/ml values by the volume of release buffer (10 ml).

5.2.7 Statistical analysis

The sizes of population data sets are expressed as (N) throughout this thesis, with values being reported as the mean averages ± standard deviation (SD), unless otherwise stated. All statistical analysis was conducted using GraphPad Prism version 8 (GraphPad Software, USA).

5.2.7.1 Student's t-test

Student's t-tests were used to determine significance levels between bacteriophage sensitivity to IL plasticiser, bacteriophage release from hydrated PLAg hydrogels, and plaque counts from direct plating of bacteriophage integrated PLAg and PVAm-PLAg. P values of < 0.05 indicate statistical significance, with the degree of significance indicated on the figures where appropriate.

5.2.7.2 Two-way ANOVA

Two-way ANOVAs were conducted to determine significance between bacteriophage adsorption and release from the surfaces of PLAg, PVAm-PLAg and Alg-PVAm-PLAg composites. In all cases, bacteriophage titres were Log transformed and normality confirmed using the Shapiro-Wilk test. Two-way ANOVA was then conducted with Tukey's multiple comparisons post-hoc test to determine significance between values. P values of < 0.05 indicate statistical significance, with the degree of significance indicated on the figures where appropriate.

5.3 Results

5.3.1 Bacteriophage sensitivity to ionic liquid plasticiser

To determine the sensitivity of bacteriophage to the plasticiser used in PLAg synthesis, bacteriophage K, 44AHJD, T4, and T3 were incubated in solution with incremental plasticiser concentrations (0 % to 50 % v/v) for 3 h at 30°C (Figure 5.3). These conditions were selected to be reflective of the conditions each bacteriophage would be exposed to during physical sorption by desiccation at the material interface (section 5.2.2.2 for method). Bacteriophage titres at 0% plasticiser concentration (bacteriophage buffer without plasticiser) were used as a control to confirm that no reductions were due to the experimental conditions (30°C for 3 h).

The *Podoviridae*, T3 and 44AHJD, had modest titre reductions following 3 h exposure to the maximum (50% v/v) tested concentrations (0.18 Log_{10} and 1.07 Log_{10}, respectively) of plasticiser. Conversely, both *Myoviridae*, bacteriophage K and T4, were notably more sensitive to plasticiser at 50% v/v (4.14 Log_{10} and 2.59 Log_{10}, respectively). From 30% w/v plasticiser concentrations, the bacteriophage T3 titre was significantly lower than the control ($P < 0.05$), whereas a statistically significant reduction was identified from 10% v/v for bacteriophage 44AHJD ($P < 0.05$). Reductions of both *Myoviridae*, bacteriophage K and T4 were considered statistically different from the control at plasticiser concentrations of 20% v/v and higher ($P < 0.0001$). From plasticiser concentrations of 25% v/v to 50% v/v, the differences in titres of all bacteriophage were considered statistically significant ($P < 0.0001$).

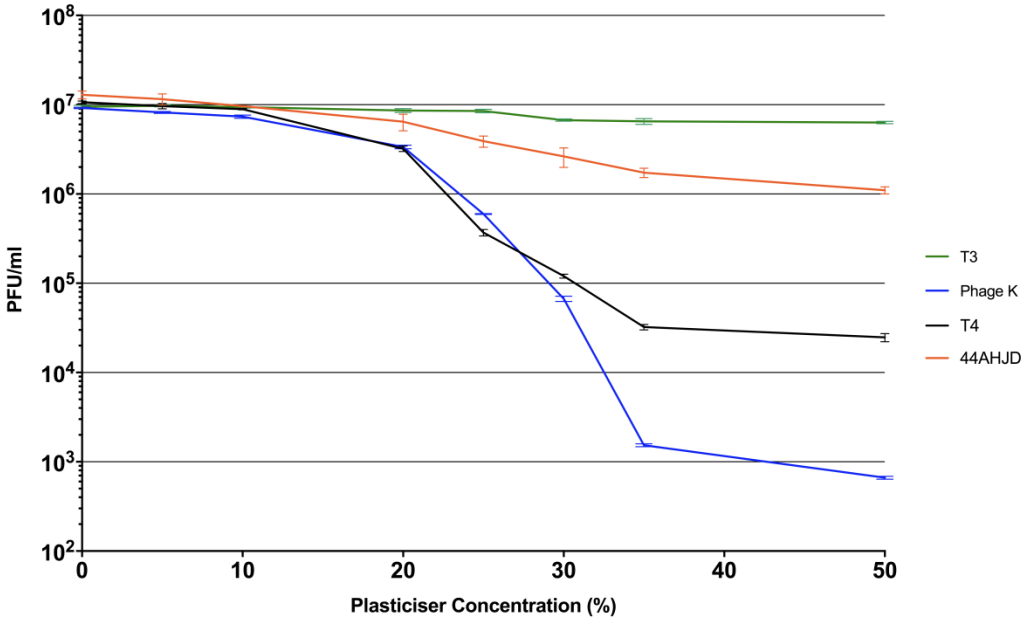

Figure 5.3 - Bacteriophage sensitivity to ionic liquid plasticiser at incremental concentrations (0% to 50% v/v) following 3 h exposure at 30°C. Each value represents the mean of three independent measurements (N=3) ± SD.

5.3.2 Bacteriophage integration within hydrated PLAg hydrogels

Bacteriophage K and T3 were incorporated within the matrix of hydrated PLAg gels to determine their viability and release prior to dehydration from a hydrated gel to a dehydrated film (Figure 5.4). Subsequent to inoculation (bacteriophage K: 4.25 x 10^7 PFU/disk and T3: 1.83 x 10^7 PFU/disk) and gelation of the agarose, individual excised gels were immediately placed in bacteriophage buffer and the PFU/ml quantified after a pre-determined release time period (24 h at 4°C) by plaque assay. Direct plating of bacteriophage loaded hydrated agarose was also included for qualitative assessment of bacteriophage release. Bacteriophage T3 demonstrated a high level of release at 7.52 Log_{10} PFU (97 % of the inoculum), indicating release and sustained lytic ability of a high proportion of the integrated bacteriophage. Conversely, bacteriophage K demonstrated restricted release from the agarose hydrogel at 4.35 Log_{10} PFU (0.07 % of the inoculum), which suggests inactivity and/or inhibited release of bacteriophage from the gel matrix. The difference between release values for bacteriophage K and T3 were statistically significant ($P < 0.001$). The images obtained from direct plating of the bacteriophage integrated PLAg gels show complete lawn clearance for bacteriophage T3 (with bacterial re-growth due to the emergence of bacteriophage resistant mutants), while individual plaques can be seen for PLAg gels loaded with bacteriophage K.

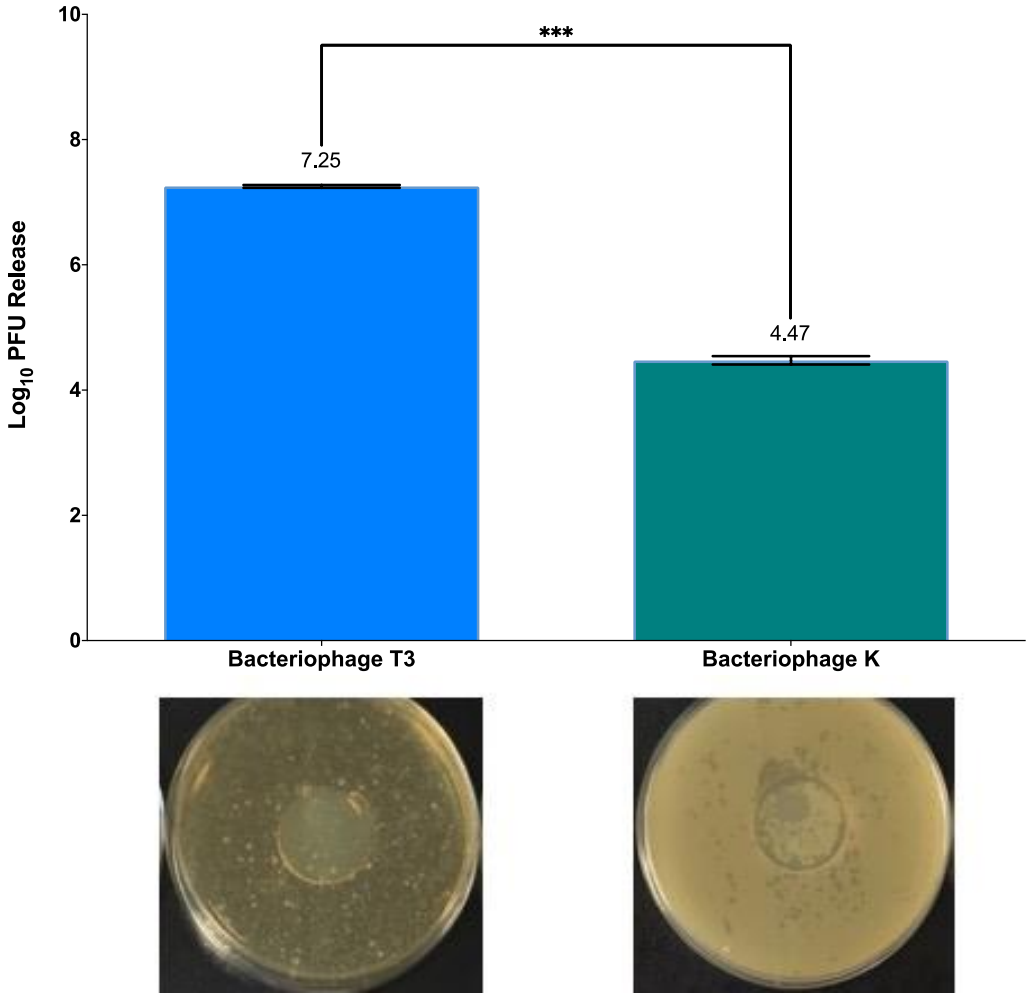

Figure 5.4 - Incorporation and release of bacteriophage K and T3 from within the PLAg gel matrix. Each value represents the mean of three independent experiments (N=3) ± SD. (A) proportional release in relation to the starting inoculum (%), and (B) qualitative measure of bacteriophage release by direct plating. Statistical significance between bacteriophage release was calculated using student's t-test. * indicates statistical significance (***** = P <0.05, ****** = P <0.01, ******* = P <0.001).

5.3.3 Bacteriophage physisorption by desiccation on the surface of PLAg films

To determine the viability and release of bacteriophage when desiccated on the surface of PLAg films, bacteriophage K and T3 were air dried on the surface of PLAg and glass cover slips (control) for 0 to 24 h at 30°C (Figure 5.5). At predetermined time points, samples were removed from the incubator and placed into glass beakers containing 10 ml of sterile bacteriophage buffer. Bacteriophage release was quantified by the reconstitution method (Section 5.2.6.1) for 24 h at 4°C, followed by plaque assay. In all cases the materials were visibly dry within 3 h of incubation at 30°C. To ensure any loss of viral titre was a result of PLAg and not temperature, bacteriophage were also held at 30°C for 24 h in bacteriophage buffer with no appreciable reduction in titre due to temperature (data not shown).

Both bacteriophage K and T3 demonstrated modest reductions in viability when desiccated on the surface of glass coverslips for 24 h at 30°C (1.39 Log_{10} and 1.32 Log_{10}, respectively), which was attributed to the desiccation process. These reductions were considered statistically significant from the starting inoculum ($P < 0.0001$). Bacteriophage T3 demonstrated significantly impeded dissociation when air dried on the surface of PLAg films (6.16 Log_{10} reduction) after a 24 h desiccation period, while bacteriophage K titres dropped to undetectable levels within 3 h of desiccation on the surface of PLAg films. From the first incubation time point onwards (>1 h), the reduction in recovery of bacteriophage K and T3 from glass and PLAg films was statistically significant ($P < 0.0001$).

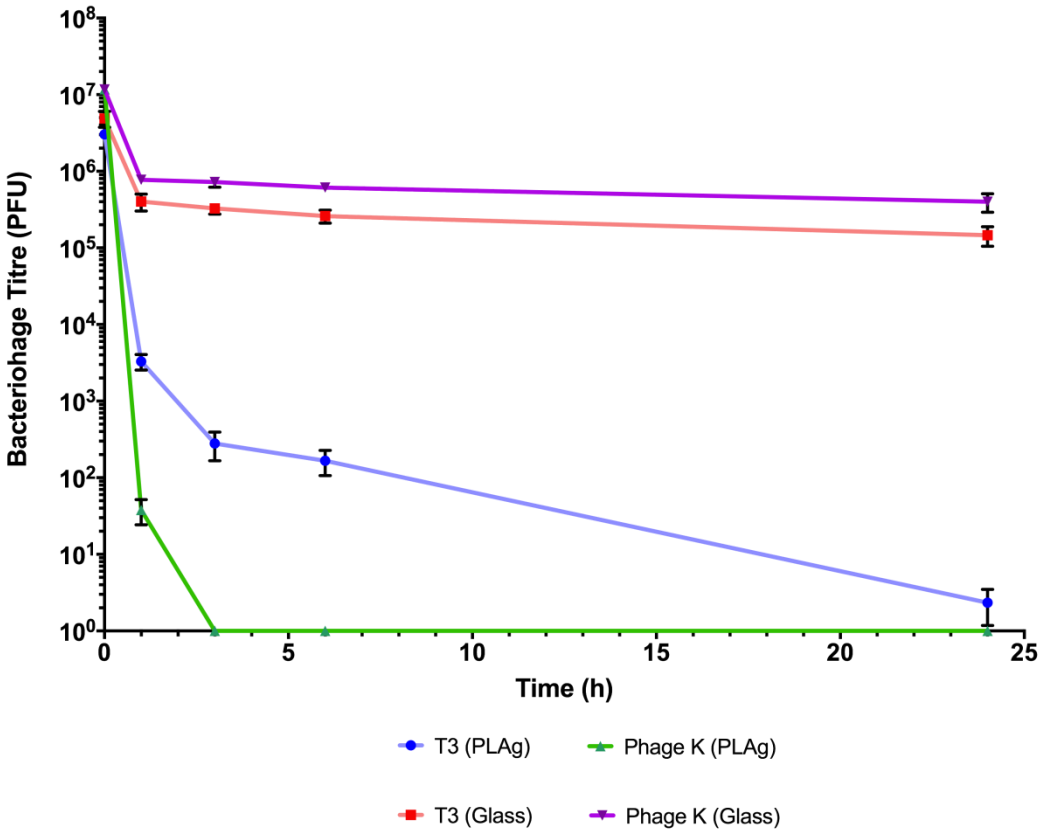

Figure 5.5 – Bacteriophage K and T3 viability subsequent to air drying at 30°C on the surface of PLAg films for 0 h to 24 h. Bacteriophage viability was quantified by the reconstitution method. Each data point represents the mean values of three independent experiments (N=3) ± SD.

5.3.4 Assessment of enumeration methods for spontaneous bacteriophage adsorption

Methodologies to enumerate spontaneous bacteriophage adsorption utilising bacterial filter units were validated using bacteriophage T3 and uncoated PLAg films due the lack of association of the bacteriophage with PLAg during preliminary studies (data not shown), and the lack of susceptibility of T3 to plasticiser mediated deactivation (Figure 5.3). Each film was secured in a filter unit as previously described (section 5.2.3) and exposed to bacteriophage T3 inocula of 1.78×10^4 PFU and 1.61×10^5 PFU suspended in 10 ml of bacteriophage buffer (pH 7.2). After 24 h incubation at 4°C, 1ml aliquots were taken from the supernatant fluid, the remaining supernatant removed, films washed (10 ml bacteriophage buffer, 2 min, 80 rpm), and an aliquot of washing buffer removed for bacteriophage enumeration. Each film was then removed from the filter unit and assessed for bacteriophage adsorption and viability by direct plating. Each PFU count indicated the following: **Supernatant**: total bacteriophage sorption, **Washing**: weakly associated bacteriophage, **Plating**: adsorbed and infective bacteriophage. The total PFU counts from each method of enumeration were then combined and compared to the starting inoculum.

Figure 5.6 shows that approximately 101.3 % (10^4 PFU inoculum) and 99.38 % (10^5 PFU inoculum), of recovered bacteriophage remained in the supernatant. 0.3 % (10^4 PFU inoculum) and 0.18 % (10^5 PFU inoculum) were recovered by washing, and 0.05 % (10^4 PFU inoculum) and 0.04 % (10^5 PFU inoculum) remained on the surface of PLAg films. By combining the PFU count from all three enumeration methods, the total PFU count could be compared with the starting inoculum. The differences between the inoculum titres and recovered titres were not considered statistically significant at 10^4 PFU ($P = 0.06$) nor 10^5 PFU ($P = 0.76$) These data show that, when enumerating bacteriophage using these three approaches, all bacteriophage were accounted for.

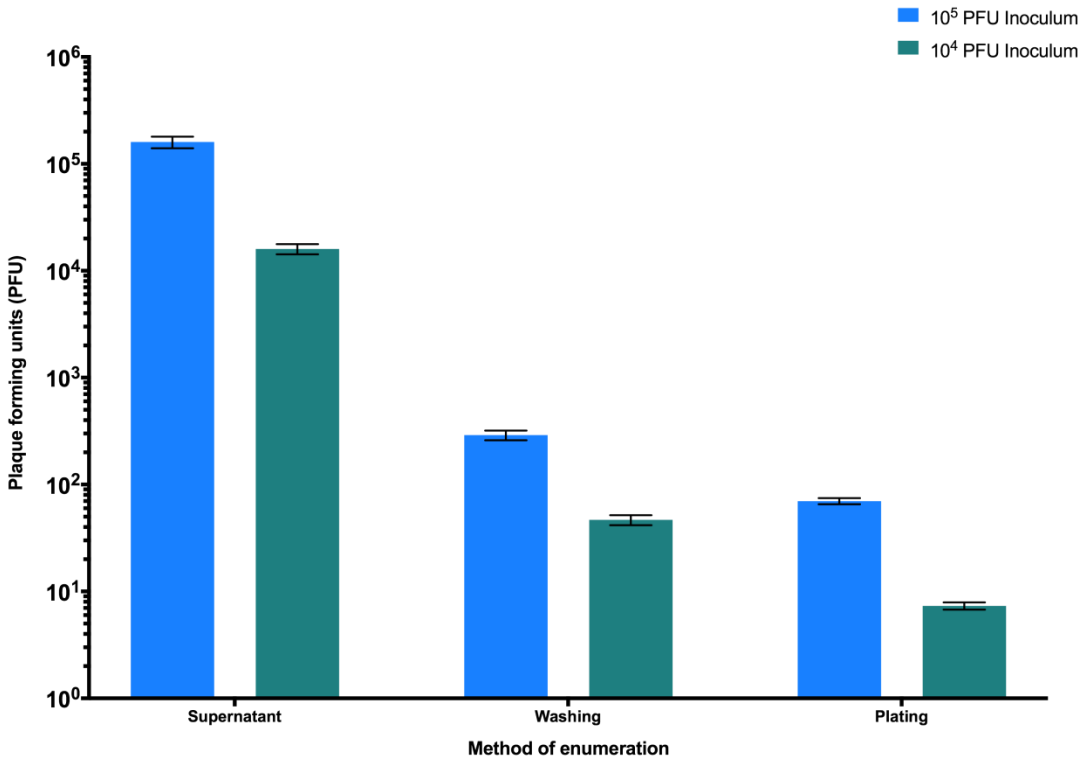

Figure 5.6 - Spontaneous adsorption methodology validation using uncoated PLAg films and bacteriophage T3 at 4ºC for 24 h. **Supernatant**: total bacteriophage sorption, **Washing**: weakly associated bacteriophage, **Plating**: adsorbed and infective bacteriophage. Each data point represents the mean values of three independent experiments (N=3) ± SD.

Preliminary studies using the same methodology for enumerating bacteriophage exposed to PVAm-PLAg resulted in the reversal of results, i.e. a high proportion of bacteriophage by direct plating and low number during washing and in supernatant titres suggesting strong adsorption to the material. The high number of plaques observed by direct plating of PVAm-PLAg, however, made enumeration using this method impossible (Figure 5.7). Therefore, supernatant measurements were used for both PLAg and PVAm-PLAg for further bacteriophage adsorption investigations.

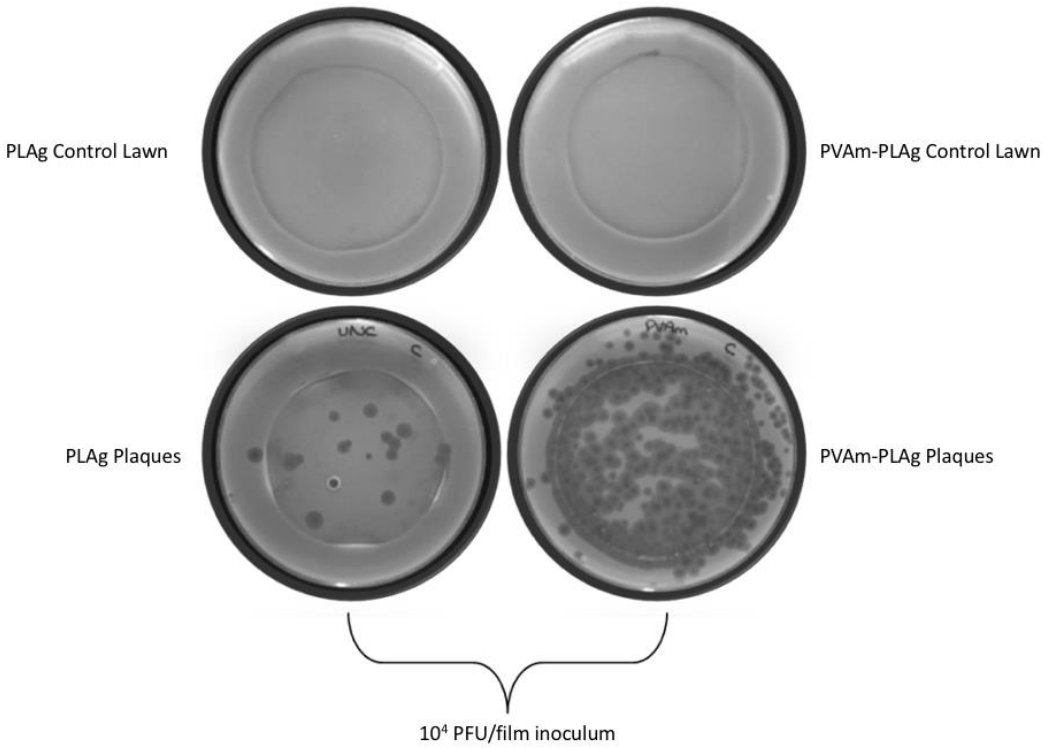

Figure 5.7 – Example of direct plating of PLAg (bottom left) and PVAm-PLAg (bottom right), subsequent to bacteriophage adsorption at an exposure inoculum of 10^4 PFU/film. Control plates are PLAg (top left) and PVAm-PLAg (top right) which had not been exposed to bacteriophage.

5.3.5 Quantification of bacteriophage adsorption to the surface of PLAg and PVAm-PLAg films

To quantify the relative adsorption of bacteriophage to negatively and positively charged films, PLAg and PVAm-PLAg films were secured in filtration units and exposed to bacteriophage suspended in 10 ml bacteriophage buffer (pH 7.2) at concentrations of 10^3 PFU, 10^4 PFU, 10^5 PFU, and 10^6 PFU. Bacteriophage adsorption efficacy was calculated by quantifying the reduction of bacteriophage in the supernatant subsequent to 24 h at 4°C under gentle agitation (80 rpm). The reduction in PFU from the starting inoculum was then determined to give the theoretical number of bacteriophage adsorbed to the material, and the proportion of bacteriophage adsorbed expressed as a percentage for graphical presentation (Figure 5.8).

At all the tested bacteriophage inocula levels, bacteriophage T3 demonstrated significantly higher levels of adsorption to PVAm-PLAg than to PLAg; 98.5 % to 100 %, and 7.04 % to 24.7, respectively ($P < 0.0001$). Adsorption of bacteriophage T4 to PVAm-PLAg and PLAg followed a similar trend, with ranges between 97.8 % to 100 %, and 7.0 % to 11.6 %, respectively, across all tested bacteriophage inocula. As with bacteriophage T3, the differences between the number of adsorbed bacteriophage T4 to PLAg and PVAm-PLAg were considered statistically significant at all tested inocula concentrations ($P < 0.0001$).

Bacteriophage 44AHJD adsorption to PLAg and PVAm-PLAg across all tested inocula ranged between 44.4 % to 90.1 %, and 97.0 % to 100 %, respectively. Adsorption to PVAm-PLAg was significantly higher than PLAg at bacteriophage inocula of 10^3 PFU, 10^4 PFU, and 10^5 PFU (all significance levels at $P < 0.0001$), however no significance was found between the two film variants at 10^6 PFU ($P = 0.16$). Bacteriophage K adsorption to PLAg and PVAm-PLAg across all tested inocula ranged from 69.7 % to 93.9 %, and 96.7 % to 100 %, respectively. While adsorption to PVAm-PLAg was considered significantly higher at all tested inocula, significance levels differed at $P < 0.0001$ (10^3 PFU, 10^4 PFU, and 10^5 PFU) and $P = 0.0013$ (10^6 PFU).

It should be noted that Figure 5.8 presents the data as proportional values (i.e. percentage adsorbed from the exposed inoculum), therefore data points which remain static with increasing concentrations do not signify consistent adsorption values. All bacteriophage and film variants did, in fact, demonstrate dose-response relationships between the inoculum and number of adsorbed bacteriophage (i.e. an increase in inoculum resulted in significantly increased adsorption ($P < 0.0001$). The dose-response relationship, however, was more pronounced in the adsorption of bacteriophage K and 44AHJD to PLAg films.

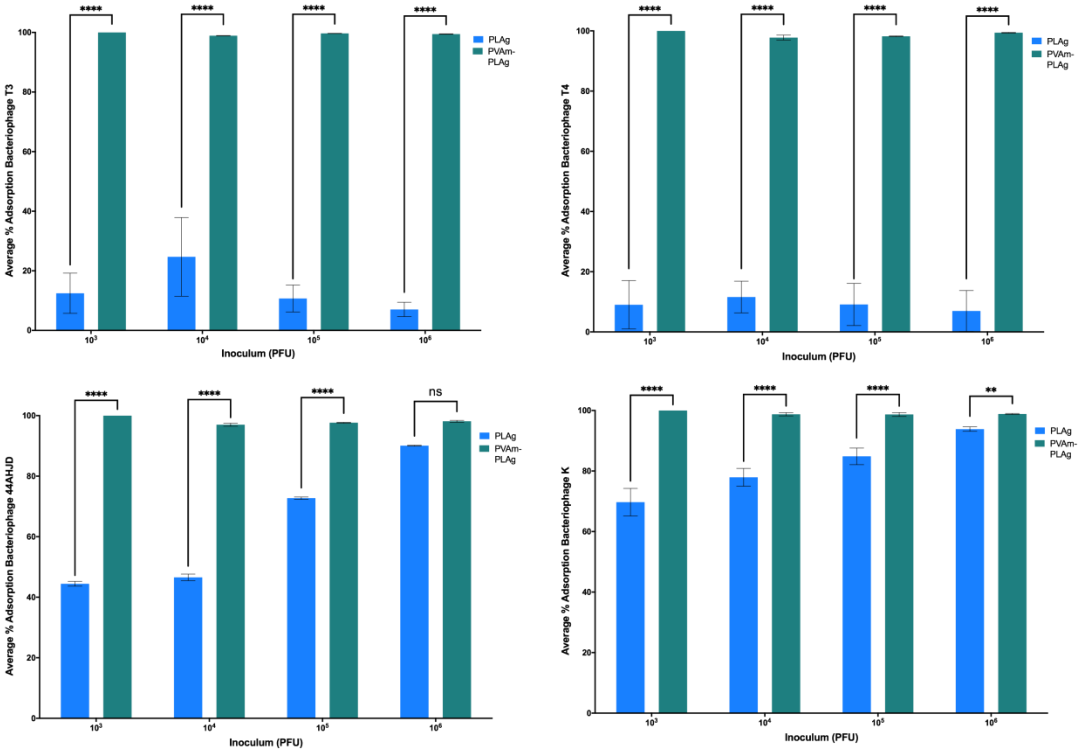

Figure 5.8 - Spontaneous adsorption of bacteriophage T3 (top left), T4 (top right), 44AHJD (bottom left), and K (bottom right), to PLAg (blue) and PVAm-PLAg (green), as determined by percentage reduction from the starting supernatant inoculum (10^3 PFU, 10^4 PFU, 10^5 PFU, and 10^6 PFU). Each data point represents the mean values of three independent experiments (N=3) ± SD. Statistical analysis between each inoculum and film variant was conducted using two-way ANOVA and Bonferroni multiple comparisons post-hoc tests, following log transformation of raw data. * indicates statistical significance (***** = P <0.05, ****** = P <0.01, ******* = P <0.001, ******** = P <0.0001).

While the proportions of bacteriophage adsorbed to the surface of PLAg and PVAm-PLAg were high in many cases, the orientation and infectivity state of the adsorbed bacteriophage remained unknown. As shown in Chapter 4, the surface charge of PLAg was negative, and PVAm-PLAg positive (bacteriophage buffer at pH 7.2 and 25°C); meaning bacteriophage tails would likely adsorb to PLAg (non-infective), and capsids to PVAm-PLAg (infective). Therefore, once an aliquot was taken to determine the reduction of bacteriophage numbers within the supernatant, each film was removed and infective bacteriophage numbers on the surface of the film quantified by direct plating. For each film variant, Table 5.1 shows the average values for bacteriophage inocula, calculated theoretical adsorption values, and mean plaque counts from direct plating of the films.

Table 5.1 - Spontaneous adsorption values of bacteriophage to PLAg and PVAm-PLAg films, showing the initial inoculum, the reduction in supernatant titre following the adsorption conditions (24 h, 4°C, 80 rpm), calculated theoretical adsorption values, and the mean plaque count obtained from direct plating of the films.

Bacteriophage	**Film variant**	**Average inoculum (PFU)**	**Average theoretical adsorption (PFU)**	**Mean plaque count (PFU ±SD)**
T3	PLAg	4.17×10^3	5.20×10^2	25 ± 4.51
		3.60×10^4	8.89×10^3	60 ± 7.02
		4.90×10^5	4.20×10^4	TNTC
		5.40×10^6	3.80×10^5	TNTC
	PVAm-PLAg	4.17×10^3	4.17×10^3	59 ± 3.21
		3.60×10^4	3.56×10^4	TNTC
		4.90×10^5	4.88×10^5	TNTC
		5.40×10^6	5.37×10^6	TNTC
T4	PLAg	3.10×10^3	2.80×10^2	0
		2.30×10^4	2.67×10^3	1 ± 1.53
		2.50×10^5	2.38×10^4	24 ± 5.03
		2.21×10^6	1.54×10^5	59 ± 11.59
	PVAm-PLAg	3.10×10^3	3.10×10^3	2 ± 1.73
		2.30×10^4	2.25×10^4	24 ± 8.5
		2.50×10^5	2.46×10^5	116 ± 14.5
		2.21×10^6	2.20×10^6	TNTC
44AHJD	PLAg	1.20×10^3	5.33×10^2	0
		1.00×10^4	4.66×10^3	7
		1.10×10^5	8.00×10^4	79
		1.30×10^6	1.17×10^6	TNTC
	PVAm-PLAg	1.20×10^3	1.20×10^3	TNTC
		1.00×10^4	9.70×10^3	TNTC
		1.10×10^5	1.07×10^5	TNTC
		1.30×10^6	1.28×10^6	TNTC
ϕK	PLAg	2.20×10^3	1.00×10^2	0
		2.42×10^4	1.89×10^4	7 ± 1.53
		1.98×10^5	1.68×10^5	79 ± 11.5
		2.10×10^6	1.97×10^6	TNTC
	PVAm-PLAg	2.20×10^3	2.20×10^3	TNTC
		2.42×10^4	2.39×10^4	TNTC
		1.98×10^5	1.95×10^5	TNTC
		2.10×10^6	2.08×10^6	TNTC

In all cases, plaque counts by direct plating were higher in PVAm-PLAg than PLAg. Difficulties arose, however, in the enumeration of plaque numbers of approximately >60 PFU due to the merging of neighbouring plaques. This was especially problematic in the enumeration of bacteriophage adsorbed to the surface of PVAm-PLAg, as plaques were almost entirely confined to within the perimeters of the film, presumably due to the strong interaction between PVAm and the viral particles.

5.3.6 Spontaneously immobilised bacteriophage T3 release from PLAg and PVAm-PLAg films

Bacteriophage T3 was allowed to spontaneously adsorb to PLAg and PVAm-PLAg films prior to the release rate being quantified (see section 5.2.6.1 for method). Bacteriophage release from PLAg and PVAm-PLAg was quantified over 48 h at 4°C and 37°C, reflective of the proposed storage and application conditions, respectively (Figure 5.9). For both film variants the initial exposed viral inoculum was approximately 1 x 10^6 PFU per film, and the estimated number of adsorbed bacteriophage was calculated from a reduction in the supernatant following the adsorption period (24 h, 4°C, 80 rpm). The calculated adsorbed number of bacteriophage is included in the figure for reference.

T3-loaded PLAg films demonstrated a rapid release of 3.59 Log_{10} (1.04 % of adsorbed PFU) and 3.68 Log_{10} (1.25 % of adsorbed PFU) within 1 h, at 4°C and 37°C, respectively. Subsequent to the initial 'burst release' of bacteriophage at 1 h, the release of bacteriophage plateaued, with the number of bacteriophage released at 48 h being 3.70 Log_{10} (1.33% of adsorbed PFU) and 3.79 Log_{10} (1.64 % of adsorbed PFU) at 4°C and 37°C, respectively. The difference between bacteriophage release from PLAg at 4°C and 37°C was not considered statistically significant between 1 h and 24 h ($P > 0.05$).

Bacteriophage T3 release from PVAm-PLAg at 4°C demonstrated similar release characteristics to PLAg, with an initial burst release from 0 h to 1 h followed by a plateau from 1 h to 48 h (Figure 5.9). However, the number of bacteriophage released was notably lower at 2.37 Log_{10} at 1 h, and 2.67 Log_{10} at 48 h. Conversely, bacteriophage T3 release from PVAm-PLAg at 37°C appeared cumulative over a 48 h time period, with a release of; 3.75 Log_{10} (1 h), 3.81 Log_{10} (2 h), 4.07 Log_{10} (6 h), 5.54 Log_{10} (24 h), and 5.88 Log_{10} (48 h). At the final time point (48 h), bacteriophage T3 release from PVAm-PLAg was 22.55% of the adsorbed PFU, compared to 0.01% release at 4°C. The difference between bacteriophage release from PVAm-PLAg at 4°C and 37°C was considered statistically significant at all time points ($P < 0.0001$).

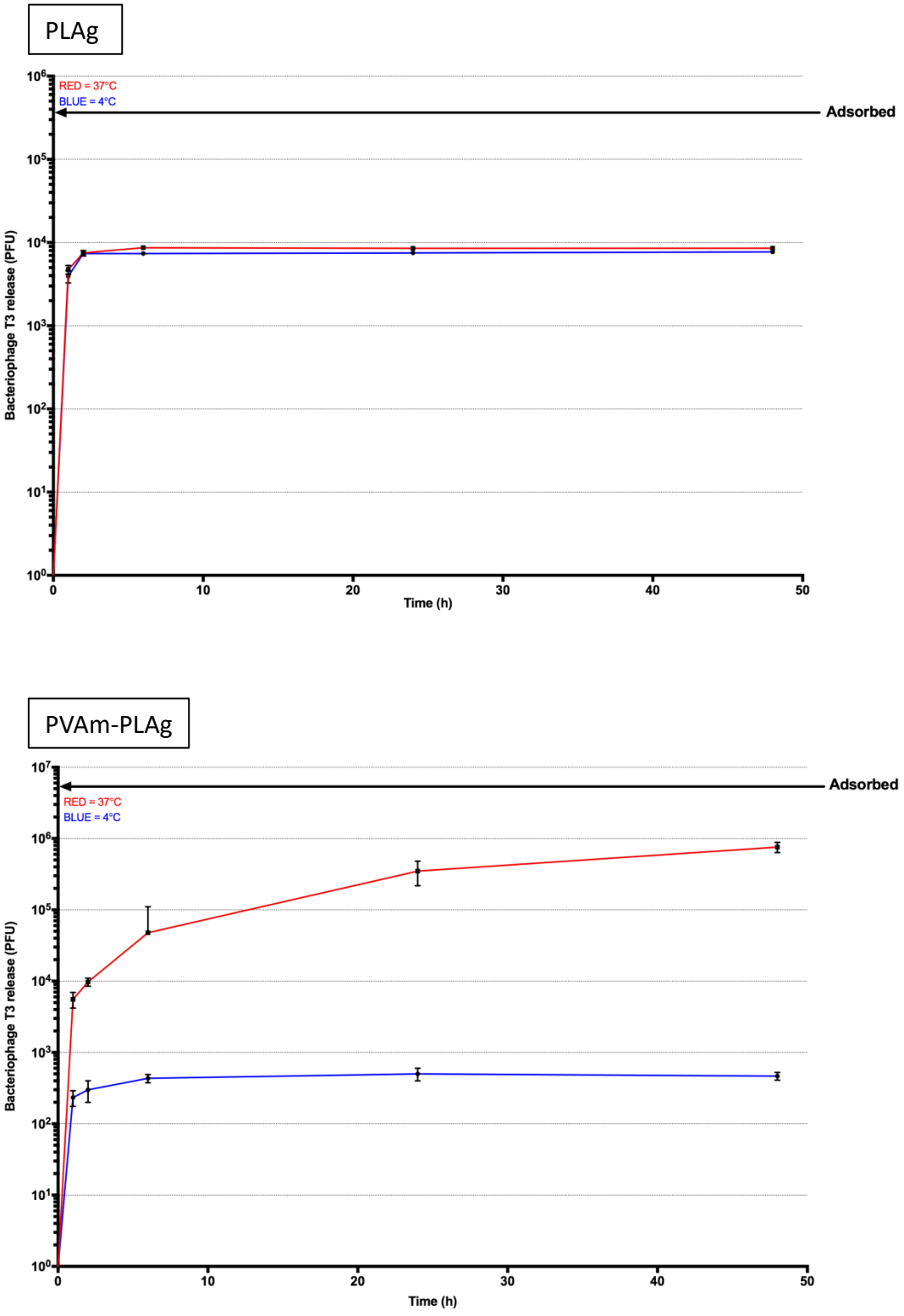

Figure 5.9 - Release of bacteriophage T3 spontaneously adsorbed to the surface of PLAg (top) and PVAm-PLAg (bottom) films, over a 48 h period at 4°C (blue line) and 37°C (red line). The number of bacteriophage adsorbed to the surface of each film variant was estimated by the reduction in supernatant titre following 24 h adsorption at 4°C. Each data point represents the mean values of three independent experiments (N=3) ± SD.

5.3.7 AFM of *E. coli* infective bacteriophage at the PVAm-PLAg film interface

E. coli infective bacteriophage, T4 and T3, were visualised at the PVAm-PLAg film interface using AFM in tapping mode. Preliminary measurements were made without fixation, using both air dried films and measurements taken in aqueous solution, however bacteriophage structures were not visible and therefore the images were omitted from this thesis. The following images were obtained at room temperature and atmospheric pressure subsequent to glutaraldehyde fixation and ethanol dehydration. Bacteriophage T3 and T4 were adsorbed at an inoculum of approximately 1 x 10^6 PFU per film (52 mm diameter).

5.3.7.1 Bacteriophage T4

Low magnification images were obtained initially to identify regions of interest on the surface of PVAm-PLAg films. Upon examination of the film interface at low magnification (5 μm^2) numerous viral particles could be identified, with capsid and tail structural components of *Myoviridae* visible (Figure 5.10). Viral deposition appeared to be fairly uniform throughout the regions, with few areas of viral aggregation.

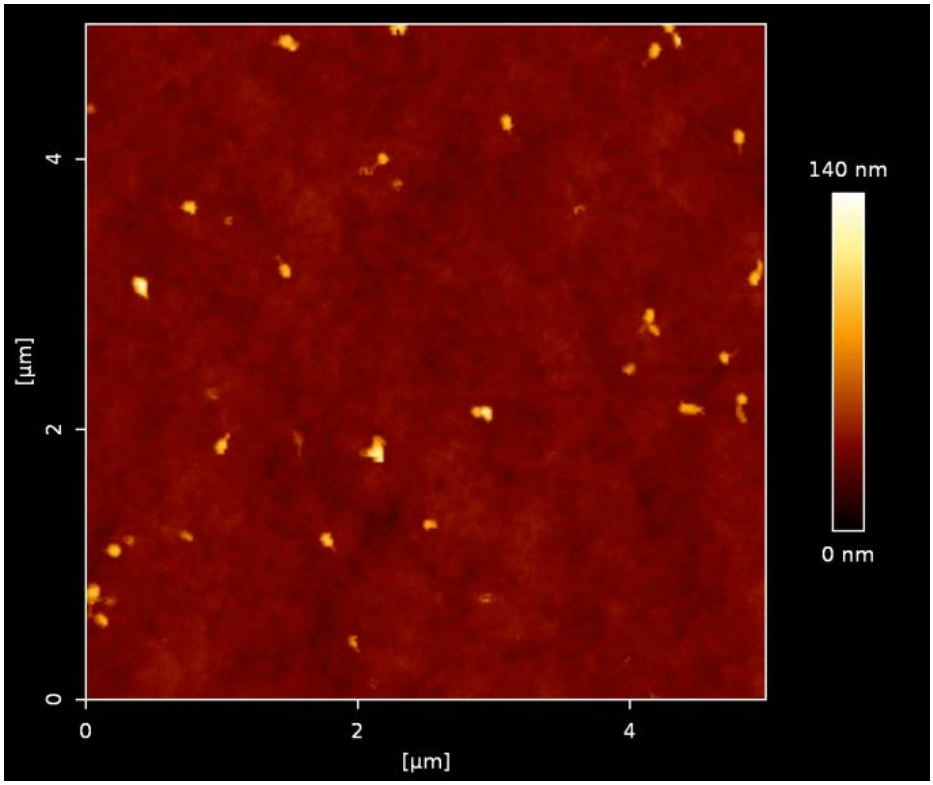

Figure 5.10 - AFM image of bacteriophage T4 adsorbed to the surface of PVAm-PLAg films. The scale is 5 μm^2, and height measurement is indicated by bar.

Once a region of interest was identified, images were acquired at increased magnification to visualise bacteriophage morphology at high resolution. Figure 5.11(A) shows four bacteriophage T4 virions on a 1.5 μm^2 region of PVAm-PLAg. Figure 5.11(B) shows a high-resolution image of a single T4 virus, and (C) a 3D perspective view (both image areas = 500 nm^2). All images allow clear identification of the bacteriophage capsid and tail structures.

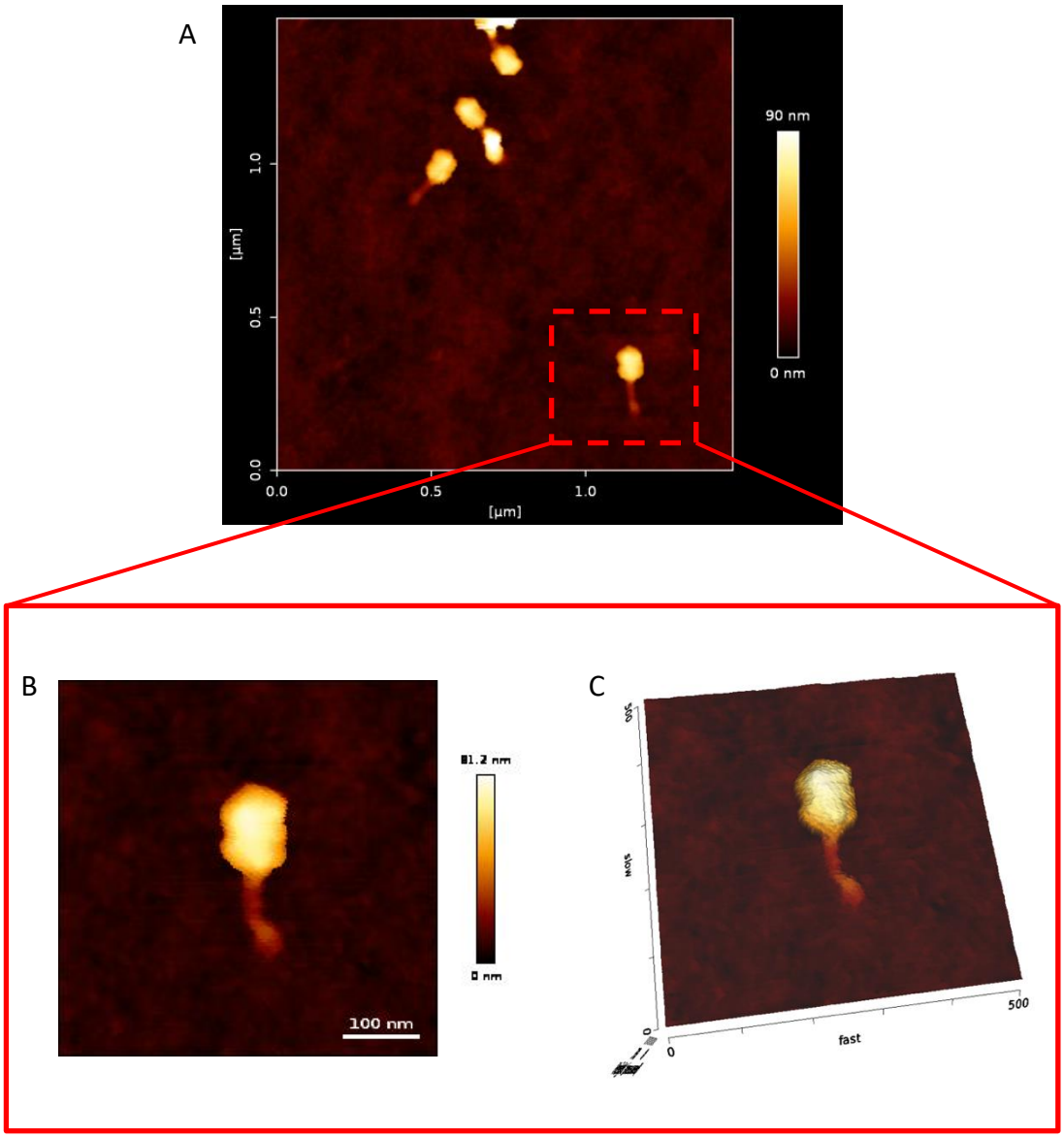

Figure 5.11 - AFM images of bacteriophage T4 adsorbed to the surface of a PVAm-PLAg film, showing the characteristic morphology of *Myoviridae*. (A) 1.5 μm^2 AFM image of four T4 bacteriophage, (B) 500 nm^2 AFM image of a single T4 bacteriophage captured from (A), and (C) 500 nm^2 3D perspective view of a single T4 bacteriophage. The scale of each image is indicated by the bars.

Height and width measurements were conducted on bacteriophage T4 capsids and tails using JPK SPM AFM data processing software (Bruker, UK). The height of each virion in relation to the PVAm-PLAg film substrate was conducted by cross-section analysis, an example of measurement placement is outlined in Figure 5.12. The average height and width of bacteriophage T4 capsids was 68.18 ± 1.3 nm and 91.76 ± 2.7 nm, respectively. Due to the symmetrical 3D structure of the icosahedral capsid, it should be expected that height and width measurements should be equal. The disparity between the two measurements could be an artefact of sample fixation and dehydration but could also indicate penetration of the virions within the superficial layer. It should also be noted that the surface of PVAm-PLAg is not entirely flat (Section 4.3.3.1). Height and width measurements of bacteriophage T4 tail also differed at 16.43 ± 1.8 nm and 26.46 ± 3.6 nm, respectively. The width measurements of both T4 capsid and tail structures obtained in this study align with those found in the literature [308].

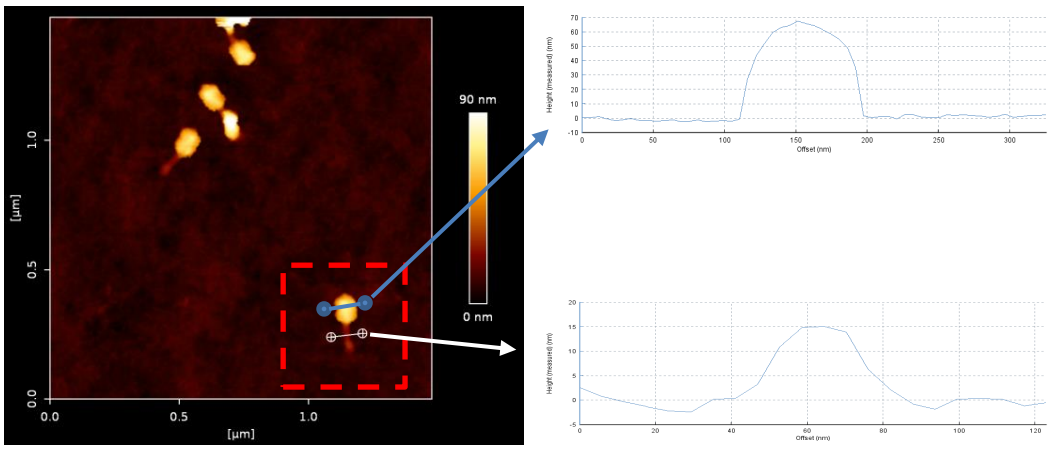

Figure 5.12 - Example height measurements of bacteriophage T4 capsid (blue line) and tail (white line) structures by cross-section analysis using JPK SPM AFM data processing software. Each graph shows the measured height (nm) of the capsid (top image) and tail (bottom image) over the selected section.

5.3.7.2 Bacteriophage T3

As with bacteriophage T4, low magnification images were obtained to identify regions of interest for further analysis. Figure 5.13(A) shows a 5 μm^2 image containing numerous particles with approximate height measurements similar to that of bacteriophage T3 (approximately 60 nm diameter – see Section 3.3.2). Viral deposition seems to be fairly uniform, however areas of particle aggregation are evident. Increasing the magnification on a region of interest allowed for size measurements of three particles (Figure 5.13(B)), with the average diameter being 63.7 ± 3.8 nm (Figure 5.13(B)). A 3D perspective image is shown in Figure 5.13(C) which shows a short tail-like structure protruding from one of the virions (white circle). The 3D perspective view is suggestive of bacteriophage being embedded within the surface, however this could be an artefact of sample fixation, or the capsid morphology and nature of AFM measurements due to the small surface area of contact between the capsid and polymer film and the cantilever increasing in height upon contact with the peripheral edge of the virion.

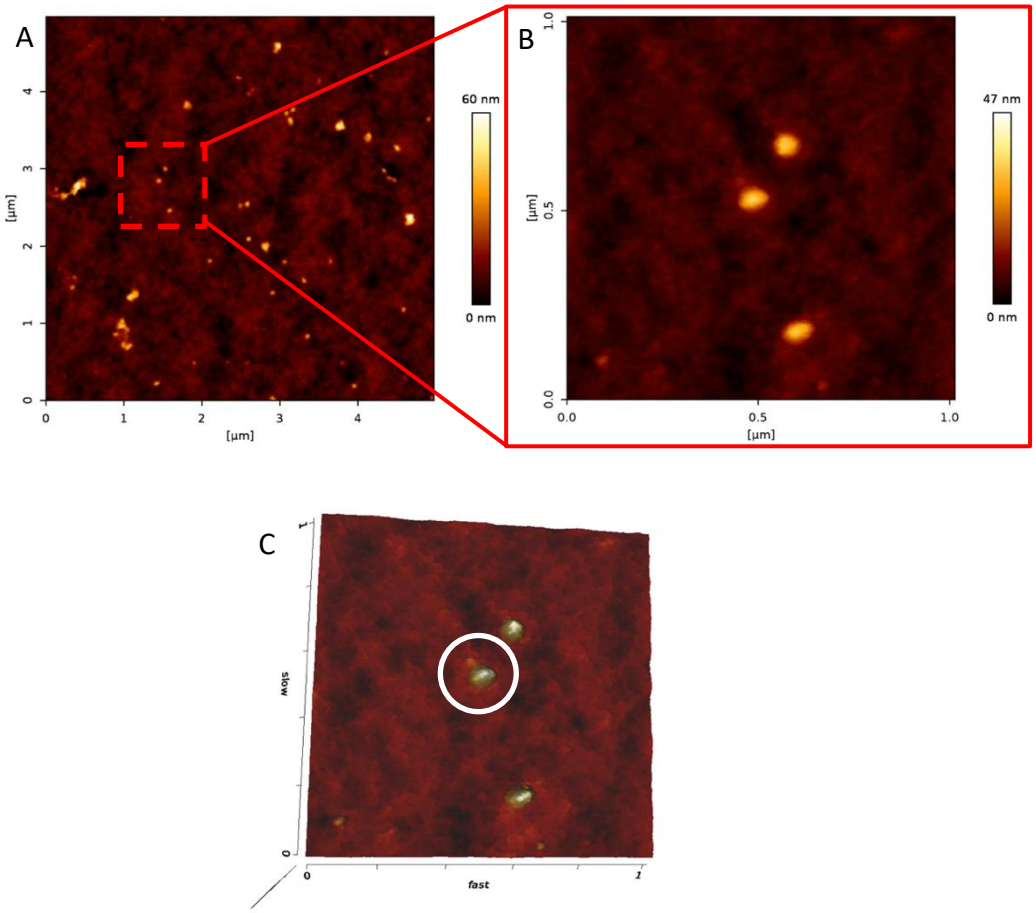

Figure 5.13 - AFM images of bacteriophage T3 adsorbed to the surface of PVAm-PLAg. (A) 5 μm^2 AFM image of numerous T3 bacteriophage, (B) 1 μm^2 AFM image of three T3 bacteriophage enlarged from (A – red box), and (C) 1 μm^2 3D perspective view of image (B) showing the tail structure of bacteriophage T3 (white circle). The scale of each image is indicated by the bars.

5.3.8 Bacteriophage release from Alg-PVAm-PLAg composite materials

Figure 5.14 shows the release rates of bacteriophage K, T3, and T4, from Alg-PVAm-PLAg composites over a 48 h time period, at 4°C (storage conditions) and 37°C (application conditions). Incremental bacteriophage concentrations (10^5, 10^6, and 10^7 PFU per material) were immobilised within the matrix of the superficial alginate hydrogel adhered to PVAm-PLAg films and release was determined by the method outlined in section 5.2.6.3. At all tested inocula and time points, recovery numbers of bacteriophage 44AHJD were near to, or below the limit of detection of $<10^2$ PFU (data not shown).

Bacteriophage K, T3, and T4 were gradually released from Alg-PVAm-PLAg composites, with consistently higher release titres (from 6 to 48 h) at 37°C when compared to release at 4°C (Figure 5.14). To demonstrate the cumulative release of bacteriophage from Alg-PVAm-PLAg, Table 5.2 shows proportion (of the release at 48 h) of released bacteriophage from 1 to 48 h, at a single bacteriophage inoculum (10^7 PFU), and release temperatures of 4°C and 37°C. At an inoculum of 10^7 PFU, the release of all three bacteriophage at 1 h and 2 h remained comparable at 4°C and 37°C. However, between 6 h and 48 h release, the number of bacteriophage released at 37°C was consistently higher than at 4°C. The release of bacteriophage K from Alg-PVAm-PLAg at both temperatures and all time points was consistently lower than that of bacteriophage T3 and T4 (as shown in Figure 5.14 and Table 5.2).

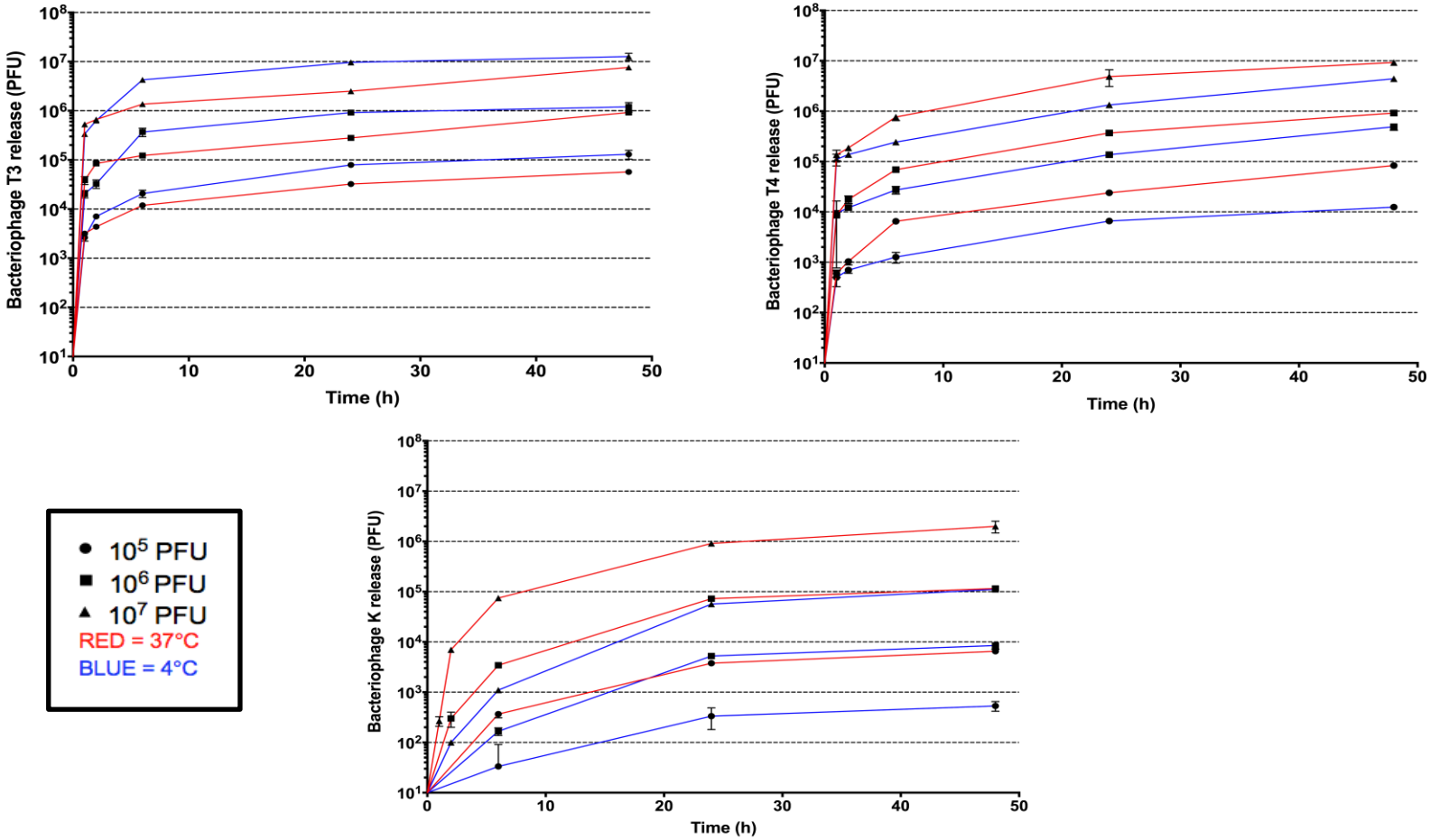

Figure 5.14 - Release kinetics of bacteriophage T3 (top left), T4 (top right), and bacteriophage K (bottom centre) from Alg-PVAm-PLAg composite materials at 4°C (blue lines) and 37°C (red lines). Three titres were tested for each bacteriophage; 10^5 PFU (circle), 10^6 PFU (square), and 10^7 PFU (triangle). Each data point represents the mean values of three independent experiments (N=3) ± SD.

Table 5.2 - Bacteriophage K, T3, and T4 release from Alg-PVAm-PLAg composites from 1 to 48 h time points, 10^7 PFU inoculum, and release temperatures of 4°C (blue) and 37°C (red).

Bacteriophage	**Release temperature**	**Time (h)**	**Proportion of bacteriophage released from 10^7 PFU inoculum (% ± SD)**
T3	4°C	1	4.08 ± 0.4
		2	5.10 ± 0.4
		6	10.51 ± 0.4
		24	19.23 ± 2.0
		48	58.72 ± 3.1
	37°C	1	2.59 ± 0.3
		2	4.87 ± 0.4
		6	32.82 ± 1.6
		24	74.10 ± 2.4
		48	97.44 ± 16.0
T4	4°C	1	1.11 ± 0.3
		2	1.38 ± 0.1
		6	2.43 ± 0.1
		24	13.33 ± 1.2
		48	44.00 ± 2.6
	37°C	1	1.36 ± 0.3
		2	1.87 ± 0.1
		6	7.67 ± 1.2
		24	48.67 ± 17.8
		48	92.67 ± 2.5
ϕK	4°C	1	0.00 ± 0.0
		2	0.00 ± 0.0
		6	0.01 ± 0.0
		24	0.57 ± 0.03
		48	1.11 ± 0.13
	37°C	1	0.00 ± 0.0
		2	0.07 ± 0.01
		6	0.75 ± 0.04
		24	9.10 ± 0.35
		48	20.00 ± 5.27

The final titres for all bacteriophage and release temperatures at 48 h were proportional to the bacteriophage inocula integrated within the hydrogel (i.e. as the inoculum increased logarithmically, so did the 48h release titre). The proportions of released bacteriophage at each integrated inoculum (10^5, 10^6, and 10^7 PFU) at 48 h are shown in Table 5.3. Bacteriophage T3 and T4 both demonstrated high release rates across all tested inocula at 37°C (83.33 % to 97.44 %). Release at 4°C was more variable, with the proportionate release ranging from 12.43 % (T4 – 10^5 PFU inoculum) to 70.77 % (T3 – 10^6 PFU inoculum). The average release of bacteriophage T3 and T4, at 48 h across all inocula at 4°C, was 57.78 % and 35.14 %, respectively. In contrast to T3 and T4, bacteriophage K demonstrated limited release from Alg-PVAm-PLAg at 4°C and 37°C, with an average proportional release at 48 h across all inoculums of 0.83 % and 12.7 %, respectively.

Table 5.3 – Bacteriophage K, T3, and T4 release from Alg-PVAm-PLAg composites at the 48 h time point (10^5, 10^6, and 10^7 PFU inoculums) and release temperatures of 4°C (blue) and 37°C (red).

Bacteriophage	**Release temperature**	**Inoculum (PFU)**	**Proportion of bacteriophage released at 48 h (% ± SD)**
T3	4°C	10^5	43.85 ± 3
		10^6	70.77 ± 5
		10^7	58.72 ± 3
	37°C	10^5	92.86 ± 19
		10^6	92.31 ± 20
		10^7	97.44 ± 16
T4	4°C	10^5	12.43 ± 1
		10^6	49.00 ± 7
		10^7	44.00 ± 3
	37°C	10^5	83.33 ± 7
		10^6	92.00 ± 4
		10^7	92.67 ± 3
ϕK	4°C	10^5	0.53 ± 0.1
		10^6	0.85 ± 0.1
		10^7	1.11 ± 0.1
	37°C	10^5	6.53 ± 1
		10^6	11.57 ± 0.4
		10^7	20.00 ± 5

5.4 Discussion

This chapter describes the integration of bacteriophage with previously synthesised and characterised (Chapter 4) PLAg, PVAm-PLAg, and Alg-PVAm-PLAg candidate wound dressing materials. Prior to integration, the sensitivity of bacteriophage to the ionic liquid plasticiser was determined. Subsequently, bacteriophage incorporation with PLAg was attempted by the integration of viral particles within the porous matrix of hydrated PLAg hydrogels and air drying on the surface of dehydrated PLAg films. Due to limitations of these methods, bacteriophage were then tethered to the surface of PVAm-PLAg, by a surface charge interaction. To determine the capture efficacy of bacteriophage to the surface of PVAm-PLAg, a number of quantification methods were investigated. Following this methodology validation, the adsorption efficacy and release rate from PVAm-PLAg was determined. Visualisation of bacteriophage on the surface of PVAm-PLAg was achieved by the use of AFM, which also allowed for size measurements of viral particles. Finally, bacteriophage were integrated with Alg-PVAm-PLAg composite materials, by incorporation of viral particles within the superficial alginate hydrogel layer.

Prior to bacteriophage integration, bacteriophage sensitivity to the plasticiser component of the materials was determined to distinguish any potential detrimental effects to bacteriophage stability and infectivity during exposure to the material. Bacteriophage K, 44AHJD, T4, and T3 were incubated with incremental concentrations of ionic liquid plasticiser (0 to 50 % w/v) for 3 h at 30°C. At 50 % w/v, the *Podoviridae* bacteriophage T3 and 44AHJD showed modest reductions in titre (0.18 Log_{10} and 1.07 Log_{10} reductions, respectively), while both *Myoviridae* bacteriophage K and T4, showed significant sensitivity (4.14 Log_{10} and 2.59 Log_{10} reductions, respectively). This phenomenon can be explained by the composition of the ionic liquid. Urea has been shown to induce tail sheath contraction in bacteriophage T4 [309], which could explain the cumulative reduction in titre of *Myoviridae*, with increasing plasticiser concentration. *Podoviridae* on the other hand, lack contractile tails, which could explain the only modest reduction in bacteriophage titre under the tested conditions. The ionic charge of the plasticiser compound could also cause viral aggregation, resulting in fewer plaques being identified during enumeration.

Bacteriophage K and T3 were integrated within the porous matrix of PLAg hydrogels and bacteriophage release quantified after 24 h submersion in bacteriophage buffer at 4°C. A high proportion (97 % of integrated PFU) of bacteriophage T3 was released from the hydrogel under the tested conditions, while the release of bacteriophage K was significantly more restricted (0.07 % of integrated PFU). The rationale for selecting bacteriophage K and T3 for this study was their size, at 280 nm length and 60 nm diameter, respectively. Agarose

pore size has been documented to be dependent on the concentration and gelling temperature of agarose; with increasing concentration resulting in decreased pore size due to closer packing of polymer chains, and increased setting temperature resulting in increased pore size as a result of weak junction degradation [310]. The agarose concentration of the gel formulations was 2 % w/v, which can produce pore sizes of approximately 100 nm to 200 nm [310]. The pore size of PLAg hydrogels could, therefore, result in the inhibited release of bacteriophage K while allowing unhindered release of T3. It should also be noted that while bacteriophage K was demonstrated to be sensitive to ionic liquid plasticiser, according to the results shown in Figure 5.3, the exposure concentration of 2 % v/v would not be sufficient to exhibit any reduction in viral titre.

While the integration of *Podoviridae* within the porous matrix of PLAg hydrogels provides a promising vehicle for small bacteriophage, the poor mechanical characteristics of these materials in the hydrated state make them unsuitable for application as wound dressings. For this reason, attempts were made to integrate bacteriophage K and T3 into the matrix of dehydrated PLAg films, by following the methods described in section 5.2.2.1, followed by dehydration of the hydrogel to form a film under mild conditions (48 h at 30°C). This proved to be unsuccessful, with no recoverable bacteriophage identified after 24 h reconstitution in bacteriophage buffer (4°C). The dehydration of PLAg gels to form PLAg films results in significant reduction in size (4 mm depth in hydrogel state to 0.14 mm depth as a film). While PLAg has been shown to swell when rehydrated (see Chapter 4) this contraction of the matrix could result in decreased bacteriophage recovery due to the exposure of bacteriophage to shear stress.

In the case of bacteriophage drying when integrated with PLAg, a more significant factor was the increasing concentration of plasticiser that bacteriophage were exposed to as the solvent evaporated from the material. At 50 % v/v plasticiser concentrations, all bacteriophage showed some reduction in titre (Figure 5.3). During the dehydration process bacteriophage would be exposed to further elevated concentrations, which would undoubtedly result in significant reductions in viability. This phenomenon was also observed when investigating the release of bacteriophage K and T3 air dried on the surface of PLAg films at 30°C for up to 24 h (Figure 5.5). Modest reductions in viable bacteriophage release were observed after 24 h drying on the surface of glass (1.3 Log_{10} reduction), which align with values found in the literature [311]. Conversely, when dried on the surface of PLAg, release of bacteriophage T3 was quantified as a 6 Log_{10} reduction of the starting inoculum at 24 h, and within 3 h desiccation bacteriophage K titres had fallen below detectable levels. Previous work has shown that plasticiser leaches from the film material upon rehydration

(see Chapter 4), and in the case of air drying bacteriophage on the surface of PLAg films, leachate would subsequently concentrate on the film surface during desiccation. This concentrated layer of plasticiser would not only affect bacteriophage stability, but also inhibit release of bacteriophage due to the high viscosity at high concentrations. These findings suggest that, while an approximate 1.3 Log_{10} reduction can be attributed to the drying process (as demonstrated by drying on the surface of glass), drying of bacteriophage when integrated with PLAg results in significant reductions in bacteriophage infectivity as a result of the plasticiser content. This section presents the first investigations of bacteriophage stability with ionic liquid plasticisers, independently and as a component of polymer films.

To overcome the challenges associated with bacteriophage desiccation, bacteriophage particles were allowed to spontaneously associate with the surface of PVAm-PLAg films by charge-based sorption. This method allowed for bacteriophage tethering under conditions which do not present challenges to bacteriophage viability; i.e. at low temperature and in aqueous conditions. To determine the best method for quantification of bacteriophage capture, three methods of quantification were evaluated during preliminary investigations: quantification of supernatant bacteriophage concentration, quantification of washing buffer bacteriophage concentration, and quantification of bacteriophage on the film surface by direct plating onto bacterial host-inoculated agar.

Supernatant bacteriophage titres were determined to estimate viral sorption by reduction compared to the starting inoculum. Each film was then washed and the number of bacteriophage in the washing buffer quantified to determine the proportion of non-associated bacteriophage. Finally, direct plating of films was used to determine the proportion of associated and infective bacteriophage at the film interface. For the validation of enumeration methods, the adsorption of bacteriophage T3 to the surface of PLAg was evaluated. The majority of bacteriophage T3 exposed to PLAg films were shown to remain in the supernatant, with only a small proportion dissociating during washing and quantifiable by direct plating. The sum of all three methods was equivalent to the starting inoculum, demonstrating that using all three methods would result in the quantification of all exposed bacteriophage. When assessing the sorption of bacteriophage T3 to PVAm-PLAg, the majority of bacteriophage were recovered by direct plating; these numbers, however, were generally too numerous to count (TNTC). For this reason, and the proportionally low number of bacteriophage recovered by direct plating and washing buffer quantification for PLAg films, supernatant measurements were selected as the chosen method of bacteriophage capture efficacy to the surface of PLAg and PVAm-PLAg.

The adsorption efficacy of bacteriophage to the surface of PLAg and PVAm-PLAg was determined at incremental bacteriophage inocula (10^3 PFU to 10^6 PFU) by quantifying the reduction of viral particles in the exposed inoculum. The adsorption of all four bacteriophage to PVAm-PLAg was significantly higher than PLAg at all tested concentrations (with the exception of bacteriophage 44AHJD at 10^6 PFU inoculum). In addition, with the exception of bacteriophage T4, the number of infective bacteriophage at the material interface (as determined by direct plating of bacteriophage integrated films) was notably higher in PVAm-PLAg compared to PLAg. The reasoning for the increased adsorption and infective capacity when adsorbed to the surface of PVAm-PLAg is likely due to the surface charge difference of the two films. As reported in Chapter 4, by application of PVAm to the surface of PLAg the surface charge is modified from negative to positive. With the net surface charge of all bacteriophage being negative (as reported in Chapter 3), it is reasonable to conclude that the increased adsorption is due to the attraction of the opposing net electrostatic charges. The rationale behind the development of PVAm-PLAg, however, was to allow for the orientated adsorption of bacteriophage to the material interface by exploiting the reported charge difference between the bacteriophage capsids (negative) and tails (positive) [200]. As demonstrated by direct plating of bacteriophage integrated films, plaque counts were significantly higher for all bacteriophage adsorbed to PVAm-PLAg; suggesting higher proportions of bacteriophage were adsorbed in the optimal orientation, presumably by their capsids. Interestingly, contact angle measurements presented in Chapter 4 showed that, while PLAg and PVAm-PLAg were both hydrophilic, the surface of PVAm-PLAg was notably 'more hydrophobic' than PLAg. This factor may also play a part in the increase of bacteriophage adsorption to PVAm-PLAg as it is generally accepted that hydrophobic surfaces adsorb more proteins than hydrophilic surfaces [312]. The increase towards hydrophobicity on the surface of PVAm-PLAg could therefore increase the affinity and consequent adsorption of bacteriophage structural proteins (i.e. the bacteriophage capsid). Data from this study, therefore, suggests that by applying PVAm to the surface of PLAg, not only is the adsorption rate increased, but the infectivity at the material interface is increased also. These findings align with a study which reported increased bacteriophage adsorption to, and infectivity of, PVAm modified cellulose membranes intended for food packaging [200]. The aforementioned study, however, used a previously developed bacteriophage cocktail and did not investigate the correlation between bacteriophage morphology and adsorption efficacy. The work conducted in this thesis suggests that some bacteriophages of the *Myoviridae* and *Podoviridae* families are suitable candidates for immobilisation on the surface of PVAm-PLAg.

Once the spontaneous adsorption of bacteriophage to the surface of PLAg and PVAm-PLAg had been quantified, the release rate of bacteriophage T3 was investigated over 48 h at 4°C (storage conditions) and 37°C (application conditions). Bacteriophage T3 adsorbed to PLAg demonstrated a rapid release of 3.59 Log_{10} (4°C) and 3.68 Log_{10} (37°C) of the adsorbed bacteriophage within 1 h, with these values rising to 3.70 Log_{10} (4°C) and 3.79 Log_{10} (37°C) after 48 h release; the lack of significance between the time points indicates passive adsorption and release from the material. The total release of bacteriophage at 48 h for both tested temperatures only accounted for a small proportion of the bacteriophage adsorbed, suggesting some interaction with PLAg, potentially association of the positively charged tail with the negatively charged material surface. Bacteriophage release from PVAm-PLAg at 4°C also demonstrated an initial burst at 1 h followed by plateau, however the number of released bacteriophage was notably lower at 2.67 Log_{10} at 48 h. Bacteriophage T3 release from PVAm-PLAg at 37°C, however, revealed a cumulative release of bacteriophage over the 48 h period, from 3.75 Log_{10} (1 h) to 5.88 Log_{10} (48 h). These data show that the addition of PVAm in PVAm-PLAg films results in a controlled, progressive and cumulative release of bacteriophage over time. This effect, however, is exclusive to release at 37°C, suggesting the controlled release occurs as a result of temperature induced phase transitions of the material. While the thermodynamic properties of PVAm-PLAg remain unknown, the T_g of PVAm has been reported to occur at approximately 55°C [313], while the T_g of PLAg films is reported to occur at 37.5°C (IL50) [262]. The T_g of a polymer is defined as the temperature at which the material's physical properties change from a glassy or crystalline rigid state ($< T_g$), to a flexible rubber like state ($> T_g$) due to increased mobility of the molecules within. The effect that this has on PVAm-PLAg, however, remains elusive and the thermodynamic properties of PVAm-PLAg should be determined in the future to elucidate the effect of temperature on bacteriophage release. The release of adsorbed bacteriophage may also occur due to ion exchange of plasticiser leachate, or ions in solution, with the PVAm surface coating; suggesting further insight into the interactions between plasticiser leachate and components of the release buffer is necessary. This could then extend to investigating the interaction and release of bacteriophage from PVAm-PLAg in artificial wound media. To date, this is the first study outlining the dissociation profile of bacteriophage from cationic surfaces at various release temperatures.

Visualisation of *E. coli* infective bacteriophage T3 and T4 using AFM revealed the deposition of viral particles on the surface of PVAm-PLAg films. Bacteriophage T4 were clearly identifiable by their characteristic morphology (capsid with long contractile tail), while bacteriophage T3 were identifiable by their small size and short tail. For both

bacteriophage, distribution seemed uniform over 5 μm^2 sections. Bacteriophage T3 showed higher levels of aggregation than bacteriophage T4. This phenomenon has been attributed to the compact morphology of non-tailed *Podoviridae* resulting in higher rates of aggregation, while steric hindrance imposed by the long tails of *Myoviridae* results in lower levels of aggregation [160]. Due to the necessity for fixation and dehydration of bacteriophage loaded PVAm-PLAg samples, the orientation of viral particles could not be elucidated. Height measurements of both bacteriophage were lower than their width, suggesting flattening of the viral particles or embedding within the superficial layer, both factors are likely to be an artefact of sample fixation.

While bacteriophage were shown to adsorb at higher rates to PVAm-PLAg when compared to PLAg, the infective yield at the material interface was much lower, suggesting that a high number of bacteriophage were adsorbed but non-infective. Determining the orientation of bacteriophage in an aqueous environment was not possible due to imaging limitations, therefore the reason for the disparity between number adsorbed and number viable remains unknown. It was also shown that the infectivity at the material interface varied between the bacteriophage under investigation, suggesting that this method of bacteriophage immobilisation could not be used universally. Another limitation of bacteriophage immobilisation on a substrate is the exposure of viral particles to the external environment, which may render them inactive or result in premature release. For these reasons, bacteriophage were integrated within the porous matrix of alginate hydrogels on the surface of Alg-PVAm-PLAg composite materials. The rationale was to provide a hydrated and protective environment which would allow for extended storage periods and provide a higher dose of bacteriophage to the wound site upon application.

Bacteriophage release from Alg-PVAm-PLAg composite materials was determined over a 48 h period at both 4°C and 37°C to be reflective of storage and application conditions, respectively. At both temperatures, bacteriophage K, T3, and T4 were shown to release cumulatively over the 48 h time period. From 6 h onwards bacteriophage were released at a higher rate at 37°C than 4°C. This could be due to relaxation of the hydrogel matrix at higher temperatures and contraction at lower temperatures. Due to the materials being synthesised at room temperature, the initial release of bacteriophage could remain similar for both temperatures up to 6 h while the materials equilibrated to the correct test temperature. At both temperatures, bacteriophage K showed a significantly lower level of release than bacteriophage T3 and T4, while bacteriophage T3 showed the highest rate of release of all bacteriophage at 48 h. While these findings may suggest that bacteriophage release from Alg-PVAm-PLAg is dependent on bacteriophage size, release of bacteriophage 44AHJD

(the smallest of the four bacteriophage) was below the limit of detection (10^2 PFU). From Table 5.4 this bacteriophage also has the highest negative charge of all three bacteriophage at -24.01 mV. The reduced release of bacteriophage 44AHJD could, therefore, be explained by the association of viral particles with excess or partially crosslinked Ca^{2+} ions within the hydrogel matrix. This factor may also explain why bacteriophage T3, which is of similar size but significantly lower zeta potential (-13.12 mV), is readily released from Alg-PVAm-PLAg composites. The inhibited release of bacteriophage K, however, cannot be explained by zeta potential values and is more likely due to the entrapment within the matrix due to its larger size. While the pore sizes of alginate hydrogels used in this study were not determined, pore sizes of between 5 nm to 200 nm have been reported for 2 % Ca^{2+} hydrogels [314]. The wide range of pore sizes observed were likely due to the concentration gradient produced by external Ca^{2+} cross-linking, therefore the internal gelation method used in this study would likely produce a more homogenous matrix. Notwithstanding, maximum pore size of 200 nm would not be sufficient to allow for the release of bacteriophage K from the hydrogel matrix. Further investigations into the pore size of alginate hydrogels synthesised using the $CaCO_3$-GDL system would be necessary to elucidate the mechanisms of bacteriophage release from Alg-PVAm-PLAg composites.

Table 5.4 - Summary of characteristics which could influence the release of bacteriophage from Alg-PVAm-PLAg composites.

Bacteriophage	**Family**	**Approximate Length (nm)**	**Zeta Potential (mV)**	**Composite Release % (48 h, 37°C, 10^7 inoculum)**
T3	*Podoviridae*	70	-13.12	97.4
T4	*Myoviridae*	200	-17.66	92.7
44AHJD	*Podoviridae*	60	-24.01	0
K	*Myoviridae*	280	-16.65	20.0

While alginate is not inherently degradable under physiological conditions, partially oxidised alginate hydrogels can degrade in aqueous media by degradation of the polymer backbone [315]. In addition, alginate hydrogels may degrade by the addition of monovalent cations in solution; by exchange reactions with the cross-linking divalent cations [191]. These characteristics provide areas of exploitation for the release of antimicrobial molecules and particles contained within the hydrogel, particularly when they are too large to have significant diffusion-based release. Targeting alginate degradation may, therefore, provide a more rapid release of small bacteriophage (< 200 nm), and facilitate the release of larger bacteriophage (> 200 nm) contained within the hydrogel layer of Alg-PVAm-PLAg.

Chapter Six: General Discussion and Conclusions

6 General Discussion and Conclusions

6.1 General discussion

The overall aim of this thesis was to select candidate bacteriophage infective against clinically reflective wound colonising bacteria and integrate them with novel wound dressing materials in order to explore their potential as alternative treatment options to traditional antibiotic therapy. Although there is growing evidence of bacteriophage efficacy in the prospective treatment of wound infections [111, 115, 135, 171, 222, 235, 301, 316-319], investigations into the integration of bacteriophage with biomaterials and their effective delivery to the infected wound are lacking; this thesis aims to contribute to building this understanding.

The first results chapter (Chapter 3) describes the characterisation of four bacteriophage active against the common wound pathogens *E. coli* and *S. aureus*. The morphology of each bacteriophage was evaluated using TEM to confirm their characteristic structural properties and to ensure purity of the preparations. The bacterial host range for each bacteriophage was then determined using a range of culture collection and clinical isolates establishing the efficacy of infection and enabling the selection of a suitable host for use in further studies. Once the bacteriophage hosts were selected, the growth characteristics of the bacteriophage were assessed, followed by investigations of their infective capabilities in planktonic bacterial culture. Finally, bacteriophage zeta potentials were measured to establish relative surface charge for each; all bacteriophage showed a net negative charge but with variation in magnitude.

The following chapter (Chapter 4) outlines the development, synthesis and extensive characterisation of candidate wound dressing materials for bacteriophage integration. Initially the characterisation of the base material (PLAg) was undertaken, building upon earlier work by Shamsuri *et al* (2012) [262]. No potential applications for this material were experimentally explored by these researchers, and so further evaluation to determine its suitability as a wound dressing was conducted by investigation of the stability of plasticiser upon film rehydration and the toxicity of leachate. Once its potential suitability was confirmed, the material was further developed by cationic modification of the film surface to produce the novel PVAm-PLAg material. The rationale for this development was to provide a positively charged surface for orientated bacteriophage immobilisation. Prior to surface modification, commercially sourced PVAm was further purified and characterised, with this thesis presenting the first investigations into the stability of purified PVAm under selected storage conditions. PVAm-PLAg was then extensively characterised and compared to PLAg

throughout, providing insight into the structural arrangement of the base material. The presence and permanence of PVAm at the material interface was confirmed by molecular techniques including FTIR, EDS and XPS; demonstrating the suitability of the surface coating technique and stability of PVAm upon rehydration. Finally, the synthesis of Alg-PVAm-PLAg is described. This material was developed to offer a protected environment for bacteriophage through their integration into the hydrated matrix of an alginate hydrogel layer, while the addition of PLAg as a base layer ensured structural support to the otherwise mechanically weak hydrogel.

The final results chapter (Chapter 5) sought to combine the selected bacteriophage characterised in Chapter 3 with the materials developed in Chapter 4, in order to produce antimicrobial biomaterials for potential wound dressing applications. Bacteriophage infectivity was shown to be inhibited at high plasticiser concentrations, particularly in *Myoviridae*, which was likely due to spontaneous tail contraction induced by urea. This feature presented complications to the physical adsorption of bacteriophage through desiccation, due to the leaching of plasticiser during the introduction of bacteriophage followed by the evaporation of the solvent; elevating plasticiser concentrations to undesirable levels. Using an alternative approach, bacteriophage were allowed to spontaneously adsorb to the surface of cationic PVAm-PLAg, which resulted in increased adsorption and surface infectivity compared to PLAg alone. The release of bacteriophage T3 from PVAm-PLAg was inhibited at 4°C (typical storage conditions where retention would be required) but was progressive at 37°C emulating in-use conditions; this behaviour suggested potentially suitable properties for the release of bacteriophage under application conditions. Finally, bacteriophage were integrated within the alginate hydrogel layer of Alg-PVAm-PLAg composites to increase antimicrobial potential further and to provide a protective environment prior to application. Release of bacteriophage K, T3 and T4 from these composites was higher at 37°C compared to 4°C. Perhaps not surprisingly given the variation in bacteriophage, no method of integration investigated in this study was equally effective for all bacteriophage tested, suggesting further study into the interactions between bacteriophage and their prospective delivery platforms is necessary. Of the four bacteriophage, however, T3 was shown to be only moderately sensitive to the ionic liquid plasticiser, demonstrated high rates of adsorption to PVAm-PLAg, and temperature induced release from PVAm-PLAg and Alg-PVAm-PLAg. This discovery could therefore be a target for future studies.

6.2 Experimental limitations

6.2.1 Microbiological

The majority of experimental limitations were encountered during investigations which required the enumeration of bacteriophage suspended in bacteriophage buffer. The standard methodology used in this study for bacteriophage enumeration was the viral plaque assay, which when plating 100 µl per plate results in an approximate limit of detection (LOD) of 10 PFU/ml. Bacteriophage release studies, however, were conducted in 10 ml of bacteriophage buffer and values expressed in PFU to correspond with the starting inoculum units; thereby increasing the LOD ten-fold to 100 PFU. As a result, viral titres of < 100 PFU would generally be non-quantifiable; a finding particularly evident in the release of bacteriophage 44AHJD from Alg-PVAm-PLAg composites, where release values were consistently on or below the LOD. While traditional plaque assays are generally considered the "gold standard' for quantifying bacteriophage titres, this method presents various other problems that should be considered. Firstly, the reproducibility is generally considered to be poor, with 1000-fold variations in viable titres of T2 reported with the change of salt concentration within the top agar layer, and variable efficacy of one bacteriophage against multiple hosts [320]. To reduce the influence of these limitations, the salt concentrations within the top agar layer were kept consistent and one bacterial host was selected for each bacteriophage for bacteriophage enumeration throughout the project. Other limitations of the plaque assay include the time taken to obtain results (usually 24 h), due to the necessity of visible bacterial lawn growth to identify clear plaques. Alternative methods to the plaque assay include QPCR and NanoSight (NS) technologies; however QPCR requires costly equipment and the synthesis of bacteriophage specific primers and NS has been reported to be less precise [321].

Further limitations relating to bacteriophage enumeration arose when attempting to quantify the number of viable bacteriophage immobilised on the surface of PVAm-PLAg by direct plating. The small plaque size of bacteriophage K, 44AHJD and T4 allowed enumeration of < 116 PFU. However, with the adsorption of 10^3 to 10^6 PFU this only allowed for enumeration at the lower adsorption titres. Bacteriophage T3 presented further challenges due to the larger plaque size, only allowing identification of < 60 PFU. Unfortunately, the diameter of the films was fixed due to the use of bacterial filter units for bacteriophage adsorption and release studies, as larger films may have allowed enumeration of a higher number of plaques. Attempts were made to adsorb lower numbers of bacteriophage by reducing the exposed inoculum, however the data presented in this thesis show that some bacteriophage show a dose-response relationship between the bacteriophage inoculum and

the proportion adsorbed. Alternative methods of bacteriophage enumeration at the material interface were considered, including AFM. This method, however, proved to be labour intensive and did not decipher whether the viral particles were viable.

6.2.2 Imaging of bacteriophage at the film interface

The rationale behind the development of PVAm-PLAg was to obtain a cationic interface for the immobilisation of negatively-charged bacteriophage capsids permitting tail fibres to remain available to initiate bacterial infection. To determine the orientation of bacteriophage which had been allowed to spontaneously adsorb to PVAm-PLAg, attempts were made to visualise viral particles using AFM. While bacteriophage T3 and T4 could be identified at the material interface, deciphering the orientation was more complex. Initially, imaging was conducted on bacteriophage-loaded PVAm-PLAg samples in an aqueous environment (bacteriophage buffer), to prevent any changes in orientation imposed by factors such as fixation and dehydration. Unfortunately, this method resulted in movement of the film on the AFM stage during the acquisition of measurements and definitive images could not be produced. Furthermore, detachment and orientation changes may have occurred during interactions with the AFM probe. In order to obtain images, bacteriophage-loaded PVAm-PLAg films were fixed with glutaraldehyde and dehydrated with ethanol, potentially altering the orientation of bacteriophage on the material surface. Therefore, no clear assumptions regarding the orientation of bacteriophage could be made.

Further attempts to visualise bacteriophage on the surface of PVAm-PLAg were made using SEM. Preliminary studies were conducted by adsorbing bacteriophage T3 on the surface of carbon grids, which proved successful with an abundance of viral particles visible (see Appendix IV). However, when imaging bacteriophage-loaded PVAm-PLAg with SEM, charging of the polymer film at high magnification and consequent heat damage and deformation of the material resulted in difficulties in obtaining images with the necessary resolution.

This study, therefore, relied significantly on indirect microbiological techniques to determine by inference the orientation of bacteriophage by direct plating of bacteriophage-loaded PVAm-PLAg films and enumeration of plaques. This method also had its limitations (Section 6.2.1), however it provided insight into whether the adsorbed bacteriophage were also capable of infection. Recently, evanescent wave light scattering and interferometric scattering microscopy (iSCAT) have been proposed as methods which have potential to provide real-time monitoring of bacteriophage orientation on a surface [197]. These methods

would be particularly useful for reducing the influence of experimental artefacts by monitoring changes in the intensity of scattered light induced by changes in viral orientation.

6.2.3 PLAg cytotoxicity assay

Due to the nature of biomaterial development, predictive toxicity of the materials in development should be assessed at an early stage to avoid unsafe clinical outcome. However, a study investigating the cytotoxic effect of sixteen, mostly commercially available, wound dressings found that only 5 did not induce cytotoxic effects [322]. This highlights the importance of appropriate methodological validity and consistency when determining the cytotoxic effect of any given material. This study presents data which suggests that plasticiser leachate from PLAg films is non-toxic, however the level of plasticiser leachate was unknown and may not reflect the potential concentrations of leachate and the associated toxicity when applied to an infected wound. In addition, the use of a single cell model in this study is considered a significant limitation, due to the potential variability in biological response and toxicity between cell types. It should also be noted that the exposed tissue of an infected wound would be a significantly different environment than that used in routine cytotoxicity assays. By quantifying plasticiser leachate in an artificial wound exudate medium and investigating the cytotoxic effect at incremental plasticiser concentrations against a panel of cell lines data could be obtained which would be more reflective of the effects when *in situ*. Using wound healing scratch assays would also allow for monitoring of cell proliferation and migration when exposed to PLAg leachate. These limitations were, however, foreseen and a choice had to be made to restrict these studies in order to focus on the primary objectives of this study. This preliminary investigation, instead, gives a general predictive insight into the cytotoxicity of PLAg leachate for future study.

6.3 Investigative outcomes, novel contributions and conclusions

The conclusions presented in this study have been drawn from the outcomes of experimental investigation and consideration of the available literature. This study has been successful in fulfilling the research aims outlined at the start of this thesis and in providing novel contributions to knowledge across multidisciplinary fields. The novel contributions for this body of research are diverse and cover aspects of the base dressing material, surface coating, composite material synthesis, and the combined bacteriophage integrated candidate materials.

6.3.1 Investigative outcomes

I. Four bacteriophage infective against the common wound pathogens *E. coli* and *S. aureus* were selected for integration with synthesised wound dressing materials. A member of the *Podoviridae* and *Myoviridae* family were selected to investigate the differences between bacteriophage morphology and integration efficacy. Each bacteriophage was characterised, including determination of the bacteriophage zeta potential which is a lesser studied but significant characteristic for this study.

II. Ionic liquid plasticiser has been shown to leach from PLAg films upon rehydration, with data obtained by FTIR and XPS suggesting solubilisation of plasticiser and the preferential release of urea. Plasticiser leachate showed no adverse effect on a fibroblast cell line, offering the potential for safe use in a wound dressing.

III. The purification method for PVAm outlined in this study results in the complete hydrolysis of the polymer precursor and the removal of side-product impurities, as shown by FTIR and NMR analysis. PVAm was shown to degrade over a 12-month period under various conditions, however long-term stability was observed when stored under nitrogen at -20°C.

IV. The surface coating technique developed in this study to create PVAm-PLAg, was shown to be effective in depositing PVAm at the material interface with a level of permanence suitable for the proposed application. The distribution of PVAm across the material interface was also proposed to be entire and equal across the film interface. PVAm-PLAg was shown to demonstrate only marginal changes in swelling and MVPR over nascent PLAg, while offering a complete reversal of surface charge from negative (PLAg) to positive (PVAm-PLAg).

V. Alg-PVAm-PLAg composite materials were successfully developed by addition of an alginate hydrogel layer to PVAm-PLAg films. The alginate hydrogels were shown to adhere to the surface of PVAm-PLAg resulting in structural stabilisation and mechanical improvement of the hydrogel. Conversely, alginate was shown to have no affinity to unmodified PLAg, suggesting a molecular interaction between the alginate hydrogel layer and PVAm.

VI. The bacteriophage used in this study were shown to be sensitive to ionic liquid plasticiser at high concentrations, potentially due to the urea component inducing spontaneous tail contraction. This presented limitations in the integration of bacteriophage by desiccation on the film surface due to increasing plasticiser concentrations arising during the drying process.

VII. Spontaneous adsorption of bacteriophage to PVAm-PLAg under aqueous conditions was consistently higher than to unmodified PLAg, potentially due to the net negative charge of bacteriophage and the complementary positive charge of PVAm-PLAg. Infectivity at the material interface was higher in PVAm-PLAg for all bacteriophage other than T4, suggesting a higher proportion of capsid association with the material interface. However, numbers of infective bacteriophage at the interface of PVAm-PLAg were not equal to the number adsorbed to the film, indicating either that not all bacteriophage were associated in the correct orientation or an unidentified factor was causing viral deactivation. Bacteriophage T3 and T4 were successfully visualised at the material interface using AFM.

VIII. The release of spontaneously adsorbed bacteriophage T3 from PVAm-PLAg was shown to be significantly higher at 37°C compared to 4°C. The cumulative, controlled release at 37°C was proposed to be due to temperature induced phase transitions of the material, however the thermodynamic properties of PVAm-PLAg are currently unknown. These findings suggest a possible temperature-dependant release of bacteriophage which may be a significant advantage when considering the storage and application of the bacteriophage integrated material.

IX. Bacteriophage were successfully integrated within the alginate hydrogel layer of Alg-PVAm-PLAg composite materials. The release of bacteriophage from Alg-PVAm-PLAg appeared to be multifactorial and dependant on both the size and zeta potential of each bacteriophage. Consistently higher release rates of bacteriophage

were observed at 37°C compared to 4°C; bacteriophage 44AHJD release, however, remained below the limit of detection suggesting strong retention possibly as a result of strong electrostatic interactions between bacteriophage particles and the material.

X. No method of bacteriophage integration investigated in this study was shown to be universally appropriate for all bacteriophage. For example, bacteriophage T4 spontaneously adsorbed at higher numbers to PVAm-PLAg compared to PLAg, however lower levels of infectivity were observed on the surface of PVAm-PLAg. Bacteriophage 44AHJD release from Alg-PVAm-PLAg composites was also inhibited, while bacteriophage K, T3 and T4 were released at high levels. These findings suggest that further study into the interactions between bacteriophage and their prospective delivery vehicles is necessary. Bacteriophage T3, however, showed desirable integration and release from PVAm-PLAg and Alg-PVAm-PLAg, presenting opportunities for further study.

6.3.2 Novel contributions

I. Further characterisation of PLAg, including studies involving plasticiser leachate and surface analysis, build upon work conducted by Shamsuri *et al* [262]. The data presented in this thesis have not only furthered our knowledge of PLAg and its potential as a wound dressing material, but also been essential in the development of PVAm-PLAg and Alg-PVAm-PLAg.

II. As PVAm-PLAg and Alg-PVAm-PLAg are novel candidate wound dressing materials, all developmental stages and characterisation of these materials can be considered as novel contributions to the current body of literature. The development of these materials has provided avenues of future exploration for the integration and release of therapeutic compounds.

III. The integration and characterisation of bacteriophage integrated PVAm-PLAg and Alg-PVAm-PLAg offers further contributions to knowledge by quantification of the integration efficacy and release profiles of bacteriophage with the developed candidate wound dressing materials.

6.3.3 Conclusions

This study has contributed to our understanding of the development and characterisation of novel wound dressing materials and the integration and release characteristics of bacteriophage. The results highlight the importance of the compatibility between the material and bacteriophage when designing suitable delivery vehicles for therapeutic bacteriophage formulations. This will require careful consideration and harmonisation of the bacteriophage characteristics (i.e. general morphology and surface charge) and those of the proposed material (i.e. pore size and antiviral properties of individual components). Whilst this study was unable to present a material capable of successfully integrating all four bacteriophage selected in Chapter 3, with at least one species presenting limitations in each material or integration technique, data presented in the current study provides definitive evidence of successful bacteriophage integration with PVAm-PLAg and Alg-PVAm-PLAg. Further investigations of the interactions between morphologically and characteristically distinct bacteriophage and candidate materials may elucidate further the factors giving rise to these limitations; allowing for the eventual development of materials capable of integrating a wide range of bacteriophage.

6.4 Future work

The experimental work presented in this thesis describes the synthesis of two novel wound dressing materials (PVAm-PLAg and Alg-PVAm-PLAg) and the evaluation of a number of techniques for bacteriophage integration to produce novel antimicrobial biomaterials. Reflecting on the identified limitations and conclusions drawn, several lines of investigation could be considered to formulate further questions and research aims to direct future research.

In terms of further biomaterial characterisation, due to time constraints the nature of the interaction between PVAm and the alginate hydrogel layer of Alg-PVAm-PLAg remains unclear offering a potential avenue for future investigation. The interaction between the two layers could be deciphered by molecular techniques such as monatomic depth profiling combined with XPS analysis. The combined use of these techniques would allow for the determination of elemental composition and further subsurface information at various depths of the material by cycles of etching and spectrum acquisition. By pinpointing the depth at which the hydrogel layer met the PVAm surface coating, the change in elemental composition and analysis of high resolution C1s core level spectra could provide insight into the molecular interactions between these two materials.

The work presented in this study suggests the need for further investigation into the interactions between the novel materials and bacteriophage during integration and subsequent release. While the reported charge difference between the bacteriophage capsid and tail has been exploited for the orientated immobilisation of bacteriophage [200], this conclusion has been drawn from investigations using capsid and tail components of the *Myoviridae*, bacteriophage T4, only. Therefore, determining the charge difference between bacteriophage capsids and tails in an array of bacteriophage of different species, families, and orders would be valuable to assess the utility of this approach for a wider range of bacteriophage. Furthermore, it was determined that amongst the four bacteriophage selected for use in this study, there was no “one size fits all” method for integration with any of the developed materials. In a clinical context, this could provide a challenge for producing broad-range antimicrobial wound dressings through the introduction of bacteriophage cocktails. An avenue of future research could therefore focus on determining the wider range of bacteriophage characteristics which allow for efficacious integration and release from PVAm-PLAg and Alg-PVAm-PLAg. By establishing these characteristics, prospective bacteriophage could be screened for these properties, or the biomaterials could be further modified to accommodate a wider range of interactions to enable incorporation of a more catholic selection of bacteriophage to target challenging wound infections.

Whilst this study gave insight into the integration and release of bacteriophage from PVAm-PLAg and Alg-PVAm-PLAg, the antimicrobial efficacy of these bacteriophage composites remains largely unstudied. Initially, further work should focus on probing the antimicrobial efficacy against bacteria in both in vitro planktonic and biofilm culture. Once established and optimised, investigations could progress to *in vitro* wound infection models and then *in vivo* animal models.

Finally, while this work has focused on the therapeutic use of bacteriophage integrated into biomaterials for application as wound dressings, the technology outlined presents future possibilities for a range of alternative applications. For example, the use of bacteriophage integrated polymer films has been investigated for application with food products to prevent meat spoilage [200, 202, 323] and PVAm-PLAg and Alg-PVAm-PLAg may offer alternative options in this industry. Furthermore, bacteriophage loaded materials may be utilised in the biosensing industries, allowing for the sensitive and highly specific detection of bacterial species in the food, clinical, and biological defence industries. The development of PVAm-PLAg and Alg-PVAm-PLAg may not be limited to the integration of bacteriophage, with these materials offering potential for the incorporation of traditional antibiotics, or novel alternatives such as antimicrobial peptides, bacteriophage-derived enzymes, therapeutic antibodies, and metal nanoparticles. These polymer composites therefore offer a technology platform that may be exploited in a wider range of industries for an array of applications.

7 References

1. Control, C.f.D. and Prevention, *Antibiotic resistance threats in the United States, 2013. Atlanta: CDC; 2013*. 2015.
2. ECDC, E., *The bacterial challenge: time to react.* Stockholm: European Center for Disease Prevention and Control, 2009.
3. Golkar, Z., O. Bagasra, and D.G. Pace, *Bacteriophage therapy: a potential solution for the antibiotic resistance crisis.* J Infect Dev Ctries, 2014. **8**(2): p. 129-136.
4. O'Neil, J., *Tackling a crisis for the health and wealth of nations*. 2014.
5. Paquette, D. and V. Falanga, *Leg ulcers.* Clin Geriatr Med, 2002. **18**(1): p. 77-88, vi.
6. WHO. *Governing Body Documentation*. 1998.
7. WHO. *Global Strategy for Containment of Antimicrobial Resistance*. 2001.
8. European-Community, *Regulation (ED) 1831/2003 of the European Parliament and of the Council of 22 September 2004 on additives for use in animal nutrition*. 2003. p. 29-43.
9. European-Commission, *Action plan against the rising threats from antimicrobial resistance*. 2011.
10. European-Council, *Council conclusions on the impact of antimicrobial resistance in the human health sector and in the veterinary sector*, E. Council, Editor. 2012. p. 1-6.
11. FDA, *Press Announcements - FDA takes steps to protect public health*. 2012.
12. DEFRA, *UK Five Year Antimicrobial Resistance Strategy 2013 - 2018*. 2013.
13. Baker, S.J., et al., *Technologies to address antimicrobial resistance.* Proceedings of the National Academy of Sciences, 2018. **115**(51): p. 12887.
14. Czaplewski, L., et al., *Alternatives to antibiotics—a pipeline portfolio review.* The Lancet infectious diseases, 2016. **16**(2): p. 239-251.
15. Zheng, K., et al., *Antimicrobial silver nanomaterials.* Coordination Chemistry Reviews, 2018. **357**: p. 1-17.
16. Wang, L., C. Hu, and L. Shao, *The antimicrobial activity of nanoparticles: present situation and prospects for the future.* International journal of nanomedicine, 2017. **12**: p. 1227-1249.
17. Pitt, S.J., et al., *Antimicrobial properties of mucus from the brown garden snail Helix aspersa.* Br J Biomed Sci, 2015. **72**(4): p. 174-81; quiz 208.

18. Pitt, S.J., et al., *Identification and characterisation of anti - Pseudomonas aeruginosa proteins in mucus of the brown garden snail, Cornu aspersum.* British Journal of Biomedical Science, 2019. **76**(3): p. 129-136.
19. Tagliaferri, T.L., M. Jansen, and H.P. Horz, *Fighting Pathogenic Bacteria on Two Fronts: Phages and Antibiotics as Combined Strategy.* Front Cell Infect Microbiol, 2019. **9**: p. 22.
20. Han, G. and R. Ceilley, *Chronic Wound Healing: A Review of Current Management and Treatments.* Advances in therapy, 2017. **34**(3): p. 599-610.
21. Snyder, R.J., *Treatment of nonhealing ulcers with allografts.* Clinics in Dermatology, 2005. **23**(4): p. 388-395.
22. Edwards, J.V., P. Howley, and I.K. Cohen, *In vitro inhibition of human neutrophil elastase by oleic acid albumin formulations from derivatized cotton wound dressings.* International Journal of Pharmaceutics, 2004. **284**(1–2): p. 1-12.
23. Mustoe, T., *Understanding chronic wounds: a unifying hypothesis on their pathogenesis and implications for therapy.* The American Journal of Surgery, 2004. **187**(5, Supplement 1): p. S65-S70.
24. Steed, D.L. and t.D.U. Study Group, *Clinical evaluation of recombinant human platelet – derived growth factor for the treatment of lower extremity diabetic ulcers.* Journal of Vascular Surgery, 1995. **21**(1): p. 71-81.
25. Mustoe, T.A., et al., *A phase ii study to evaluate recombinant platelet-derived growth factor-bb in the treatment of stage 3 and 4 pressure ulcers.* Archives of Surgery, 1994. **129**(2): p. 213-219.
26. Bishop, J.B., et al., *A prospective randomized evaluator-blinded trial of two potential wound healing agents for the treatment of venous stasis ulcers.* Journal of Vascular Surgery, 1992. **16**(2): p. 251-257.
27. Percival, S.L., et al., *Surgical-site Infectionsâ Biofilms, Dehiscence, and Delayed Healing.* 2008.
28. Kingsley, A., *The wound infection continuum and its application to clinical practice.* Ostomy Wound Manage, 2003. **49**(7A Suppl): p. 1-7.
29. Bowler, P.G., *The 10 (5) bacterial growth guideline: reassessing its clinical relevance in wound healing.* Ostomy/wound management, 2003. **49**(1): p. 44-53.

30. Krizek, T.J. and M.C. Robson, *Evolution of quantitative bacteriology in wound management.* The American Journal of Surgery, 1975. **130**(5): p. 579-584.
31. Breidenbach, W.C. and S. Trager, *Quantitative culture technique and infection in complex wounds of the extremities closed with free flaps.* Plast Reconstr Surg, 1995. **95**(5): p. 860-5.
32. Bowler, P.G., et al., *Infection control properties of some wound dressings.* Journal of Wound Care, 1999. **8**(10): p. 499-502.
33. Hansis, M., *Pathophysiology of infection--a theoretical approach.* Injury, 1996. **27 Suppl 3**: p. Sc5-8.
34. Kingston, D. and D.V. Seal, *Current hypotheses on synergistic microbial gangrene.* Br J Surg, 1990. **77**(3): p. 260-4.
35. Negut, I., V. Grumezescu, and A.M. Grumezescu, *Treatment Strategies for Infected Wounds.* Molecules (Basel, Switzerland), 2018. **23**(9): p. 2392.
36. Bowler, P., *The anaerobic and aerobic microbiology of wounds. A review.* Wounds, 1998. **10**: p. 170-178.
37. Agnihotri, N., V. Gupta, and R.M. Joshi, *Aerobic bacterial isolates from burn wound infections and their antibiograms--a five-year study.* Burns, 2004. **30**(3): p. 241-3.
38. Bayram, Y., et al., *Three-year review of bacteriological profile and antibiogram of burn wound isolates in Van, Turkey.* Int J Med Sci, 2013. **10**(1): p. 19-23.
39. NNIS, *National Nosocomial Infections Surveillance (NNIS) Report, data summary from October 1986–April 1996, issued May 1996.* American Journal of Infection Control, 1996. **24**(5): p. 380-388.
40. Citron, D.M., et al., *Bacteriology of Moderate-to-Severe Diabetic Foot Infections and In Vitro Activity of Antimicrobial Agents.* Journal of Clinical Microbiology, 2007. **45**(9): p. 2819-2828.
41. Benwan, K.A., A.A. Mulla, and V.O. Rotimi, *A study of the microbiology of diabetic foot infections in a teaching hospital in Kuwait.* Journal of Infection and Public Health. **5**(1): p. 1-8.
42. Frank, D.N., et al., *The Human Nasal Microbiota and Staphylococcus aureus Carriage.* PLOS ONE, 2010. **5**(5): p. e10598.
43. T, F., *Staphylococcus*. Medical Microbiology, ed. B. S. Vol. 4. 1996, Galveston (TX): University of Texas.
44. Uhlen, M., et al., *Complete sequence of the staphylococcal gene encoding protein A. A gene evolved through multiple duplications.* J Biol Chem, 1984. **259**(3): p. 1695-702.

45. Patel, A.H., et al., *Virulence of protein A-deficient and alpha-toxin-deficient mutants of Staphylococcus aureus isolated by allele replacement.* Infect Immun, 1987. **55**(12): p. 3103-10.
46. Berube, B.J. and J. Bubeck Wardenburg, *Staphylococcus aureus α-toxin: nearly a century of intrigue.* Toxins, 2013. **5**(6): p. 1140-1166.
47. Lacey, K.A., J.A. Geoghegan, and R.M. McLoughlin, *The role of Staphylococcus aureus virulence factors in skin infection and their potential as vaccine antigens.* Pathogens, 2016. **5**(1): p. 22.
48. Becker, K., et al., *Prevalence of genes encoding pyrogenic toxin superantigens and exfoliative toxins among strains of Staphylococcus aureus isolated from blood and nasal specimens.* Journal of clinical microbiology, 2003. **41**(4): p. 1434-1439.
49. Bernal, A., et al., *Superantigens in human disease.* Journal of clinical immunology, 1999. **19**(3): p. 149-157.
50. McCormick, J.K., J.M. Yarwood, and P.M. Schlievert, *Toxic shock syndrome and bacterial superantigens: an update.* Annual Reviews in Microbiology, 2001. **55**(1): p. 77-104.
51. Costa, A.R., et al., *Staphylococcus aureus virulence factors and disease.* Microbial pathogens and strategies for combating them: science, technology and education, 2013. **1**: p. 702-710.
52. Kwiecinski, J., et al., *Staphylokinase promotes the establishment of Staphylococcus aureus skin infections while decreasing disease severity.* J Infect Dis, 2013. **208**(6): p. 990-9.
53. Bentley, R. and R. Meganathan, *Biosynthesis of vitamin K (menaquinone) in bacteria.* Microbiol Rev, 1982. **46**(3): p. 241-80.
54. Hudault, S., J. Guignot, and A. Servin, *Escherichia coli strains colonising the gastrointestinal tract protect germfree mice against Salmonella typhimurium infection.* Gut, 2001. **49**(1): p. 47-55.
55. Tourmousoglou, C.E., et al., *Surgical-site infection surveillance in general surgery: a critical issue.* J Chemother, 2008. **20**(3): p. 312-8.
56. Rodgers, G.L., et al., *Predictors of infectious complications after burn injuries in children.* The Pediatric infectious disease journal, 2000. **19**(10): p. 990-995.
57. Moet, G.J., et al., *Contemporary causes of skin and soft tissue infections in North America, Latin America, and Europe: Report from the SENTRY Antimicrobial Surveillance Program (1998–*

2004). Diagnostic Microbiology and Infectious Disease, 2007. **57**(1): p. 7-13.
58. Petkovšek, Ž., et al., *Virulence potential of Escherichia coli isolates from skin and soft tissue infections.* Journal of clinical microbiology, 2009. **47**(6): p. 1811-1817.
59. Stumpe, S., et al., *Identification of OmpT as the Protease That Hydrolyzes the Antimicrobial Peptide Protamine before It Enters Growing Cells of Escherichia coli.* Journal of Bacteriology, 1998. **180**(15): p. 4002-4006.
60. Haiko, J., et al., *Invited review: breaking barriers—attack on innate immune defences by omptin surface proteases of enterobacterial pathogens.* Innate immunity, 2009. **15**(2): p. 67-80.
61. Fabbri, A., S. Travaglione, and C. Fiorentini, *Escherichia coli Cytotoxic Necrotizing Factor 1 (CNF1): Toxin Biology, in Vivo Applications and Therapeutic Potential.* Toxins, 2010. **2**(2): p. 283-296.
62. Bhakdi, S., et al., *Escherichia coli hemolysin may damage target cell membranes by generating transmembrane pores.* Infect Immun, 1986. **52**(1): p. 63-9.
63. Bhakdi, S., et al., *Effects of Escherichia coli hemolysin on human monocytes. Cytocidal action and stimulation of interleukin 1 release.* J Clin Invest, 1990. **85**(6): p. 1746-53.
64. Gadeberg, O.V., I. Orskov, and J.M. Rhodes, *Cytotoxic effect of an alpha-hemolytic Escherichia coli strain on human blood monocytes and granulocytes in vitro.* Infect Immun, 1983. **41**(1): p. 358-64.
65. Grimminger, F., et al., *Escherichia coli hemolysin is a potent inductor of phosphoinositide hydrolysis and related metabolic responses in human neutrophils.* J Clin Invest, 1991. **88**(5): p. 1531-9.
66. Suttorp, N., et al., *Effects of Escherichia coli hemolysin on endothelial cell function.* Infect Immun, 1990. **58**(11): p. 3796-801.
67. Giedraitiene, A., et al., *Antibiotic resistance mechanisms of clinically important bacteria.* Medicina (Kaunas), 2011. **47**(3): p. 137-46.
68. Fukuda, K., *Antimicrobial drug resistance threat: our duty towards future generations.* East Mediterr Health J, 2013. **19**(5): p. 399.
69. Schmitz, F. and A. Fluit, *Mechanisms of Resistance in Infectious Diseases.* 1999, London: Mosby Ltd.

70. Azeredo, J. and I.W. Sutherland, *The use of phages for the removal of infectious biofilms.* Curr Pharm Biotechnol, 2008. **9**(4): p. 261-6.
71. Dissemont, J., et al., *Methicillin resistant Staphylococcus aureus (MRSA) in chronic wounds: therapeutic options and perspectives.* J. Dermatol. Ges, 2005. **3**: p. 25662.
72. King, M.D., et al., *Emergence of community-acquired methicillin-resistant Staphylococcus aureus USA 300 clone as the predominant cause of skin and soft-tissue infections.* Annals of internal medicine, 2006. **144**(5): p. 309-317.
73. Frazee, B.W., et al., *High prevalence of methicillin-resistant Staphylococcus aureus in emergency department skin and soft tissue infections.* Annals of emergency medicine, 2005. **45**(3): p. 311-320.
74. Klevens, R.M., et al., *Invasive methicillin-resistant Staphylococcus aureus infections in the United States.* Jama, 2007. **298**(15): p. 1763-71.
75. Mera, R.M., et al., *Increasing role of Staphylococcus aureus and community-acquired methicillin-resistant Staphylococcus aureus infections in the United States: a 10-year trend of replacement and expansion.* Microb Drug Resist, 2011. **17**(2): p. 321-8.
76. DeLeo, F.R., et al., *Community-associated methicillin-resistant Staphylococcus aureus.* Lancet, 2010. **375**(9725): p. 1557-1568.
77. Stapleton, P.D. and P.W. Taylor, *Methicillin resistance in Staphylococcus aureus: mechanisms and modulation.* Science progress, 2002. **85**(Pt 1): p. 57-72.
78. Chambers, H.F., *Methicillin-resistant Staphylococcus aureus. Mechanisms of resistance and implications for treatment.* Postgrad Med, 2001. **109**(2 Suppl): p. 43-50.
79. Arias , C.A. and B.E. Murray *Antibiotic-Resistant Bugs in the 21st Century — A Clinical Super-Challenge.* New England Journal of Medicine, 2009. **360**(5): p. 439-443.
80. Fernández, L. and R.E.W. Hancock, *Adaptive and Mutational Resistance: Role of Porins and Efflux Pumps in Drug Resistance.* Clinical Microbiology Reviews, 2012. **25**(4): p. 661-681.
81. Little, M.L., et al., *Molecular diversity in mechanisms of carbapenem resistance in paediatric Enterobacteriaceae.* International Journal of Antimicrobial Agents, 2012. **39**(1): p. 52-57.

82. Gisele, P., et al., *Global Incidence of Carbapenemase-Producing Escherichia coli ST131.* Emerging Infectious Disease journal, 2014. **20**(11): p. 1928.
83. Queenan, A.M. and K. Bush, *Carbapenemases: the Versatile β-Lactamases.* Clinical Microbiology Reviews, 2007. **20**(3): p. 440-458.
84. Poirel, L., et al., *Carbapenem-hydrolysing metallo-beta-lactamases from Klebsiella pneumoniae and Escherichia coli isolated in Australia.* Pathology, 2004. **36**(4): p. 366-7.
85. Gauthier, L., et al., *Diversity of Carbapenemase-Producing Escherichia coli Isolates in France in 2012-2013.* Antimicrobial Agents and Chemotherapy, 2018. **62**(8): p. e00266-18.
86. Percival, S.L., S.M. McCarty, and B. Lipsky, *Biofilms and Wounds: An Overview of the Evidence.* Advances in Wound Care, 2015. **4**(7): p. 373-381.
87. Agladze, K., X. Wang, and T. Romeo, *Spatial periodicity of Escherichia coli K-12 biofilm microstructure initiates during a reversible, polar attachment phase of development and requires the polysaccharide adhesin PGA.* Journal of bacteriology, 2005. **187**(24): p. 8237-8246.
88. Moormeier, D.E. and K.W. Bayles, *Staphylococcus aureus biofilm: a complex developmental organism.* Molecular microbiology, 2017. **104**(3): p. 365-376.
89. Amalaradjou, M.A.R. and K. Venkitanarayanan, *Role of bacterial biofilms in catheter-associated urinary tract infections (CAUTI) and strategies for their control.* In: Recent Advances in the Field of Urinary Tract Infections. InTech. http://dx. doi. org/10.5772/46044, 2013.
90. Lauriano, C.M., et al., *The sodium-driven flagellar motor controls exopolysaccharide expression in Vibrio cholerae.* Journal of bacteriology, 2004. **186**(15): p. 4864-4874.
91. Karatan, E. and P. Watnick, *Signals, regulatory networks, and materials that build and break bacterial biofilms.* Microbiology and Molecular Biology Reviews, 2009. **73**(2): p. 310-347.
92. Hammar, M.r., et al., *Expression of two csg operons is required for production of fibronectin-and Congo red-binding curli polymers in Escherichia coli K-12.* Molecular microbiology, 1995. **18**(4): p. 661-670.
93. Mack, D., et al., *The intercellular adhesin involved in biofilm accumulation of Staphylococcus epidermidis is a linear beta-1,6-linked glucosaminoglycan: purification and structural analysis.* J Bacteriol, 1996. **178**(1): p. 175-83.

94. Solano, C., et al., *Genetic analysis of Salmonella enteritidis biofilm formation: critical role of cellulose.* Molecular microbiology, 2002. **43**(3): p. 793-808.
95. Stevenson, G., et al., *Organization of the Escherichia coli K-12 gene cluster responsible for production of the extracellular polysaccharide colanic acid.* Journal of bacteriology, 1996. **178**(16): p. 4885-4893.
96. Vuong, C., et al., *Polysaccharide intercellular adhesin (PIA) protects Staphylococcus epidermidis against major components of the human innate immune system.* Cellular microbiology, 2004. **6**(3): p. 269-275.
97. Henke, J.M. and B.L. Bassler, *Bacterial social engagements.* Trends in cell biology, 2004. **14**(11): p. 648-656.
98. Stewart, P.S. and J.W. Costerton, *Antibiotic resistance of bacteria in biofilms.* The lancet, 2001. **358**(9276): p. 135-138.
99. Perfeito, L., et al., *Adaptive mutations in bacteria: high rate and small effects.* Science, 2007. **317**(5839): p. 813-815.
100. Fenton, M., et al., *Recombinant bacteriophage lysins as antibacterials.* Bioengineered Bugs, 2010. **1**(1): p. 9-16.
101. Kennedy, J. and G. Bitton, *Bacteriophages in foods.* Phage ecology. New York: John Wiley & Sons, 1987: p. 286-316.
102. Bergh, Ø., et al., *High abundance of viruses found in aquatic environments.* Nature, 1989. **340**(6233): p. 467-468.
103. Danovaro, R., et al., *Determination of Virus Abundance in Marine Sediments.* Applied and Environmental Microbiology, 2001. **67**(3): p. 1384-1387.
104. Sulakvelidze, A., *Safety by Nature: Potential Bacteriophage Applications-Bacteriophages offer opportunities for safely managing bacterial infections.* Microbe, 2011. **6**(3): p. 122.
105. Hatfull, G.F. and R.W. Hendrix, *Bacteriophages and their genomes.* Current opinion in virology, 2011. **1**(4): p. 298-303.
106. Abedon, S.T., *Phage evolution and ecology.* Advances in applied microbiology, 2009. **67**: p. 1-45.
107. Mc Grath, S. and D. van Sinderen, *Bacteriophage: genetics and molecular biology*. 2007: Horizon Scientific Press.
108. Ackermann, H.W., *Phage classification and characterization.* Methods Mol Biol, 2009. **501**: p. 127-40.
109. Fischetti, V.A., *Bacteriophage lytic enzymes: novel anti-infectives.* Trends in microbiology, 2005. **13**(10): p. 491-496.
110. Kumari, S., K. Harjai, and S. Chhibber, *Topical treatment of Klebsiella pneumoniae B5055 induced burn wound infection in*

mice using natural products. J Infect Dev Ctries, 2010. **4**(6): p. 367-77.
111. Fish, R., et al., *Bacteriophage treatment of intransigent Diabetic toe ulcers: A case series.* Journal of Wound Care, 2016. **25**: p. S27-S33.
112. Merabishvili, M., et al., *Quality-Controlled Small-Scale Production of a Well-Defined Bacteriophage Cocktail for Use in Human Clinical Trials.* PLOS ONE, 2009. **4**(3): p. e4944.
113. Oechslin, F., et al., *Synergistic Interaction Between Phage Therapy and Antibiotics Clears Pseudomonas Aeruginosa Infection in Endocarditis and Reduces Virulence.* The Journal of Infectious Diseases, 2017. **215**(5): p. 703-712.
114. Wright, A., et al., *A controlled clinical trial of a therapeutic bacteriophage preparation in chronic otitis due to antibiotic-resistant Pseudomonas aeruginosa; a preliminary report of efficacy.* Clin Otolaryngol, 2009. **34**(4): p. 349-57.
115. Seth, A.K., et al., *Bacteriophage therapy for Staphylococcus aureus biofilm-infected wounds: a new approach to chronic wound care.* Plast Reconstr Surg, 2013. **131**(2): p. 225-34.
116. Semler, D.D., et al., *Aerosol phage therapy efficacy in Burkholderia cepacia complex respiratory infections.* Antimicrob Agents Chemother, 2014. **58**(7): p. 4005-13.
117. Huff, W.E., et al., *Prevention of Escherichia coli infection in broiler chickens with a bacteriophage aerosol spray.* Poultry Science, 2002. **81**(10): p. 1486-1491.
118. Singla, S., et al., *Bacteriophage-loaded nanostructured lipid carrier: improved pharmacokinetics mediates effective resolution of Klebsiella pneumoniae-induced lobar pneumonia.* J Infect Dis, 2015. **212**(2): p. 325-34.
119. Chhibber, S., S. Kaur, and S. Kumari, *Therapeutic potential of bacteriophage in treating Klebsiella pneumoniae B5055-mediated lobar pneumonia in mice.* Journal of Medical Microbiology, 2008. **57**(12): p. 1508-1513.
120. Debarbieux, L., et al., *Bacteriophages Can Treat and Prevent Pseudomonas aeruginosa Lung Infections.* Journal of Infectious Diseases, 2010. **201**(7): p. 1096-1104.
121. Morello, E., et al., *Pulmonary Bacteriophage Therapy on Pseudomonas aeruginosa Cystic Fibrosis Strains: First Steps Towards Treatment and Prevention.* PLOS ONE, 2011. **6**(2): p. e16963.

122. Carmody, L.A., et al., *Efficacy of bacteriophage therapy in a model of burkholderia cenocepacia pulmonary infection.* Journal of Infectious Diseases, 2010. **201**(2): p. 264-271.
123. Stanford, K., et al., *Oral Delivery Systems for Encapsulated Bacteriophages Targeted Escherichia coli O157: H7 in Feedlot Cattle.* Journal of Food Protection, 2010. **73**(7): p. 1304-1312.
124. Colom, J., et al., *Liposome-encapsulated bacteriophages for enhanced oral phage therapy against Salmonella spp.* Applied and Environmental Microbiology, 2015. **81**(14): p. 4841-4849.
125. Colom, J., et al., *Microencapsulation with alginate/CaCO3: A strategy for improved phage therapy.* Scientific Reports, 2017. **7**: p. 41441.
126. Atterbury, R.J., et al., *Bacteriophage therapy to reduce Salmonella colonization of broiler chickens.* Applied and Environmental Microbiology, 2007. **73**(14): p. 4543-4549.
127. Yen, M., L.S. Cairns, and A. Camilli, *A cocktail of three virulent bacteriophages prevents Vibrio cholerae infection in animal models.* Nature Communications, 2017. **8**: p. 14187.
128. Tanji, Y., et al., *Therapeutic use of phage cocktail for controlling Escherichia coli O157:H7 in gastrointestinal tract of mice.* Journal of Bioscience and Bioengineering, 2005. **100**(3): p. 280-287.
129. Nale, J.Y., et al., *Bacteriophage combinations significantly reduce Clostridium difficile growth in vitro and proliferation in vivo.* Antimicrobial Agents and Chemotherapy, 2016. **60**(2): p. 968-981.
130. Smith, H.W. and M.B. Huggins, *Successful treatment of experimental Escherichia coli infections in mice using phage: its general superiority over antibiotics.* Journal of General Microbiology, 1982. **128**(2): p. 307-318.
131. Barrow, P., M. Lovell, and A. Berchieri Jr, *Use of lytic bacteriophage for control of experimental Escherichia coli septicemia and meningitis in chickens and calves.* Clinical and Diagnostic Laboratory Immunology, 1998. **5**(3): p. 294-298.
132. Biswas, B., et al., *Bacteriophage therapy rescues mice bacteremic from a clinical isolate of vancomycin-resistant Enterococcus faecium.* Infection and Immunity, 2002. **70**(1): p. 204-210.
133. Oliveira, A., et al., *The influence of the mode of administration in the dissemination of three coliphages in chickens.* Poultry Science, 2009. **88**(4): p. 728-733.

134. Wills, Q.F., C. Kerrigan, and J.S. Soothill, *Experimental bacteriophage protection against Staphylococcus aureus abscesses in a rabbit model.* Antimicrobial Agents and Chemotherapy, 2005. **49**(3): p. 1220-1221.
135. McVay, C.S., M. Velasquez, and J.A. Fralick, *Phage therapy of Pseudomonas aeruginosa infection in a mouse burn wound model.* Antimicrob Agents Chemother, 2007. **51**(6): p. 1934-8.
136. Capparelli, R., et al., *Experimental phage therapy against Staphylococcus aureus in mice.* Antimicrobial Agents and Chemotherapy, 2007. **51**(8): p. 2765-2773.
137. Clark, J.R. and J.B. March, *Bacteriophages and biotechnology: vaccines, gene therapy and antibacterials.* Trends in biotechnology, 2006. **24**(5): p. 212-218.
138. Alemayehu, D., et al., *Bacteriophages ϕMR299-2 and ϕNH-4 can eliminate Pseudomonas aeruginosa in the murine lung and on cystic fibrosis lung airway cells.* MBio, 2012. **3**(2): p. e00029-12.
139. Drilling, A.J., et al., *Fighting sinus-derived Staphylococcus aureus biofilms in vitro with a bacteriophage-derived muralytic enzyme.* Int Forum Allergy Rhinol, 2015.
140. Becker, S.C., et al., *Differentially conserved staphylococcal SH3b_5 cell wall binding domains confer increased staphylolytic and streptolytic activity to a streptococcal prophage endolysin domain.* Gene, 2009. **443**(1-2): p. 32-41.
141. Hausler, T., *Viruses vs. Superbugs*. 2006: Springer.
142. Lu, T.K. and M.S. Koeris, *The next generation of bacteriophage therapy.* Current opinion in microbiology, 2011. **14**(5): p. 524-531.
143. Leiman, P.G., et al., *Three-dimensional rearrangement of proteins in the tail of bacteriophage T4 on infection of its host.* Cell, 2004. **118**(4): p. 419-29.
144. Yan, J., J. Mao, and J. Xie, *Bacteriophage polysaccharide depolymerases and biomedical applications.* BioDrugs, 2014. **28**(3): p. 265-74.
145. Hanlon, G.W., et al., *Reduction in exopolysaccharide viscosity as an aid to bacteriophage penetration through Pseudomonas aeruginosa biofilms.* Appl Environ Microbiol, 2001. **67**(6): p. 2746-53.
146. Bartell, P.F. and T.E. Orr, *Origin of polysaccharide depolymerase associated with bacteriophage infection.* J Virol, 1969. **3**(3): p. 290-6.

147. Abedon, S.T., et al., *Phage treatment of human infections.* Bacteriophage, 2011. **1**(2): p. 66-85.
148. Leiman, P., et al., *Structure and morphogenesis of bacteriophage T4.* Cellular and Molecular Life Sciences, 2003. **60**(11): p. 2356-2370.
149. Leiman, P.G., et al., *Structure and morphogenesis of bacteriophage T4.* Cellular and Molecular Life Sciences CMLS, 2003. **60**(11): p. 2356-2370.
150. Rakhuba, D., et al., *Bacteriophage receptors, mechanisms of phage adsorption and penetration into host cell.* Pol. J. Microbiol, 2010. **59**(3): p. 145-155.
151. Yu, F. and S. Mizushima, *Roles of lipopolysaccharide and outer membrane protein OmpC of Escherichia coli K-12 in the receptor function for bacteriophage T4.* Journal of Bacteriology, 1982. **151**(2): p. 718-722.
152. Doolittle, M.M., J.J. Cooney, and D.E. Caldwell, *Lytic infection of Escherichia coli biofilms by bacteriophage T4.* Can J Microbiol, 1995. **41**(1): p. 12-8.
153. Glonti, T., N. Chanishvili, and P.W. Taylor, *Bacteriophage-derived enzyme that depolymerizes the alginic acid capsule associated with cystic fibrosis isolates of Pseudomonas aeruginosa.* Journal of Applied Microbiology, 2010. **108**(2): p. 695-702.
154. Latka, A., et al., *Bacteriophage-encoded virion-associated enzymes to overcome the carbohydrate barriers during the infection process.* Applied microbiology and biotechnology, 2017. **101**(8): p. 3103-3119.
155. Fraser, D. and R.C. Williams, *Details of frozen-dried T3 and T7 bacteriophages as shown by electron microscopy.* Journal of bacteriology, 1953. **65**(2): p. 167-170.
156. Hausmann, R., *The genetics of T-odd phages.* Annual Reviews in Microbiology, 1973. **27**(1): p. 51-68.
157. Rao, R. and M. Pereira, *Behavior of a hybrid F'ts114 lac+, his+ factor (F42-400) in Klebsiella pneumoniae M5a1.* Journal of bacteriology, 1975. **123**(3): p. 792-805.
158. Brunovskis, I. and R. Burns, *Growth of coliphage T7 in Salmonella typhimurium.* Journal of virology, 1973. **11**(5): p. 621-629.
159. Krüger, D. and C. Schroeder, *Bacteriophage T3 and bacteriophage T7 virus-host cell interactions.* Microbiological reviews, 1981. **45**(1): p. 9.

160. Cinquerrui, S., et al., *Nanoencapsulation of Bacteriophages in Liposomes Prepared Using Microfluidic Hydrodynamic Flow Focusing.* Frontiers in Microbiology, 2018. **9**(2172).
161. Tkhilaishvili, T., et al., *Real-time assessment of bacteriophage T3-derived antimicrobial activity against planktonic and biofilm-embedded Escherichia coli by isothermal microcalorimetry.* Res Microbiol, 2018. **169**(9): p. 515-521.
162. Serwer, P. and E.T. Wright, *Nanomedicine and Phage Capsids.* Viruses, 2018. **10**(6).
163. Rountree, P.M., *The serological differentiation of staphylococcal bacteriophages.* J Gen Microbiol, 1949. **3**(2): p. 164-73.
164. O'Flaherty, S., et al., *Genome of Staphylococcal Phage K: a New Lineage of Myoviridae Infecting Gram-Positive Bacteria with a Low G+C Content.* Journal of Bacteriology, 2004. **186**(9): p. 2862-2871.
165. Gill, J.J., *Revised genome sequence of staphylococcus aureus bacteriophage K.* Genome announcements, 2014. **2**(1): p. e01173-13.
166. Chatterjee, A.N., *Use of Bacteriophage-resistant Mutants to Study the Nature of the Bacteriophage Receptor Site of Staphylococcus aureus.* Journal of Bacteriology, 1969. **98**(2): p. 519-527.
167. Burnet, F. and D. Lush, *The staphylococcal bacteriophages.* The Journal of Pathology and Bacteriology, 1935. **40**(3): p. 455-469.
168. Pantůček, R., et al., *The polyvalent staphylococcal phage φ812: its host-range mutants and related phages.* Virology, 1998. **246**(2): p. 241-252.
169. Rees, P. and B. Fry, *The morphology of staphylococcal bacteriophage K and DNA metabolism in infected Staphylococcus aureus.* Journal of General Virology, 1981. **53**(2): p. 293-307.
170. O'Flaherty, S., et al., *Potential of the Polyvalent Anti-Staphylococcus Bacteriophage K for Control of Antibiotic-Resistant Staphylococci from Hospitals.* Applied and Environmental Microbiology, 2005. **71**(4): p. 1836-1842.
171. Alves, D.R., et al., *Combined use of bacteriophage K and a novel bacteriophage to reduce Staphylococcus aureus biofilm formation.* Appl Environ Microbiol, 2014. **80**(21): p. 6694-703.
172. Lungren, M.P., et al., *Bacteriophage K for reduction of Staphylococcus aureusbiofilm on central venous catheter material.* Bacteriophage, 2013. **3**(4): p. e26825.

173. Narasimhaiah, M.H., et al., *Therapeutic potential of Staphylococcal bacteriophages for nasal decolonization of Staphylococcus aureus in mice.* 2013.
174. Vybiral, D., et al., *Complete nucleotide sequence and molecular characterization of two lytic Staphylococcus aureus phages: 44AHJD and P68.* FEMS Microbiol Lett, 2003. **219**(2): p. 275-83.
175. Sau, K., et al., *Synonymous codon usage bias in 16 Staphylococcus aureus phages: implication in phage therapy.* Virus research, 2005. **113**(2): p. 123-131.
176. Aindow, D. and M. Butcher, *Films or fabrics: is it time to reappraise postoperative dressings?* British journal of nursing, 2005. **14**(19).
177. Scales, J.T., A. Towers, and N. Goodman, *Development and evaluation of a porous surgical dressing.* British medical journal, 1956. **2**(4999): p. 962.
178. Petrulyte, S., *Advanced textile materials and biopolymers in wound management.* Danish medical bulletin, 2008. **55**(1): p. 72-77.
179. Handfield-Jones, S.E., et al., *Comparison of a hydrocolloid dressing and paraffin gauze in the treatment of venous ulcers.* Br J Dermatol, 1988. **118**(3): p. 425-7.
180. Boulton, A.J., P. Meneses, and W.J. Ennis, *Diabetic foot ulcers: A framework for prevention and care.* Wound Repair Regen, 1999. **7**(1): p. 7-16.
181. Maitz, M.F., *Applications of synthetic polymers in clinical medicine.* Biosurface and Biotribology, 2015. **1**(3): p. 161-176.
182. Awadhiya, A., et al., *Agarose bioplastic-based drug delivery system for surgical and wound dressings.* Engineering in Life Sciences, 2016.
183. Carlsson, J., *Physical and nutritional factors in gel culture of mammalian cells.* In vitro, 1978. **14**(10): p. 860.
184. Natarajan, S., et al., *Replica plating of mammalian cells using low melt agarose.* Cytotechnology, 2007. **54**(3): p. 145-147.
185. Kurkus, J., et al., *Biocompatibility of a Novel Avidin-Agarose Adsorbent for Extracorporeal Removal of Redundant Radiopharmaceutical From the Blood.* Artificial organs, 2007. **31**(3): p. 208-214.
186. Fernández-Cossío, S., et al., *Biocompatibility of agarose gel as a dermal filler: histologic evaluation of subcutaneous implants.* Plastic and reconstructive surgery, 2007. **120**(5): p. 1161-1169.

187. Maniatis, T., E.F. Fritsch, and J. Sambrook, *Molecular cloning: a laboratory manual*. Vol. 545. 1982: Cold Spring harbor laboratory Cold Spring Harbor, NY.
188. Wypych, G., *Handbook of plasticizers*. 2004: ChemTec Publishing.
189. Vieira, M.G.A., et al., *Natural-based plasticizers and biopolymer films: A review.* European Polymer Journal, 2011. **47**(3): p. 254-263.
190. Bial·ecka-Florjańczyk, E. and Z. Florjańczyk, *Solubility of Plasticizers, Polymers and Environmental Pollution-Chapter 22.* 2007.
191. Lee, K.Y. and D.J. Mooney, *Alginate: properties and biomedical applications.* Progress in polymer science, 2012. **37**(1): p. 106-126.
192. Meyer, T., et al., *Radical grafting polymerization of vinylformamide with functionalized silica particles.* Macromolecular Chemistry and Physics, 2003. **204**(4): p. 725-732.
193. Pelton, R., *Polyvinylamine: a tool for engineering interfaces.* Langmuir, 2014. **30**(51): p. 15373-15382.
194. Boateng, J.S., et al., *Wound healing dressings and drug delivery systems: A review.* Journal of Pharmaceutical Sciences, 2008. **97**(8): p. 2892-2923.
195. Jończyk, E., et al., *The influence of external factors on bacteriophages—review.* Folia Microbiologica, 2011. **56**(3): p. 191-200.
196. Iriarte, F.B., et al., *Factors affecting survival of bacteriophage on tomato leaf surfaces.* Appl Environ Microbiol, 2007. **73**(6): p. 1704-11.
197. Hosseinidoust, Z., A.L. Olsson, and N. Tufenkji, *Going viral: designing bioactive surfaces with bacteriophage.* Colloids Surf B Biointerfaces, 2014. **124**: p. 2-16.
198. Bhardwaj, N., et al., *Bacteriophage immobilized graphene electrodes for impedimetric sensing of bacteria (Staphylococcus arlettae).* Analytical Biochemistry, 2016. **505**: p. 18-25.
199. Hosseinidoust, Z., A.L.J. Olsson, and N. Tufenkji, *Going viral: Designing bioactive surfaces with bacteriophage.* Colloids and Surfaces B: Biointerfaces, 2014. **124**(Supplement C): p. 2-16.
200. Anany, H., et al., *Biocontrol of Listeria monocytogenes and Escherichia coli O157:H7 in Meat by Using Phages Immobilized on Modified Cellulose Membranes.* Applied and Environmental Microbiology, 2011. **77**(18): p. 6379-6387.

201. Cademartiri, R., et al., *Immobilization of bacteriophages on modified silica particles.* Biomaterials, 2010. **31**(7): p. 1904-1910.
202. Lone, A., et al., *Development of prototypes of bioactive packaging materials based on immobilized bacteriophages for control of growth of bacterial pathogens in foods.* International Journal of Food Microbiology, 2016. **217**: p. 49-58.
203. Lvov, Y., et al., *Successive Deposition of Alternate Layers of Polyelectrolytes and a Charged Virus.* Langmuir, 1994. **10**(11): p. 4232-4236.
204. Lin, Y., et al., *Layer-by-layer assembly of viral capsid for cell adhesion.* Acta Biomaterialia, 2008. **4**(4): p. 838-843.
205. Steinmetz, N.F., et al., *Layer-By-Layer Assembly of Viral Nanoparticles and Polyelectrolytes: The Film Architecture is Different for Spheres Versus Rods.* ChemBioChem, 2008. **9**(10): p. 1662-1670.
206. Suci, P.A., et al., *Assembly of Multilayer Films Incorporating a Viral Protein Cage Architecture.* Langmuir, 2006. **22**(21): p. 8891-8896.
207. Yoo, P.J., et al., *Spontaneous assembly of viruses on multilayered polymer surfaces.* Nature Materials, 2006. **5**: p. 234.
208. Yoo, P.J., et al., *Solvent-Assisted Patterning of Polyelectrolyte Multilayers and Selective Deposition of Virus Assemblies.* Nano Letters, 2008. **8**(4): p. 1081-1089.
209. Pearson, H.A., et al., *Phage-Bacterium War on Polymeric Surfaces; Can Surface-Anchored Bacteriophages Eliminate Microbial Infections?* Biomacromolecules, 2013. **14**(5): p. 1257-1261.
210. Singh, A., et al., *Immobilization of bacteriophages on gold surfaces for the specific capture of pathogens.* Biosensors and Bioelectronics, 2009. **24**(12): p. 3645-3651.
211. Klem, M.T., et al., *2-D Array Formation of Genetically Engineered Viral Cages on Au Surfaces and Imaging by Atomic Force Microscopy.* Journal of the American Chemical Society, 2003. **125**(36): p. 10806-10807.
212. Tolba, M., et al., *Oriented Immobilization of Bacteriophages for Biosensor Applications.* Applied and Environmental Microbiology, 2010. **76**(2): p. 528-535.
213. Naidoo, R., et al., *Surface-immobilization of chromatographically purified bacteriophages for the optimized capture of bacteria.* Bacteriophage, 2012. **2**(1): p. 15-24.

214. Dixon, D.V., Z. Hosseinidoust, and N. Tufenkji, *Effects of environmental and clinical interferents on the host capture efficiency of immobilized bacteriophages.* Langmuir, 2014. **30**(11): p. 3184-90.
215. Kopeček, J., *Hydrogel biomaterials: a smart future?* Biomaterials, 2007. **28**(34): p. 5185-5192.
216. Lutolf, M.P., *Biomaterials: Spotlight on hydrogels.* Nature materials, 2009. **8**(6): p. 451-453.
217. Patel, A. and K. Mequanint, *Hydrogel biomaterials*, in *Biomedical engineering-frontiers and challenges*. 2011, InTech.
218. Puapermpoonsiri, U., J. Spencer, and C.F. van der Walle, *A freeze-dried formulation of bacteriophage encapsulated in biodegradable microspheres.* European Journal of Pharmaceutics and Biopharmaceutics, 2009. **72**(1): p. 26-33.
219. Desai, E.S., et al., *Critical factors affecting cell encapsulation in superporous hydrogels.* Biomedical Materials, 2012. **7**(2): p. 024108.
220. Park, J.H. and Y.H. Bae, *Hydrogels based on poly (ethylene oxide) and poly (tetramethylene oxide) or poly (dimethyl siloxane): synthesis, characterization, in vitro protein adsorption and platelet adhesion.* Biomaterials, 2002. **23**(8): p. 1797-1808.
221. Bean, J.E., et al., *Triggered Release of Bacteriophage K from Agarose/Hyaluronan Hydrogel Matrixes by Staphylococcus aureus Virulence Factors.* Chemistry of Materials, 2014. **26**(24): p. 7201-7208.
222. Markoishvili, K., et al., *A novel sustained-release matrix based on biodegradable poly(ester amide)s and impregnated with bacteriophages and an antibiotic shows promise in management of infected venous stasis ulcers and other poorly healing wounds.* Int J Dermatol, 2002. **41**(7): p. 453-8.
223. Sulakvelidze, A. and E. Kutter, *Bacteriophage Therapy in Humans.* Bacteriophages: biology and applications, 2004: p. 377-428.
224. Li, J. and D.J. Mooney, *Designing hydrogels for controlled drug delivery.* Nature reviews. Materials, 2016. **1**(12): p. 16071.
225. Seo, J.Y., et al., *Electrostatically Interactive Injectable Hydrogels for Drug Delivery.* Tissue Engineering and Regenerative Medicine, 2018. **15**(5): p. 513-520.
226. Pertici, V., et al., *Degradable and Injectable Hydrogel for Drug Delivery in Soft Tissues.* Biomacromolecules, 2019. **20**(1): p. 149-163.

227. Puvirajesinghe, T.M., et al., *Tailoring drug release rates in hydrogel-based therapeutic delivery applications using graphene oxide.* Journal of The Royal Society Interface, 2018. **15**(139): p. 20170949.
228. Dzhonova, D., et al., *Local release of tacrolimus from hydrogel-based drug delivery system is controlled by inflammatory enzymes in vivo and can be monitored non-invasively using in vivo imaging.* PLOS ONE, 2018. **13**(8): p. e0203409.
229. Li, D., X. An, and Y. Mu, *A liposomal hydrogel with enzyme triggered release for infected wound.* Chemistry and Physics of Lipids, 2019. **223**: p. 104783.
230. Jiang, H., et al., *A Smart Capsule With a Hydrogel-Based pH-Triggered Release Switch for GI-Tract Site-Specific Drug Delivery.* IEEE Transactions on Biomedical Engineering, 2018. **65**(12): p. 2808-2813.
231. Yamamoto, K.R., et al., *Rapid bacteriophage sedimentation in the presence of polyethylene glycol and its application to large-scale virus purification.* Virology, 1970. **40**(3): p. 734-744.
232. Abbott, A.P., et al., *Novel solvent properties of choline chloride/urea mixtures.* Chemical Communications, 2003(1): p. 70-71.
233. Narayanan, R.P., et al., *Photodegradable iron(III) cross-linked alginate gels.* Biomacromolecules, 2012. **13**(8): p. 2465-71.
234. Kuhl, S.J. and H. Mazure, *d'Hérelle. Preparation of Therapeutic Bacteriophages, Appendix 1 from: Le Phénomène de la Guérison dans les maladies infectieuses: Masson et Cie, 1938, Paris—OCLC 5784382.* Bacteriophage, 2011. **1**(2): p. 55-65.
235. Pallavali, R.R., et al., *Isolation and in vitro evaluation of bacteriophages against MDR-bacterial isolates from septic wound infections.* PLOS ONE, 2017. **12**(7): p. e0179245.
236. Casey, E., D. van Sinderen, and J. Mahony, *In Vitro Characteristics of Phages to Guide 'Real Life' Phage Therapy Suitability.* Viruses, 2018. **10**(4): p. 163.
237. Khan Mirzaei, M. and A.S. Nilsson, *Isolation of phages for phage therapy: a comparison of spot tests and efficiency of plating analyses for determination of host range and efficacy.* PloS one, 2015. **10**(3): p. e0118557-e0118557.
238. Ackermann, H.W., *Bacteriophage electron microscopy.* Adv Virus Res, 2012. **82**: p. 1-32.
239. Winey, M., et al., *Conventional transmission electron microscopy.* Molecular biology of the cell, 2014. **25**(3): p. 319-323.

240. Miller, E.S., et al., *Bacteriophage T4 Genome.* Microbiology and Molecular Biology Reviews, 2003. **67**(1): p. 86.
241. Pajunen, M.I., et al., *Complete nucleotide sequence and likely recombinatorial origin of bacteriophage T3.* J Mol Biol, 2002. **319**(5): p. 1115-32.
242. Adams, M.H. and B.H. Park, *An enzyme produced by a phage-host cell system. II. The properties of the polysaccharide depolymerase.* Virology, 1956. **2**(6): p. 719-36.
243. Chan, B.K. and S.T. Abedon, *Bacteriophages and their enzymes in biofilm control.* Curr Pharm Des, 2015. **21**(1): p. 85-99.
244. Gallet, R., S. Kannoly, and I.-N. Wang, *Effects of bacteriophage traits on plaque formation.* BMC microbiology, 2011. **11**: p. 181-181.
245. Abedon, S.T. and R.R. Culler, *Bacteriophage evolution given spatial constraint.* J Theor Biol, 2007. **248**(1): p. 111-9.
246. You, L. and J. Yin, *Amplification and spread of viruses in a growing plaque.* J Theor Biol, 1999. **200**(4): p. 365-73.
247. Abedon, S.T., *Lysis from without.* Bacteriophage, 2011. **1**(1): p. 46-49.
248. Hyman, P. and S.T. Abedon, *Bacteriophage host range and bacterial resistance.* Adv Appl Microbiol, 2010. **70**: p. 217-48.
249. Shao, Y. and I.-N. Wang, *Bacteriophage adsorption rate and optimal lysis time.* Genetics, 2008. **180**(1): p. 471-482.
250. Gallet, R., Y. Shao, and I.-N.J.B.E.B. Wang, *High adsorption rate is detrimental to bacteriophage fitness in a biofilm-like environment.* 2009. **9**(1): p. 241.
251. Karam, J.D. and E.S.J.V.J. Miller, *Bacteriophage T4 and its relatives.* 2010. **7**(1): p. 293.
252. Abedon, S.T., *Selection for bacteriophage latent period length by bacterial density: A theoretical examination.* Microb Ecol, 1989. **18**(2): p. 79-88.
253. Choi, C., et al., *The effect of cell size on the burst size of T4 bacteriophage infections of Escherichia coli B23.* J Exp Microbiol Immunol, 2010. **14**: p. 85-91.
254. Brock, T.D., *The emergence of bacterial genetics*. 1990: Cold Spring Harbor Laboratory Press Cold Spring Harbor, NY.
255. Abedon, S.T., T.D. Herschler, and D. Stopar, *Bacteriophage Latent-Period Evolution as a Response to Resource Availability.* 2001. **67**(9): p. 4233-4241.
256. Golec, P., et al., *Bacteriophage T4 can produce progeny virions in extremely slowly growing Escherichia coli host: comparison*

of a mathematical model with the experimental data. 2014. **351**(2): p. 156-161.
257. Gu, J., et al., *A Method for Generation Phage Cocktail with Great Therapeutic Potential.* PLOS ONE, 2012. **7**(3): p. e31698.
258. Zemb, O., et al., *Phage adsorption to bacteria in the light of the electrostatics: A case study using E. coli, T2 and flow cytometry.* Journal of Virological Methods, 2013. **189**(2): p. 283-289.
259. Esteban, P.P., A.T.A. Jenkins, and T.C. Arnot, *Elucidation of the mechanisms of action of Bacteriophage K/nano-emulsion formulations against S. aureus via measurement of particle size and zeta potential.* Colloids and Surfaces B: Biointerfaces, 2016. **139**: p. 87-94.
260. Gottenbos, B., et al., *Antimicrobial effects of positively charged surfaces on adhering Gram-positive and Gram-negative bacteria.* Journal of Antimicrobial Chemotherapy, 2001. **48**(1): p. 7-13.
261. Bull, J.J. and J.J. Gill, *The habits of highly effective phages: population dynamics as a framework for identifying therapeutic phages.* Frontiers in microbiology, 2014. **5**: p. 618-618.
262. Shamsuri, A.A. and R. Daik, *Plasticizing effect of choline chloride/urea eutectic-based ionic liquid on physicochemical properties of agarose films.* BioResources, 2012. **7**(4): p. 4760-4775.
263. Zakrewsky, M., et al., *Ionic liquids as a class of materials for transdermal delivery and pathogen neutralization.* Proceedings of the National Academy of Sciences, 2014. **111**(37): p. 13313-13318.
264. Klein-Marcuschamer, D., B.A. Simmons, and H.W. Blanch, *Techno-economic analysis of a lignocellulosic ethanol biorefinery with ionic liquid pre-treatment.* Biofuels, Bioproducts and Biorefining, 2011. **5**(5): p. 562-569.
265. Morrow, T.I. and E.J. Maginn, *Density, local composition and diffusivity of aqueous choline chloride solutions: a molecular dynamics study.* Fluid Phase Equilibria, 2004. **217**(1): p. 97-104.
266. Björklund, S., et al., *Glycerol and urea can be used to increase skin permeability in reduced hydration conditions.* European Journal of Pharmaceutical Sciences, 2013. **50**(5): p. 638-645.
267. Ma, Y., et al., *Microencapsulation of Bacteriophage Felix O1 into Chitosan-Alginate Microspheres for Oral Delivery.* Applied and Environmental Microbiology, 2008. **74**(15): p. 4799-4805.

268. Boggione, D.M., et al., *Evaluation of microencapsulation of the UFV-AREG1 bacteriophage in alginate-Ca microcapsules using microfluidic devices.* 2017. **158**: p. 182-189.
269. Moghtader, F., et al., *Phages in modified alginate beads.* 2017. **45**(2): p. 357-363.
270. Soto, M.J., et al., *Encapsulation of specific Salmonella Enteritidis phage f3αSE on alginate-spheres as a method for protection and dosification.* Electronic Journal of Biotechnology, 2018. **31**: p. 57-60.
271. Bruchet, M. and A. Melman, *Fabrication of patterned calcium cross-linked alginate hydrogel films and coatings through reductive cation exchange.* Carbohydrate Polymers, 2015. **131**: p. 57-64.
272. Machida-Sano, I., et al., *Effects of composition of iron-cross-linked alginate hydrogels for cultivation of human dermal fibroblasts.* 2012. **2012**.
273. Kuo, C.K. and P.X. Ma, *Ionically crosslinked alginate hydrogels as scaffolds for tissue engineering: Part 1. Structure, gelation rate and mechanical properties.* Biomaterials, 2001. **22**(6): p. 511-521.
274. Bozzola, J.J. and L.D. Russell, *Electron microscopy: principles and techniques for biologists*. 1999: Jones & Bartlett Learning.
275. Misell, D. and C. Stolinski, *Scanning electron microscopy and X-ray microanalysis. A text for biologists, material scientists and geologists| JI Goldstein, DE Newbury, P. Echlin, DC Joy, C. Fiori and E. Lifshin. Plenum Press, New York and London, 1981. XIII+ 673 pp.£ 29.50*. 1983, Pergamon.
276. Noor, P., et al., *Evaluation of ATR-FTIR spectrometry in the fingerprint region combined with chemometrics for simultaneous determination of benzene, toluene, and xylenes in complex hydrocarbon mixtures.* Monatshefte für Chemie-Chemical Monthly, 2018. **149**(8): p. 1341-1347.
277. Günther, H., *NMR spectroscopy: basic principles, concepts and applications in chemistry*. 2013: John Wiley & Sons.
278. Zambonin, P. and E. Desimoni, *X-ray photoelectron spectroscopy: principles, instrumentation, data processing and molten salt applications*, in *Molten Salt Chemistry*. 1987, Springer. p. 425-445.
279. Corbett, J.C.W., et al., *Measuring surface zeta potential using phase analysis light scattering in a simple dip cell arrangement.* Colloids and Surfaces A: Physicochemical and Engineering Aspects, 2012. **396**: p. 169-176.

280. Witek, E., M. Pazdro, and E. Bortel, *Mechanism for Base Hydrolysis of Poly(N-vinylformamide).* Journal of Macromolecular Science, Part A, 2007. **44**(5): p. 503-507.
281. Ingar Draget, K., K. Østgaard, and O. Smidsrød, *Homogeneous alginate gels: A technical approach.* Carbohydrate Polymers, 1990. **14**(2): p. 159-178.
282. Waters, E.M., et al., *Phage therapy is highly effective against chronic lung infections with Pseudomonas aeruginosa.* Thorax, 2017.
283. Pernodet, N., M. Maaloum, and B. Tinland, *Pore size of agarose gels by atomic force microscopy.* Electrophoresis, 1997. **18**(1): p. 55-58.
284. Tenhunen, T.-M., et al., *Understanding the interactions of cellulose fibres and deep eutectic solvent of choline chloride and urea.* 2018. **25**(1): p. 137-150.
285. Macário, I.P.E., et al., *Cytotoxicity profiling of deep eutectic solvents to human skin cells.* Scientific reports, 2019. **9**(1): p. 3932-3932.
286. Pinschmidt, R.K., et al., *N-Vinylformamide – Building Block for Novel Polymer Structures.* Journal of Macromolecular Science, Part A, 1997. **34**(10): p. 1885-1905.
287. Winter, G.D., *Formation of the Scab and the Rate of Epithelization of Superficial Wounds in the Skin of the Young Domestic Pig.* Nature, 1962. **193**(4812): p. 293-294.
288. Queen, D., et al., *The preclinical evaluation of the water vapour transmission rate through burn wound dressings.* Biomaterials, 1987. **8**(5): p. 367-71.
289. White, R.J. and K.F. Cutting, *Interventions to avoid maceration of the skin and wound bed.* Br J Nurs, 2003. **12**(20): p. 1186-201.
290. McColl, D., B. Cartlidge, and P. Connolly, *Real-time monitoring of moisture levels in wound dressings in vitro: an experimental study.* Int J Surg, 2007. **5**(5): p. 316-22.
291. Mi, F.-L., et al., *Fabrication and characterization of a sponge-like asymmetric chitosan membrane as a wound dressing.* Biomaterials, 2001. **22**(2): p. 165-173.
292. Xu, R., et al., *Controlled water vapor transmission rate promotes wound-healing via wound re-epithelialization and contraction enhancement.* Scientific Reports, 2016. **6**: p. 24596.
293. Yasuda, T., T. Okuno, and H. Yasuda, *Contact Angle of Water on Polymer Surfaces.* Langmuir, 1994. **10**(7): p. 2435-2439.

294. Abbott, A.P., et al., *Cationic functionalisation of cellulose using a choline based ionic liquid analogue.* 2006. **8**(9): p. 784-786.
295. Bruening, M. and M. Adusumilli, *Polyelectrolyte-multilayer-films-and-membrane-functionalization.* Mater. Matters, 2011. **6**(3): p. 76-81.
296. Sun, J. and H. Tan, *Alginate-based biomaterials for regenerative medicine applications.* Materials, 2013. **6**(4): p. 1285-1309.
297. Jones, V., J.E. Grey, and K.G. Harding, *Wound dressings.* BMJ (Clinical research ed.), 2006. **332**(7544): p. 777-780.
298. Jault, P., et al., *Efficacy and tolerability of a cocktail of bacteriophages to treat burn wounds infected by Pseudomonas aeruginosa (PhagoBurn): a randomised, controlled, double-blind phase 1/2 trial.* The Lancet Infectious Diseases, 2018.
299. Esteban, P.P., et al., *Enhancement of the antimicrobial properties of bacteriophage-K via stabilization using oil-in-water nano-emulsions.* Biotechnol Prog, 2014. **30**(4): p. 932-44.
300. Merabishvili, M., et al., *Stability of bacteriophages in burn wound care products.* PLOS ONE, 2017. **12**(7): p. e0182121.
301. Nogueira, F., et al., *Immobilization of bacteriophage in wound-dressing nanostructure.* Nanomedicine, 2017. **13**(8): p. 2475-2484.
302. Jain, K.K., *Drug Delivery Systems - An Overview*, in *Drug Delivery Systems*, K.K. Jain, Editor. 2008, Humana Press: Totowa, NJ. p. 1-50.
303. Singla, S., et al., *Encapsulation of Bacteriophage in Liposome Accentuates Its Entry in to Macrophage and Shields It from Neutralizing Antibodies.* PLOS ONE, 2016. **11**(4): p. e0153777.
304. Hosseinidoust, Z., T.G. Van de Ven, and N. Tufenkji, *Bacterial capture efficiency and antimicrobial activity of phage-functionalized model surfaces.* Langmuir, 2011. **27**(9): p. 5472-80.
305. Serwer, P., *Agarose gel electrophoresis of bacteriophages and related particles.* Journal of Chromatography B: Biomedical Sciences and Applications, 1987. **418**(Supplement C): p. 345-357.
306. Samtlebe, M., et al., *Carrier systems for bacteriophages to supplement food systems: Encapsulation and controlled release to modulate the human gut microbiota.* LWT - Food Science and Technology, 2016. **68**: p. 334-340.
307. Ma, Y., et al., *Enhanced alginate microspheres as means of oral delivery of bacteriophage for reducing staphylococcus aureus*

intestinal carriage. Food Hydrocolloids, 2012. **26**(2): p. 434-440.
308. Yap, M.L. and M.G. Rossmann, *Structure and function of bacteriophage T4.* Future microbiology, 2014. **9**(12): p. 1319-1327.
309. Coombs, D. and F. Arisaka, *T4 tail structure and function.* Molecular biology of bacteriophage, 1994. **4**: p. 259-281.
310. Narayanan, J., J.-Y. Xiong, and X.-Y. Liu. *Determination of agarose gel pore size: Absorbance measurements vis a vis other techniques*. in *Journal of Physics: Conference Series*. 2006. IOP Publishing.
311. Chen, L.-K., et al., *Potential of bacteriophage ΦAB2 as an environmental biocontrol agent for the control of multidrug-resistant Acinetobacter baumannii.* BMC microbiology, 2013. **13**: p. 154-154.
312. Wertz, C.F. and M.M. Santore, *Effect of Surface Hydrophobicity on Adsorption and Relaxation Kinetics of Albumin and Fibrinogen: Single-Species and Competitive Behavior.* Langmuir, 2001. **17**(10): p. 3006-3016.
313. Belfiore, L.A. and E.M. Indra, *Transition metal compatibilization of poly(vinylamine) and poly(ethylene imine).* Journal of Polymer Science Part B: Polymer Physics, 2000. **38**(4): p. 552-561.
314. Smidsrød, O. and G. Skja, *Alginate as immobilization matrix for cells.* Trends in biotechnology, 1990. **8**: p. 71-78.
315. Bouhadir, K.H., et al., *Degradation of partially oxidized alginate and its potential application for tissue engineering.* Biotechnol Prog, 2001. **17**(5): p. 945-50.
316. Chhibber, S., T. Kaur, and K. Sandeep, *Co-therapy using lytic bacteriophage and linezolid: effective treatment in eliminating methicillin resistant Staphylococcus aureus (MRSA) from diabetic foot infections.* PLoS One, 2013. **8**(2): p. e56022.
317. Mendes, J.J., et al., *Wound healing potential of topical bacteriophage therapy on diabetic cutaneous wounds.* Wound Repair Regen, 2013. **21**(4): p. 595-603.
318. Miao, J., et al., *Lysostaphin-functionalized cellulose fibers with antistaphylococcal activity for wound healing applications.* Biomaterials, 2011. **32**(36): p. 9557-67.
319. Rhoads, D.D., et al., *Bacteriophage therapy of venous leg ulcers in humans: results of a phase I safety trial.* J Wound Care, 2009. **18**(6): p. 237-8, 240-3.

320. Kutter, E. and A. Sulakvelidze, *Bacteriophages: biology and applications*. 2004: CRC Press.
321. Anderson, B., et al., *Enumeration of bacteriophage particles: Comparative analysis of the traditional plaque assay and real-time QPCR- and nanosight-based assays.* Bacteriophage, 2011. **1**(2): p. 86-93.
322. van Luyn, M.J., et al., *Cytotoxicity testing of wound dressings using methylcellulose cell culture.* Biomaterials, 1992. **13**(5): p. 267-75.
323. Alves, D., et al., *Bacteriophage varphiIBB-PF7A loaded on sodium alginate-based films to prevent microbial meat spoilage.* Int J Food Microbiol, 2019. **291**: p. 121-127.

8 Appendices

Appendix I - Preparation of lambda buffer

Lambda buffer was prepared as follows; stock solutions of 2 % w/v gelatine, and 1 M Tris solution at pH 7.2 (altered with concentrated HCl) were prepared and autoclaved to sterilise. 2.5 g $MgSO_4(7H_2O)$, 6 ml Tris buffer and 2.5 ml 2 % gelatine were added to a volumetric flask and made up to 1 L with reverse osmosis water. The buffer was then divided into appropriate aliquots and autoclaved at 121°C for 15 min to sterilise.

Appendix II - Preparation of overlay agar

TSA and technical agar were added to reverse osmosis water at 3 % w/v and 0.4 % w/v, respectively, and placed over a Bunsen burner until the agar had completely dissolved. 5ml aliquots for plaque assay and 10 ml aliquots for direct plating methods were dispensed in Bijoux bottles and autoclaved at 121°C for 15 min to sterilise. Prior to use the individual Bijoux bottles containing overlay agar were boiled in a water bath until molten, then placed in a water bath at 45°C until required.

Appendix III - Surface zeta potential validation and tracer particle selection

The addition of tracer particles to the medium of interest is to detect electrophoretic and electro-osmotic mobility by light scattering (see section 4.2.10 for background). Due to the nature of surface zeta potential measurements, compatibility of the tracer particles needs to be assessed prior to conducting surface zeta potential measurements. Compatibility of the tracer particles with the medium of interest should be determined to avoid aggregation and flocculation of the particles, this can be achieved using dynamic light scattering (DLS) measurements to characterise particle size in the dispersant. It is also important to use minimum concentrations of tracer particles to further avoid interaction with the material interface. Excessive tracer particle mediated interaction with the sample surface can be investigated by performing multiple surface zeta potential measurements with incremental tracer concentrations. A correlation between the mean surface zeta potential and tracer concentration would indicate a possible interaction between the tracer and the material interface.

The compatibility of tracer particles with the material surface should also be assessed to avoid adsorption of particles to the interface. For example, positively charged tracer particles should not be used with negatively charged surfaces as adsorption would result in charging

of the surface and incorrect surface zeta potential measurements. Tracer particles should therefore have no affinity to the sample under investigation. As the surface charge of the material may not be known, sterically stabilised tracer particles (i.e. PEGylated) can be used in these cases. Tracer suitability can also be determined by comparison of the tracer zeta potential in the dispersant of interest, with the zeta potential value of the tracer dispersed in the same medium in the presence of the sample. If the difference in zeta potential values is less than 5 mV, the tracer chemistry is suitable for the sample under investigation (MALVERN). A difference in zeta potential of more than 5 mV would indicate strong particle-matrix interactions and an alternative tracer should be sought.

Tracer particle selection

Prior to experimental development, zeta potential and size measurements were validated using -42 mV transfer standard and a 100 nm polystyrene latex standard, respectively.

Standard	Particle Size (nm)	Polydispersity Index (PdI)	Zeta potential (mV ± SD)
-42 ± 4.2 mV Transfer Standard	N/A	N/A	-45.9 ± 1.5 mV
100 nm PL Standard (in water)	112.52 ± 0.94	0.016	N/A

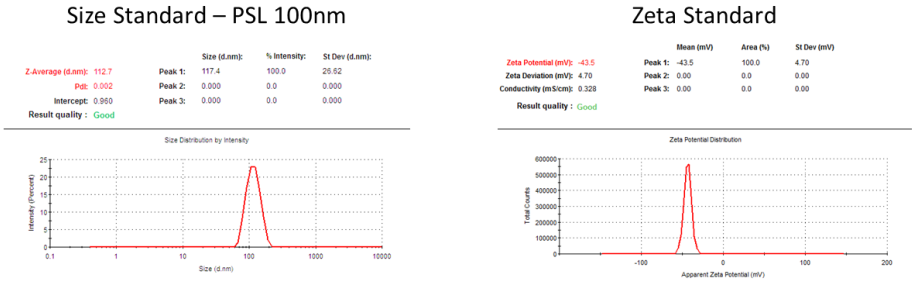

Validation data for the ZetaSizer Nano ZS90, including transfer standard zeta potential and polystyrene latex (PL) particle size standard, in tabular (top) and graphical (bottom) format.

Tracer compatibility with the dispersant of interest (bacteriophage buffer, pH 7.2, 25°C) was determined by DLS size measurements to identify aggregation of tracer particles. The tracer zeta potentials in lambda buffer were then determined and compared to the tracer zeta potential measurements obtained during preliminary surface zeta potential measurements. A difference of over 5 mV would indicate particle-matrix interactions and the tracer would therefore be discounted for the sample.

Tracer particle size, PdI, and zeta potential values in lambda buffer (pH 7.2, 25°C).

Tracer	Particle Size (nm)	Polydispersity Index (PdI)	Zeta potential in dispersant (mV ± SD)	Zeta Potential in dispersant containing sample (mV)
100 nm NR3+ PL	105.4 ± 0.67	0.17	19.84 ± 1.46	20.17 ± 1.69
500 nm PEG300 PL	652.05 ± 75.06	0.055	-12.66 ± 0.38	-
100 nm PL	105.02 ± 1.07	0.015	-14.98 ± 0.86	-19.27 ± 0.68
100 nm – COOH PL	105.08 ± 1.67	0.067	-15.80 ± 0.61	-

Based on the assumption that PLAg samples with surfaces modified with a cationic polymer would be positively charged, NR3+ tracer particles were selected for use on such samples, confirmed by compatibility with both material and dispersant. Polystyrene latex particles were selected for use with unmodified PLAg films based on their stability in lambda buffer and the compatibility with the material interface.

Appendix IV – SEM of bacteriophage T3 adsorbed to the surface of carbon grids

Bacteriophage T3 was adsorbed to the surface of carbon SEM grids by placing 100 μl of bacteriophage lysate at 1 x 10^8 PFU/ml on the adhesive surface and leaving to adsorb for 5 minutes before blotting excess liquid with filter paper. The carbon grids were then allowed to air dry for 1 h at room temperature and atmospheric pressure prior to analysis by SEM with no further sample preparation.

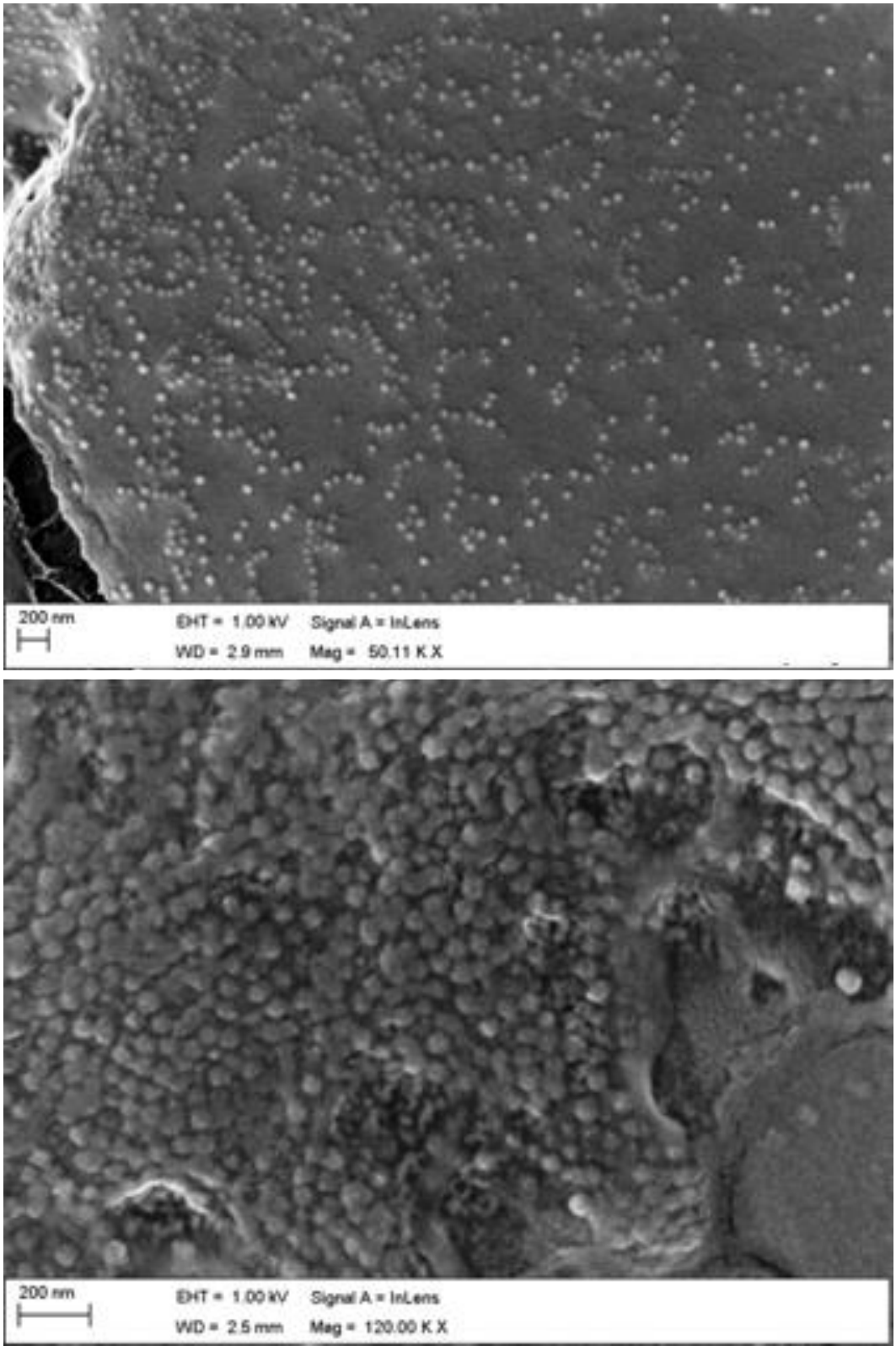

SEM micrographs of bacteriophage T3 adsorbed to the surface of carbon SEM grids at 50 K (top) and 120 K (bottom) magnification.

Appendix V – Schematic outlining areas of experimental exploration, rationales and investigative findings.